EXPERIMENTAL AND NUMERICAL STUDY OF THE IN-PLANE AND OUT-OF-PLANE BEHAVIOUR OF UNREINFORCED MASONRY INFILLS BOUNDED BY RC FRAMES

by

Ehsan Nasiri

Submitted in partial fulfilment of the requirements

for the degree of Doctor of Philosophy

at

Dalhousie University

Halifax, Nova Scotia

June 2019

I dedicate this dissertation to my parents

for their endless love, support, and encouragement.

Table of Contents

List of Tables ix

List of Figures x

Abstract xvi

List of Abbreviations and Symbols Used xvii

Acknowledgements xxiii

Chapter 1 Introduction 1

1.1 Masonry Infilled Frames 1

1.2 Method of Analysis 2

1.3 In-Plane and Out-of-Plane Behaviour of Infills 3

1.4 Research Objectives 3

1.5 Thesis Layout 5

Chapter 2 Literature Review 6

2.1 Introduction 6

2.2 General Behaviour 6

2.2.1 In-Plane Behaviour 6

2.2.1.1 Aspect Ratio (h/l) 8

2.2.1.2 Interfacial Gaps 8

2.2.1.3 Openings 9

2.2.1.4 Cyclic Loading 9

2.2.2 Out-of-Plane Behaviour 10

2.2.2.1 Interfacial Gaps 11

2.2.2.2 Slenderness Ratio 13

2.2.2.3 Frame Rigidity 13

2.2.2.4 Openings 14
2.3 Analytical Modelling 14
2.3.1 Macro-Modelling Methods 15
2.3.1.1 In-Plane Behaviour 15
2.3.1.2 Out-of-Plane Behaviour 19
2.3.2 Micro-Modeling Methods 24
2.4 Code and Practice 30
2.4.1 In-Plane Behaviour 30
2.4.2 Out-of-Plane Behaviour 33
2.5 Summary 33
Chapter 3 Experimental Program 35
3.1 Introduction 35
3.2 Infilled Frame Specimens 35
3.3 In-Plane Test Setup and Procedure 37
3.4 Out-of-Plane Test Setup and Procedure 38
Chapter 4 Development of a Detailed 3D FE Model for Analysis of the In-Plane Behaviour of Masonry Infilled Concrete Frames 41
4.1 Abstract 41
4.2 Introduction 42
4.3 Experimental Program 45
4.3.1 Test Setup and Instrumentation 48
4.3.2 Material Properties 48
4.4 Finite Element Model 49
4.4.1 Nonlinear Behaviour of Concrete and CMUs 50
4.4.2 Yield Surface 51

4.4.3 Flow Rule 52
4.4.4 Compressive Stress-strain Relationship 53
4.4.5 Tensile Behaviour Model 55
4.5 Material Model for Reinforcement 57
4.6 Behaviour Model of Interface Elements 59
4.7 Analysis Procedure 63
4.8 Verification of the Model 64
4.9 Investigation on the Interface Parameters 72
4.9.1 Effect of Failure Surface Parameters 75
4.9.2 Effect of Fracture Energy Parameters 76
4.9.3 Effect of Dilation Angle 77
4.10 Conclusion 79
4.11 Acknowledgement 80
Chapter 5 The Out-of-Plane Behaviour of Concrete Masonry Infills Bounded by Reinforced Concrete Frames 81
5.1 Abstract 81
5.2 Introduction 82
5.3 Experimental Program 84
5.3.1 Test Setup, Instrumentation, and Procedure 87
5.3.2 Material Properties 89
5.4 Finite Element Model 90
5.4.1 Nonlinear Behaviour of Concrete and CMUs 91
5.4.1.1 Compressive Behaviour Model 92
5.4.1.2 Tensile Behaviour Model 93

5.4.2 Behaviour Model of Interface Between the CMUs and Between the CMUs and the Frame 95

5.4.3 Material Model for Reinforcement 97

5.4.4 Analysis Procedure 98

5.5 Validation of the Model 98

5.6 Parametric Study 103

5.6.1 Effect of Infill Aspect Ratio 105

5.6.2 Effect of Frame Stiffness 106

5.6.3 Effect of Infill Slenderness Ratio 108

5.6.4 Effect of Size and Aspect Ratio of Openings 112

5.6.5 Effect of Interfacial Gaps 115

5.6.6 Effect of CMU Web Thickness 119

5.7 Conclusion 121

5.8 Acknowledgement 123

Chapter 6 Study of Arching Behaviour and Strength of Concrete Masonry Infills under Out-of-Plane Loading 124

6.1 Abstract 124

6.2 Introduction 125

6.3 Finite Element Modelling Method 130

6.3.1 Nonlinear Behaviour of Concrete and CMUs 130

6.3.2 Behaviour Model of Interface Elements 132

6.4 One-Way Arching with Rigid Supports 133

6.5 Two-Way Arching with Rigid Bounding Frames 138

6.6 Experimental Investigation 139

6.7 Two-Way Arching in Flexible Bounding Frames 147

6.7.1 Proposed Modification Based on Dawe and Seah's Method 153
6.7.2 Performance of the Proposed Equation.....156
6.8 Conclusion 161
6.9 Acknowledgement.....162
Chapter 7 Effect of Prior In-Plane Damage on the Out-of-Plane Performance of Concrete Masonry Infills 163
7.1 Abstract 163
7.2 Introduction.....164
7.3 Finite Element Modelling Method 168
7.4 Experimental Investigation 170
7.5 Validation of the Model 175
7.6 Parametric Study.....178
7.6.1 In-Plane Behaviour.....180
7.6.2 Out-of-Plane Behaviour with In-Plane Damage 182
7.6.3 Consideration of Infill Slenderness.....187
7.6.4 Consideration of Cyclic Loading 189
7.7 Evaluation of the Existing Analytical Method 192
7.8 Suggested Reduction Factor 195
7.9 Limitations.....197
7.10 Conclusion 198
7.11 Acknowledgement.....199
Chapter 8 Summary and Conclusions 200
8.1 In-Plane Behaviour.....201
8.1.1 Experimental Observations.....201
8.1.2 FE Modelling.....201

8.2 Out-of-Plane Behaviour 202
8.2.1 General behaviour 202
8.2.2 Effect of Interfacial Gap 202
8.2.3 Effect of Infill Opening 203
8.2.4 Effect of Infill Aspect Ratio 203
8.2.5 Effect of Infill Slenderness Ratio 204
8.2.6 Effect of Frame Stiffness 204
8.2.7 One-Way and Two-Way Arching 204
8.2.8 Effect of In-Plane Damage 205
8.3 Recommendations for Future Research 206
References 208
Appendix A: Copyright Permissions 221

List of Tables

Table 2.1. Strut methods in TMS 402/602-16 and CSA S304-14 32

Table 3.1. Summary of frame specimens 36

Table 4.1. Summary of test specimens 46

Table 4.2. Summary of material properties for test specimens 49

Table 4.3. The CDP model parameters for concrete and CMUs 53

Table 4.4. Summary of interface parameters 63

Table 4.5. Stiffness and strength comparison of the experimental and FE results 67

Table 4.6. Summary of input parameters used in the sensitivity study 74

Table 4.7. Material properties used for the sensitivity study 75

Table 5.1. Summary of material properties for the specimens 89

Table 5.2. The CDP model parameters for concrete and CMUs 92

Table 5.3. Summary of interface parameters 97

Table 5.4. Material properties used for the parametric study 104

Table 6.1. Details of tested RC framed masonry infill specimens 142

Table 6.2. Summary of FE model results 149

Table 6.3. Comparison of results from FE analysis and proposed equation 157

Table 6.4. Comparison of results from the proposed equation and experimental studies 160

Table 7.1. Details of RC framed masonry infill specimens 170

Table 7.2. Material properties used in the parametric study 179

Table 7.3.Comparison of experimental and analytical reduction factor 197

List of Figures

Figure 2.1. Failure modes of infilled RC frames (Asteris et al. 2013) 7

Figure 2.2. Illustration of arching action 11

Figure 2.3. Arching action in rigid and gapped conditions (Gabrielsen and Kaplan 1976)..... 12

Figure 2.4. Masonry infill-frame deformed shape interaction (Asteris et al. 2013) 16

Figure 2.5. Stafford Smith's test setup and equivalent strut replaced for infill (Smith 1966)..... 16

Figure 2.6. Two-strut with shear spring model proposed by Crisafulli and Carr (2007) 18

Figure 2.7. Idealized cracking pattern..... 21

Figure 2.8. Modelling strategies for masonry: (a) detailed micro-modelling; (b) simplified micro-modelling; (c) continuum element micro-modelling (Roca et al. 1998)..... 25

Figure 3.1. Test setup details, main LVDT locations and side view of the test setup 37

Figure 3.2. Out-of-plane LVDTs and LVDT 1 38

Figure 3.3. Out-of-plane test setup: (a) Schematic side view; and. (b) setup components 39

Figure 3.4. LVDTs position for out-of-plane test 40

Figure 4.1. Geometric properties of infilled frame specimens and reinforcement details in the RC frame..... 47

Figure 4.2. Schematic test set-up 48

Figure 4.3. Three dimensional geometric model used in the FE analysis 51

Figure 4.4. Failure surface of the CDP model in plane stress (D.S.Simulia 2010)..... 52

Figure 4.5. Compression stress-strain curve for: (a) Concrete; and (b) CMUs..... 55

Figure 4.6. Tension stress-strain curve for concrete 56

Figure 4.7. Tensile behaviour of CMU material: (a) stress-strain curve; and (b) stress-displacement curve 57

Figure 4.8. Modified stess-strain curve for the reinforcement 59

Figure 4.9. Hyperbolic Drucker-Prager yield surface (D.S.Simulia 2010) 61

Figure 4.10. Hardening and flow rule for the hyperbolic Drucker-Prager model (D.S.Simulia 2010) 61

Figure 4.11. Tensile and shear strength softening curves and corresponding fracture energies 62

Figure 4.12. Load-displacement curves for different number of elements 65

Figure 4.13. Comparison of lateral load vs. displacement curves obtained from tests and FE analysis for all specimens. 68

Figure 4.14. Deformed geometry and cracking pattern comparison for: (a) IFNG, (b) IFW16, (c) IFTG12 and (d) IFSG12 71

Figure 4.15. Detailed crushing comparison (specimen IFW16) 72

Figure 4.16. Yield lines in the p-q plane 74

Figure 4.17. Lateral load vs. displacement curves for interface failure surface parameters 75

Figure 4.18. Deformed shape (6x magnified) and cracking patterns for interface failure surfaces 76

Figure 4.19. Lateral load vs. displacement curves for interface fracture energy parameters 77

Figure 4.20. Lateral load vs. displacement curves for different interface dilation angles 78

Figure 4.21. Deformed shape (10x magnified) and cracking pattern at 25 mm lateral displacement for dilation angles 79

Figure 5.1. Geometric properties of specimens and reinforcement details in the RC frames 86

Figure 5.2. Test set-up for out-of-plane loading of the specimens 88

Figure 5.3. Schematic test set-up for in-plane loading of specimens IF-D1 and IF-D2 88

Figure 5.4. Load vs. lateral displacement curve for the laterally loaded infilled frame specimens 89

Figure 5.5. Three-dimensional geometric model used in the FE analysis 91

Figure 5.6. Compressive stress-strain curve for: (a) concrete; and (b) CMUs 93

Figure 5.7. Tensile stress-strain curve for concrete 94

Figure 5.8. Tensile behaviour of CMUs: (a) stress-strain curve; and (b) stress-displacement curve 95

Figure 5.9. Behaviour of the mortar joint interaction 96

Figure 5.10. Finite element stress-strain curves and failure modes for CMUs and masonry prisms 99

Figure 5.11. Comparison of out-of-plane pressure vs. displacement curves obtained from tests and FE analysis 100

Figure 5.12. Comparison of FE and experimental results for IFW16: (a) tensile cracks on the windward face and; (b) compressive crushing in the mid-plane of the infill 103

Figure 5.13. Development of cracks in the CMU blocks: (a) initiation of cracking; (b) at the ultimate capacity of the infill; and (c) after collapse of the infill 103

Figure 5.14. Infill aspect ratio study: (a) geometric configuration; and (b) failure mode for varying aspect ratios 106

Figure 5.15. Effect of infill aspect ratio and frame rigidity on the out-of-plane strength 107

Figure 5.16. Effect of frame stiffness on the out-of-plane strength 108

Figure 5.17. Failure mode and deformation contours (unit: m): (a) AR4; and (b) AR4-W 108

Figure 5.18. Slenderness ratio study: (a) out-of-plane pressure vs. slenderness for varying aspect ratios; and (b) out-of-plane pressure vs. slenderness for rigid and model frames 110

Figure 5.19. Cracking patterns shown at mid-plane of infill at ultimate pressure for slenderness ratio study: h/l=1 111

Figure 5.20. Infill opening size study: (a) geometry of models with different opening sizes; (b) normalized strength vs. opening area ratios 113

Figure 5.21. Infill opening aspect ratio study (FE results): (a) geometry of models; and, (b) out-of-plane pressure vs. displacement curves 114

Figure 5.22. Cracking pattern for different opening aspect ratios at 42 kPa pressure 115

Figure 5.23. Interfacial gap study: (a) out-of-plane pressure vs. displacement curves; and (b) normalized strength for different gap sizes/locations.....117

Figure 5.24. Effect of beam gap and column gap on the infills with different aspect ratios.....119

Figure 5.25. Maximum compressive stress contours (unit: N/m^2) for model AR2 with gaps at 32 kPa out-of-plane pressure.....119

Figure 5.26. CMU web thickness study: normalized strength vs. web thickness.....120

Figure 5.27. Cracking development in the webs of different thickness at 30 kPa out-of-plane pressure.....121

Figure 6.1. Behaviour of the interface interaction.....133

Figure 6.2. Geometric configuration of vertical and horizontal strips and masonry block dimensions.....134

Figure 6.3. Out-of-plane strength in vertical and horizontal arching vs. slenderness ratio.....135

Figure 6.4. Failure modes in vertical strips with different h/t ratios (5× magnified deformations).....136

Figure 6.5. Failure modes in horizontal strips with different l/t ratios (5× magnified deformations).....137

Figure 6.6. Two-way and one-way arching comparison for rigid frames.....138

Figure 6.7. Normalized pressure and arching froces in vertical and horizontal directions.....139

Figure 6.8. Geometric properties of specimens and reinforcement details in the RC frames.....141

Figure 6.9. Test set-up for out-of-plane loading of the specimens.....143

Figure 6.10. Comparison of out-of-plane pressure vs. displacement curves obtained from tests and FE analysis: (a) IFNG; (b) IF-TG; (c) IF-SG; and (d) Combined results.....144

Figure 6.11. Comparison of FE and experimental results for cracking patterns: (a) IFNG; (b) IF-SG; and (c) IF-TG.....146

Figure 6.12. Geometric configuration of the models in parametric study.....148

Figure 6.13. Comparison of strength value vs aspect ratio for different frame stiffness 152

Figure 6.14. Comparison of strength value vs frame stiffness for different infill aspect ratio 153

Figure 6.15. Two-way and one-way arching comparison for non-rigid frames.....155

Figure 7.1. Behaviour of the interface interaction 169

Figure 7.2. Geometric properties of specimens and reinforcement details in the RC frame.....171

Figure 7.3. Lateral load vs. drift ratio obtained from in-plane tests.....173

Figure 7.4. Comparison of FE and experimental results for cracking patterns: (a) IF-D1; (b) IF-D2; and (c) IF-D3 (magnified deformation) 173

Figure 7.5. Out-of-plane test results: (a) Out-of-plane pressure vs displacement curves; and (b) normalized out-of-plane strength vs. prior in-plane drift....174

Figure 7.6. Comparison of out-of-plane pressure vs. displacement curves obtained from tests and FE analysis 177

Figure 7.7. Comparison of FE and experimental cracking pattern in IF-D2 at out-of-plane loading stage 178

Figure 7.8. Geometric configuration of the models and reinforcement details in the RC frame in the parametric study 179

Figure 7.9. Prior damage pattern at: (a) 0.25%, and (b) 2% in-plane drift (AR=0.8, f′m = 16 MPa) 181

Figure 7.10. Damage patterns for a square panel with: (a) weak, (b) intermediate; and, (c) strong infill. 181

Figure 7.11. In-plane load vs. drift ratio for AR=1.0 model 182

Figure 7.12. Pressure vs. displacement curves: (a) Weak; (b) Intermediate; and, (c) Strong infill 183

Figure 7.13. Normalized out-of-plane strength vs. in-plane drift ratios for different infill strength and aspect ratios: (a) Weak infill; (b) Intermediate infill; (c) Strong infill; and, (d) Average of all aspect ratios.....185

Figure 7.14. In-plane cracking pattern for AR=0.8 and AR=1.3 strong infill models at 1% drift.....186

Figure 7.15. Normalized out-of-plane strength vs. prior in-plane drift curves for different slenderness ratios.....188

Figure 7.16. Cracking pattern for: (a) SR=14; and, (b) SR=28 with 0.5% in-plan drift at the ultimate out-of-plane pressure (magnified deformation).....188

Figure 7.17. Cyclic in-plane loading analysis for out-of-plane strength reduction: (a) Cyclic loading history; (b) AR=0.8 infill; (c) AR=1.0 infill; and, (d) AR=1.3 infill.....191

Figure 7.18. Cyclic and monotonic cracking comparison in different steps (6×magnified deformations): (a) Monotonic in-plane; (b) Cyclic in-plane; (c) Monotonic out-of-plane; and, (d) Cyclic out-of-plane.....192

Figure 7.19. Out-of-plane strength reduction comparison between Angel et al.'s method and: (a) test results; and, (b) finite element results 194

Figure 7.20. Proposed reduction factor equation with FE and test results 196

Abstract

A literature review revealed that there is limited technical information available on the subject of masonry infilled frames, in particular, the interaction between the infill and its bounding frame and how this interaction affects the infilled system behaviour and strength. This research was then conducted to further the understanding of the infill-to-frame interaction considering a range of geometric, material, loading characteristics of the infilled frame systems. To that end, both experimental and numerical studies were performed with the focus on the concrete masonry infills bounded by reinforced concrete frames. Both in-plane and out-of-plane loading situations on the infilled frames were considered. The experimental testing was designed to provide physical results of failure modes, behaviour and strength of infilled frames as affected by several key parameters. The numerical study began with development of a 3D finite element model capable of incorporating properties of masonry infilled frames using ABAQUS. An extensive validation process on the model ensued using the physical results. Once verified, the model was used in a finite element study where several geometric and material parameters with extended range of variations were systematically studied.

In the experimental study, a total of 17 specimens were tested of which 1) ten were subjected to in-plane loading; 2) four were subjected to out-of-plane loading; and 3) three were tested under in-plane loading first and then tested under out-of-plane loading to failure. Infill openings and infill-to-frame interfacial gaps were designed as two varying parameters for 1) and 2) test scenarios. The varying in-plane damage was the parameter for 3) testing scenario. While the diagonal cracking followed by corner crushing predominated the in-plane failure, two-way arching with the shear cracking through the concrete masonry unit webs was identified as the main load-resisting mechanism in out-of-plane tests. As for the in-plane damaged specimens, the out-of-plane capacity was reduced as a function of experienced in-plane drift ratio.

In the numerical study, the finite element model was shown to be capable of predicting the load-displacement responses as well as the cracking pattern and failure modes accurately for both in-plane and out-of-plane loading scenarios. The correlations between each studied parameter and the behaviour and strength of masonry infilled frames were presented and discussed. Modifications on the out-of-plane design method currently adopted by the American masonry standard (TMS 402/602-16) were proposed and was shown to improve the performance of the method. A lower-bound equation for evaluating the out-of-plane strength of masonry infills with prior in-plane damage was proposed and it showed to produce better estimate when compared to the existing method.

List of Abbreviations and Symbols Used

Abbreviations

ASTM	American society for testing and materials
BF	Bare frame
CC	Corner crushing
CDP	Concrete damaged plasticity
CMU	Concrete masonry unit
COV	Coefficient of variation
CSA	Canadian standards association
FEMA	Federal emergency management agency
IFD	Infilled frame with a door opening
IF-D	Infilled frame with in-plane damage
IFNG	Infilled frame with no gaps
IFSG	Infilled frame with side gaps
IFTG	Infilled frame with a top gap
IFW	Infilled frame with a window opening

LVDT	Linear variable differential transformer
MSJC	Masonry society joint committee
NBCC	National building code of Canada
RC	Reinforced concrete
SS	Shear sliding
TMS	The masonry society

Symbols

A	Area of diagonal compressive strut
A_e	Effective infill area
C_d	Wave velocity in the material
d	Length of diagonal compressive strut
d'	Initial shear strength
d_v	Effective depth for the shear calculation
EI	Flexural stiffness of the bounding frame
E_s^*	Modified elastic modulus
E_f	Modulus of elasticity of frame

E_m	Modulus of elasticity of masonry
f_{cr}	Cracking stress
f_y	Yield stress
f_y^*	Modified yield stress
f_c'	Compressive strength of concrete
f_m'	Compressive strength of masonry
f_t	Tensile strength
G	Flow potential function
G_f	Mode I fracture energy
g_0	Deflection in the direction of arching due to axial shortening or gaps
h	Height of the infill
I_b	Moment of inertia of the beam
I_c	Moment of inertia of the column
J_b, J_c	Torsional constant of bounding beam, bounding column
K_c	Ratio of the tensile meridian to the compressive meridian

K_{nn}, K_{ss}, K_{tt}	Normal and two shear stiffness of the mortar joint interface
k_i	Stiffness of infill at initial cracking load
k_{cra}	Stiffness of infill at the first major crack load
k_{ult}	stiffness of infill at ultimate load
l	Length of the infill
L_e	Characteristic length of the smallest element
M_f	Factored moment
M_{yh}	Moment resistance for horizontal arching
M_{yv}	Moment resistance for vertical arching
N_u	Compressive force on the shear surface
$\bar{p}$	hydrostatic pressure stress
p_t	Initial tensile strength
$\bar{q}$	Von Mises equivalent effective stress
q_{cr}	Out-of-plane load at the occurrence of boundary crushing of infill
q_{max}	Out-of-plane load at the occurrence of transverse instability of infill

q_{ult}	Ultimate out-of-plane pressure of the infill
R_1	Reduction factor to account for the prior in-plane damage
R_2	Reduction factor for the bounding frame stiffness
t	Thickness of infill, CMU
$\dot{u}$	Velocity in equation of motion
$\ddot{u}$	Acceleration in equation of motion
V_f	Factored shear force
w	Width of the diagonal strut
w_{eff}	The effective width of diagonal compressive strut as defined by CSA S304-14
x_{yh}	Displacement of the infill corresponding to horizontal arching at failure
x_{yv}	Displacement of the infill corresponding to vertical arching at failure
β	Frictional angle of the material in the p-q plane
γ	Factor accounting for the contact area during arching action
Δ_{cr}	Lateral deflection required for the cracking of the infill
ϵ	Eccentricity

$\tilde{\varepsilon}_c^{pl}$	Plastic compressive strain
$\tilde{\varepsilon}_t^{pl}$	Plastic tensile strain
$\varepsilon_t, \varepsilon_c$	Tensile and compressive strain
λ	Slenderness effect
μ	Coefficient of friction
ν	Poisons ratio
ρ	Reinforcement ratio
$\hat{\bar{\sigma}}_{max}$	Maximum principal effective stress
σ_{b0}	Initial biaxial compressive yield stress
σ_{c0}	Initial uniaxial compressive yield stress
σ_t, σ_c	Tensile and compressive stress
φ	Friction angle in the Mohr-Coulomb failure surface
ψ_c, ψ_i	Dilation angle of concrete and mortar joint

Acknowledgements

First and foremost, I would like to thank my supervisor Dr. Yi Liu for her generous support, guidance and mentorship. This dissertation would not have been possible without her leadership.

I would also like to thank my supervisory committee members Dr. Gordon Fenton and Dr. Fadi Oudah, and my external examiner, Dr Tony Yang for taking the time to review this dissertation, attending my defense, and providing valuable feedback.

Additionally, I would like to thank the civil engineering department staff, Mrs. June Ferguson and Mrs. Shelley Parker for their help throughout my studies as well as the laboratory technicians Mr. Blair Nickerson, Mr. Brian Kennedy, Mr. Jesse Keane, and Mr. Brian Liekens for their assistance with my project.

I would like to thank my fellow colleagues, Chuanjia Hu, Xiaoyan Zeng, Chongyang Wang, Reza Sepasdar, and Reza Rahimi for their helpful collaboration in completing the experiments.

I wish to acknowledge the financial contributions from the Canadian Concrete Masonry Producers Association.

Finally, I would like to thank friends and family for providing their love and support throughout the past five and a half years. I thank Farzaneh, Parvar, Hosein, Sara, Sahar, Setareh, Vahid, Ehsan, and all my amazing friends who made this journey unforgettable.

Chapter 1 Introduction

1.1 Masonry Infilled Frames

Masonry is the most ancient construction material and its use dates back as early as 10,000 years ago from natural stone and sun-dried brick then developing into the modern manufactured clay bricks and concrete masonry blocks. In modern construction, masonry walls are commonly used in steel and concrete frame buildings as infill walls either as partitions to separate spaces or as cladding to complete the building envelope. Previous studies have shown that the presence of masonry infill in a framed structure affects the behaviour of the system significantly. Once the masonry infill participates in the load sharing of the system, the interaction between the infill and its bounding frame becomes crucial in determining the strength of the framed system. Most early research has been focused on understanding the contribution of masonry infills to the frame behaviour when subjected to in-plane loading. Studies conducted since the 1950s have shown that the infill results in increasing the stiffness, strength, ductility, and energy dissipation of the frame system. A design approach based on "diagonal strut" concept has been adopted in the Canadian and American masonry design standards (CSA S304-14, TMS 402/602-16), albeit with different design formulations. In comparison, the out-of-plane behaviour of the infilled frame has been researched much less with only a handful of existing experimental studies. While a design guideline is provided in the American masonry design standard, the Canadian standard in this regard is blank and it only directs designers to apply principles of mechanics for design. It is also worth to point out that the current design guidelines, if available, need a thorough examination as the work on which the existing design equations were based was conducted on very limited physical specimens of one type

or another. Recent experimental studies have reported large disparities between the measured strengths when compared with the code values (Pasca et al. 2017, Ricci et al. 2018). It is also recognized that due to the complexity of the system consisting of one brittle material (infill) and one ductile material (frame) and many variations of material and geometric properties of each, more in-depth studies are in need to advance the understanding of the infilled frame behaviour and lead to improvement of the current design provisions in the standards.

1.2 Method of Analysis

Studies of infilled frames in general dates back to the 1950s. Till 1990s, most studies were experiment-based, and some led to simplified analytical models with restriction for use (Mainstone 1971, McDowell et al. 1956a, Monk 1958, Smith and Carter 1969). Although the parameters studied in the early research were limited, the test set-up, specimen design, and testing procedure provided foundation on which the later work can be built. With the advancement in computing technology, finite element modeling techniques have been increasingly implemented in studies to supplement the experimental results and extend parameters beyond those that are feasible in laboratory testing. Since 2000s, finite element (FE) methods encoded in commercial software such as ANSYS, ABAQUS or open source software OpenSees have achieved various successes in simulation of masonry infilled frames (Hashemi 2007, Minaie et al. 2014, Mohyeddin et al. 2013, Rahimi and Liu 2017, Stavridis and Shing 2010). These FE studies also identified challenges and inadequacies in modeling techniques. Nonetheless, FE methods have been considered to be an effective tool for analysis of masonry infilled frames. For this study, both experimental and FE

studies were conducted where the experimental results were used to validate the FE model which was in turn used in an extensive parametric study to predict results on a wider range of parameters.

1.3 In-Plane and Out-of-Plane Behaviour of Infills

As mentioned, most early research was dedicated to the in-plane behaviour of masonry infilled frames. The focus was to study the performance of the infilled frame as the lateral load resisting system where the infill in-plane behaviour and strength plays a critical role in the system lateral load resistance. A large volume of literature is available for the in-plane studies of masonry infilled frames. A summary of the literature review on the subject can be found in (Asteris et al. 2013, Chen 2016). In the case of out-of-plane research of masonry infilled frames, some experimental studies were conducted but with a very limited number of parameters and limited variations in masonry and frame types. There is a greater gap in the current standards for design of masonry infills subjected to out-of-plane loading. This research was focused on the out-of-plane behaviour of masonry infills. If the masonry infilled frame is considered as a lateral load resisting system, its out-of-plane behaviour and strength are integral parts of design since the loading is applied in both directions in a seismic event.

1.4 Research Objectives

This study involved an experimental and numerical investigation of the in-plane and out-of-plane behaviour and strength of masonry infills with a focus on the latter. Various parameters deemed influential were considered in the study. The main objectives of the

research were to advance the FE modeling technique in simulation of masonry infilled frames; to provide reliable physical and numerical results of masonry infilled frames subjected to in-plane/out-of-plane loading; and to propose a rational design method for out-of-plane strength of masonry infills bounded by frames.

The scope of work includes the following:

- To develop a robust finite element model to simulate the in-plane and out-of-plane behaviour of the infilled frames and verification of the model using the obtained experimental data. Focus is given to a three-dimensional model with the least amount of simplification that is capable of considering the main influencing materials and geometric parameters.
- To investigate the effect of several key parameters including infill opening, interfacial gaps, and prior in-plane damage on the out-of-plane behaviour and strength of infilled RC frames.
- To study the one-way and two-way arching action in concrete masonry infills and compare the results with the state of the art in analysis of arching.
- To study the effect of various parameters including frame stiffness, aspect ratio, slenderness ratio, arching direction, and prior in-plane damage on the out-of-plane behaviour and strength of infills.
- To develop correlations between the studied parameters and the strength of masonry infills.
- To assess the efficiency of the existing design methods in the literature and current standards for the infill design and propose new design methods as appropriate.

1.5 Thesis Layout

This dissertation is organized in a paper format with eight chapters. The present chapter presents the subject and objectives of the research. Chapter 2 presents a comprehensive literature review of the numerical modelling approaches available for masonry infill analysis. Important experimental studies pertinent to in-plane and out-of-plane behaviour have also been reported in this chapter. Chapter 3 provides an overview of the experimental program. Chapters 4 to 7 consist of four papers. Chapter 4 describes the details of the three-dimensional FE model and validation of the model for in-plane analysis. Chapter 5 focuses on the application of the proposed FE model for out-of-plane analysis of infills. Verification of the model using the test results is presented and an investigation on the effects of various influencing parameters is carried out. Chapter 6 presents a detailed experimental and numerical analysis on the arching behaviour and out-of-plane resistance in concrete masonry units. Chapter 7 investigates the effect of in-plane damage on the out-of-plane behaviour of the infills. Effects of different in-plane damage modes observed in experiments and other factors investigated numerically are summarized and used to provide recommendations for estimation of damaged out-of-plane capacity. Finally, a summary of results, main conclusions and recommendations for future work are presented in Chapter 8.

Chapter 2 Literature Review

2.1 Introduction

Research on the behaviour of masonry infilled frames dates back to the 1950s. Studies have been conducted to investigate the behaviour of masonry infilled frames of various material and geometric properties subjected to static, quasi-static, or seismic loading. The common objective of these studies was to quantify the effect of the infill on the strength and stiffness of the infilled system and to propose guidelines for design of infilled frames. While early research focused mainly on experimental work, the numerical modeling using finite element methods has gained popularity in the last two decades with the development of computing technology. The following chapters deal with a specific subject on the behaviour of masonry infills furnished with a detailed literature review on that subject. Rather than repeating the information, this chapter serves as a more general summary of the important findings that are deemed most relevant to this research. Since this research is more numerical modelling focused, the following section begins with a description of general behaviour of infilled frames observed in the experiments and then focuses more on the review of the state-of-the-art in numerical and analytical studies conducted particularly on RC frames with infills.

2.2 General Behaviour

2.2.1 In-Plane Behaviour

The in-plane behaviour deals with the behaviour of masonry infilled frames subjected to in-plane lateral loading. In general, the previous studies showed that the behaviour depends

on many factors such as material and geometric properties of both the frame and infill; the relative stiffness of the frame and infill and loading conditions to just name a few.

Some general behavioural trend and characteristics of infilled frames have been identified and studied. It was shown that regardless of steel or RC frames, the presence of infills resulted in significant increases in both stiffness and strength of infilled frame systems when compared with bare frames. However, the degree of increase was dependent on the type of frame. Infilled frames can develop a number of possible failure mechanisms. The following four failure modes have been identified as common types of failure observed in masonry infilled RC frames; 1) Corner Crushing (CC) which is the compressive failure of the infill in the loaded corners; 2) Sliding Shear (SS) that usually happens in infills with weak mortar joints; 3) Diagonal Cracking (DC) that occurs along the diagonal direction of the infill due to shear sliding or principal tensile stresses; and 4) Frame Failure (FF) that can be in the form of ductile plastic hinge development or sudden shear failure of the columns. The schematic representation of these modes is shown in Figure 2.1.

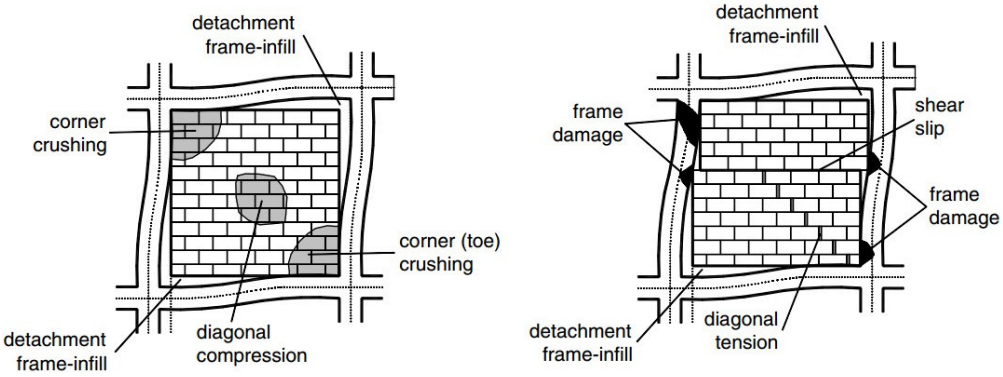

Figure 2.1. Failure modes of infilled RC frames (Asteris et al. 2013)

The corner crushing failure mode the most common one for infilled frames with typical material and geometric properties while shear sliding is ranked the second (Ghosh and Amde 2002, Mehrabi and Shing 1997, Saneinejad and Hobbs 1995).

In these previous studies, effects of several geometric and material parameters that are deemed influential to the behaviour and capacity of masonry infilled frames were the focus and the general findings are presented in the following.

2.2.1.1 Aspect Ratio (h/l)

The aspect ratio of infills (h/l) has been shown to affect the stiffness and strength of the infilled frames. Studies by Mehrabi et al. (1996) and Flanagan and Bennett (1999a, 1999c) showed that increase in the aspect ratio of the infill reduces the ultimate capacity and stiffness of the infill. Shear failure is dominant for low aspect ratio (squat) walls whereas the failure is more controlled by flexural stresses with toe crushing for larger aspect ratios (tall, slender infills).

2.2.1.2 Interfacial Gaps

The interfacial gaps, whether at beam-infill or column-infill, have been shown to reduce the stiffness and strength of the infilled system. However, the magnitude of the reduction and the correlation between the gap size, location and the reduction were not consistent in reported studies. Yong (1984) and Dawe and Seah (1989a) observed that presence of top beam-infill gap of 20 mm significantly reduces the initial stiffness and capacity of infilled frames by about 50%. Flanagan (1994) reported that a 25 mm column-infill gap did not result in a reduction in ultimate capacity, but a non-symmetrical cracking pattern occurred.

All previous research did point to a much softer behaviour of infilled frame at early loading stage when gap was present. Once the gap was closed at the loaded corner, a sudden increase in stiffness was observed.

2.2.1.3 Openings

Openings are also proven to reduce the initial stiffness and capacity of the infills. This reduction is correlated to the size of the infill and to the location of the opening albeit on a lesser degree. Mallick and Garg (1971) recommended that the best location for opening is at the center of the infill. However, experiments on RC infilled frames by Kakaletsis and Karayannis (2007) showed that the best performance of the system was obtained when the opening is located as close as possible to the edges of the infill panel where a better crack distribution takes place in the remaining solid sections of the infills. Experiments by Tasnimi and Mohebkhah (2011) indicated that infills with openings usually develop more extensive diagonal tension cracking prior to failure than infills without openings. Soon (2011) suggested that the relationship between the reduction in infill ultimate strength and the opening size is not linear.

2.2.1.4 Cyclic Loading

Shake table tests on half-scaled single storey infilled frame specimens by Mehrabi et al. (1996) and Klingner et al. (1996) showed that strength of the infilled system was sustained through many hysteretic cycles without major damage. Results showed that infills can significantly increase the stiffness, strength and energy dissipation capacity of the system, even under simultaneous in- and out-of-plane lateral forces.

Pujol and Fick (2010) conducted full-scale experimental testing on three-storey concrete buildings with and without masonry infills to investigate the effect of infills on the drift capacity of concrete frames. The presence of infills was found to improve the behaviour of the frame in terms of controlling the inter-storey drift and increasing the base shear strength and lateral stiffness up to 100% and 500%, respectively.

2.2.2 Out-of-Plane Behaviour

One critical aspect of analyzing the behaviour of masonry infills bounded by frames subjected to out-of-plane loading is the confinement provided by the frame. While behaviour and capacity of a typical flexural wall is controlled by masonry tensile strength, confinement of the bounding frame has shown to change a tension-controlled failure to a compression-controlled failure. When the infill is restrained by a relatively rigid frame, the out-of-plane pressure causes tensile cracks that divide the infill into two or more segments. These segments then push against the boundary supports which induces in-plane compressive forces that transfer the out-of-plane pressure through a mechanism called arching where failure is characterized by compression failure of masonry. The shift from a tension-controlled mechanism to a compression-controlled mechanism enables the infills to resist much higher out-of-plane pressures compared to their flexural wall counterparts. Figure 2.2 illustrates the arching of an infill supported on two boundaries.

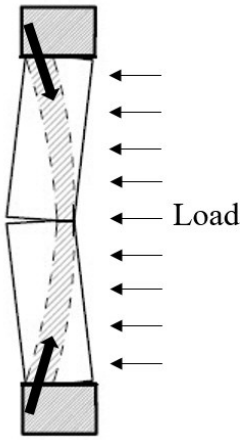

Figure 2.2. Illustration of arching action

The principles of mechanics can be used to find the capacity of the infill by utilizing equilibrium between the internal compressive forces and out-of-plane pressure. Different failure modes have been observed and included compressive crushing in the loaded corners of the arched segments, compressive/shear failure of the faceshells and buckling of the infill without major damage (Angel et al. 1994, Dawe and Seah 1989b, Flanagan and Bennett 1999b, McDowell et al. 1956a). Effects of several geometric parameters influential to the arching behavior and failure mode have been studied and some main findings are presented in the following.

2.2.2.1 Interfacial Gaps

Gaps between the masonry infill and its bounding frame are common occurrence due to the wall shrinkage, workmanship defects or intentional movement joints to separate the infill from the frame. As development of arching is dependent on the compressive force induced by the restraints on the boundary frame member, presence of gaps was found to reduce the out-of-plane resistance of the infill. Gabrielsen et al. (1975) carried out blast load tests on masonry walls with 2.5 and 5 mm gaps between the wall panel and the top

support. Compared to the control specimen, the gapped walls only resisted 1/6 to 1/8 of the out-of-plane load. However, these walls were still significantly stronger than the cantilever panels without confinement. Gabrielsen and Kaplan (1976) reported that wall with tight rigid supports would form a symmetric arching mechanism when subjected to out-of-plane loads while the presence of a gap at the top of the wall causes larger displacement and unsymmetrical arching as shown in Figure 2.3.

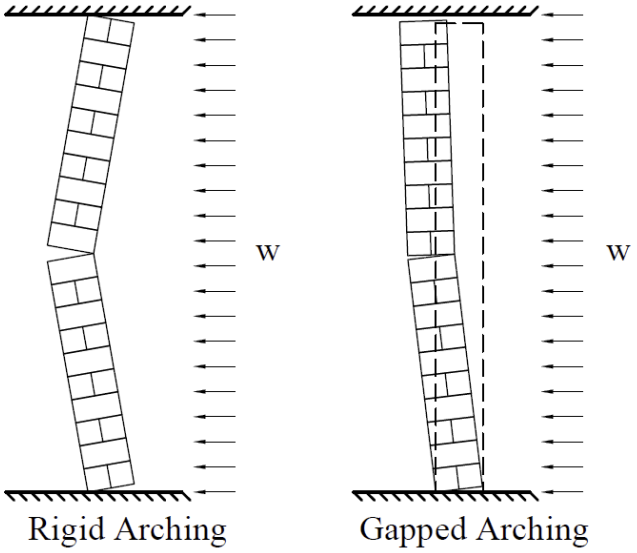

Figure 2.3. Arching action in rigid and gapped conditions (Gabrielsen and Kaplan 1976)

Drysdale et al. (1994) studied the arching action using mechanics of rigid body movement and concluded that the maximum gap that could exist for arching to develop is controlled by the diagonal distance between the compression forces at the hinges and it can be expressed as:

$$g \leq \frac{4(\gamma t)^2}{h} \tag{2.1}$$

Where g is the gap size, h is the height of the infill, t is the thickness of masonry, and γ=0.9.

2.2.2.2 Slenderness Ratio

Experimental studies conducted by Anderson (1984) showed that the out-of-plane strength of masonry panels has an inverse relationship with the slenderness ratio (h/t) of the panel. Further, the failure mode for smaller slenderness ratios was governed by compressive crushing of the masonry while for larger slenderness ratios (35-40 in their tests) the failure was governed by instability of the panel.

Angel et al. (1994) tested eight infill specimens with a wide range of slenderness ratios from 9 to 34 and reported that the out-of-plane strength greatly depended on the slenderness ratio of the panel. the strength from arching action becomes insignificant for slenderness ratios greater than 30.

2.2.2.3 Frame Rigidity

Dawe and Seah (1989b) conducted a comprehensive experimental study on the masonry infilled steel frames that showed the importance of flexural and torsional stiffness of the bounding frame on the out-of-plane strength of the infill. They included the effect of beam and column stiffness in their proposed equation for out-plane strength calculation for the first time.

Angel et al. (1994) also recognized the effect of the frame stiffness in their analytical model but set an upper limit for the effect of frame's flexural stiffness (EI) (equal to 2.6×10^{13} N-mm^2) beyond which the increase in out-of-plane strength as a result of frame stiffness is considered insignificant.

Flanagan and Bennett (1999a) evaluated the performance of different analytical models proposed by Dawe and Seah and Angel at al. and concluded that the flexural stiffness of the boundary frame has a much greater impact on the out-of-plane strength than its torsional stiffness.

2.2.2.4 Openings

Experiments by Gabrielsen et al. (1975) showed that the arching action can still develop on infills with openings.

Dawe and Seah (1989b) tested a 3.6×2.8 m infill specimen with 1.6×1.2 m central opening under uniform out-of-plane pressure and observed a 19% reduction in the strength and significantly smaller deflection at failure compared to the control specimen without opening.

Experiments conducted by Akhoundi et al. (2016) showed that presence of an opening with 13% area of the infill did not change the out-of-plane strength however, it reduced the deformation at failure to 1/4 of the solid infill.

2.3 Analytical Modelling

In the case of analytical modeling, the following two categories of techniques have been used by various researchers.

1- Macro-modeling which uses data from experiments and analytical approaches to develop structural behaviour models (usually simplified methodology, practice-

oriented) that can be used in conjunction with other structural frame elements in design of structural systems.

2- Micro-modeling which uses advanced mathematical and numerical methods to simulate the behaviour of masonry, as accurate as possible, in order to obtain a wide range of results (stress, deformation, strength, stiffness, constitutive law and cyclic behaviour) to be used in detailed analysis and design or to replace expensive experimental programs.

2.3.1 Macro-Modelling Methods

2.3.1.1 In-Plane Behaviour

The most widely accepted macro-model to simulate the infill contribution to the stiffness and strength of the infilled system subjected to in-plane loading is the "diagonal strut method". This method was originally proposed by Polliakov (1963) and Holmes (1961) based on experimental tests where strut-like behaviour was observed in infills under lateral loading conditions (Figure 2.4). The strut width was associated with the contact area between the infill and the frame beam and column. In this method, the masonry infill is replaced by one or more pin-jointed equivalent struts connecting loaded corners in the infill diagonal direction. Once the width of the strut or struts is known, assuming the strut having the thickness and material property of the infill, a frame analysis can be performed to determine the system stiffness incorporating the infill contribution. Since its inception, most research followed has been dedicated in determining the strut width expression that can provide accurate simulation of frame behaviour.

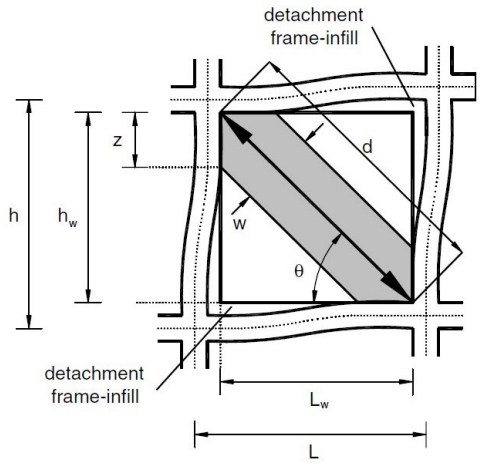

Figure 2.4. Masonry infill-frame deformed shape interaction (Asteris et al. 2013)

The first equation for determination of strut width, *w*, was proposed by Polliakov (1963):

$$\frac{w}{d} = \frac{1}{3} \tag{2.2}$$

where *d* is the diagonal length of the panel.

Smith (1966, 1967) and Smith and Carter (1969) proposed a series of equations for the contact length and the width of equivalent strut. The contact length α (Figure 2.5) was determined by the following equation:

$$\frac{\alpha}{l} = \frac{\pi}{2\lambda l} \tag{2.3}$$

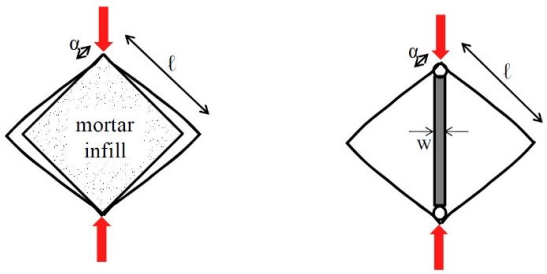

Figure 2.5. Stafford Smith's test setup and equivalent strut replaced for infill (Smith 1966)

where λ is a dimensionless parameter which calculates the relative stiffness of the frame and infill and can be determined as:

$$\lambda = \sqrt[4]{\frac{E_c t \sin 2\theta}{4EIh_w}} \tag{2.4}$$

where E_c is the modulus of elasticity of the infill, t is the thickness of the infill, E is the modulus of elasticity of the frame, I is the moment of inertia of the frame elements, h_w is the height of the infill panel, and θ is the angle that its tangent is the infill height to length aspect ratio.

The width of infill w can be correlated to stiffness parameters of the frame and infill using contact length α and relative stiffness λh.

$$w = 0.58\left(\frac{l}{h}\right)^{-0.445}(\lambda\, h_{col})^{0.335} d \left(\frac{l}{h}\right)^{0.064} \tag{2.5}$$

Based on the diagonal strut approach, Mainstone (1971) proposed an empirical equation for calculating the strut width based on the experimental and numerical results:

$$w = 0.175(\lambda l\, h_{col})^{-0.4} d \tag{2.6}$$

In addition to single-strut approach, several studies (Buonopane and White 1999, Saneinejad and Hobbs 1995, Thiruvengadam 1985) showed that a single strut might be inadequate to simulate the local infill-frame interaction effects, especially when the shearing force and bending moment in frame members at loaded corners are concerned. To address these effects, using of two or more struts were suggested by some researchers

(Chrysostomou et al. 2002, El-Dakhakhni et al. 2003, Syrmakezis and Vratsanou 1986). These struts have different width expressions and can be placed diagonally connected to the beam-column joints or off-diagonally and connected to either beams or columns.

Crisafulli et al. (2000) adopted a multi-strut method to analyze the structural response of RC infilled frames, focusing on the actions induced in the surrounding frame. Numerical results on single, two and three strut methods showed that all of the methods can simulate the infilled frame behaviour with more accurate results for two (Schmidt 1989) and three strut (Chrysostomou 1991) cases. Finally, it was concluded that the two-strut method is accurate enough with less complication compared to other methods.

Crisafulli and Carr (2007) proposed a two-strut method, as shown in Figure 2.6, where struts were connected together with a shear spring to account for shear behaviour of the infill. This four-node panel element was found capable of capturing both corner crushing and shear sliding failure mechanisms of the masonry infill when compared with experimental results obtained by the authors.

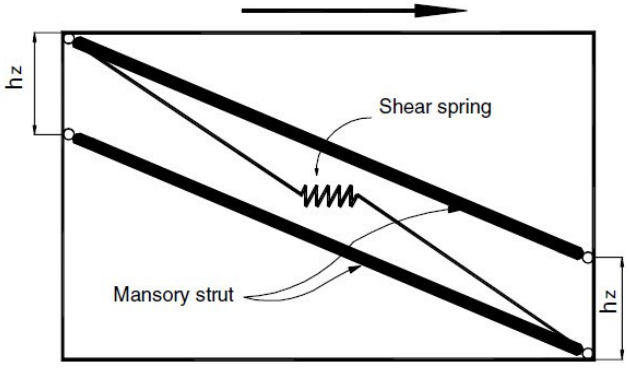

Figure 2.6. Two-strut with shear spring model proposed by Crisafulli and Carr (2007)

Turgay et al. (2014) summarized results of 51 experiments on masonry infilled RC frames conducted by 24 researchers. They proposed the following expressions for strut width in stiffness calculation:

$$w = 0.18(\lambda h_{col})^{-0.25} r_{inf} \tag{2.7}$$

$$\lambda = \sqrt[4]{E_{me} t \sin 2\theta \Big/ 4 E_{fe} I_{col} h_{inf}} \tag{2.8}$$

Di Trapani et al. (2017) carried out cyclic lateral loading experiments on infilled RC frames and investigated the use of the strut model to reflect degradation of infill stiffness subjected to cyclic loading. They proposed a multi-linear plastic behaviour for the strut and showed that the strength and stiffness of the specimens could be predicted using this behaviour model.

2.3.1.2 Out-of-Plane Behaviour

The very first methodology for arching action was proposed by McDowell et al. (1956a). To investigate arching, they conducted lateral loading tests on strips of brick masonry supported rigidly at the ends and formulated the strength equation in one-way arching based on compressive strength of masonry (f'_m) as shown in Eq. (2.9).

$$q_u = \frac{\gamma f'_m}{2(\frac{h}{t})^2} \tag{2.9}$$

Where q_u is the arching strength, γ is a function of *h/t* ratio and f'_m is the compressive strength of masonry.

This theory was further extended to two-way arching in a study by Dawe and Seah (1989b) where they conducted a series of tests on steel frames infilled with concrete masonry blocks with different thicknesses. They developed an analytical model by introducing the arching action in the yield-line theory to calculate the out-of-plane strength of the infills. In this model, compressive crushing of masonry was assumed as the main failure mode for ultimate capacity estimation. They proposed an empirical design equation to calculate the ultimate out-of-plane capacity (Eq. (2.10)-(2.13))

$$q_{ult} = 4.5(f'_m)^{0.75} t^2 \alpha / L^{2.5} \quad \text{(infill panel bounded on three sides and top side is free)} \tag{2.10}$$

$$q_{ult} = 4.5(f'_m)^{0.75} t^2 \{\alpha / L^{2.5} + \beta / H^{2.5}\} \quad \text{(infill panel bounded on four sides)} \tag{2.11}$$

where,

$$\alpha = {}^{1}/_{H} \, (EI_c H^2 + GJ_c tH)^{0.25} \leq 50 \; (\leq 75 \text{ for panel bounded on three sides}) \tag{2.12}$$

$$\beta = {}^{1}/_{L} \, (EI_b L^2 + GJ_b tL)^{0.25} \leq 50 \tag{2.13}$$

and *t, L*, and *H* are the thickness, length, and height of the infill panel, respectively. Parameters α and β are factors accounting for the stiffness effect of boundary frame where E and G are the Young's modulus and shear modulus of the frame members respectively, and *I* and *J* are the moment of inertia and torsional constant of the frame members with subscript *b* and *c* indicating beam and columns respectively.

An upper limit is set for α and β, indicating that the effect of boundary frame stiffness diminishes as the stiffness becomes greater and at the set limit, the frame can be considered

as rigid. The method also provides simple treatment for gaps at frame-to-infill interface, by setting α or β equal to zero for frame-column or frame-beam gap, respectively.

Klingner et al. (1996) considered the yield-line cracking pattern shown in Figure 2.7 and proposed the following expression for out-of-plane capacity calculation:

$$q = \frac{8}{h^2 l}\left\{M_{yv}[(l-h) + h\ln 2] + M_{yh}\left(\frac{x_{yv}}{x_{yh}}\right)\ln\left(\frac{1}{1-h/2}\right)l\right\} \tag{2.14}$$

where M_{yv} is the moment resistance for vertical arching and x_{yv} is the displacement of the infill corresponding to vertical arching at failure:

$$M_{yv} = \frac{0.85 f'_m}{4}(t - x_{yv})^2 \tag{2.15}$$

$$x_{yv} = \frac{t f'_m}{1000E\left[1-\frac{h}{2\sqrt{(h/2)+t^2}}\right]} \tag{2.16}$$

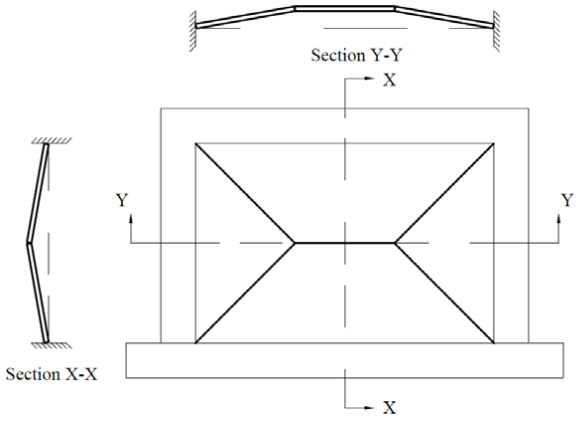

Figure 2.7. Idealized cracking pattern

The moment resistance for horizontal arching (M_{yh}) and the displacement of the infill corresponding to horizontal arching (x_{yh}) are denoted by h instead of v in Eq. (2.14). These values can be calculated by using Eq. (2.15) and Eq. (2.16) by replacing h with l.

Angel et al. (1994) proposed an analytical method for arching based on experimental and numerical results. They conducted in-plane and out-of-plane tests on masonry infilled concrete frames to investigate the effect of in-plane damage on the out-of-plane behaviour of infills. The analytical model was developed for one-way arching of masonry strips cracked at mid-height considering both compressive crushing of masonry at the boundaries and snap-through of the panel due to buckling as potential failure modes. They proposed the following for out-of-plane capacity of masonry infills:

$$q = \frac{2f'_m}{(\frac{h}{t})} R_1 R_2 \lambda \tag{2.17}$$

$$R_2 = 0.357 + 2.49 \times 10^{-14} EI \leq 1.0 \tag{2.18}$$

$$\lambda = 0.154 \exp\left(-0.0985 \frac{h}{t}\right) \tag{2.19}$$

where, R_1 is a reduction factor for prior in-plane loading as defined in Eq. (2.20); R_2 is a reduction factor accounting for bounding frame flexibility; and λ is a function of h/t and EI is the flexural stiffness of the smallest member of the bounding frame.

This equation was originally formulated based on a one-way mechanism, however, it was calibrated using two-way arching tests on infills with 1.5 aspect ratio.

$$R_1 = 1, \qquad \frac{\Delta}{\Delta_{cr}} < 1$$

$$R_1 = \left[1.08 + \left(\frac{h}{t}\right)\left(-0.015 + \left(\frac{h}{t}\right)\left(-0.00049 + 0.000013\left(\frac{h}{t}\right)\right)\right)\right]^{\frac{\Delta}{2\Delta_{cr}}}, \quad \frac{\Delta}{\Delta_{cr}} \geq 1 \tag{2.20}$$

where Δ is the maximum lateral deflection experienced by the infill and Δ_{cr} is the lateral deflection required for the cracking of the infill.

Flanagan and Bennett (1999a) investigated the reliability of the equations suggested by Dawe and Seah (1989b), Angel et al. (1994) and Klingner et al. (1996) and concluded that Dawe and Seah (1989b) method provides the best results in prediction of out-of-plane capacity. They also suggested that for most practical frames, the GJ_ctH and GJ_btL terms in Dawe and Seah (1989b) method are much smaller than the EI_cH^2 and EI_bL^2 terms and eliminated the torsional terms (GJ_ctH and GJ_btL). The final modified version of their method for out-of-plane strength calculation is expressed as follows:

$$q_{ult} = 4.1(f'_m)^{0.75} t^2 \alpha / L^{2.5} \tag{2.21}$$

$$\alpha = {}^{1}/_{H} \, (EI_c H^2)^{0.25} \leq 50 \tag{2.22}$$

$$\beta = {}^{1}/_{L} \, (EI_b L^2)^{0.25} \leq 50 \tag{2.23}$$

This formulation was adopted in the current American masonry design standard TMS 402/602-16 for design of masonry infills subjected to out-of-plane loading.

Moghaddam and Goudarzi (2010) proposed two equations based on the masonry crushing at the boundary (q_{cr}) and transverse instability of the infill (q_{max}) for out-of-plane strength calculation. They suggested that the lesser of the two criteria be considered as the strength of the infill:

$$q = Min \begin{cases} q_{cr} = \left[0.85 - \left(0.12 + \dfrac{0.045}{\alpha}\right)\dfrac{f'_m}{E_m}\lambda^2\right]\dfrac{f'_m}{\lambda^2} \\ q_{max} = \dfrac{0.18E_m}{\left(0.12 + \dfrac{0.045}{\alpha}\right)\lambda^4} \end{cases} \tag{2.24}$$

The q_{cr} is a function of the infill slenderness ratio (λ), masonry compressive strength (f'_m) and elastic modulus (E_m), and the ratio of the frame stiffness to the masonry stiffness (α) that is shown in Eq. (2.27)

$$\alpha = \frac{K}{(E_m t l/h)}$$
$$K = \frac{384 E_f I_b}{l^3} \tag{2.25}$$

where K is the frame stiffness for uniformly distributed arching force on the beam.

2.3.2 Micro-Modeling Methods

In micro-model approaches, Finite Element Method (FEM) is commonly adopted as the analysis tool because of its capability in handling geometrically complex structures and nonlinear behaviour. Moreover, many interface models have been developed that enables FEM to be used in simulation of both continuum and discrete media. Other methods such as Discrete Element Method (DEM) and Boundary Element Method (BEM) have also been used but with less success.

Most important factors in using micro-models are the types of simplifications and assumptions used to discretize the system and define material behaviour as well as the choice of interaction models and interface elements. In general, there are three main categories in discretization and representation of masonry structures depending on the level of accuracy and simplicity desired (Lourenco 1996). As shown in Figure 2.8, those are (a) Detailed micro-modelling, in which blocks and mortars are modeled with continuum elements and contact behaviour can be used for mortar-block interface; (b) Simplified

micro-modelling, in which the masonry is discretized at block level (i.e. the mortar is not modeled physically) and mortar joints are replaced with zero-thickness contact behaviour between blocks; and, (c) Continuum element (or composite) micro-modelling, in which the blocks and mortars are simplified to a homogenous medium that represents the overall behaviour of the masonry.

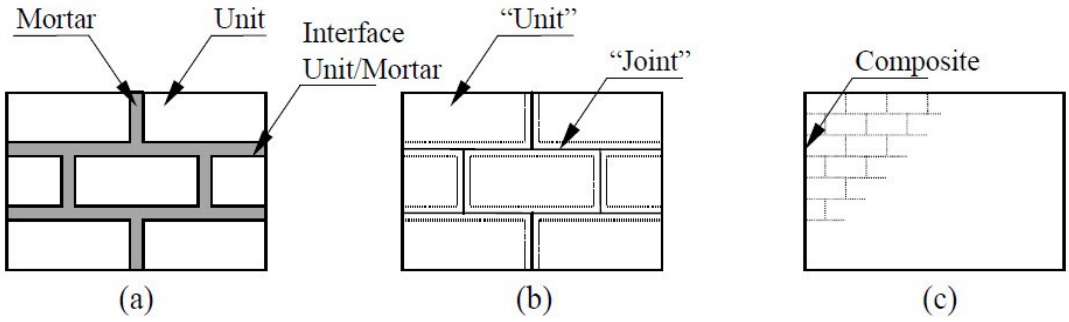

Figure 2.8. Modelling strategies for masonry: (a) detailed micro-modelling; (b) simplified micro-modelling; (c) continuum element micro-modelling (Roca et al. 1998)

The first approach is considered as potentially the most accurate one because the geometry and mechanical characteristics of both mortar and block as well as crack/slip phenomena inside the joints may be incorporated in the model. In the second approach, the masonry is discretized with expanded blocks to keep the geometry unchanged while the mortar joints are removed and replaced with zero-thickness interface elements which can include the nonlinear behaviour and failure modes expected in relatively thin mortar joints. However, since the material of mortar is not modeled, the Poisson effect of the mortar joints cannot be taken into account. Because of the discrete nature of the first two approaches, they can represent reasonably well the behaviour and failure of masonry components but at expenses of large computing cost. The third approach, continuum element method, is the simplest micro-model technique that has been more widely used for engineering practice, and in

modelling of big structures where computational efficiency is desired. This method is preferred for preliminary design when detailed results in masonry components is not required and the global behaviour of the system is intended. The drawback of this method is that many simplifying assumptions in terms of masonry anisotropic and nonlinear behaviour as well as failure criteria and mortar-masonry unit have to be made.

Following is a summary of important aspects of the micro-modelling approaches reported in the literature to simulate the behaviour of masonry infilled frames. It is noted that very few numerical models have been developed for the infill out-of-plane analysis. Unless otherwise specified, the summarized studies provided in the following are for the in-plane analysis of infills.

Mallick and Severn (1967) were among the first to use FEM to analyze the masonry infilled frames in which shell element with plane stress behaviour was used to simulate the infill and elastic beam elements were used for frame members. Infill-to-frame interface was modeled using a simple contact element that was capable of simulating separation at the interface.

Liauw and Lo (1988) adopted a nonlinear simplified micro-model FEM to analyze infilled steel frames. Beam and plane-stress elements were used to simulate the steel frame members and infills, respectively. Elasto-plastic behaviour was used for beams and tensile stress-controlled failure criterion was combined with elastic isotropic behaviour to represent the infill behaviour. In this model, when tensile stress exceeds tensile strength, both normal and shear stiffnesses were set equal to zero, thus, it was unable to consider residual stresses and predict post-failure response in cracked regions.

Smeared crack formulation was developed and employed in FE analysis of infilled RC frames by Lotfi and Shing (1991) to account for nonlinear behaviour of masonry blocks and concrete. Cracking of the material was determined by a Rankine tension-cut off criterion. The drawback of this model was its inability in prediction of shear failure.

Mehrabi and Shing (1997) conducted nonlinear finite element analysis for the 14 infilled RC frames that they tested. They used simplified micro-model method and developed interface models for shear cracking of concrete and mortar joints as well as bond-slip behaviour of steel bars in concrete. The model accounted for the compressive hardening behaviour of cementitious interfaces. It was observed that bond-slip behaviour had an important influence on the response of bare frame but did not affect the response of the infilled frame significantly.

Syrmakezis and Asteris (2001) developed an anisotropic failure criterion for masonry under biaxial stress condition for different level of shear stress. To validate this failure criterion, they used experimental results conducted by Page (1981) and categorized the results based on the direction of loading and amount of shear stress. They showed that an increase in the shear stress can substantially reduce the size of the failure surface of the masonry.

Al-Chaar et al. (2008) used DIANA commercial finite element program to reproduce test results by Mehrabi et al. (1996). Smeared crack quadrilateral elements for concrete and masonry blocks and cohesive interface model for simulation of the mortar behaviour and shear failure of concrete were assumed. They pointed out that for specimens with column

shear failure, using of interface elements between concrete elements has a significant effect in obtaining accurate results.

Stavridis and Shing (2010) proposed a 2D simplified micro finite element model for analysis of masonry infilled RC frames. This model considered both nonlinear behaviour and shear failure for concrete and masonry by using smeared crack elements and cohesive crack interface elements of Lotfi and Shing (1994) model. Smeared crack model was used to simulate the diffused cracks in concrete and masonry units and the cohesive crack interface was adopted to simulate the major displacement cracks in concrete, masonry and mortar joints. Triangular elements were used and configured to represent the shear crack in concrete as well as normal cracks. This model also accounted for shear and flexural reinforcements. All the interface elements for both concrete and masonry were zero-thickness. In their approach, uncracked material was modeled using a plastic-elastic law governed by Von-Mises failure criteria with tension cut-off. They used test results of three infilled frames obtained by Mehrabi et al. (1996) and concluded that the strength and ductility of an infilled frame are most sensitive to the shear parameters of the mortar joints.

Koutromanos et al. (2011a) extended the work done by Stavridis and Shing (2010) and used the model in seismic analysis of infilled RC frames. They added a new cohesive crack interface model and an improved smeared crack model to capture the cyclic behaviour. The model was calibrated with large scale shake table tests on one-story and three-story frames and showed that the model can predict the failure modes of specimens accurately.

Manos et al. (2012) used LUSAS commercial finite element package to simulate the shear behaviour of masonry panels. They considered three different micro-modelling techniques

in their research where 1) the masonry infill considered as linear elastic blocks connected through interface spring elements at mortar joints; 2) using linear elastic blocks and 2D nonlinear continuum elements with Mohr-coulomb failure criteria for the mortar; and 3) nonlinear blocks with Von-Mises failure criterion and 2D nonlinear continuum elements with Mohr-coulomb failure criterion. They concluded that all these methods can produce appropriate results and in most of the cases the simpler method (elastic model) is preferred because of less computational effort required to obtain the results.

Mohyeddin et al. (2013) used ANSYS to analyze the in-plane and out-of-plane behaviour of masonry infilled RC frames. They used 3D simplified micro-modelling approach and a novel method to consider the mortar effect in which the mortar at the joints was divided into two layers and an elastic interaction was defined between these two nonlinear mortar layers. They showed that with this simplification the results are accurate enough for most of the masonry simulation purposes.

Minaie et al. (2014) used Concrete Damaged Plasticity (CDP) model in ABAQUS to investigate the bi-directional loading behaviour of fully and partially grouted masonry shear walls. Masonry blocks and mortar joints were combined into three-dimensional solid element model. This model was capable of considering nonlinear cyclic behaviour of masonry in tension and compression as well as damage due to large plastic strains. They used in-plane and out-of-plane experimental data to validate the FE model and conducted parametric studies on the effects of aspect ratio, axial stress and combined in/out of plane loadings on the strength of the walls.

Pantò et al. (2018) and Pantò et al. (2019) developed a hybrid approach that incorporates 3D discrete FE model for masonry and concentrated plasticity beam-column elements for the frame. A 3D nonlinear element was also used to capture the flexural and sliding behaviour of the contact between the frame and the infill. In this method the masonry is discretized into smaller so called "panels" with 4 rigid edges that interact with each other through diagonal springs to capture shear behaviour and through nonlinear springs with adjacent panels to capture the interface behaviour under in-plane and out-of-plane loadings. The model was able to capture the deformed shape and global cracking pattern but it was dependent on the number of panels used for discretization. Also, this model was unable to capture the cracking inside the panels.

2.4 Code and Practice

2.4.1 In-Plane Behaviour

The diagonal strut method described previously has been adopted in most international design standards and codes to evaluate the stiffness and strength of masonry infilled frames subjected to in-plane lateral loading. These standards and codes include the Canadian standard CSA S304-14, American standard TMS 402/602-16 and European seismic design of buildings: Eurocode 8 for new construction as well as for retrofit/repair of existing buildings. However, the strut width equations are all in different forms since they are calibrated against different sets of experimental results that are representative of the materials and practice used in the regions. Table 2.1 summarizes the equations for calculation of the stiffness and strength for masonry infilled frames as proposed by CSA S304-14 and TMS 402/602-16.

CSA S304-14 adopts the equation proposed by Smith (1962) in strut width calculation. Based on work of Hendry (1981), the compressive stress can be considered relatively uniformly distributed over only half of the diagonal strut width. The effective width used in the stiffness calculation is the lesser of ($^{w}/_{2}$, $^{d}/_{4}$) where d is the diagonal length of the infill. The stipulation $^{d}/_{4}$ was based on the upper limit of width suggested by Smith (1962). Three possible failure mechanisms are considered in CSA S304-14 standard: 1) compressive failure of the strut; 2) diagonal tension cracking; and 3) shear sliding. Three equations representing the lateral capacity corresponding to these failure mechanisms are shown in Table 2.1.

TMS 402/602-16 adopted the diagonal strut width equation proposed by Flanagan and Bennett (2001). Corner crushing, lateral displacement limit and shear sliding failure are considered in the lateral capacity calculation.

For both Canadian and American standards, the design guidelines only apply for the hollow and fully grouted infill. Both are silent on the treatment of partially grouted infills. Neither standards provide any provisions on the effect of opening, joint reinforcement, the presence of vertical load and the potential gap on the lateral resistance of the infill.

Table 2.1. Strut methods in TMS 402/602-16 and CSA S304-14

Model	Strut width model	Strength model
TMS 402/602-16	$\lambda = \sqrt[4]{\frac{E_m t_{inf} \sin 2\theta}{4 E_f I_{col} h_w}}$ $w = \frac{0.3}{\lambda \cos\theta}$ $E_m = 900 f'_m$	$V_u \leq \begin{cases} 150 t_{inf} f'_m \ (Compressive\ failure) \\ -\ Hor.component\ of\ the\ force\ in \\ \quad the\ strut\ at\ 25mm\ racking\ disp. \\ 0.33 A_n \sqrt{f'_m}/_{1.5} \ (Diagonal\ cracking) \\ 0.83 A_n/_{1.5} \ (Shear\ slip) \\ 0.26 A_n + 0.45 N_u/_{1.5} \ (Shear\ slip) \end{cases}$
CSA S304-14	$w = \sqrt{\alpha_h^2 + \alpha_l^2}$ $\alpha_h = \frac{\pi}{2} \sqrt[4]{\frac{4 E_f I_c h}{E_m t_e \sin 2\theta}}$ $\alpha_l = \pi \sqrt[4]{\frac{4 E_f I_b l_{inf}}{E_m t_e \sin 2\theta}}$ $w_e \leq \begin{cases} w/_2 \\ r_{inf}/_4 \end{cases}$ $E_m = 850 f'_m$	$V_u \leq \begin{cases} 0.85 \varphi_m \chi f'_m A_e \cos\theta \ (Compressive\ failure) \\ 0.16 \varphi_m \sqrt{f'_m} A_{uc} + \varphi_m \mu P \ (Diagonal\ cracking) \\ \varphi_m \left(0.16 \left(2 - \frac{M_f}{V_f d_v} \right) \sqrt{f'_m} b_w d_v + 0.25 P \right) \gamma_g \\ (Shear\ slip) \end{cases}$

A_n is the cross-sectional area of the masonry in shear, N_u and P are the compressive force on the shear surface, A_e is the effective cross-sectional area, M_f is the moment, V_f is the shear force, d_v is the effective depth for the shear calculation, b_w is the web width of the masonry, γ_g is grouted/ungrouted factor, μ is the friction coefficient, A_{uc} is the uncracked area of the cross-sections, $\theta = \tan^{-1} h/_l$

2.4.2 Out-of-Plane Behaviour

There are no design provisions in the current CSA S304-14 for calculating of the out-of-plane strength of infill walls. Rather, it specifies that basic principles of mechanics be relied upon for analysis. In the American masonry design standard TMS 402/602-16, the nominal capacity to resist out-of-plane forces of the infill is given in the following. These expressions were based on the work of Dawe and Seah (1989b).

$$q_{n\,inf} = 4.1(f'_m)^{0.75}\, {t_{inf}}^2 \left(\frac{\alpha_{arch}}{l^{2.5}} + \frac{\beta_{arch}}{h^{2.5}}\right) \tag{2.26}$$

$$\alpha_{arch} = \frac{1}{h}(E_{bc} I_{bc} {h_{inf}}^2)^{0.25} < 50 \tag{2.27}$$

$$\beta_{arch} = \frac{1}{h}(E_{bb} I_{bb} {l_{inf}}^2)^{0.25} < 50 \tag{2.28}$$

where E_{bc} and E_{bb} are the modulus of the frame columns and frame beam, respectively and t_{inf} shall not exceed $^1/_8\, h_{inf}$.

2.5 Summary

A literature review of the state-of-the-art research on masonry infilled frames is provided in this chapter. Main experimental studies, numerical modeling development, as well as the current code and practice on the subject are presented. It is shown that the behaviour of masonry infilled frames is complex as it is affected by many factors of geometric, material, and loading characteristics of the system. While some advancement in understanding of the behaviour has been made, inadequacies of the previous studies are summarized in the following paragraph.

In terms of experimental studies, the range of variations in studied parameters was limited so that there were few developed correlations between the geometric and material parameters and the in-plane and out-of-plane capacity. A large portion of these studies are dedicated to steel infilled frames with normal infills and less information is available for infilled RC frames. In terms of numerical studies, the existing models were generally developed and validated for specific conditions with certain assumptions and none was found to be able to provide universally satisfactory estimates for infills with different material and geometric properties. Also, details of the modeling are commonly not available in the public domain and thus cannot be easily reproduced for studies of other parameters. As a result, the design provisions contained in the North American masonry standards are only applicable to simple infill situations. In view of this, more research is needed to further the understanding and development of design guidelines for masonry infills.

Chapter 3 Experimental Program

3.1 Introduction

Concurrent to the numerical study, an experimental program was conducted to obtain physical results on the in-plane and out-of-plane loading response of masonry infilled RC frames. This experimental investigation aimed to analyze the effect of several influential parameters on the behaviour of infilled frame that are either not available in the literature or the reported data are not applicable to concrete masonry units bounded by RC frames. These results were also used in the validation of the finite element model.

While the experimental work is included and discussed in each following chapter in different focuses, this chapter is to provide an overall description and summary of the experimental portion of the research. Along with infilled frame specimens, auxiliary tests were also conducted to obtain mechanical properties of each component of the infilled system. These components include concrete masonry units (CMUs), mortar, masonry prisms, concrete cylinders and reinforcing steel. The obtained results were used in numerical modeling as input property parameters. Description of the specimens, test setup, and testing procedure are briefly presented in this chapter.

3.2 Infilled Frame Specimens

A total of seventeen specimens were constructed and tested and they included one bare frame, two control infilled frames, six infilled frames with side and top interfacial gaps, five infilled frames with window and door openings, and three regular infilled frames with prior in-plane damage tested under out-of-plane loading. Table 3.1 presents a summary of

the specimens. The numbers in specimen ID denotes either the magnitude of gap between infill and concrete frame or the percentage of opening (ratio of the opening area to the total area of the wall) in specimens with gaps and openings.

Table 3.1. Summary of frame specimens

Number	Specimen ID	Gap	Opening	In-plane damage
In-plane test				
1	BF	-	-	-
2	IFNG	-	-	-
3	IFTG7	7 mm at top	-	-
4	IFTG12	12 mm at top	-	-
5	IFSG7	3.5 mm at each side	-	-
6	IFSG12	6 mm at each side	-	-
7	IFW8	-	8% Window opening	-
8	IFW16	-	16% Window opening	-
9	IFD19	-	19% Door opening	-
10	IFW22	-	22% Window opening	-
Out-of-plane test				
11	IFNG (IF-ND)	-	-	-
12	IF-TG	5 mm at top	-	-
13	IF-SG	5 mm at each side	-	-
14	IFW16	-	16% Window opening	-
In-pane test followed by out-of-plane test				
15	IF-D1	-	-	0.66% in-plane drift
16	IF-D2	-	-	1.37% in-plane drift
17	IF-D3	-	-	2.7% in-plane drift

3.3 In-Plane Test Setup and Procedure

The lateral load was applied using a hydraulic actuator with a capacity of 250 kN. A load cell was placed between the actuator and the RC frame to measure the load during the test. In-plane lateral displacements were measured at both the top beam and the bottom beam locations using linear variable differential transformers (LVDTs). In addition, two LVDTs were positioned at the central point of the top beam and at the centre of the infill to monitor possible out-of-plane movements of the RC frame and infill. Test setup configuration and LVDT locations are shown in Figure 3.1 and Figure 3.2 respectively.

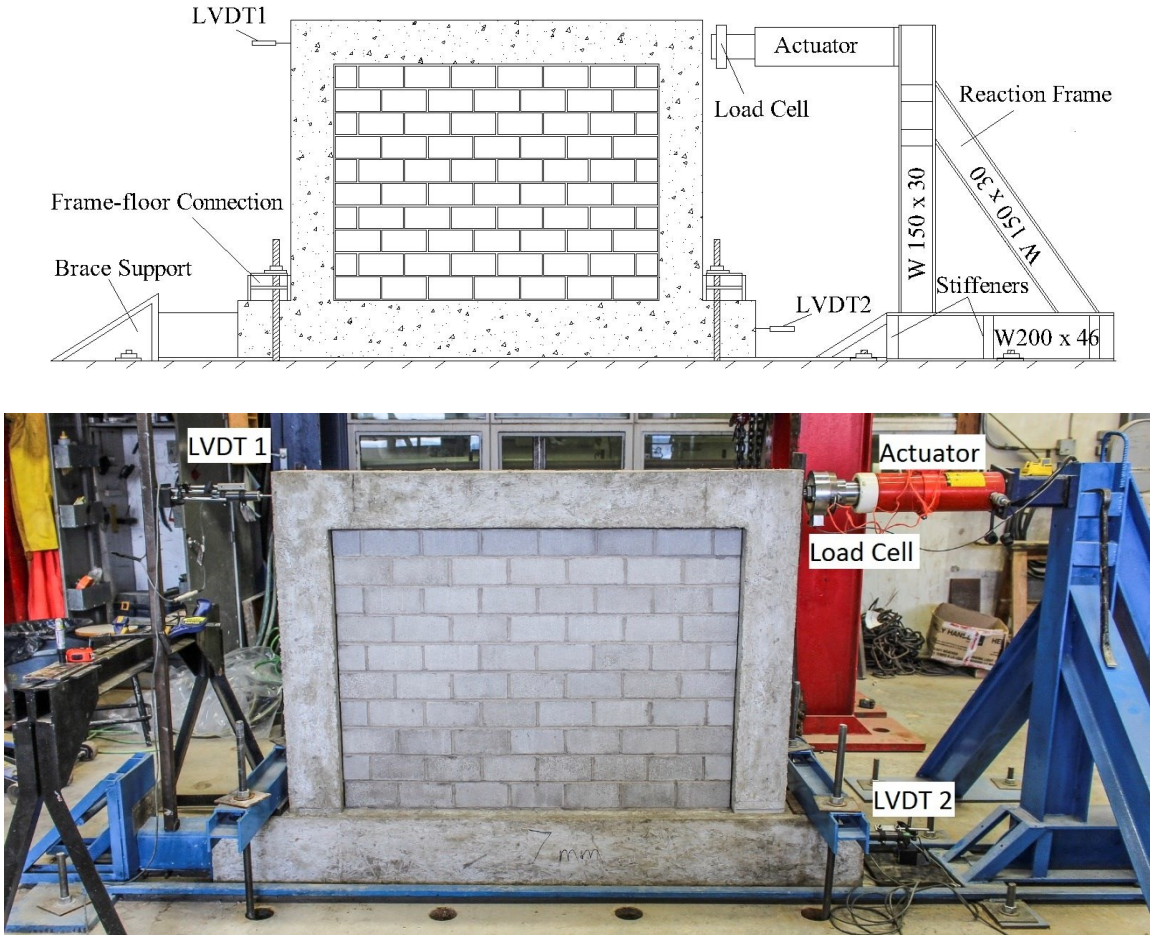

Figure 3.1. Test setup details, main LVDT locations and side view of the test setup

Figure 3.2. Out-of-plane LVDTs and LVDT 1

Prior to each test, the specimens were positioned in place and aligned in both the in-plane and out-of-plane directions, and the load cell and LVDTs were mounted. The lateral load was then applied at the centreline of the top beam until the failure of the specimen. The loading rate was approximately 6 kN per minute which is considered slow enough to represent quasi-static loading conditions. Load cell and LVDT readings were recorded with an interval of 0.2 seconds throughout the test using an electronic data acquisition system. Cracking loads, ultimate loads and cracking patterns were noted for each test.

3.4 Out-of-Plane Test Setup and Procedure

The out-of-plane load was applied to the masonry infills using an airbag through a self-equilibrating system as shown in Figure 3.3. The airbag was placed in between the masonry infill and a reaction frame that in turn connected to the corners of the RC frame through threaded rods. The reaction frame was made of a 15 mm thick plywood board covering the entire surface area of the infill stiffened with steel HSS sections. Similar to the in-plane

tests, the bottom beam of the frame was clamped down to the strong floor using threaded steel rods. An air compressor was used to inflate the airbag and the pressure in the air bag was measured and recorded using a pressure transducer during the test.

(a)

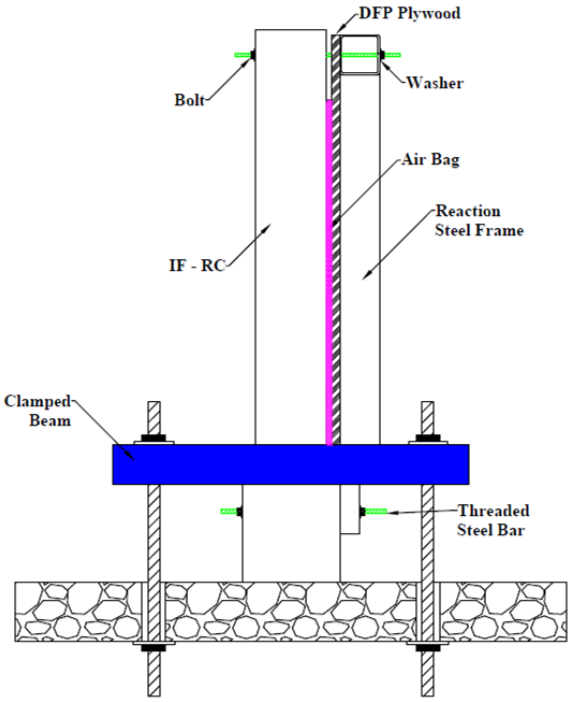

(b)

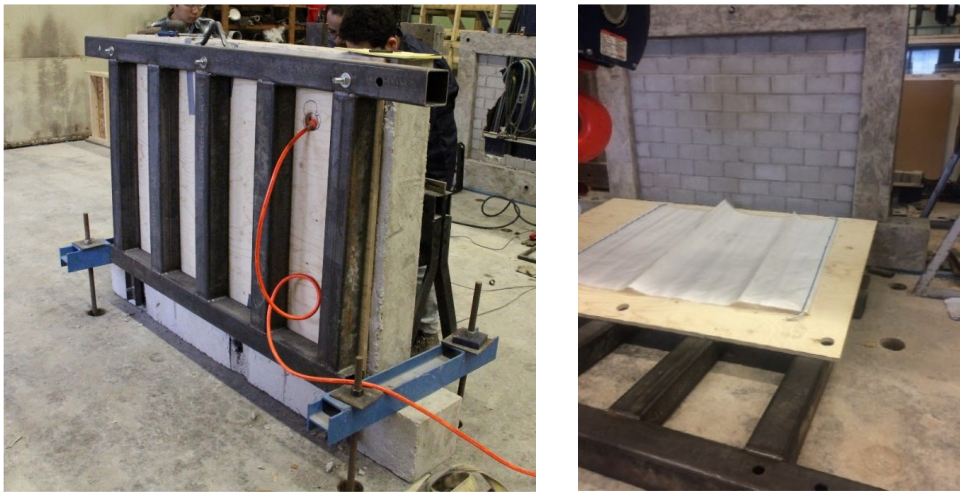

Figure 3.3. Out-of-plane test setup: (a) Schematic side view; and. (b) setup components

Six linear variable differential transformers (LVDTs) were used to measure the out-of-plane displacements of infills which their location is shown in Figure 3.4 except for infill

with opening where LVDT 1 was removed and LVDTs 2-5 were placed around the opening boundary.

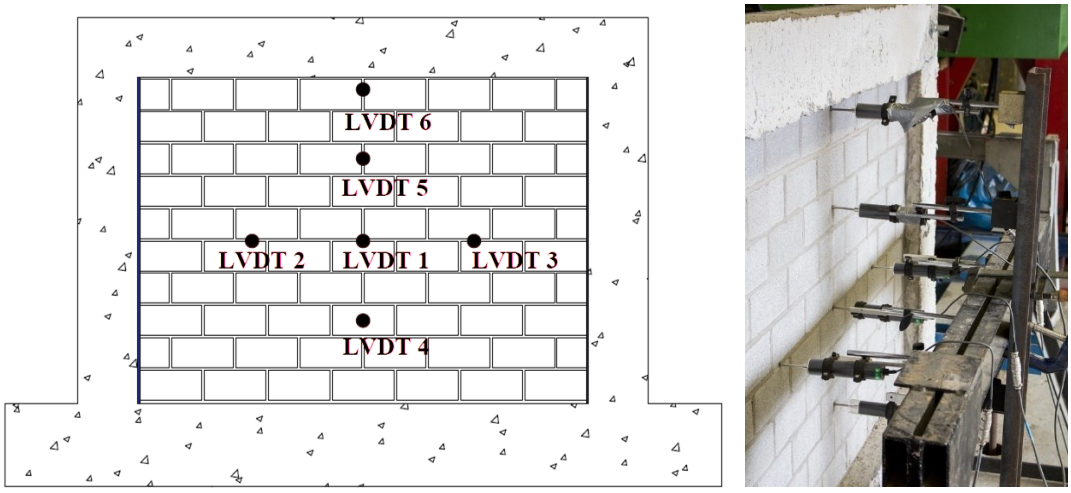

Figure 3.4. LVDTs position for out-of-plane test

To carry out the out-of-plane test, the air bag assembly and measuring devices were mounted and checked to ensure that they worked properly and zeroed for initial recording. The air bag pressure was increased gradually at a rate of 1.5 kPa per minute to the failure of the specimen. The pressure and out-of-plane displacement were recorded at a 0.1 second interval using a data acquisition system. The cracking load, ultimate load, cracking pattern and failure mode were recorded and marked during each test.

Chapter 4 Development of a Detailed 3D FE Model for Analysis of the In-Plane Behaviour of Masonry Infilled Concrete Frames

Ehsan Nasiri, Yi Liu

Published in Engineering Structures, Volume 143, 15 July 2017, Pages 603-616

https://doi.org/10.1016/j.engstruct.2017.04.049

4.1 Abstract

This paper detailed the development of a numerical model for simulating the nonlinear behaviour of the concrete masonry infilled RC frames subjected to in-plane lateral loading. The ABAQUS finite element software was used in the modeling. Nonlinear behaviour as well as cracking and crushing of concrete and masonry blocks were simulated using the Concrete Damaged Plasticity (CDM) model. The cohesive element method combined with hyperbolic Drucker-Prager and shear and tensile failure criteria were used to capture the possible failure mechanisms in mortar joints. Concurrent with the finite element modeling, an experimental study was also conducted and results of masonry infilled RC frame specimens incorporating infill openings and interfacial gaps were used to validate the model. The validation showed that the model can accurately simulate the behaviour and predict the strength of masonry infilled RC frames. A sensitivity study was subsequently conducted where the influence of mortar joint failure surface parameters, mortar dilatancy, and fracture energy on the lateral behaviour of infilled RC frames was investigated. Results showed that the in-plane behaviour of infilled RC frames was significantly affected by the input parameters of mortar's Drucker-Prager yield surface and dilatancy and less affected by those of mortar fracture energy.

Keywords: concrete masonry infills; RC frame; in-plane behavior; finite element; failure surface; mortar dilation; fracture energy

4.2 Introduction

Masonry walls are often used to infill reinforced concrete (RC) or steel frames in modern construction to act as either interior partitions or exterior cladding. It is understood that if an infill is built in tight contact with its surrounding frame, its inherent large in-plane stiffness will attract large forces and in turn alter the dynamic characteristics of the entire structure. Thus, an accurate assessment of the infill-frame interaction is crucial for a safe design. However, the frame, commonly made of steel or reinforced concrete materials, deforms in a ductile and flexural mode while the masonry infill, made of brittle materials, tends to deform in a shear mode. This difference in behaviour, coupled with development of inelasticity of both materials at high load levels, makes it difficult to quantify the exact extent of the infill-frame interaction for the entire loading history. For the past six decades, both experimental and numerical studies (Chen and Liu 2015, Dawe and Seah 1989a, Haach et al. 2009, Koutromanos et al. 2011b, Liu and Manesh 2013, Mehrabi et al. 1996, Mehrabi and Shing 1997, Mosalam et al. 1997, Smith 1962) have been conducted in an effort to provide rational methods for considering the infill contribution to the system stiffness and strength. The diagonal strut method has then emerged as the most adopted method for evaluating the capacity and stiffness of infilled frames. In this case, the infilled frame may be considered as a braced frame where the infill is replaced by a diagonal strut connecting loaded corners. Once the strut width is known, a simple frame analysis can be performed to determine the stiffness of the system. The strength of the infill can also be

related to the strut width. Based on the diagonal strut concept, much research work was contributed to the development of this method to incorporate effects of material nonlinearities, various failure mechanisms, geometric properties of the infill and frame, and boundary conditions (Mosalam et al. 1997, Smith 1962). The effect of infill openings, infill-to-frame interfacial gaps, and vertical loading on the infill behaviour was investigated in more recent research (Chen and Liu 2016, Dawe and Seah 1989a, Kakaletsis and Karayannis 2007, Liu and Manesh 2013, Liu and Soon 2012, Mehrabi et al. 1996, Tasnimi and Mohebkhah 2011).

With the development of computing technology in the last two decades, numerical modeling encoded in computer programs has been increasingly used to simulate the behaviour of masonry infilled frames. Both finite element methods (FEM) (Koutromanos et al. 2011b, Lourenco 1996, Mehrabi and Shing 1997, Mohyeddin et al. 2013, Stavridis and Shing 2010) and discrete element methods (DEM) (Mohebkhah et al. 2008, Sarhosis et al. 2014) have been employed in modeling with the former being the more popular one. While the DEM is robust in simulating mortar joint effect between blocks, it is quite limited in providing different geometry and material models for continuums such as the block itself or frame members. In the case of reinforced concrete frames, interaction between reinforcing bars and continuum medium of concrete cannot be adequately defined using DEM. In this study, the FEM was used and thus the following literature review is focused on studies of FEM in masonry infilled frames. Mehrabi and Shing (1997) developed interface models for shear cracking of concrete and mortar joints as well as bond-slip behaviour of steel bars in concrete. Lotfi and Shing (1991) developed a smeared crack formulation to account for nonlinear behaviour of masonry blocks and concrete in infilled

RC frames. Al-Chaar et al. (2008) adopted smeared crack quadrilateral elements for masonry blocks and cohesive interface model for simulation of mortar behaviour and shear failure of concrete. Stavridis and Shing (2010) proposed a 2D simplified micro-model for analysis of masonry infilled RC frames adopting the cohesive crack interface elements developed by Lotfi and Shing (1994) to consider mortar effect. Mohyeddin et al. (2013) used a 3D simplified micro-model in which the mortar at joints was halved and an elastic interaction model was defined between the two mortar layers. Minaie et al. (2014) used Concrete Damaged Plasticity (CDP) model in ABAQUS to investigate bi-directional loading behaviour of fully and partially grouted masonry shear walls. Despite that previous numerical studies have shown capability of FE models in simulation of masonry infills or masonry shear walls, some limitations of these models are noted as follows. Although simple to use, the 2D models were not adequate to capture many aspects of infilled frames such as non-typical geometric properties, stress concentration, local reinforcement effects, and out-of-plane behaviour. For the existing 3D model studies, there is commonly a lack of information provided on the input material parameters, which makes it difficult for others to reproduce the model and associated results. Moreover, these models were calibrated against test results of a specific type of masonry infill and bounding frame, their effectiveness for a wide range of material and geometric parameters was not investigated.

In view of the above, this study was then motivated to develop a 3D finite element model to study the in-plane behaviour of masonry infilled RC frames. Encoded in ABAQUS software, the model development, analysis procedure, and input parameters were described in detail in this paper. Concurrent with the finite element modelling, ten masonry infilled RC frames were tested, and experimental parameters included interfacial gaps and infill

openings. Detailed validation of the model against experimental results was discussed. Once verified, the model was used in a sensitivity study of several critical material input parameters on the behaviour and strength of infilled RC frames. Recommendations were provided on the efficacy of the model in simulation of infilled RC frames covering a wide range of these parameters.

4.3 Experimental Program

The experimental program involved the testing of ten masonry infilled RC frames subjected to a monotonically increased lateral load to failure. The objectives of the experimental program were to provide test results to 1) investigate the behaviour of masonry infilled RC frames as affected by infill openings and infill-to-frame interfacial gaps; and 2) validate the numerical model. Information on test specimens, test setup, and results considered relevant to this paper is provided in the following section. A detailed description of the test program and discussion of results can be found elsewhere (Hu 2015).

Ten specimens included one bare frame (BF), one infilled frame control specimen (IFNG), four infilled frame specimens with interfacial gaps between either the top frame beam and the infill (IFTG) or the frame columns and the infill (IFSG), and four infilled frame specimens with window or door openings (IFW and IFD). Table 4.1 presents a detailed description of the test specimens.

Table 4.1. Summary of test specimens

Number	Specimen ID	Gap		Opening type (Opening/infill area)
		Location	Size (mm)	
1	BF		-	-
2	IFNG		None	-
3	IFTG7	Top	7	-
4	IFTG12	Top	12	-
5	IFSG7	Side	3.5 (on each side)	-
6	IFSG12	Side	6 (on each side)	-
7	IFW8		-	Window (8%)
8	IFW16		-	Window (16%)
9	IFD19		-	Door (19%)
10	IFW22		-	Window (22%)

All infilled frame specimens had the same dimension as shown in Figure 4.1, yielding a height-to-length aspect ratio of about 0.73. The masonry infill was constructed using the custom-made, half-scale 200 mm standard concrete masonry units laying in the running bond. The interfacial gaps for those four specimens were achieved by adjusting the thickness of the mortar joints. The RC frame was designed according to CSA A23.3-04 and reinforcement detailing including size, spacing, arrangement of longitudinal bars and stirrups complied with requirements to provide ductility and avoid brittle shear failure.

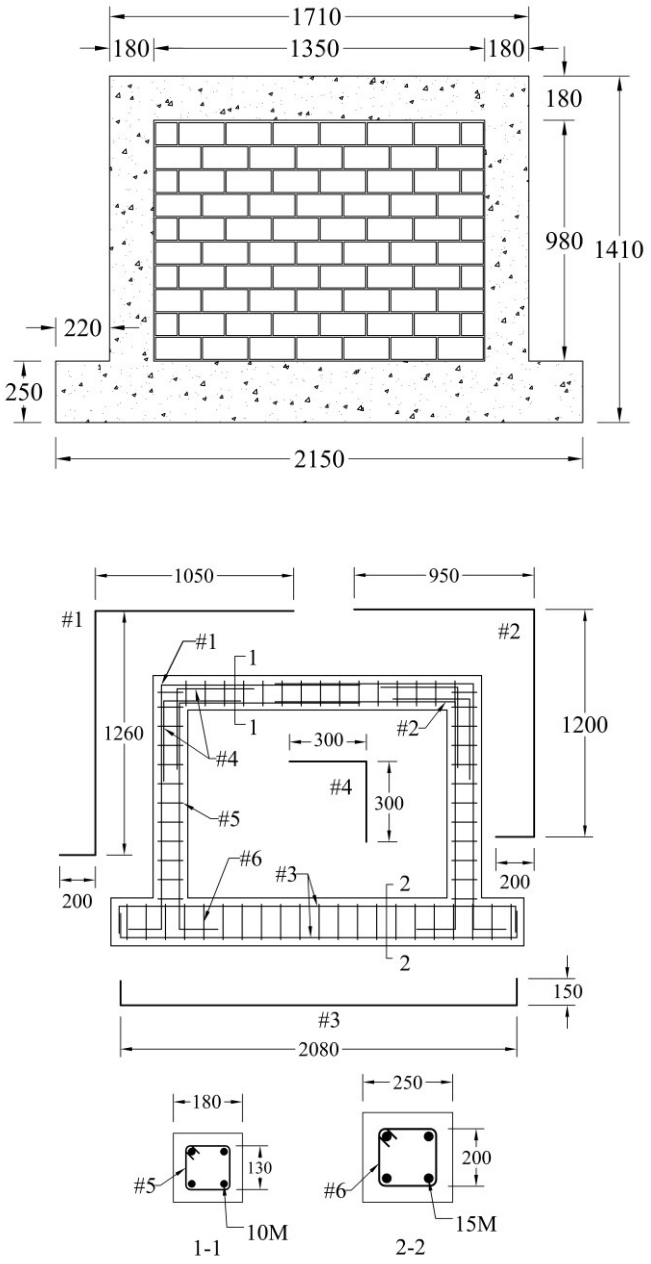

Figure 4.1. Geometric properties of infilled frame specimens and reinforcement details in the RC frame

4.3.1 Test Setup and Instrumentation

The experimental set-up is illustrated in Figure 4.2. The specimens were connected to the strong floor through high strength bolts and the lateral load was applied at the top beam level using a hydraulic actuator with a capacity of 250 kN. Two linear variable differential transformers (LVDTs) (LVDT 1 and 2) were mounted at the centerline of the top and bottom beam respectively to measure the in-plane lateral displacements. Another two LVDTs (not shown) were positioned at the half height of the masonry infill wall and at the central point of the top beam respectively, both on the back side, to monitor any possible out-of-plane movements of the infill wall and the concrete frame, respectively.

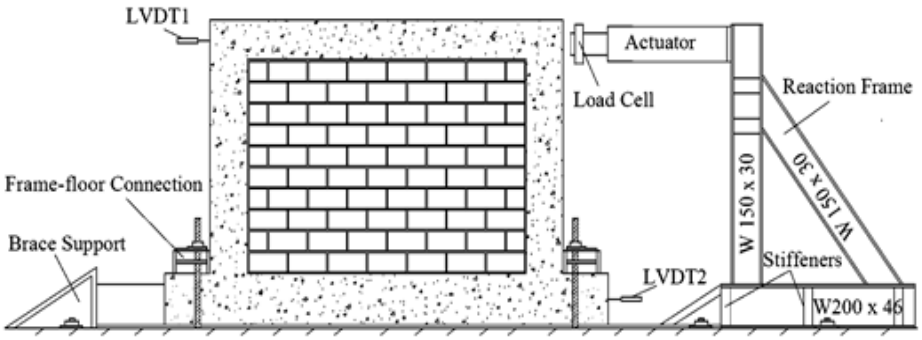

Figure 4.2. Schematic test set-up

4.3.2 Material Properties

The mechanical properties of CMUs, mortar, and masonry prisms for the infill and those of concrete and reinforcement for the frame were obtained experimentally in accordance with ASTM specifications. A summary of the material properties is presented in Table 4.2.

Table 4.2. Summary of material properties for test specimens

	Elastic modulus E (MPa)	Compressive strength (MPa)	Tensile strength (MPa)	Yield strength (MPa)	Ultimate (yield) strain
Concrete	27800	43.8	3.5	-	0.0025
CMUs	3500	25.0	2.5	-	0.008
Mortar	2600	21.3	1.7	-	-
Prisms	2980	17.1	-	-	-
Reinforcement	220000	-	665	446	0.85 (0.003)

4.4 Finite Element Model

In this study, the so-called simplified micro-modelling approach (Lourenco 1996) was adopted and the key characteristic of this approach is that the mortar joints are not physically modeled, rather, they are replaced with zero-thickness interface elements. The geometry and the meshing of the model is shown in Figure 4.3. The ABAQUS software was used in the model development. The concrete masonry units (CMU) as well as RC frame members were modeled using 8-node reduced integration solid elements (C3D8R). The CMU dimensions were increased by the half thickness of the mortar joint in both horizontal and vertical directions so that the discrete CMUs were connected and interact with each other through zero-thickness interface elements. The simplified micro-model was shown to provide desired accuracy (Haach et al. 2009, Lourenco 1996, Mehrabi and Shing 1997, Stavridis and Shing 2010) and is considered as a more computing efficient modeling technique than a detailed micro-modelling approach where mortar joints are

modelled. The following sections describe modeling details of each component of the infilled frame. It is noted that while ABAQUS provides the general material constitutive and interfacial behaviour models for different structural applications, the contribution of this study lies in the determination of appropriate models and critical material parameters and conducting computationally efficient and accurate simulation of masonry infilled RC frames.

4.4.1 Nonlinear Behaviour of Concrete and CMUs

Different from ideal brittle materials such as glass, concrete and CMUs are considered as quasi-brittle materials with high toughness after subcritical cracking (Anderson and Anderson 2005). The Concrete Damaged Plasticity (CDP) model for quasi-brittle materials in ABAQUS (Lubliner et al. 1989) was used to simulate the behaviour of concrete and CMUs in this study. The CDP model is a continuum, plasticity-based, damage model. Both isotropic damaged elasticity and tensile and compressive plasticity are considered in this model and failure mechanisms are defined in terms of tensile cracking and compressive crushing.

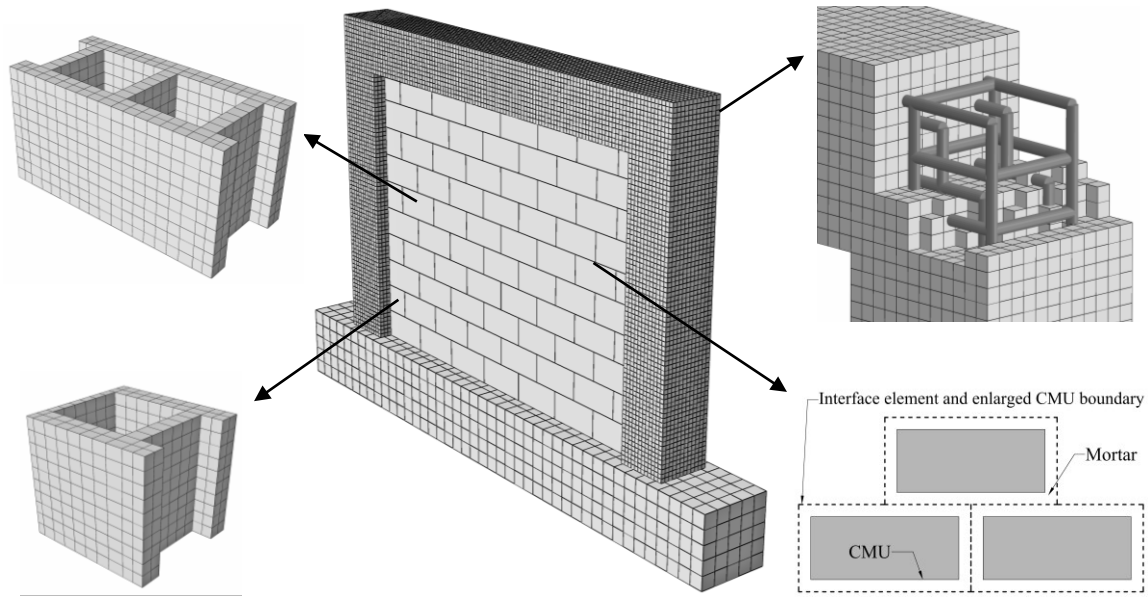

Figure 4.3. Three dimensional geometric model used in the FE analysis

4.4.2 Yield Surface

In a general form, the yield function, *F*, of the CDP model in terms of effective stresses is defined according to Eq. (4.1):

$$F = \frac{1}{1-\alpha}\left(\bar{q} - 3\alpha\bar{p} + \beta(\tilde{\varepsilon}^{pl})\langle\hat{\bar{\sigma}}_{max}\rangle - \gamma\langle\hat{\bar{\sigma}}_{max}\rangle\right) - \sigma_c\left(\tilde{\varepsilon}_c^{pl}\right) = 0$$

$$\alpha = \frac{\left({}^{\sigma_{b0}}/_{\sigma_{c0}}\right) - 1}{2\left({}^{\sigma_{b0}}/_{\sigma_{c0}}\right) - 1}; \quad 0 \le \alpha \le 0.5 \tag{4.1}$$

$$\beta = {}^{\bar{\sigma}_c\left(\tilde{\varepsilon}_c^{pl}\right)}\Big/_{\bar{\sigma}_t\left(\tilde{\varepsilon}_t^{pl}\right)}(1-\alpha) - (1+\alpha) \qquad \gamma = {}^{3(1-K_c)}/_{2K_c - 1}$$

where $\bar{p}$ is the hydrostatic pressure stress, $\bar{q}$ is the Von Mises equivalent effective stress, $\hat{\bar{\sigma}}_{max}$ is the maximum principal effective stress, ${}^{\sigma_{b0}}/_{\sigma_{c0}}$ is the ratio of initial biaxial compressive yield stress to initial uniaxial compressive yield stress, K_c is the ratio of the tensile meridian to the compressive meridian and defines the shape of the yield surface in

the deviatory plane, $\bar{\sigma}_t\left(\tilde{\varepsilon}_t^{pl}\right)$ and $\bar{\sigma}_c\left(\tilde{\varepsilon}_c^{pl}\right)$ are the effective tensile and compressive cohesion stress respectively, corresponding to the plastic strains indicated in the bracket.

The yield surface in the plane-stress and deviatoric conditions is shown in Figure 4.4. The intercepting points of yield line at principal stress axes specify the uniaxial tension and compression capacities of the material. Reduced tension and increased compression capacities in biaxial stress conditions are illustrated in the graph.

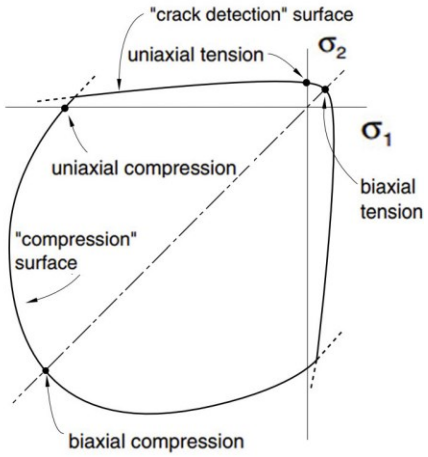

Figure 4.4. Failure surface of the CDP model in plane stress (D.S.Simulia 2010)

4.4.3 Flow Rule

A non-associated potential flow was assumed in the CDP model as follows:

$$\dot{\varepsilon}^{pl} = \dot{\lambda}\frac{\partial G(\bar{\sigma})}{\partial \bar{\sigma}} \tag{4.2}$$

The flow potential G chosen for this model was the Drucker-Prager hyperbolic function defined as follows:

$$G(\sigma) = \sqrt{(\epsilon\sigma_{t0}\tan\psi_c)^2 + \bar{q}^2} - \bar{p}\tan\psi_c \tag{4.3}$$

where ϵ is the eccentricity that gives the rate at which the plastic potential function approximates the asymptote, ψ_c is the dilation angle measured in the $p-q$ plane at high confining pressure and is an indicator of the direction of the plastic strain increment, and σ_{t0} is the uniaxial tensile stress at failure.

Determining the yield surface and flow rule parameters for concrete and CMUs requires accurate biaxial and triaxial tests on the materials. However, the available literature showed that the lateral response of the infilled frame is not overly sensitive to these parameters. The values used in this study were then based on experimental results obtained by Kupfer et al. (1969) and Jankowiak and Lodygowski (2005) as well as numerical values used by Lubliner et al. (1989), Lee and Fenves (1998), Jiang and Wu (2012), and Genikomsou and Polak (2015), and they are summarized in Table 4.3.

Table 4.3. The CDP model parameters for concrete and CMUs

	Dilation angle ψ_c	Eccentricity ϵ	σ_{b0}/σ_{c0}	K_c
Concrete	40	0.1	1.16	0.66
CMU	30	0.1	1.16	0.66

4.4.4 Compressive Stress-strain Relationship

The compressive behaviour of concrete and CMUs is defined using the stress-strain constitutive model proposed by Sima et al. (2008) as follows:

$$\begin{cases} \sigma_c = \varepsilon_c E_0 & \varepsilon_c \le \varepsilon_{c0} \\ \sigma_c = \left[\varepsilon_{c0}(1-A) + A\varepsilon_c e^{\left(\frac{\varepsilon_{c0}-\varepsilon_c}{\varepsilon_c'}\right)}\right] E_0 & \varepsilon_c > \varepsilon_{c0} \end{cases}$$

$$A = \frac{f_c' - \varepsilon_{c0} E_0}{E_0\left(\varepsilon_c' e^{\left(\frac{\varepsilon_{c0}}{\varepsilon_c'}-1\right)} - \varepsilon_{c0}\right)} \tag{4.4}$$

where σ_c and ε_c are the compressive stress and strain values, respectively; f_c' is the compressive strength of the material; ε_{c0} is the linear elastic strain limits; ε_c' is the strain at the peak stress and E_0 is the Young's modulus of the material. It should be noted that no damage parameter (i.e. reduction in the elastic modulus after cracking/crushing) was not considered in the modeling of concrete and CMU due to monotonic nature of simulations.

Incorporating experimentally obtained mechanical properties into Eq. (4.4), the compressive stress-strain curves for concrete and CMUs were obtained and shown in Figure 4.5.

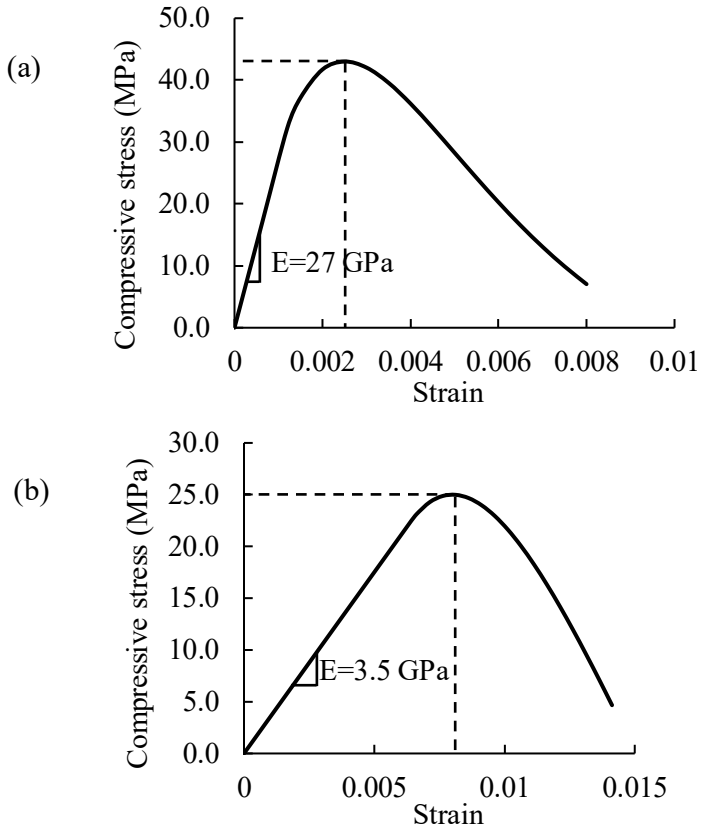

Figure 4.5. Compression stress-strain curve for: (a) Concrete; and (b) CMUs

4.4.5 Tensile Behaviour Model

In this study, the tensile behaviour of concrete was given special consideration due to presence of reinforcement. Since in plasticity-based smeared cracking models the cracks in concrete are not simulated physically and each finite element might include a cracked and uncracked material, an averaged tensile stress-strain curve between cracked and uncracked concrete can be used. Based on the results of uniaxial tension and pullout tests on RC members conducted by Maekawa et al. (2003), the tensile stress-strain curve for concrete reflecting the tension stiffening effect can be expressed using Eq. (4.5). This model was shown to be independent of element size, crack spacing, reinforcement ratio, and orientation of reinforcement (Maekawa et al. 2003).

$$\begin{cases} \sigma_t = \varepsilon_t E_0 & \varepsilon_t \leq \varepsilon_{t0} \\ \sigma_t = \sigma_{t0}\left(\dfrac{\varepsilon_{t0}}{\varepsilon_t}\right)^{0.4} & \varepsilon_t > \varepsilon_{t0} \end{cases} \tag{4.5}$$

where σ_t and ε_t are the tensile stress and strain values, respectively; σ_{t0} and ε_{t0} are the linear elastic stress and strain limit, respectively. Incorporating experimental results of concrete modulus and elastic stress and strain limit, the tensile stress-strain curve for concrete was obtained as illustrated in Figure 4.6.

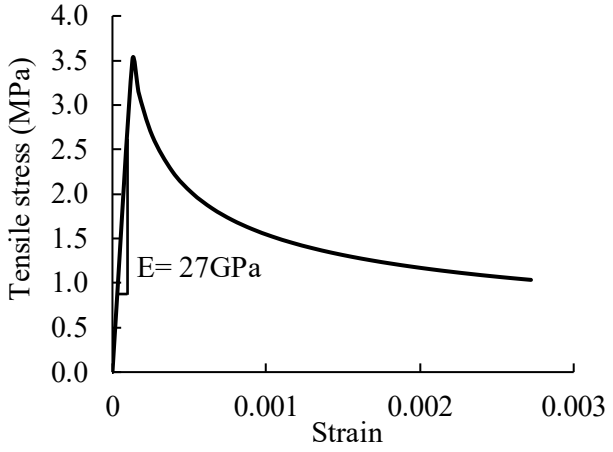

Figure 4.6. Tension stress-strain curve for concrete

In the case of CMUs, due to the absence of steel reinforcement, the tensile behaviour is more dependent on localized cracks which initiates a sharp stress drop. This type of behaviour is better described using a stress-crack displacement curve in which the area under the curve represents the Mode I fracture energy of the material (G_f) (Hillerborg et al. 1976). Thus, the tensile behaviour model for CMUs was defined by a linear elastic behaviour in the pre-cracking phase and a stress-crack displacement curve in the post-cracking phase as shown in Figure 4.7. The fracture energy of the CMU material was estimated using Eq. (4.6) as suggested by Fib: Model Code (2012).

$$G_f = 73\, f_c^{\,0.18} \tag{4.6}$$

where f_c is the compressive strength of the CMU. In this equation f_c is in MPa and G_f is in $^{N}/_{m}$.

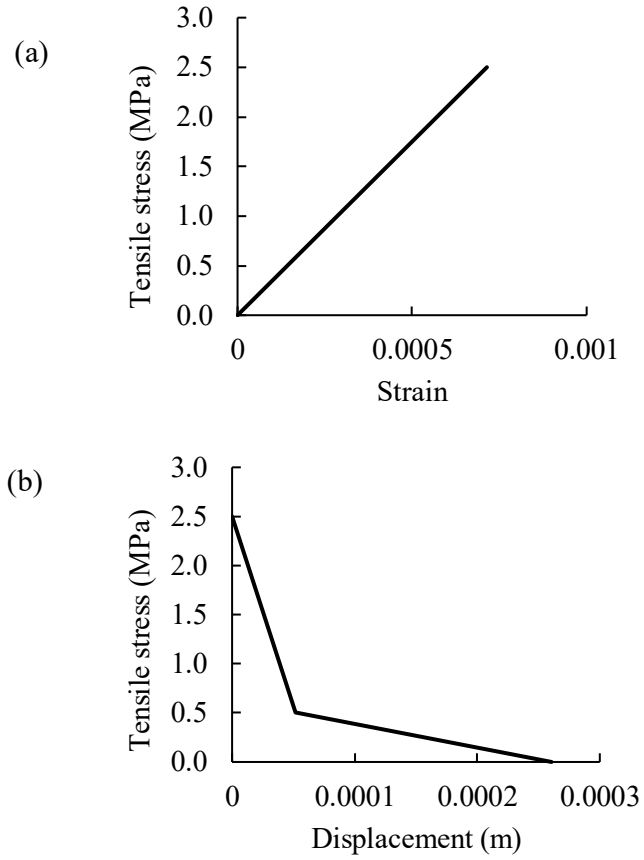

Figure 4.7. Tensile behaviour of CMU material: (a) stress-strain curve; and (b) stress-displacement curve

4.5 Material Model for Reinforcement

Modeling of the steel reinforcement in the concrete frame members requires consideration of the bond-slip effect. Previous FE studies on reinforced concrete (Abdeldjelil and Thomas , Dehestani and Mousavi 2015, Kwak and Kim 2006) showed that for a steel bar

embedded in concrete, its stress-strain curve averaged at the cracked region and that adjacent to cracks does not show a pronounced yield plateau and the "apparent yield stress" is lower than the yield stress of a bare steel bar. This phenomenon, known as bond-slip effect, is often implemented in models by reducing the elastic modulus or yield stress, or both of the steel bars. Based on this concept, the method proposed by Dehestani and Mousavi (2015) was adopted in this study to account for the bond-slip effect in the modeling of the reinforcement. In this method, the modified elastic modulus, E_s^*, hardening modulus, E_{sp}^*, and yield stress, f_y^*, can be calculated using Eqs. (4.7) to (4.9). The experimentally obtained curve on tensile coupons and the corresponding modified curve are both shown in Figure 4.8.

$$\frac{f_y^*}{f_y} = (0.93 - 2B) \quad , \quad B = \left.(\frac{f_{cr}}{f_y})^{1.5}\right/ \rho \tag{4.7}$$

$$E_s^* = \frac{f_y^*}{\varepsilon_s + (\frac{\delta}{l})} \tag{4.8}$$

$$E_{sp}^* = 0.03E_s^* \tag{4.9}$$

where f_y is the yield stress of the reinforcing bars, f_{cr} is the cracking stress of the concrete, ρ is the reinforcement ratio in the RC frame section, ε_s is the strain of the steel bar corresponding to the stress f_y^*, l is the transmission length of bond strength between the steel bar and the surrounding concrete and δ is the slip of the steel bar. More information on determination of the transmission length l and the maximum slip δ is available elsewhere (Dehestani and Mousavi 2015).

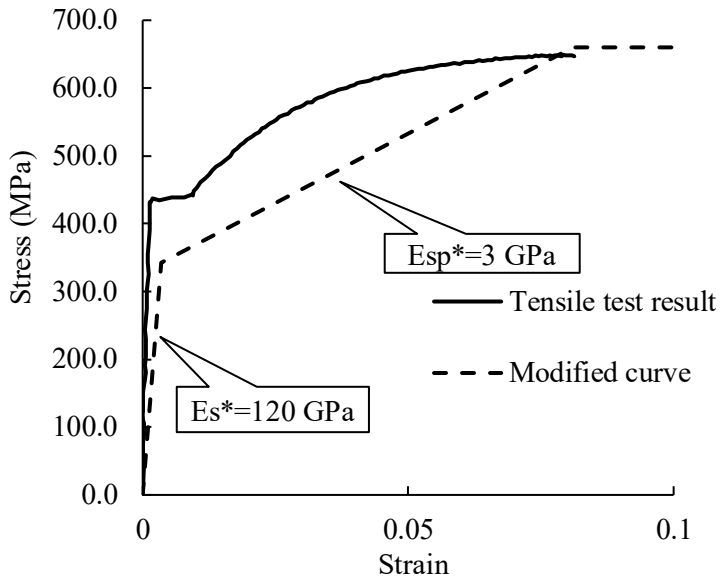

Figure 4.8. Modified stess-strain curve for the reinforcement

4.6 Behaviour Model of Interface Elements

The interface elements used between CMUs need to account for plastic behaviour and possible failure modes of the mortar. For this purpose, the cohesive element in ABAQUS was used in combination with the hyperbolic Drucker-Prager plasticity criterion. The shear and normal stress damage models were also implemented to allow for degradation and removal of elements after failure to create the frictional interaction between the CMUs. Subsequent to the failure of mortar, interaction between the blocks is controlled by Mohr-Coulomb friction behaviour. The cohesive element is an eight-node three-dimensional element (COH3D8) with a very small thickness (0.1 mm) to satisfy the zero-thickness assumption, which also ensures that the separation between masonry blocks can be obtained with sufficient accuracy after removal of the element at normal or shear stress failure. In the elastic state, the behaviour of these elements is controlled by an elastic traction-separation response (D.S.Simulia 2010). Traction stress vector t consists of three

components, t_n, t_s and t_t, which represent the normal and two shear tractions. The corresponding displacements are denoted by δ_n, δ_s and δ_t. The elastic stress- displacement behaviour for this case is expressed as:

$$t = \begin{Bmatrix} t_n \\ t_s \\ t_t \end{Bmatrix} = \begin{bmatrix} K_{nn} & 0 & 0 \\ 0 & K_{ss} & 0 \\ 0 & 0 & K_{tt} \end{bmatrix} \begin{Bmatrix} \delta_n \\ \delta_s \\ \delta_t \end{Bmatrix} = K\delta \tag{4.10}$$

This elastic relationship is combined with a hyperbolic Drucker-Prager yield criterion that controls the tension cracking and shear sliding failure of mortar joints. The advantage of hyperbolic Drucker-Prager yield criterion over the Mohr-Coulomb or regular Drucker-Prager criterion is that the tension cut-off can be considered in the failure surface. The shape of this yield surface in the p-q plane is shown in Figure 4.9 and expressed as:

$$F = \sqrt{l_0^2 + q^2} - p \tan\beta - d' = 0 \tag{4.11}$$

where $l_0^2 = \sqrt{d' - p_t \tan\beta}$, d' is the shear yield stress, p_t is the hydrostatic tensile strength and β is the frictional angle of the material in the $p - q$ plane and it can be determined from the friction angle in the Mohr-Coulomb failure surface (slope of the $\sigma - \tau$ failure surface), φ, as follows:

$$\tan\beta = \frac{6\sin\varphi}{3 - \sin\varphi} \tag{4.12}$$

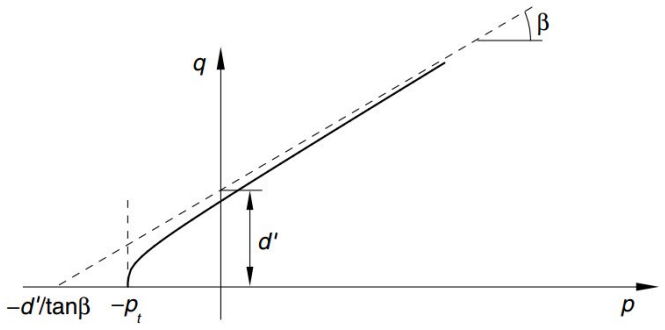

Figure 4.9. Hyperbolic Drucker-Prager yield surface (D.S.Simulia 2010)

Experimental and numerical studies have shown that the dilation during shear failure of a mortar joint has a significant effect on the deformation and strength of the interface (Lotfi and Shing 1994, Mosalam et al. 1997). In this study, this effect was considered by implementing the dilation angle (ψ) in flow potential as defined in Eq. (4.13) and illustrated in Figure 4.10. The dilation angle controls the amount of plastic volumetric strain developed during plastic shearing and is assumed constant during plastic yielding. To be distinguished from the dilation angle ψ_c for concrete and CMUs, this dilation angle for the interface element is labelled as ψ_i.

$$G = q - p\tan\psi_i \tag{4.13}$$

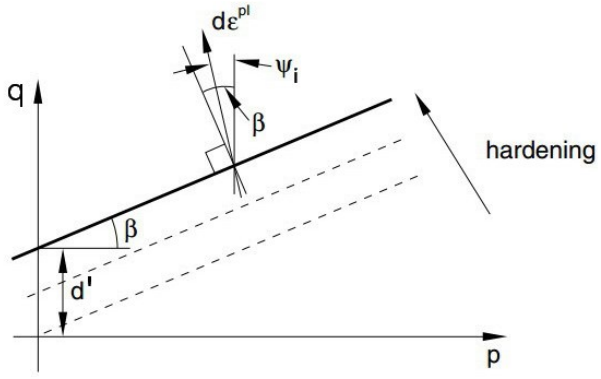

Figure 4.10. Hardening and flow rule for the hyperbolic Drucker-Prager model (D.S.Simulia 2010)

Once failure is detected by Drucker-Prager criterion, two damage models (normal and shear stress damage) control the degradation and elimination of the interface elements. The normal and shear stress damage criteria were implemented using the fracture energy approach. As shown in Figure 4.11, the areas under the tensile stress-displacement and shear stress-displacement curves after the peak stresses were set to be equal to the Mode I and Mode II fracture energy of the mortar material (Lourenco 1996, Rots 1991). Upon the full degradation of the interface elements they were deleted from the model to allow for the Coulomb frictional contact between the masonry units or between the masonry units and the concrete frame. At this stage, contacting surfaces can carry shear stresses up to a certain magnitude before sliding, which is known as sticking. The critical shear stress at which sliding of the surfaces starts, is defined as $\tau_{crit} = \mu N$ where, N is the contact pressure and μ is the coefficient of friction.

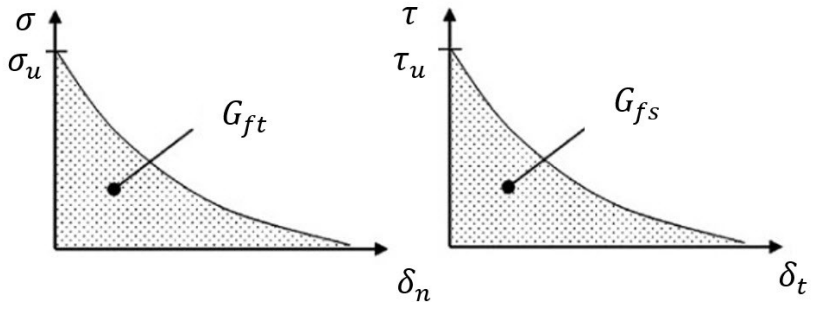

Figure 4.11. Tensile and shear strength softening curves and corresponding fracture energies

Table 4.4 summarizes values of aforementioned input parameters used in the interface element modeling. Due to a lack of standard testing procedures for determining some of these parameters, the available literature was mainly relied on for obtaining the reasonable

range of values. The final selection of values was conducted through an extensive calibration process against the experimental results obtained in this study.

Table 4.4. Summary of interface parameters

Symbol	Description	Value	Unit	Source/Reference
E	Elastic modulus	2600	MPa	Experiment
ν	Poisson's ratio	0.16	-	Experiment
β	Angle of friction in Drucker-Prager model	75	degree	(Atkinson et al. 1989, Mosalam et al. 1997, Van der Pluijm 1993)
p_t	Initial tensile strength	0.2	MPa	(Atkinson et al. 1989, Masia et al. 2012, Van der Pluijm 1993)
ψ_i	Dilation angle	20	degree	(Mosalam et al. 1997, Van der Pluijm 1993)
d'	Initial shear strength	1.0	MPa	(Atkinson et al. 1989, Masia et al. 2012, Van der Pluijm 1993)
G_{fs}	Shear fracture energy	400	N/m	(Lotfi and Shing 1994, Van der Pluijm 1993)
G_{ft}	Tension fracture energy	40	N/m	(Lotfi and Shing 1994, Van der Pluijm 1993)
μ	Coulomb friction coefficient	0.7	-	(Lotfi and Shing 1994, Mehrabi and Shing 1997, Van der Pluijm 1993)

4.7 Analysis Procedure

In this study, graphical interface of ABAQUS, ABAQUS/CAE, and the explicit solver, ABAQUS/EXPLICIT, were chosen for generation and analysis of the model, respectively. The ABAQUS/EXPLICIT uses the central difference method (CDM) to solve the equation of motion of a nonlinear problem. The advantage of CDM is that the time-marching update

equations are EXPLICIT, meaning that no iterations are needed to find the new displacements which satisfy the equation of motion. This method is preferred for computation problems involving complicated nonlinear constitutive laws and large deformations and is especially effective for prediction of post-failure behaviour. The EXPLICIT procedure uses a large number of small time increments to ensure the accuracy of analysis. The EXPLICIT central difference integration rule is shown as (D.S.Simulia 2010):

$$\dot{u}^{(i+\frac{1}{2})} = \dot{u}^{(i-\frac{1}{2})} + \frac{\Delta t^{(i+\frac{1}{2})} + \Delta t^{(i)}}{2} \ddot{u}^{(i)} \tag{4.14}$$

$$u^{(i+1)} = u^{(i)} + \Delta t^{(i+1)} \dot{u}^{(i+\frac{1}{2})} \tag{4.15}$$

where $\dot{u}$ is velocity and $\ddot{u}$ is acceleration corresponding to equations of motion. The superscript (i) refers to the increment number. In order to have a stable solution, the time increment should be less than the stability limit set as:

$$\Delta t_{max} \leq \frac{L_e}{C_d} \tag{4.16}$$

where L_e is the characteristic length of the smallest element (length of a line across an element for a first-order element) and $C_d = \sqrt{E/\rho}$ is the wave velocity in the material.

4.8 Verification of the Model

A mesh convergence study was first performed on the model. Using specimen IFNG as an example, the FE lateral load vs. displacement curves with varying element sizes used to discretize the masonry infill are compared with the experimental curve in Figure 4.12. It can be seen that while the results in elastic range and pre-peak region are less affected by

the mesh density, the ultimate force and the post-ultimate behaviour is somewhat sensitive to the mesh size. While the finest mesh (5 mm) produced the ultimate load closest to the experimental value, the mesh size of 10 mm yielded a response approximately similar to that produced by mesh size 5 mm. To balance the result accuracy and computational efficiency, the mesh size of 10 mm was used for the model in the following validation process.

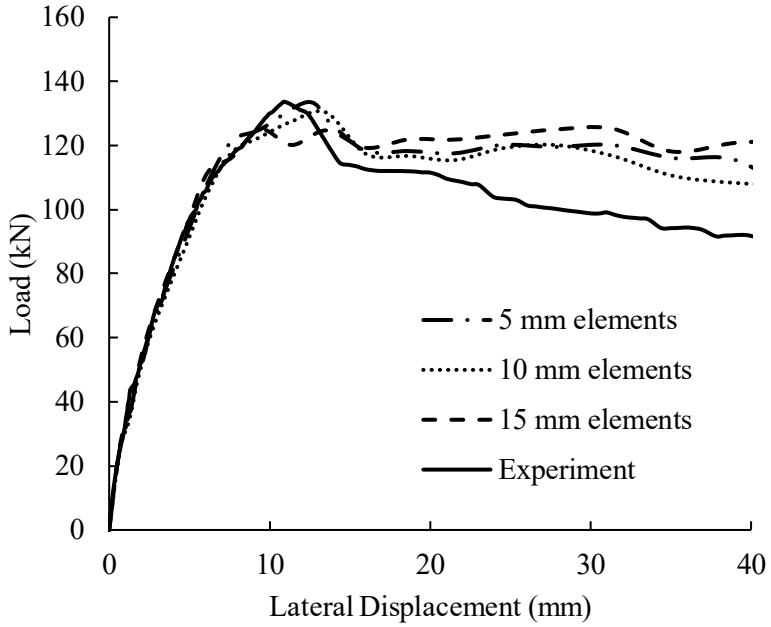

Figure 4.12. Load-displacement curves for different number of elements

The FE model was then validated using the test results. Table 4.5 summarizes the comparison results in terms of the initial and crack stiffness, and ultimate strength of specimens. Table 4.5 shows that the average of $\frac{P_{u,\mathrm{EXP}}}{P_{u,\mathrm{FE}}}$ is 1.03 with a COV of 7%, indicating that the FE model is capable of predicting the ultimate lateral load capacity of the infilled RC frames with a reasonably good accuracy. In terms of the initial stiffness which is defined as the slope of initial linear portion of the curve connecting the origin and the 10

kN in-plane point, the average $\frac{K_{i,\mathrm{EXP}}}{K_{i,\mathrm{FE}}}$ is 1.44 with a COV of 28%. High variations in the initial stiffness comparison was also reported in previous work conducted by Liu and Soon (2012). The imperfection in the specimen, difficulty in achieving a totally "tight" contact between the infill and the frame, as well as potential movements and deformations in the test setup were identified to contribute to the high variation of initial stiffness. Therefore, the crack stiffness, K_{cra}, was also obtained and compared in the table as a more reliable indicator of the system stiffness. The crack stiffness is defined as the secant stiffness connecting the origin and the point on the response curve where the first major crack occurred. The average $\frac{K_{cra,\mathrm{EXP}}}{K_{cra,\mathrm{FE}}}$, determined to be 1.24 with a COV of 17%, shows much improved estimate on the system stiffness using crack stiffness.

The experimental and FE lateral load vs. displacement curves are plotted in Figure 4.13 for all specimens. The finite element curves, in general, compare reasonably well with their experimental counterparts. The figure shows that the finite element curves are capable of capturing the cracking reflected by the sudden drops in lateral resistance during the rising portion of the curve. The immediate load increase at a lower stiffness indicates the degradation of the stiffness due to cracking development and the infill's ability to find alternative loading paths to carry additional load. It also should be pointed out that the same values of input parameters as described in the previous section were used for all specimens and there was no "tweaking" of these values to achieve a "perfect" fit for each specimen. Although there is some less than "perfect" fit in the curves, it is felt that the comparison has demonstrates the robustness and efficacy of the model.

Table 4.5. Stiffness and strength comparison of the experimental and FE results

Specimen ID	$K_{i,\mathrm{EXP}}$ ($\mathrm{kN/mm}$)	$K_{i,\mathrm{FE}}$ ($\mathrm{kN/mm}$)	$\frac{K_{i,\mathrm{EXP}}}{K_{i,\mathrm{FE}}}$	$K_{cra,\mathrm{EXP}}$ ($\mathrm{kN/mm}$)	$K_{cra,\mathrm{FE}}$ ($\mathrm{kN/mm}$)	$\frac{K_{cra,\mathrm{EXP}}}{K_{cra,\mathrm{FE}}}$	$P_{u,\mathrm{EXP}}$ (kN)	$P_{u,\mathrm{FE}}$ (kN)	$\frac{P_{u,\mathrm{EXP}}}{P_{u,\mathrm{FE}}}$
BF	20.8	22.1	0.94	17	18.6	0.91	58.5	57.3	1.02
IFNG	52.9	39.5	1.34	12.2	9.6	1.27	133.6	130.2	1.03
IFTG7	46.6	27.6	1.69	12.2	8.3	1.47	129.3	124.7	1.04
IFTG12	40.3	32.4	1.24	21.3	17.5	1.22	102.4	90.3	1.13
IFSG7	30.7	25.6	1.20	11.7	6.9	1.70	134.1	124.6	1.08
IFSG12	31.9	24.5	1.30	5.9	5.3	1.11	114.4	104.7	1.09
IFW8	36.3	33.5	1.08	12.2	9.8	1.24	108.2	105.2	1.03
IFW16	46.8	29.6	1.58	7.5	7.1	1.06	86.4	98.6	0.88
IFD19	48.6	30.0	1.62	8.4	6.5	1.29	96.0	95.3	1.01
IFW22	63.5	27.0	2.35	9.6	8.2	1.17	86.4	86.2	1.00
Avg			1.44			1.24			1.03
COV (%)			28			17			7

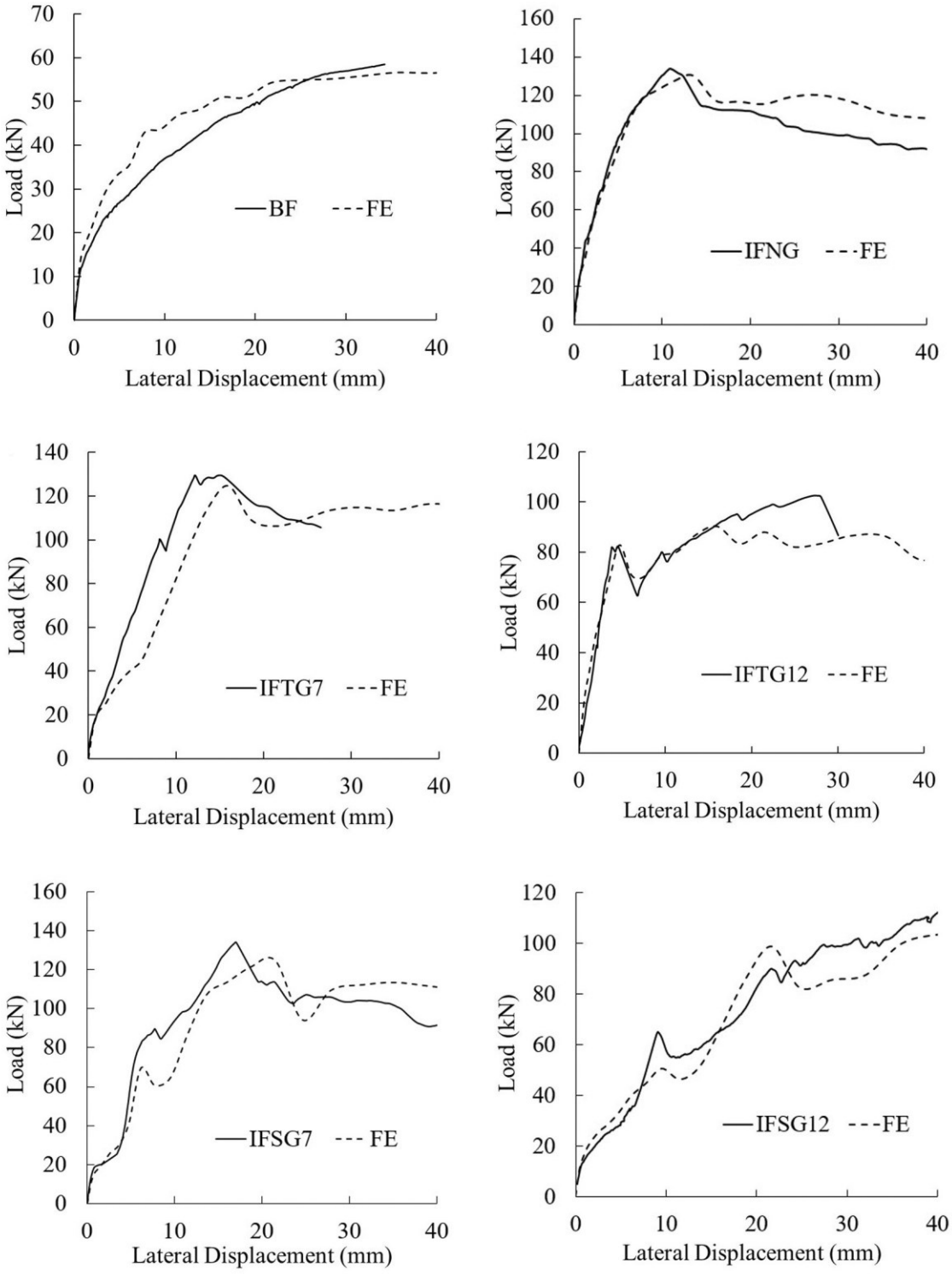

Figure 4.13. Comparison of lateral load vs. displacement curves obtained from tests and FE analysis for all specimens.

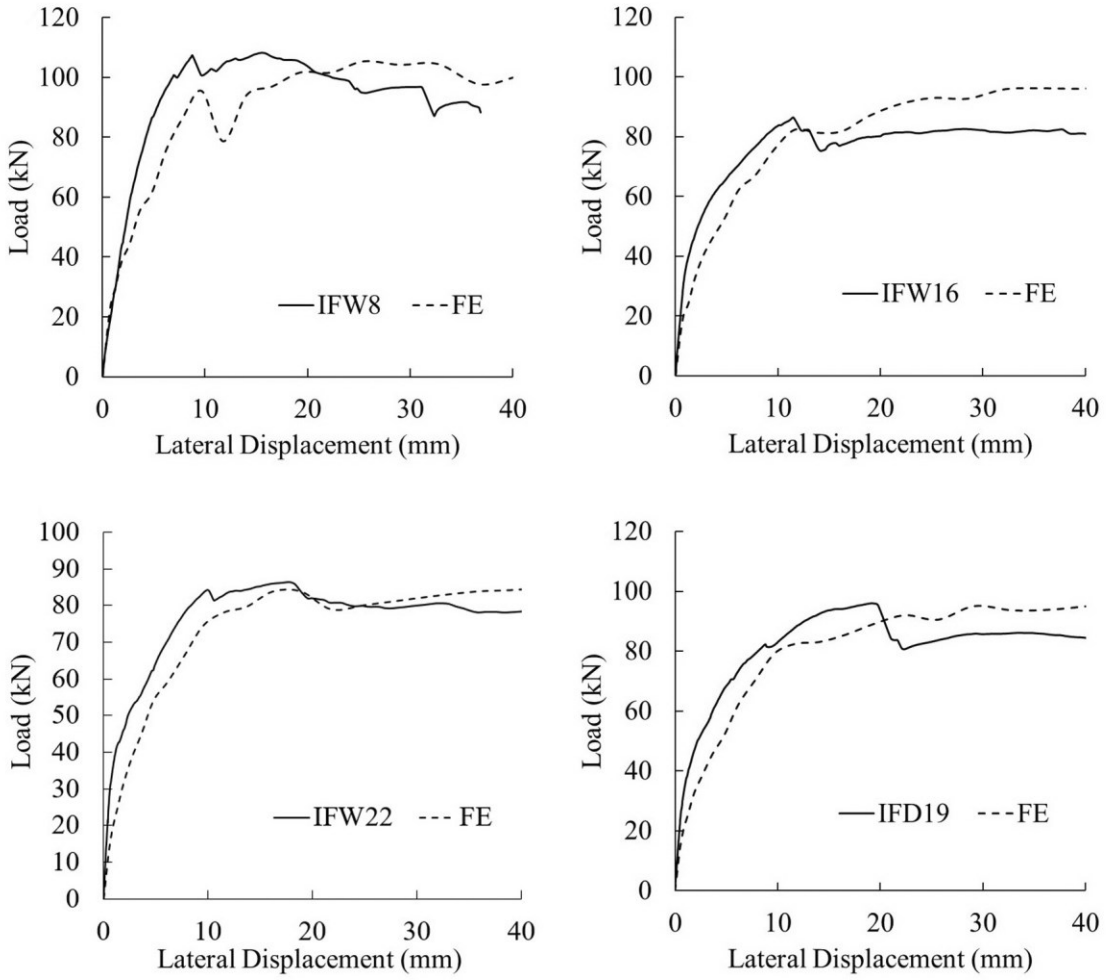

Figure 4.13. (Continued)

Figure 4.14 compares the deformed geometry and cracking patterns obtained from the FE model and tests. The red contours shown in the FE results represent the regions where stresses were well beyond the cracking stress whereas the green contours represent the regions that just began to crack. In all specimens, corner crushing was observed to be the final failure mode which usually occurred after formation and development of diagonal cracking.

For the control specimen, IFNG (Figure 4.14a), the FE model exhibited a similar cracking pattern and failure mode as the tested specimen where cracking formed and developed in the general diagonal direction of the infill, and crushing of the infill was observed at the loaded corners. For the specimen with an opening (Figure 4.14b), the FE model accurately simulated the diagonal cracks formed and developed around the corners of the opening. As the load increased, the distortion of the opening (left bottom corner and right top corner) was also captured. For the specimen with a top gap (Figure 4.14c), the FE model is capable of predicting a cracking pattern that was different from the control specimen where two main cracking regions were developed due to the presence of gap. For the specimen with side gaps (Figure 4.14d), the initiation of failure was shear sliding along the bed joints which also transformed into the cracking of masonry blocks at some regions. As load increased, both the model and test showed that the infill was pushed against the lower part of the frame column at the unloaded side and crushing of the infill was observed at the loaded corner. Figure 4.15 details the ability of the model in predicting the corner crushing failure where the crushed element contours are compared with crushed CMUs in the test.

The above comparisons further demonstrate that in addition to the ultimate strength and stiffness, the FE model is also capable of predicting the complete behaviour including both loading and unloading stages as well as the cracking pattern and failure mode of the specimens. Noting that the specimens had either infill openings or varying interfacial conditions, the comparison indicates the robustness of the model in incorporating infill frame conditions different from a “regular” infilled frame.

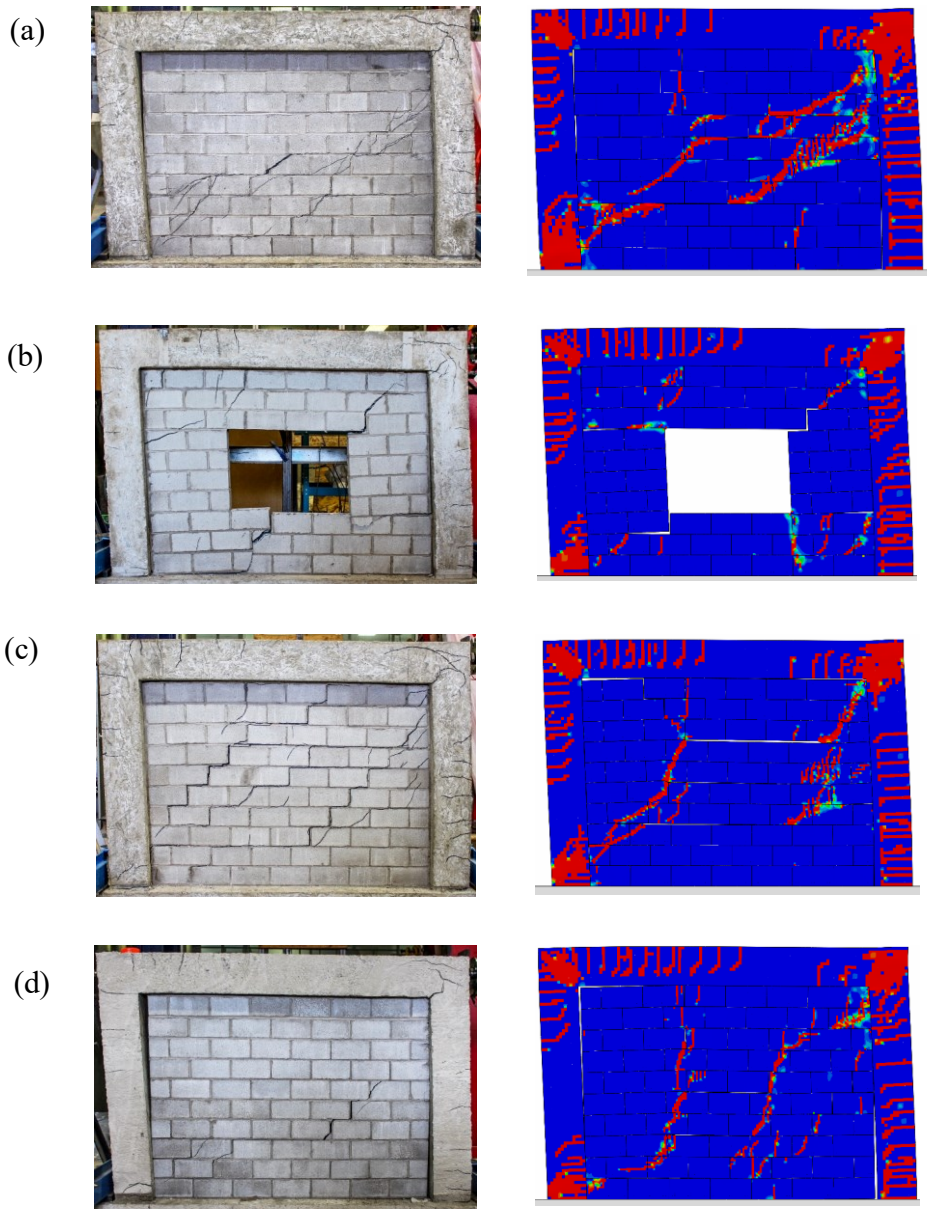

Figure 4.14. Deformed geometry and cracking pattern comparison for: (a) IFNG, (b) IFW16, (c) IFTG12 and (d) IFSG12

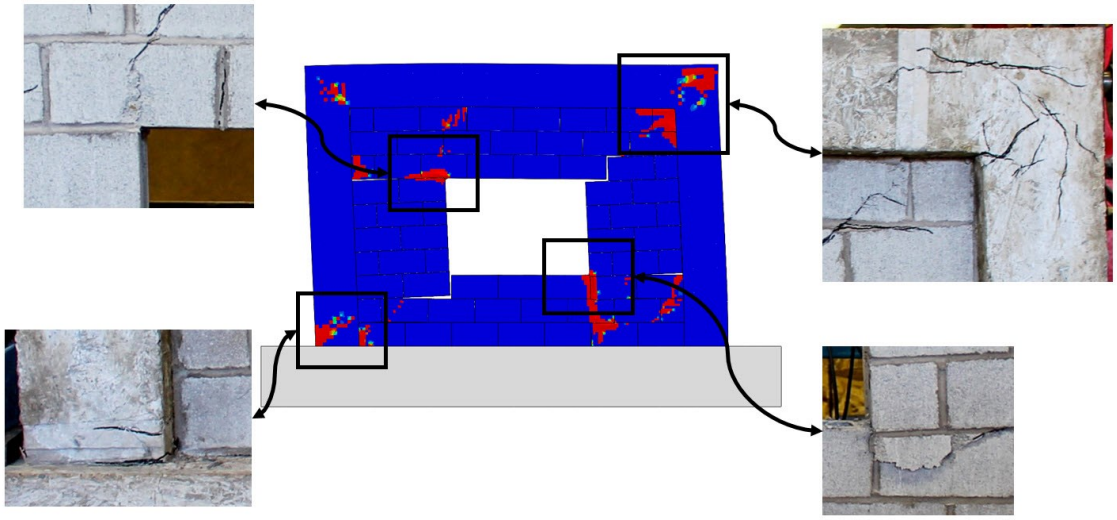

Figure 4.15. Detailed crushing comparison (specimen IFW16)

4.9 Investigation on the Interface Parameters

The validation of the model shows that the model is effective and accurate in simulating the in-plane behaviour and strength of the infilled RC frames. However, as several input material parameters were assumed based on the available literature, it is important to investigate the influence of variation in these parameters on the results. Section 4.4 showed that the interface parameters are most critical to the overall behaviour simulation and have the most uncertainty due to the lack of available technical information. Hence, in this section, the effect of several interface parameters on the behaviour and failure prediction of infill frames is investigated. These parameters covered three aspects of the interface behaviour. Group I parameters define the failure surface and include initial tensile strength (p_t), initial shear strength (d'), and frictional angle of the interface (β); Group II parameters define fracture energy of the interface and include tensile and shear fracture energies of the interface (G_{ft}, G_{fs}); and Group III parameter defines the shear behaviour of a mortar joint and is the dilation angle of the interface (ψ_i). These parameters were commonly used in

various FE models and deemed crucial in model performance (Al-Chaar et al. 2008, Bolhassani et al. 2015, Dolatshahi and Aref 2011, Koutromanos et al. 2011a, Lotfi and Shing 1994, Lourenco 1996, Mehrabi and Shing 1997, Stavridis and Shing 2010). However, in almost all of these cited studies they were calibrated for a specific masonry infill case based on limited experimental information (Atkinson et al. 1989, Van der Pluijm 1993) and no information was given for the effect if different values were used.

Table 4.6 summarizes the values of the aforementioned parameters used in this study. The values selected were considered within a reasonable range of variation as reported in the literature (Alecci et al. 2013, Atkinson et al. 1989, Dhanasekar 2010, Dolatshahi and Aref 2011, Lourenço et al. 1998, Mehrabi and Shing 1997, Stavridis and Shing 2010) covering the expected lower and upper bounds. It should be pointed out that in the case of failure surface parameters (Group I), the friction angle was reported to vary from 30 to 50 degrees in the $\sigma - \tau$ plane which corresponds to 50 to 80 degrees in the $p - q$ plane. The mortar joint strength was reported to vary from 0.05 to 0.4 MPa and 0.3 to 0.8 MPa for tensile and shear, respectively. As three of them are related through the hyperbolic Drucker-Prager function (Eq. (4.13)), the two more important parameters, shear strength (d') and frictional angle (β), were chosen first and the third parameter, tensile strength (p_t), was then calculated using the equation. The three failure surface lines formed are illustrated in Figure 4.16 where FS1 to FS3 parameter combination represent weak, intermediate and strong mortar.

Table 4.6. Summary of input parameters used in the sensitivity study

Case ID	Description	Type of mortar	Initial tensile strength, p_t (MPa)	Initial shear strength, d' (MPa)	Frictional angle, β (degree)	Dilation angle, ψ_i (degree)	Fracture Energy (N.m)	
							Tensile G_{ft}	Shear G_{fs}
FS1	Failure surface parameters	Weak	0.3	0.4	50			
FS2		Intermediate	0.4	0.8	60			
FS3		Strong	0.5	1.2	70			
FG1	Fracture energy of interface	Weak					20	200
FG2		Intermediate					40	400
FG3		Strong					60	600
DA1	Dilation angle of interface	Weak				0		
DA2		Intermediate				10		
DA3		Strong				20		

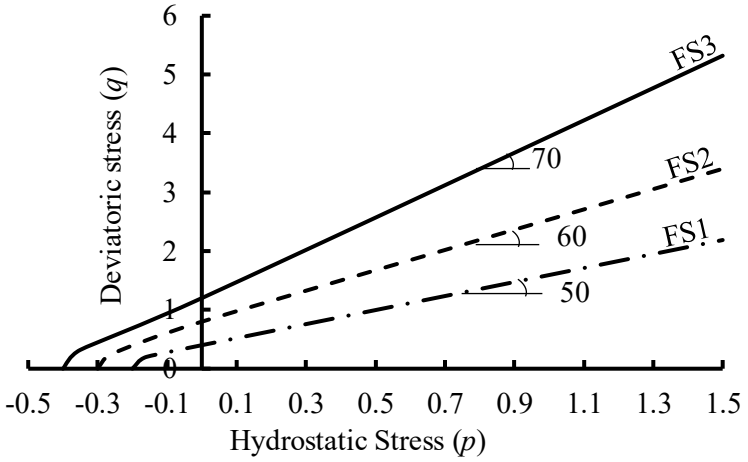

Figure 4.16. Yield lines in the p-q plane

The model used in the parametric study was a 4×3 m (W×H) RC frame infilled with 400×200 mm concrete masonry units with Type S mortar. The design of the concrete frame was based on CSA A23.3-04 in a similar manner as the tested specimens. The mechanical properties of different components used in the study are summarized in Table 4.7.

Table 4.7. Material properties used for the sensitivity study

Property	CMUs	Mortar	Concrete	Reinforcement
Compressive Strength (MPa)	20.0	15.0	35.0	-
Elastic Modulus (MPa)	20000	2600	30000	220000
Tensile strength (MPa)	2.0	1.5	3.5	400 (600)*

* Yield and (ultimate) strength

4.9.1 Effect of Failure Surface Parameters

The effect of the interface failure surface parameters on the load vs. displacement response is shown in Figure 4.17. Results indicate that these parameters have a significant effect on the cracking stiffness, ultimate capacity and post-ultimate behaviour of the infilled frame but a minimal effect on the initial stiffness. As expected, strong mortar parameters (FS3) yielded the greatest ultimate load and post-ultimate strength.

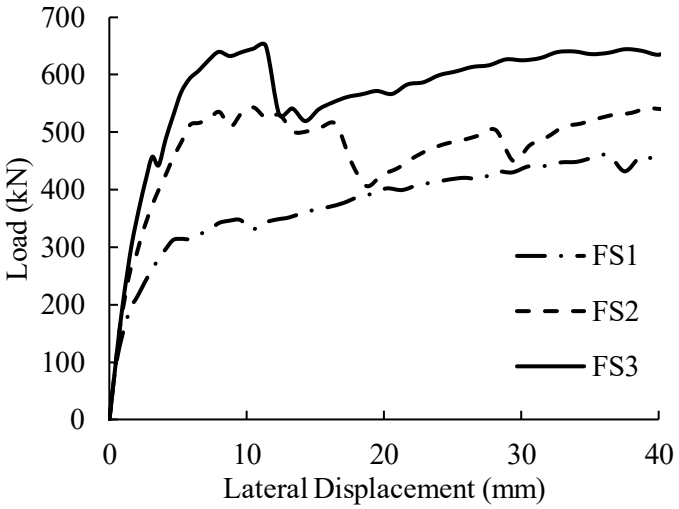

Figure 4.17. Lateral load vs. displacement curves for interface failure surface parameters

Deformed shapes as well as cracking and crushing patterns in both the infill and RC frame for three failure surface parameters are presented in Figure 4.18. Results indicate that the choice of failure surface parameters influence the failure mode and the extent of damage in both the infill and RC frame. In the weak mortar case the failure was initiated by shear sliding in horizontal mortar joints while, as the mortar becomes stronger, the failure was predominated by diagonal cracking and more extensive corner crushing of the CMUs. Figure 4.18 shows increasingly more extensive developemnt of cracking and crushing in the masonry infill as well as in the frame as the mortar becomes stronger. This is consistent with the observation that stronger mortar failure parameters produced higher ultimate load as stronger mortar allows the system to deform, crack and crush to a greater extent.

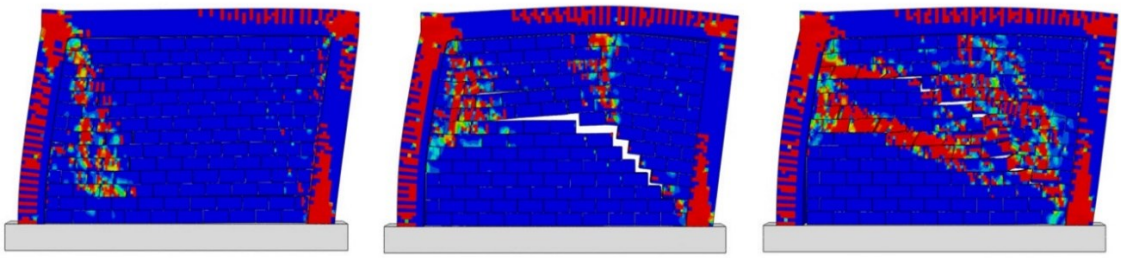

Figure 4.18. Deformed shape (6x magnified) and cracking patterns for interface failure surfaces

4.9.2 Effect of Fracture Energy Parameters

For the fracture energy parameters, values of 20, 40, 60 for tensile fracture energy and 200, 400, 600 for shear sliding energy were chosen (Table 4.6). According to the available literature the tensile fracture energy is commonly correlated with the compressive strength of the material (FIB 2012) and the shear fracture energy is usually assumed to be ten times the tensile fracture energy (Lotfi and Shing 1994, Mehrabi and Shing 1997, Stavridis and

Shing 2010). The effect of interface fracture energy parameters on the lateral load vs. displacement response of the infilled frame is illustrated in Figure 4.19. It can be seen that these parameters have a negligible effect on the pre-ultimate portion of the response curve. A noted difference is that while the ultimate strength remained practically the same for different fracture energies, in the high fracture energy case it occurs at a greater lateral displacement after development of more cracking (shown as the flat portion before the ultimate load) to correspond to a higher energy release. A minor effect was also observed on the post-ultimate behaviour where higher fracture energy values showed more residual capacity.

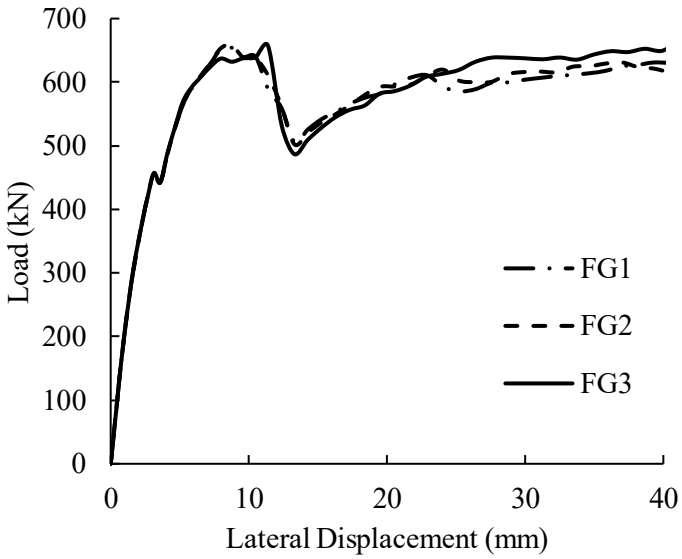

Figure 4.19. Lateral load vs. displacement curves for interface fracture energy parameters

4.9.3 Effect of Dilation Angle

In a mortar joint under shear, dilatancy is the occurrence of a displacement perpendicular to the imposed shear displacement, at and beyond the peak shear strength. Consideration of dilatancy of mortar has been inconsistent in previous numerical studies where some

researchers (Bolhassani et al. 2015, Dolatshahi and Aref 2011) ignored its effect totally while others (Lotfi and Shing 1994, Lourenço and Rots 1997, Mehrabi and Shing 1997) believed that it significantly affects the mortar shear failure. In this study, dilation angles of 0, 10, and 20 degrees were considered. The upper bound was chosen as 20 degrees as values greater than that would produce unrealistic lateral capacities. Lateral load vs. displacement responses with different dilation angles are shown in Figure 4.20. Large variation between the ultimate strengths for different dilation angles indicate that this parameter has a considerable influence on the ultimate capacity prediction. This is mainly due to effect of dilation angle in increasing the shear strength of the mortar joint interface. Dilation angle also affects the cracking load and cracking stiffness of the structure such that the initial cracking occurs roughly at 200, 300 and 450 kN for DA1, DA2 and DA3, respectively.

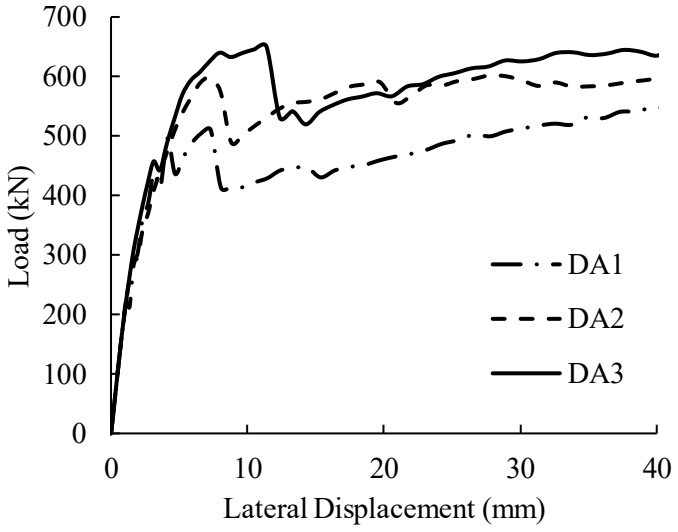

Figure 4.20. Lateral load vs. displacement curves for different interface dilation angles

A comparison between deformed shapes and cracking patterns for different dilation angles is shown in Figure 4.21. It is seen that in the case of small dilation angles, cracking is more

concentrated in mortar joints and sliding shear with wide cracks in bed joints is observed; while as the dilation angle becomes larger, sliding shear and cracking in bed joints is reduced and the mortar joints and CMUs are behaving increasingly more as a unit and cracking is mainly concentrated in CMUs.

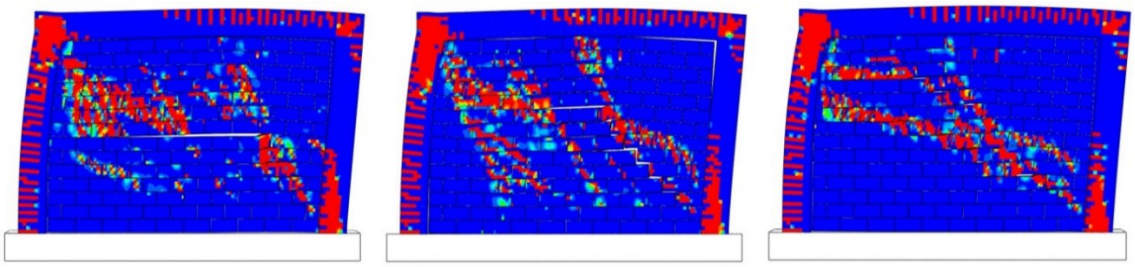

Figure 4.21. Deformed shape (10x magnified) and cracking pattern at 25 mm lateral displacement for dilation angles

4.10 Conclusion

A nonlinear three-dimensional finite element model was developed to simulate the in-plane behaviour of masonry infilled RC frames. A concurrent experimental program was conducted where ten masonry infilled RC frame specimens incorporating either interfacial gaps or infill openings were tested to failure. The finite element model was extensively validated using the test results. A sensitivity study of several critical interface input parameters on the behaviour of the infilled frame was also conducted. Some conclusions stemming from this study are as follows:

1. The 3D nonlinear model developed is capable of producing accurate results in analysis of masonry infilled RC frames and its capability in incorporating infill openings and interfacial gaps is also demonstrated.

2. The interface element input parameters for failure surface, fracture energy, and mortar dilation were analyzed. Of the parameters studied, failure surface parameters and dilation angle were shown to have a significant effect on the ultimate strength, cracking stiffness, as well as pre and post-ultimate behaviour of the models while those for fracture energy were shown to only have a small degree of influence on the ultimate load and post-ultimate behaviour of the models.

3. Contrary to recommendations from some researchers, FE results of this study showed that the dilatancy of mortar should be considered in the numerical models. Since there is little experimental information in the available literature, it is suggested that accurate methods for experimentally obtaining the dilatancy of mortar need to be developed and implemented.

4.11 Acknowledgement

The authors wish to recognize the contribution of financial assistance by the Canadian Concrete Masonry Producers Association and Natural Sciences and Engineering Research Council of Canada.

Chapter 5 The Out-of-Plane Behaviour of Concrete Masonry Infills Bounded by Reinforced Concrete Frames

Ehsan Nasiri, Yi Liu

Published in Engineering Structures, Volume 184, 1 April 2019, Pages 406-420

https://doi.org/10.1016/j.engstruct.2019.01.098

5.1 Abstract

The paper presents results of a finite element (FE) study of several critical geometric parameters on the out-of-plane behaviour of concrete masonry infills bounded by reinforced concrete (RC) frames. The development of FE model adopted a three-dimensional simplified micro-modeling technique considering detailed geometry and behaviour characteristics of concrete and masonry units through Concrete Damaged Plasticity (CDP) method. The surface-based cohesive interaction was incorporated to capture the behaviour and failure mechanisms of mortar joints. A concurrent experimental study was also conducted on four infilled RC frames and the results were used to validate the FE model. The model was shown to be capable of simulating accurately the out-of-plane behaviour and strength as well as capturing the cracking pattern and failure modes of infilled RC frames for different geometric and loading situations. The parameters considered in the FE study included infill aspect ratio, infill slenderness ratio, bounding frame stiffness, frame-to-infill interfacial gap, infill opening size and aspect ratio, and web thickness of masonry blocks. The numerical results showed that the out-of-plane behaviour of infilled RC frames was dependent on these parameters and the correlation between each parameter and its effect on the infill strength was described as appropriate.

Keywords: concrete masonry infills; RC frames; out-of-plane; strength; finite element; arching action; nonlinear analysis

5.2 Introduction

The out-of-plane behaviour and strength of masonry walls bounded by concrete or steel frames is an important aspect of structural design for buildings subjected to out-of-plane forces such as wind and impact loads as well as inertial forces induced during earthquake. Early experimental work (Gabrielsen et al. 1975, McDowell et al. 1956b, Thomas 1953) showed that these masonry walls, often referred to as masonry infills, had much greater capacity than that predicted by flexural analysis. This capacity increase has been attributed to a mechanism referred to as arching action. When a wall is butted up against the frame acting as a rigid support, in-plane compressive forces are induced in the wall as it bends under out-of-plane forces, and the compressive forces can delay cracking and produce a subsequent arching of the wall. Based on this concept, McDowell et al. (1956b) proposed an equation to calculate the out-of-plane resistance of masonry infills using simple equilibrium conditions of arching phenomenon. Maksoud and Drysdale (1993) showed that the arching can still develop even when gaps existed between the infill and the frame member, only to a lesser degree. More recent research (Angel et al. 1994, Flanagan 1994, Flanagan and Bennett 1999a, Griffith and Vaculik 2007) found that the arching action was dependent on the masonry compressive strength, infill geometry, and boundary conditions between the infill and the frame; and development of arching action can enhance the stability of infills even after the ultimate capacity was achieved. Based on test results, Dawe and Seah (1989b) developed a semi-empirical equation for determination of the out-of-

plane strength of infills taking into account of infill geometry and bending and torsional stiffness of the bounding frame. Flanagan (1994) simplified this equation by removing the terms for torsional stiffness of the frame member as they argued that the mathematical value of torsional stiffness is significantly small in comparison to the flexural stiffness. Their work formed the basis for the out-of-plane strength equation in the current American masonry design standard TMS 402/602-16. Angel et al. (1994) developed an equation for accounting for the effect of prior in-plane damage on the out-of-plane strength of infills. Klingner et al. (1996) proposed an equation considering two-way arching action that may be developed in an infill. In practice, the Canadian masonry design standard CSA S304-14 suggests using the first principle mechanics based on equilibrium of moments caused by internal thrust forces and external loading to calculate the out-of-plane strength but does not provide design equations for the internal thrust force. One such approach is presented in Drysdale et al. (1994). Comparing with the in-plane behaviour of masonry infilled frames, research on the out-of-plane behaviour of masonry infills is limited and experimental results are scarce in the literature. Although several analytical methods were proposed as described above, they often produce inconsistent, and even conflicting results due to the fact that these methods were calibrated with different experimental programs containing a limited number of physical results. More results, from either experimental or numerical studies on infilled frames with different material and geometric parameters are needed to provide better understanding of the behaviour as well as to examine the accuracy of available methods.

With the advancement of computing technology, numerical modeling has been increasingly used as an effective tool to supplement experimental results. Two-dimensional

(2D) finite element models have been commonly used in the simulation of in-plane behaviour of masonry infilled frames. The simulation of out-of-plane behaviour using 2D continuum models has also been reported in a few studies (Lourenço 2000, Minaie et al. 2014, Noor-E-Khuda et al. 2016a, Noor-E-Khuda et al. 2016b). While these models were shown to produce acceptable results for infills with large slenderness (height/thickness) ratios, for intermediate and low slenderness, the 2D continuum geometry has difficulty to accurately capture the non-homogeneous characteristics of masonry, and effect of shear deformations and associated failure modes. For out-of-plane behaviour simulation, it is believed that a three-dimensional model (3D) would be desirable to fully capture the behaviour and failure modes unique to infilled frames subjected to out-of-plane loading.

This study was then motivated to develop a 3D finite element model to systematically study the out-of-plane behaviour of masonry infilled RC frames. Concurrent with the finite element modelling, four masonry infilled RC frames were tested under out-of-plane loading and the experimental results were used to validate the model. A subsequent parametric study focusing on several critical geometric parameters was conducted using the model. Correlations between each studied parameter and the out-of-plane behaviour and strength of infills bounded by RC frames were discussed in detail.

5.3 Experimental Program

Four masonry infilled RC frames were tested in the experimental program included one infilled frame as the control specimen (IFNG), an infilled frame with 16% (opening/infill area) opening (IFW16), and two infilled frames having in-plane damage sustained prior to being subjected to out-of-plane loading. The prior damage was diagonal cracking (IF-D1)

and corner crushing (IF-D2) respectively. The test results were used to validate the model and thus information on specimens, test setup, and results deemed relevant to the validation is provided in the following section. The detailed analysis of the results is available elsewhere (Sepasdar 2017).

All specimens had the same dimension as shown in Figure 5.1, yielding an infill height-to-length aspect ratio of about 0.73. The masonry infill was constructed using the custom-made, half-scale standard 200 mm concrete masonry units (CMUs) laid in the running bond. Type S mortar was used in construction with an average joint thickness of 7 mm. The RC frame consisted of two 180 mm square columns, a 180 mm square top beam, and a 250 mm square bottom beam. The member reinforcement details including size, spacing, arrangement of longitudinal bars and stirrups was designed according to CSA A23.3-14 and complied with requirements to provide ductility and avoid brittle shear failure.

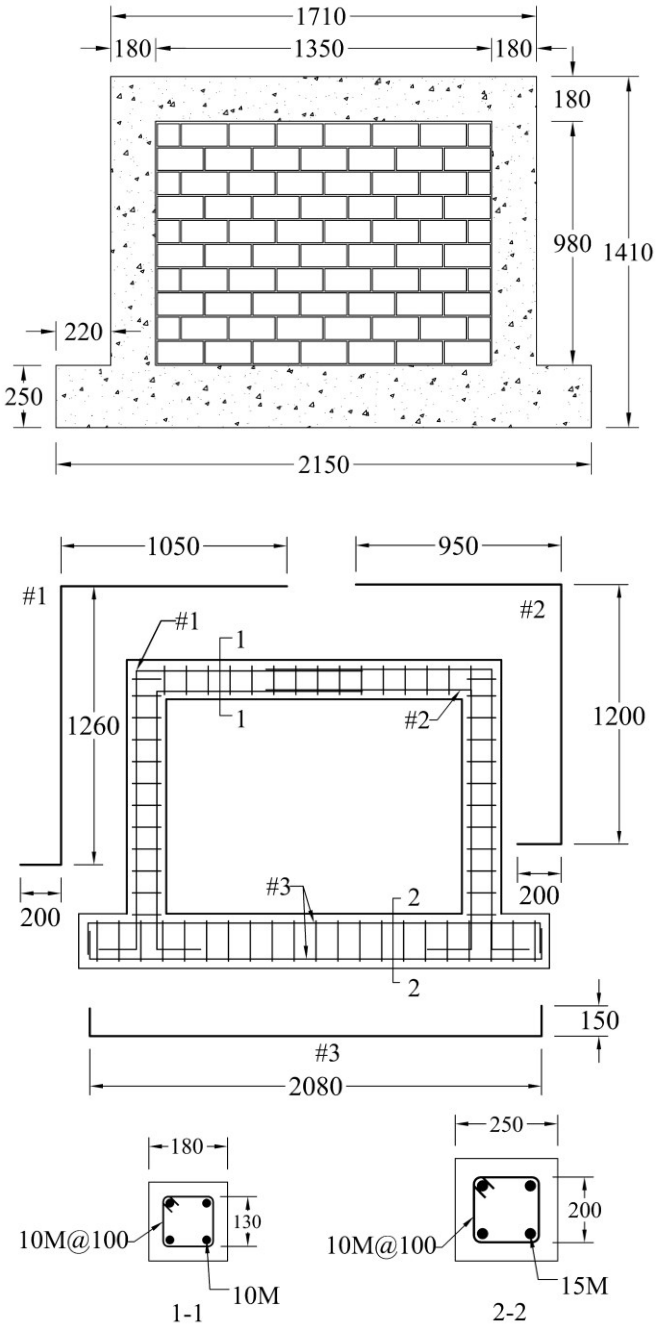

Figure 5.1. Geometric properties of specimens and reinforcement details in the RC frames

5.3.1 Test Setup, Instrumentation, and Procedure

The out-of-plane loading was applied through a self-equilibrating system as shown in Figure 5.2. The out-of-plane pressure was applied to the infill surface using an airbag that was housed in a reaction box made from plywood boards and stiffened with steel sections. The reaction box was in turn connected to the RC frame using high strength bolts. All specimens were clamped down to the strong floor using steel W-sections on either end of the frame beam stem to prevent potential lateral or transverse movement. An air compressor was used to inflate the airbag and the real-time pressure was measured using a pressure transducer. The air pressure was applied gradually at a rate of approximately 1.5 kPa per minute until failure of the infill.

For the in-plane loading set up for specimens IF-D1 and IF-D2, a lateral in-plane load was applied at the top beam level using a hydraulic actuator with a capacity of 250 kN. As shown in Figure 5.3, the hydraulic actuator was attached to the column of an independent reaction frame. A load cell was mounted at the end of the actuator to measure the applied load. The bottom beam of the frame was braced against lateral movement. An example load vs. displacement curve shown in Figure 5.4 indicates the pre-load and deformation levels of specimens IF-D1 and IF-D2. Specimen IF-D1 was first subjected to in-plane loading to the onset of first major diagonal cracking on the surface of the infill and then the in-plane loading was removed. The specimen was subsequently subjected to the out-of-plane pressure to failure. For specimen IF-D2, the in-plane loading was continued after the first major diagonal cracking of the specimen till the specimen reached its lateral in-plane capacity. At this point, the specimen has sustained extensive diagonal cracking as

well as exhibiting corner crushing at loaded corners. Then the in-plane loading was removed, and the specimen was subsequently subjected to the out-of-plane pressure to failure. Linear variable differential transformers (LVDTs) were used in all cases to measure either the lateral or out-of-plane displacements of the infill and the frame (Figure 5.3). The load and LVDT readings were monitored and recorded with an interval of 0.2 seconds throughout the test using an electronic data acquisition system. For each test, the cracking load, cracking pattern, ultimate load, and failure mode were noted.

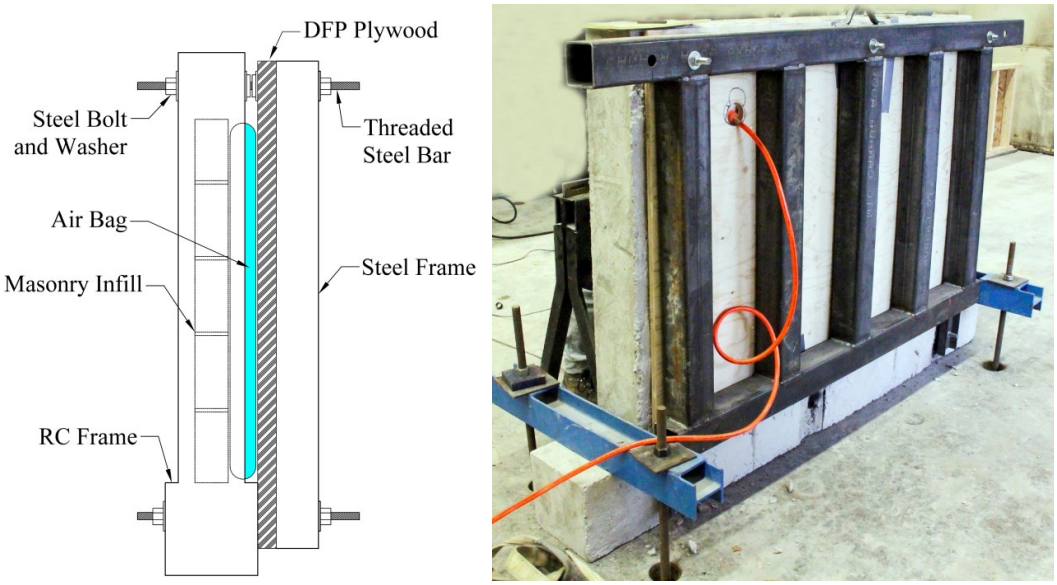

Figure 5.2. Test set-up for out-of-plane loading of the specimens

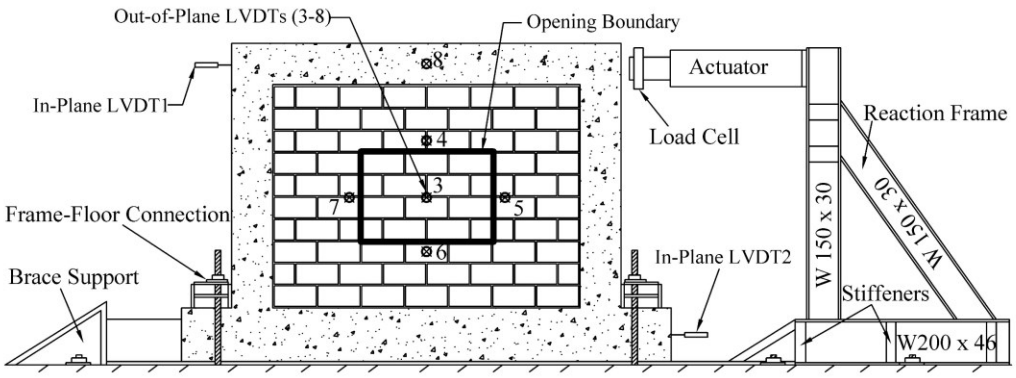

Figure 5.3. Schematic test set-up for in-plane loading of specimens IF-D1 and IF-D2

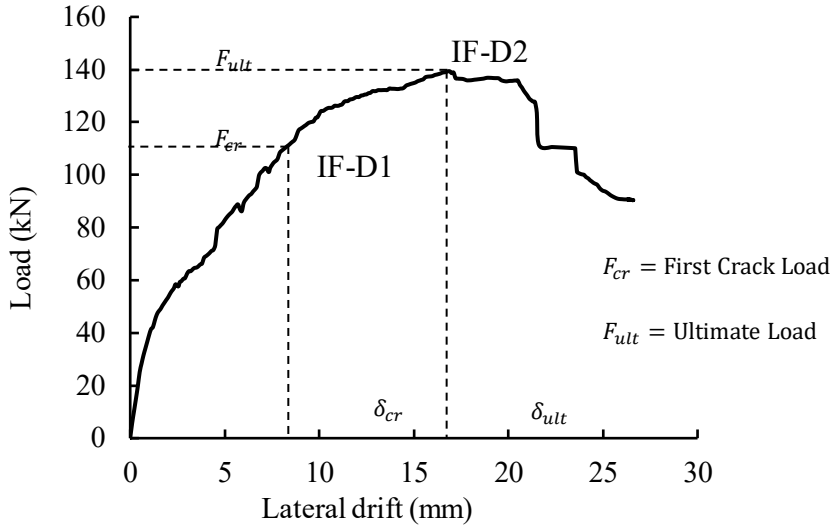

Figure 5.4. Load vs. lateral displacement curve for the laterally loaded infilled frame specimens

5.3.2 Material Properties

The mechanical properties of CMUs, mortar, and masonry prisms for the infill and those of concrete and reinforcement of the frame were obtained experimentally in accordance with ASTM specifications. A material property summary is presented in Table 5.1 (also see Nasiri and Liu (2017)).

Table 5.1. Summary of material properties for the specimens

	Elastic modulus (GPa)	Compressive strength (MPa)	Tensile strength (MPa)	Yield strength (MPa)	Ultimate (yield) strain
Concrete ASTMS C39-16	27.8	43.8	3.5	-	0.0025
CMUs ASTM C140-16	3.5	25.0	2.5	-	0.0080
Mortar ASTM C270-14	2.6	21.3	1.7	-	-
Prisms ASTM C1314-16	3.0	17.1	-	-	-
Reinforcement ASTM E8-16	220	-	665	446	0.085 (0.003)

5.4 Finite Element Model

In this study, the mortar joints were not physically modeled, and the CMU dimensions were thus increased by half thickness of the mortar joint in both horizontal and vertical directions. The CMUs were connected and interact with each other through zero-thickness interface interaction. Often referred to as the "simplified micro-modelling" (Lourenco 1996), this modeling technique is considered effective in achieving a balance of simulation accuracy and computational efficiency in comparison to the detailed micro-modelling technique where mortar joints are modelled (Haach et al. 2009, Lourenco 1996, Mehrabi and Shing 1997, Stavridis and Shing 2010). The meshing of the model is shown in Figure 5.5. The bottom beam of the frame was fully restrained to simulate the condition of a foundation beam while the rest of the RC frame members were only restrained against the out-of-plane displacement in the FE model. Uniform pressure was applied to the surface of the infill through a monotonically load-controlled procedure. A detailed description of the model development is reported in Nasiri and Liu (2017). For easy reference, key aspects for various components of the model are summarized in the following sections.

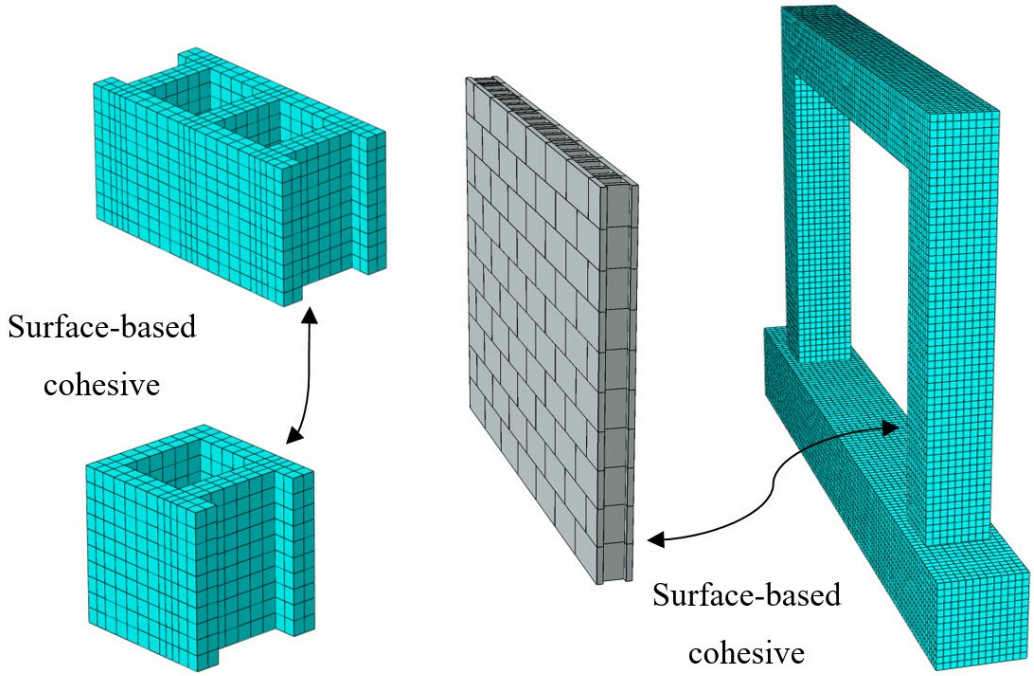

Figure 5.5. Three-dimensional geometric model used in the FE analysis

5.4.1 Nonlinear Behaviour of Concrete and CMUs

The solid elements, in this case, the eight-node brick elements with reduced integration formulation, C3D8R, were used to model the CMUs as well as the RC frame members. Their behaviour model adopted the Concrete Damaged Plasticity (CDP) model in ABAQUS (Lubliner et al. 1989). The CDP model is a continuum, plasticity-based, damage model that is commonly used for quasi-brittle materials. Both isotropic damaged elasticity and tensile and compressive plasticity are considered in this model and failure mechanisms are defined in terms of tensile cracking and compressive crushing. The Drucker-Prager hyperbolic function and a non-associated potential flow are used in the CDP model. In this study, values for the parameters that are needed to define the yield function and flow rule in the CDP model were based on experimental results obtained by Kupfer et al. (1969) and Jankowiak and Lodygowski (2005) as well as numerical values used by Lubliner et al.

(1989), Lee and Fenves (1998), Jiang and Wu (2012), and Genikomsou and Polak (2015) and they are summarized in Table 5.2. This table was also used in Nasiri and Liu (2017).

Table 5.2. The CDP model parameters for concrete and CMUs

	Dilation angle ψ_c	Eccentricity ϵ	σ_{b0}/σ_{c0}	K_c
Concrete	40	0.1	1.16	0.66
CMU	30	0.1	1.16	0.66

ϵ: the rate at which the plastic potential function approximates the asymptote; σ_{b0}/σ_{c0}: the ratio of initial biaxial compressive yield stress to initial uniaxial compressive yield stress; K_c: the ratio of the tensile meridian to the compressive meridian

5.4.1.1 Compressive Behaviour Model

The compressive behaviour of concrete and CMUs is defined using the stress-strain constitutive model proposed by Sima et al. (2008) as follows:

$$\begin{cases} \sigma_c = \varepsilon_c E_0 & \varepsilon_c \le \varepsilon_{c0} \\ \sigma_c = \left[\varepsilon_{c0}(1-A) + A\varepsilon_c e^{\left(\frac{\varepsilon_{c0}-\varepsilon_c}{\varepsilon_c'}\right)}\right] E_0 & \varepsilon_c > \varepsilon_{c0} \end{cases}$$

$$A = \frac{f_c' - \varepsilon_{c0}E_0}{E_0\left(\varepsilon_c' e^{\left(\frac{\varepsilon_{c0}}{\varepsilon_c'}-1\right)} - \varepsilon_{c0}\right)} \tag{5.1}$$

where σ_c and ε_c are the compressive stress and strain values, respectively; f_c' is the compressive strength of the material; ε_{c0} is the linear elastic strain limit; ε_c' is the strain at the peak stress and E_0 is the Young's modulus of the material. Incorporating experimentally obtained mechanical properties into Eq. (5.1), the compressive stress-strain

curves for concrete and CMUs were obtained and are shown in Figure 5.6 (Nasiri and Liu 2017).

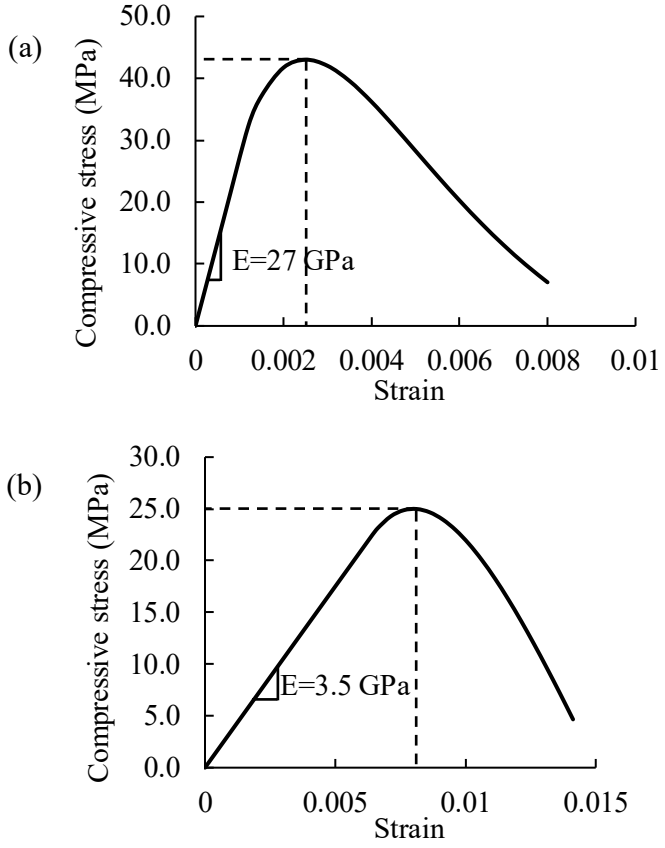

Figure 5.6. Compressive stress-strain curve for: (a) concrete; and (b) CMUs

5.4.1.2 Tensile Behaviour Model

The tensile behaviour model used in this study adopted an averaged tensile stress-strain curve between cracked and uncracked concrete suggested by Shima et al. (1987) to account for the tension stiffening effect. This model was shown to be independent of element size, crack spacing, and orientation of reinforcement. For concrete material, the tensile stress-strain curve used in this study can be expressed using Eq. (5.2).

$$\begin{cases} \sigma_t = \varepsilon_t E_0 & \varepsilon_t \leq \varepsilon_{t0} \\ \sigma_t = \sigma_{t0}\left(\dfrac{\varepsilon_{t0}}{\varepsilon_t}\right)^{0.4} & \varepsilon_t > \varepsilon_{t0} \end{cases} \quad (5.2)$$

where σ_t and ε_t are the tensile stress and strain values, respectively; σ_{t0} and ε_{t0} are the linear elastic stress and strain limits, respectively. Incorporating experimental results of concrete modulus and elastic stress and strain limit, the tensile stress-strain curve for concrete was obtained as illustrated in Figure 5.7 (Nasiri and Liu 2017).

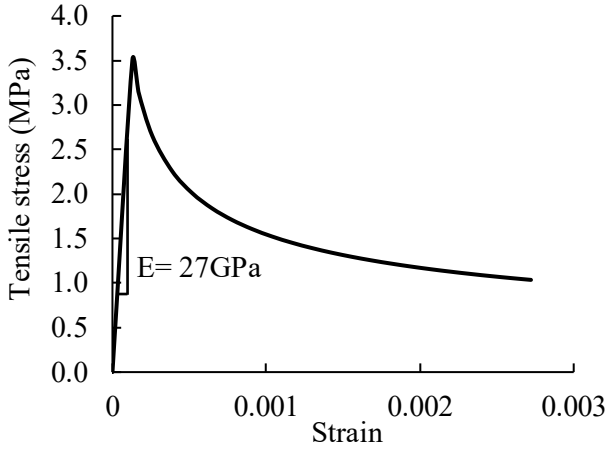

Figure 5.7. Tensile stress-strain curve for concrete

For CMUs, the tension stiffening effect described above is non-existent due to the absence of steel reinforcement. The tensile behaviour is better described using a stress-crack displacement curve in which the area under the curve represents the Mode I fracture energy of the material (G_f) (Hillerborg et al. 1976). Thus, the tensile behaviour model for CMUs was defined by a linear elastic behaviour in the pre-cracking phase and a stress-crack displacement curve in the post-cracking phase as shown in Figure 5.8 (Nasiri and Liu 2017). The fracture energy of the CMU material can be related to the compressive strength of CMUs using Eq. (5.3) as suggested by Fib: Model Code (2012).

$$G_f = 73\, f_c^{\,0.18} \tag{5.3}$$

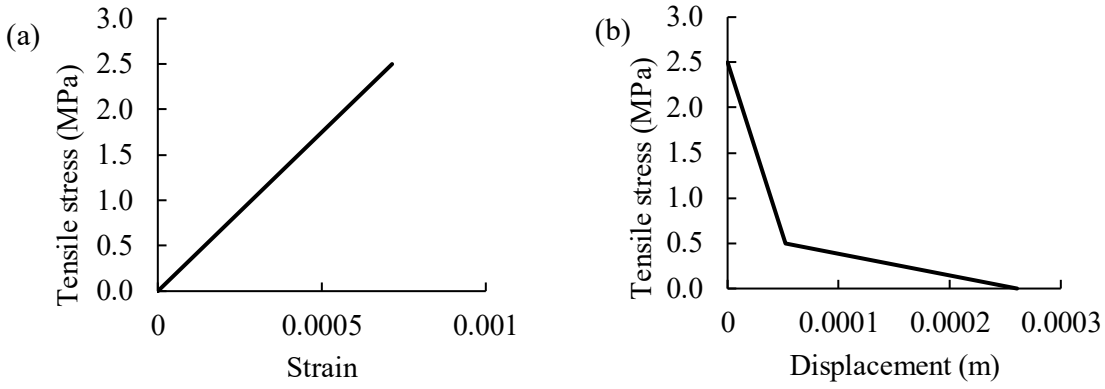

Figure 5.8. Tensile behaviour of CMUs: (a) stress-strain curve; and (b) stress-displacement curve

5.4.2 Behaviour Model of Interface Between the CMUs and Between the CMUs and the Frame

In this study, the surface-based cohesive behaviour model in ABAQUS was used for the interface between the CMUs and between the CMUs and the frame. This behaviour model uses the traction-separation constitutive relationship incorporating shear and tensile failure criteria to capture the possible failure modes of interface. In the elastic state, the traction-separation law is controlled by an elastic response for both normal and transverse deformations as expressed in Eq. (5.4). Traction stress vector t consists of three components, t_n, t_s and t_t, which represent the tensile and two shear tractions. The corresponding separations are denoted by δ_n, δ_s and δ_t.

$$t = \begin{Bmatrix} t_n \\ t_s \\ t_t \end{Bmatrix} = \begin{bmatrix} K_{nn} & 0 & 0 \\ 0 & K_{ss} & 0 \\ 0 & 0 & K_{tt} \end{bmatrix} \begin{Bmatrix} \delta_n \\ \delta_s \\ \delta_t \end{Bmatrix} = K\delta \tag{5.4}$$

Once failure is detected by tensile and shear strength criteria, two damage models (normal and shear stress damage) control degradation and elimination of the interaction. The normal

and shear stress damage criteria were based on the fracture energy approach (Lourenco 1996, Rots 1991). In this approach, the area under either the tensile or shear traction-separation curve after the peak stress was set to be equal to the Mode I and Mode II fracture energy of the mortar material (Lourenco 1996, Rots 1991). Upon full degradation of the interface, the model adopts the Coulomb frictional contact between the CMUs or between the CMUs and the frame. At this stage, contacting surfaces can carry shear stress up to a certain magnitude before sliding, which is known as sticking. The sticking stress is defined as $\tau_{crit} = \mu N$ where, N is the contact pressure and μ is the coefficient of friction. The damage criteria and evolution law are schematically illustrated in Figure 5.9.

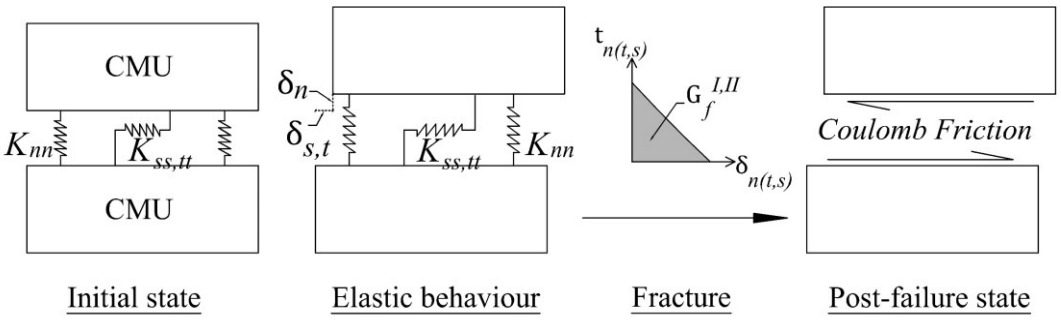

Figure 5.9. Behaviour of the mortar joint interaction

The input parameters used in the interface element modeling are summarized in Table 5.3. More detailed description can be found elsewhere (Nasiri and Liu 2017). Due to a lack of standard testing procedures for determining some of these parameters, the available literature was mainly relied on for obtaining the reasonable range of values and the final selection of values was conducted through an extensive calibration process against the experimental results obtained in this study.

Table 5.3. Summary of interface parameters

Symbol	Description	Value	Unit	Source/Reference
E	Elastic modulus	2600	MPa	Experiment
ν	Poisson's ratio	0.16	-	Experiment
t_n^0	Tensile strength of mortar	0.4	MPa	(Atkinson et al. 1989, Masia et al. 2012, Van der Pluijm 1993)
$t_{s,t}^0$	Shear strength of mortar	1.0	MPa	(Atkinson et al. 1989, Masia et al. 2012, Van der Pluijm 1993)
G_f^{II}	Shear fracture energy	400	N/m	(Lotfi and Shing 1994, Van der Pluijm 1993)
G_f^I	Tension fracture energy	40	N/m	(Lotfi and Shing 1994, Van der Pluijm 1993)
μ	Coulomb friction coefficient	0.7	-	(Lotfi and Shing 1994, Mehrabi and Shing 1997, Van der Pluijm 1993)

5.4.3 Material Model for Reinforcement

For infilled RC frames subjected to out-of-plane loading, material properties of steel reinforcement embedded in the RC frame and their interaction with the surrounding concrete have insignificant effect as the frame experiences limited cracking. Nonetheless, nonlinear material model for steel reinforcement in concrete considering bond-slip effect was adopted and the details are provided in Nasiri and Liu (2017). The "embedded elements" technique was used to simulate the interaction between reinforcing bars and concrete. In this method, the translational degrees of freedom of the embedded nodes (reinforcements) are coupled with surrounding nodes from the host region (concrete) so that they undergo equal displacements.

5.4.4 Analysis Procedure

A mesh density study was first performed. The FE load vs. displacement curves with varying element sizes were compared and it was determined that 10 and 20 mm elements were adequate for discretization of the CMUs and RC frame, respectively. The mesh density was increased at the webs of the CMUs by using 5 mm elements to capture the effects of stress concentration and large deformation in the webs of masonry units.

In this study, ABAQUS/CAE and ABAQUS/EXPLICIT were chosen for generation and analysis of the model, respectively. The ABAQUS/EXPLICIT uses the central difference method (CDM) to solve the equation of motion of a nonlinear problem. The advantage of CDM is that the time-marching update equations are EXPLICIT, so that no iterations are needed to find the new displacements which satisfy the equation of motion. This method is preferred for computation problems involving complicated nonlinear constitutive laws and large deformations and is especially effective for prediction of post-failure behaviour. The EXPLICIT procedure uses a large number of small time increments to ensure the accuracy of analysis (D.S.Simulia 2010).

5.5 Validation of the Model

As the discretization is carried out at the masonry unit block level, the constitutive relationship of the CMUs and the interaction model between CMUs are critical to the accuracy of the final infill model. The validation of the model was then first performed using the prism test results. The FE obtained stress-strain relationships for CMUs and three-high prisms are shown in Figure 5.10. Referring to Figure 5.10, the FE results predicted the strength and modulus of elasticity of both CMUs and prisms with marked

accuracy. The failure mode also agrees well with experimental observations. It is then concluded that the constitutive relationship and the interaction model between CMUs are accurate.

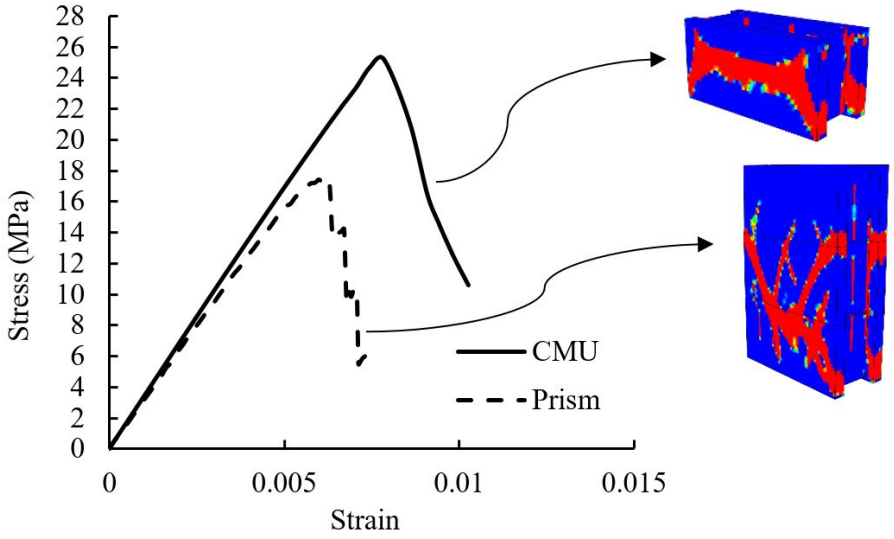

Figure 5.10. Finite element stress-strain curves and failure modes for CMUs and masonry prisms

For specimens IFNG, IFW16, a uniform pressure was applied to the surface of the infill through a monotonically load-controlled procedure. For specimens IF-D1 and IF-D2 with prior in-plane damage, the lateral in-plane load was first applied at the top beam-column joint to cause the desired level of damage in the infill (onset of first major diagonal cracking in the infill in IF-D1 and ultimate lateral capacity of the system in IF-D2). Then, the in-plane load was removed, and the out-of-plane pressure was applied on the infill surface using the same approach as described above. In all cases, the LVDT (LVDT 8) mounted at the center of the bounding frame top beam indicated that there was negligible out-of-plane displacement (< 1 mm) of the frame top beam during the out-of-plane loading of the infills. The out-of-plane pressure vs. displacement curves for IFNG, IFW16, IF-D1 and IF-D2

obtained from the experiments and FE models are compared in Figure 5.11 with the out-of-plane strengths indicated in the figure. The node with the largest recorded (by LVDTs) out-of-plane displacement was chosen for the plots.

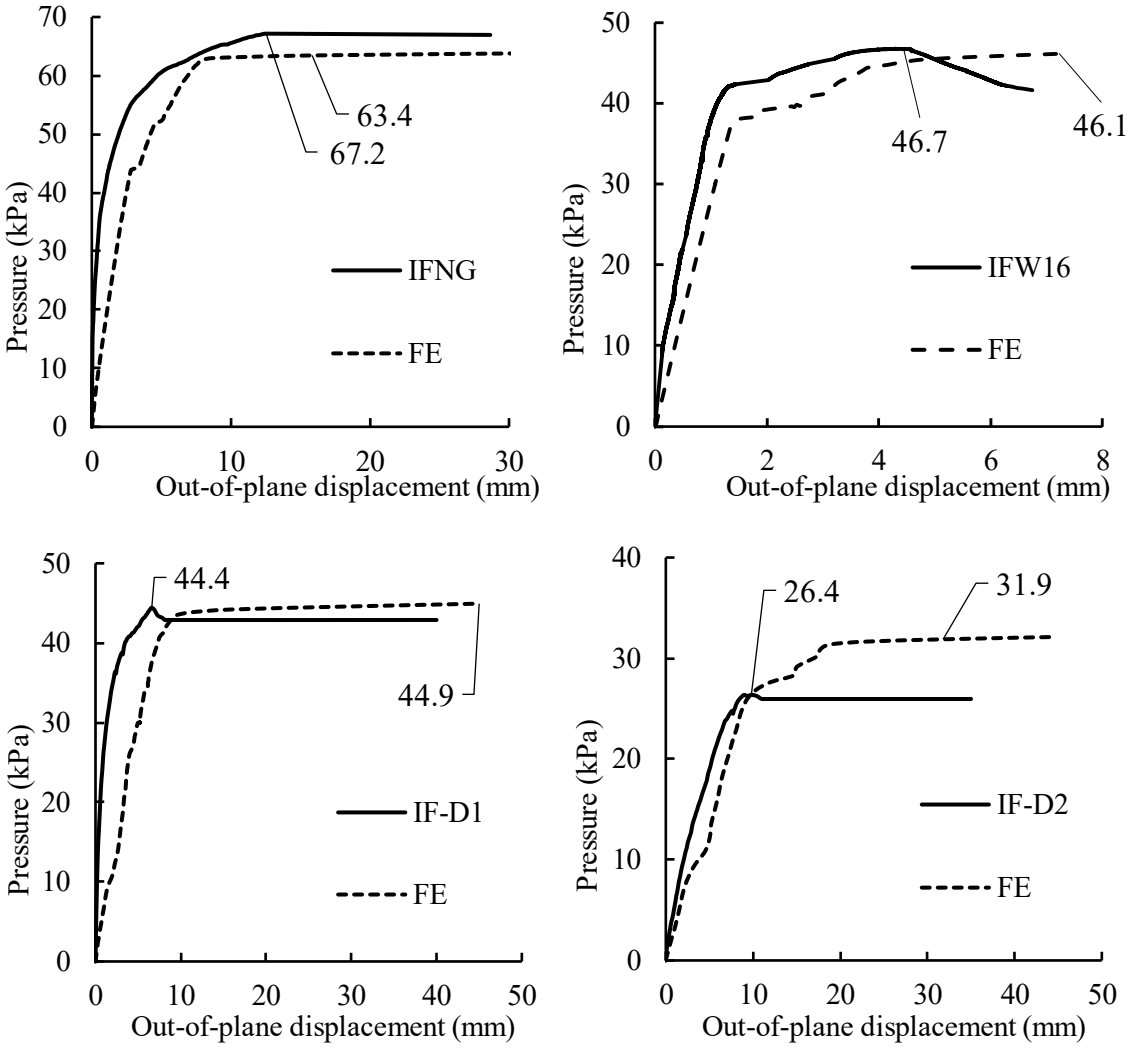

Figure 5.11. Comparison of out-of-plane pressure vs. displacement curves obtained from tests and FE analysis

The FE load vs. displacement responses compare reasonably well with the experimental curves and the potential reasons for some discrepancies are explained in the following. One, the FE initial stiffness, in general, was lower than the experimental result. The "softer" FE predicted response is believed to be attributed to several factors including the

use of reduced integration elements, reduced elastic modulus used in steel reinforcements to account for bond-slip, and the manner that the contact was modelled in the FE method. In this study, the contact behaviour between CMUs was essentially modelled with "springs" (Figure 5.9). The stiffness of these springs was adjusted during analysis to limit the penetration of the two contacting CMU surfaces based on a set penetration tolerance value, an approach referred to as "penalty method" in ABAQUS. Although this value is set to be very small, it needs to be simulated in all mortar joints throughout the height and width of the infill, and the accumulated effect causes the infill to be less stiff than the actual situation. This discrepancy can be reduced to certain degree by assuming a much higher spring stiffness or a smaller penetration tolerance value or using a finer mesh but all at the expense of a significant increase in computing time. Since the overall response trend and the ultimate load compare well with the experimental results, it is felt that the assumption used in this study achieved a balance of reasonable accuracy and computing efficiency. Second, the most significant difference in response was observed in IF-D2. This deviation is believed to be attributed to inherent weakness of the finite element model in general in handling excessive deformations. As in this case, large diagonal cracks and crushing of the infill which have occurred during the in-plane loading stage caused large distortions in the elements, resulting in lower accuracy in the out-of-plane simulation. It should be pointed out that same values of the input parameters were used for all specimens and no "tweaking" of these values was performed to achieve a "perfect" fit for each specimen. Although there is some less than "perfect" fit in the curves, it is felt that the comparison has demonstrated the robustness and efficacy of the model.

To provide some insight on the performance of exiting analytical methods, the analytical out-of-plane capacity of the control specimen IFNG was determined using TMS 402/602-16 method and the arching method presented in Drysdale et al. (1994). They were determined to be 86.8 kPa and 109 kPa, respectively. In comparison with the experimental capacity of 67.2 kPa, the disparity is significant. This underscores the necessity for further research.

Figure 5.12 shows the deformed geometry, cracking pattern, and compressive crushing obtained from the experiments and FE model for IFW16. Figure 5.12(a) shows the tensile cracking regions on the loading surface of the infill and Figure 5.12(b) shows the compressive crushing regions in the mid-plane of the infill, which was made possible by 3D modelling for the stress distribution through the thickness of blocks. The red regions shown in the FE results indicate stresses beyond the cracking or compressive strength whereas the green regions indicate that cracking and crushing was about to occur. It shows that the FE model accurately simulated the cracking formed and developed in the infill and RC frame. Figure 5.12(b) indicates that collapse was initiated through shear failure of the infill webs. A close-up view obtained from the FE simulation in Figure 5.13 agrees with experimental results showing cracking development through the web of the units.

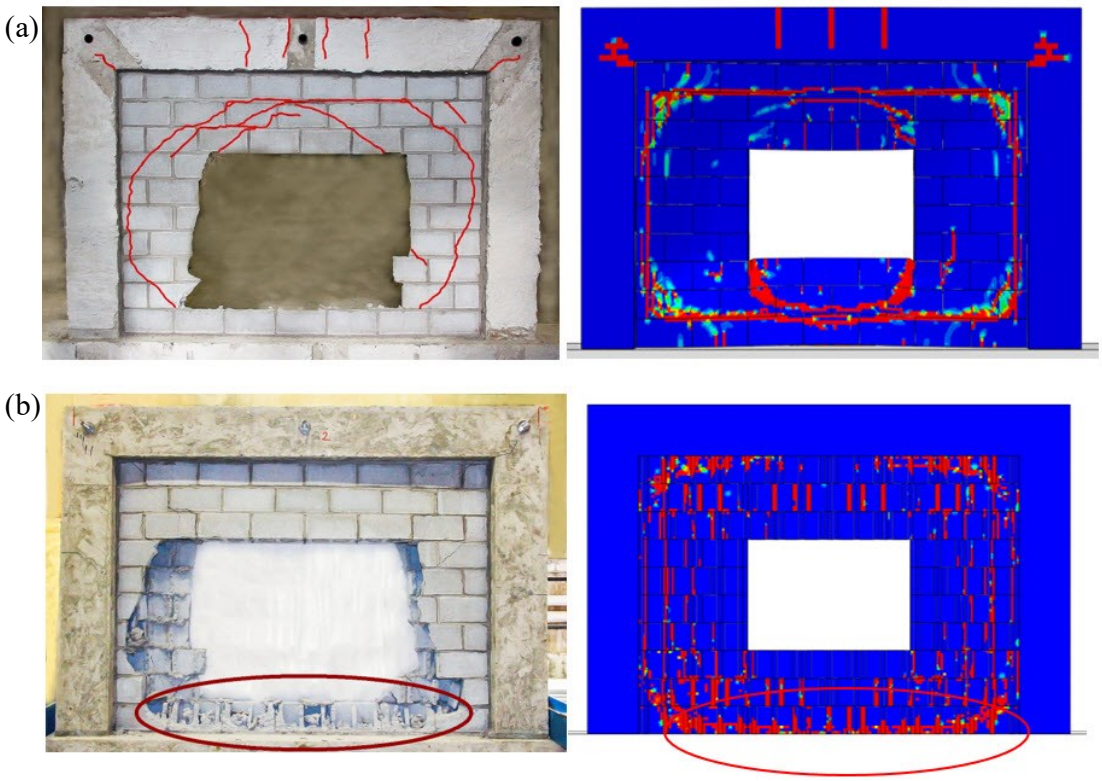

Figure 5.12. Comparison of FE and experimental results for IFW16: (a) tensile cracks on the windward face and; (b) compressive crushing in the mid-plane of the infill

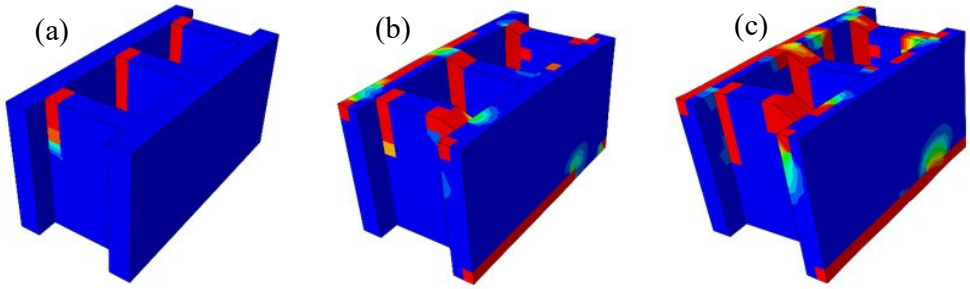

Figure 5.13. Development of cracks in the CMU blocks: (a) initiation of cracking; (b) at the ultimate capacity of the infill; and (c) after collapse of the infill

5.6 Parametric Study

In this section, the influence of several parameters on the out-of-plane behaviour and strength of infilled RC frames are studied. The parameters selected are believed to be

influential to arching action and failure mode of the infill but with limited studies available in literature. They included infill aspect ratio, bounding frame stiffness, infill slenderness ratio, size and aspect ratio of the infill opening, frame-to-infill interfacial gap, and web thickness of the CMUs.

For the reference model, the RC frame consisted of 400 mm square members with the bottom beam fully restrained to simulate the rigidity of a foundation beam. The infill was constructed with standard 200 mm concrete masonry units and Type S mortar. The web thickness of the CMU is assumed to be 30 mm. The design of the concrete frame was based on CSA A23.3-14 in compliance with requirements for minimum flexural and shear reinforcement, reinforcement spacing, and concrete cover. It was done to ensure that adequate ductility is provided, and no shear or brittle failure occurs during analysis. Unless otherwise specified, the material properties of masonry, concrete and reinforcement used in the parametric study are as shown in Table 5.4. It is also pointed out that these values are not the same as those used in the validation study.

Table 5.4. Material properties used for the parametric study

	Compressive strength (MPa)	Elastic modulus (GPa)	Tensile strength (MPa)
CMUs	20.0	20.0	2.0
Mortar	15.0	2.6	1.5
Concrete	35.0	30.0	3.5
Reinforcement	-	220.0	400 (600)*

* Yield and (ultimate) strength

5.6.1 Effect of Infill Aspect Ratio

Four different infill aspect ratios (*h/l*) equal to 1.40, 1.00, 0.70, 0.54, as shown in Figure 5.14(a), were considered. These values were selected to cover a wide range of infills in practice ranging from slender to squat infills. In all cases a tight contact between the infill and the frame members was assumed and their interface was assumed to have the same nonlinear interfacial model behaviour described in Section 3.2. The FE predicted deformation and cracking pattern of the models at failure is shown in Figure 5.14(b). It shows that for the studied aspect ratios, two-way arching action to different degrees developed. The exact extent and the associated cracking pattern are dependent on the aspect ratio of the infill. For a given infill height, as the aspect ratio decreases from 1.0 to 0.70 and to 0.54, the two-way action shifts increasingly towards one-way action in the vertical (short) direction, accompanied by a decrease in strength. It is also observed that as the aspect ratio decreases, the length of beam increases, resulting in an increasingly smaller stiffness (EI/L) for the top beam and thus less rigid support. Hence, it is believed that the effect of aspect ratio is also related to the stiffness of the frame. The normalized out-of-plane strength (with respect to model AR2) vs. infill aspect ratio is plotted in a solid line in Figure 5.15. It shows that the correlation between the decrease in the infill aspect ratio and the decrease in the out-of-plane strength is more or less in a linear manner.

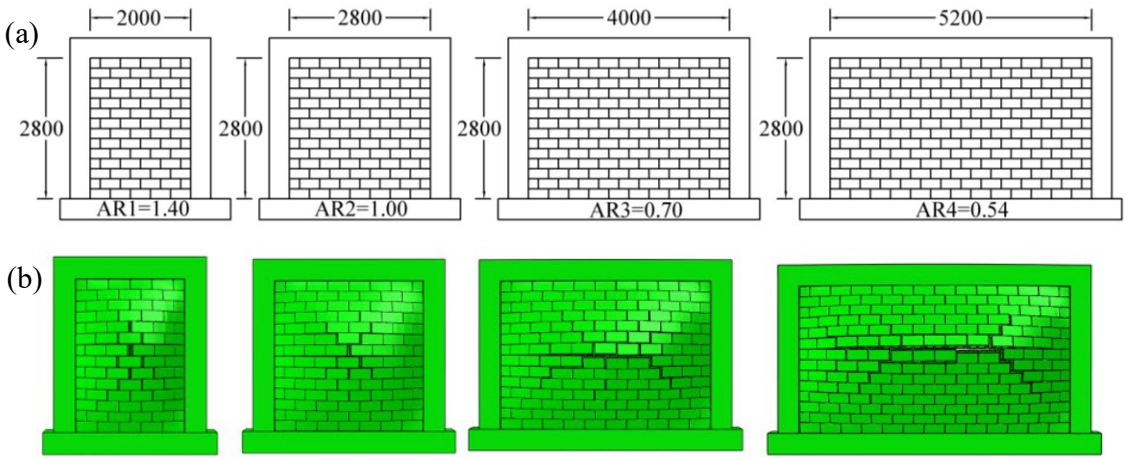

Figure 5.14. Infill aspect ratio study: (a) geometric configuration; and (b) failure mode for varying aspect ratios

5.6.2 Effect of Frame Stiffness

In the frame stiffness study, two steps were taken. First, the FE analysis was repeated on models AR1 to AR4 but with a fully rigid frame (stiffness approaches infinity). The results are plotted in Figure 5.15 in a dotted line where the normalized out-of-plane strength (with respect to model AR2) is used. It shows that when a rigid frame is assumed, the decreasing trend in the infill strength with the decrease in infill aspect ratio is still valid. However, the correlation is nonlinear. The out-of-plane strength is shown to be greater than that of the original frame. The degree of increase is the greatest for model AR4 with a 28% increase which is followed by model AR3 with a 14%, model AR1 with a 6% and model AR2 with a 3% increase. This confirms that the effect of infill aspect ratio is dependent on the bounding frame stiffness. As the original model AR4 has the lowest top beam stiffness, implementation of a rigid beam would result in the maximum strength increase. Secondly, while maintaining the aspect ratio, the FE analysis was repeated for all models with beam

and column dimensions changed to 400×250 mm (AR-W) and 400×550 mm (AR-S) respectively to simulate a weaker and stronger RC frame.

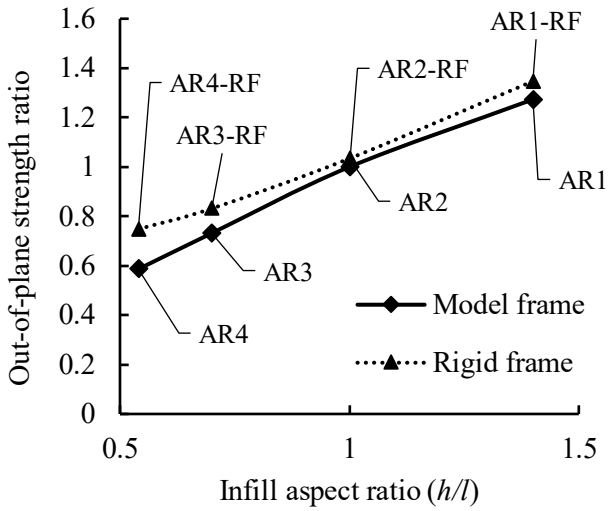

Figure 5.15. Effect of infill aspect ratio and frame rigidity on the out-of-plane strength

The normalized out-of-plane strength (with respect to the rigid model of each aspect ratio) vs. frame flexural stiffness (EI/L) is plotted in Figure 5.16. The least member stiffness of the frame is used to reflect both column and beam effect for various aspect ratios. The figure shows that the trend of infill strength increases as affected by frame stiffness is influenced by the infill aspect ratio. The rate of strength increase diminishes as frame stiffness increases. There appears to be a frame stiffness limit beyond which its benefit to infill strength is equivalent to a rigid frame and this limit is different for different aspect ratios. Deformation contours comparison between models AR4 and AR4-W plotted in Figure 5.17 further reveal that as bounding frame stiffness decreases, the failure mode of the infill changed from the horizontal cracking in model AR4 to inclined cracks between the bottom corners and the center of top beam in model AR4-W. This indicates that in model AR4-W, the top beam undergoes large deflections under arching forces and fails to

provide rigid support for the infill. Also noted is that the tight contact was assumed in both cases at the infill-to-frame interface and the nonlinear interface behaviour allows for separation of the contacting surfaces if the shear or normal failure is detected which is observed in Figure 5.17(b).

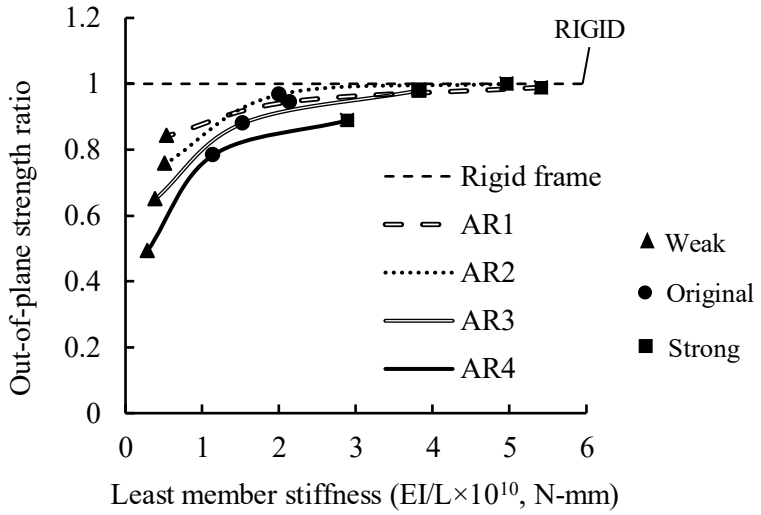

Figure 5.16. Effect of frame stiffness on the out-of-plane strength

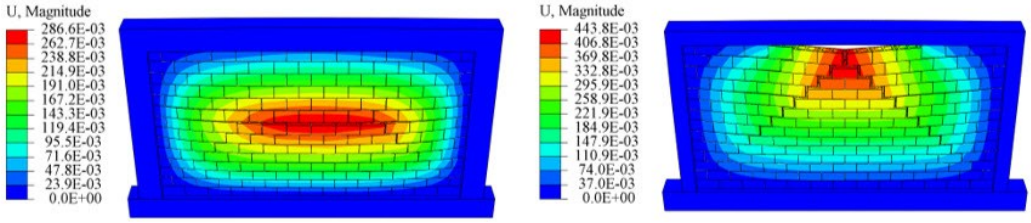

(a) 400×400 mm members (b) 400×250 mm members

Figure 5.17. Failure mode and deformation contours (unit: m): (a) AR4; and (b) AR4-W

5.6.3 Effect of Infill Slenderness Ratio

In this study, five different slenderness ratios (h/t) of 10, 14, 18, 24, and 30 were considered. The desired slenderness ratio was obtained by changing the height of infill while maintaining the infill CMU geometry. To eliminate the compounding effect of frame

stiffness due to changing the infill height, the FE analysis was first carried out assuming fully rigid frames. The resulted out-of-plane pressure vs. slenderness ratios curves are plotted in Figure 5.18(a) for four aspect ratios (h/l) of the infill. The figure shows that the slenderness ratio effect is dependent on the infill aspect ratio. For a given aspect ratio, an increase in slenderness ratio resulted in an exponential decrease in the out-of-plane strength. While the reduction trend was similar for all aspect ratios, the difference is noted that for a given slenderness ratio, infills with a higher aspect ratio (slender infills) attained a higher strength than squat infills, and this increase in strength is most pronounced in the low slenderness region. Next, the FE analysis was carried out on the model frame (400 mm square sections for both beams and columns) as specified in the parametric study and the results for a square panel (h/l=1) are shown in Figure 5.18(b). It shows that the slenderness ratio effect is also dependent on the stiffness of the bounding frame. For the model frame, while the general exponential decreasing trend in strength as slenderness increases remains valid, when compared with the fully rigid frame, the strength reduction is increasingly significant for the higher slenderness region ($h/t>15$). In the lower slenderness region ($h/t<15$), the reduction trend between the fully rigid and the model frame is nearly identical, it is reasonable to deduce that the larger strength deviation observed in the higher slenderness region is mainly due to the decrease in frame stiffness as a result of infill panel size increase rather than the reduction in frame member section size.

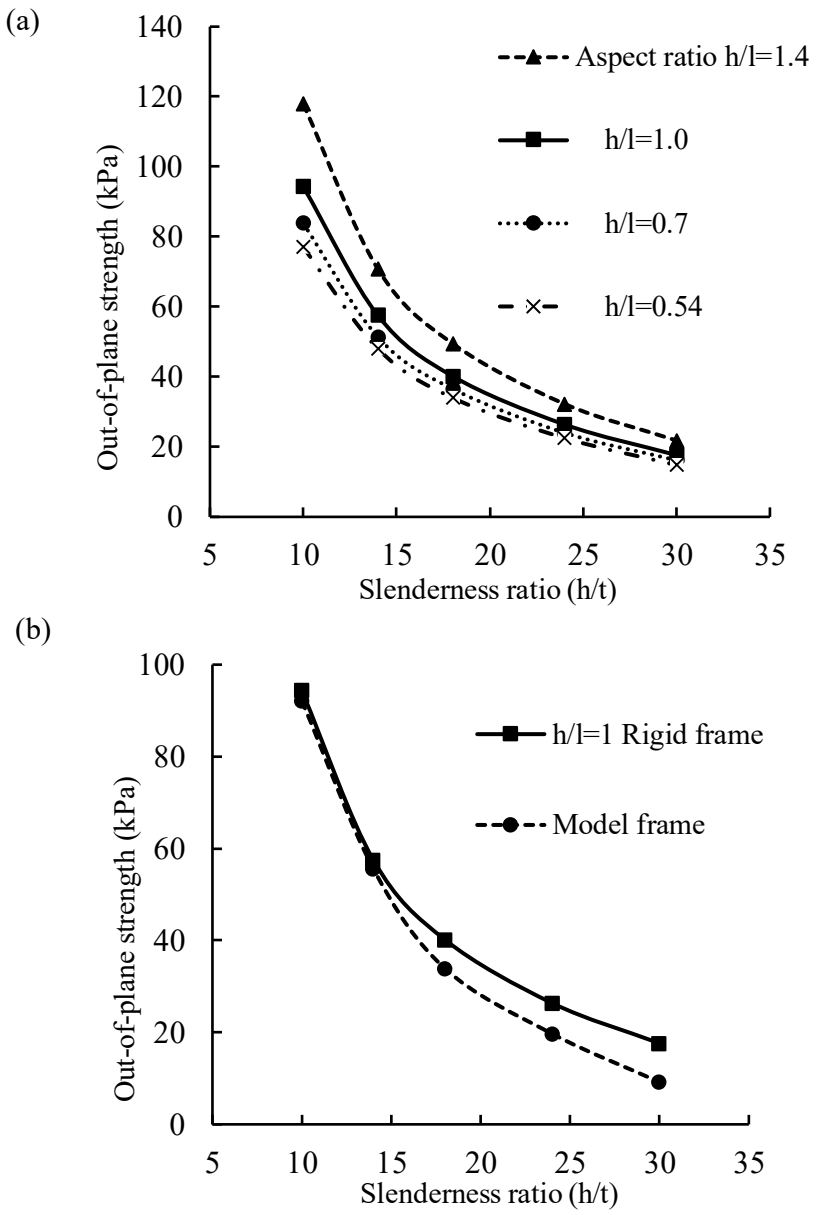

Figure 5.18. Slenderness ratio study: (a) out-of-plane pressure vs. slenderness for varying aspect ratios; and (b) out-of-plane pressure vs. slenderness for rigid and model frames

Figure 5.19 further demonstrates cracking regions (in red) observed at the mid-plane of the infill for the slenderness ratio study. A comparison of Figure 5.19(a) and (b) indicates that for a rigid bounding frame, the failure is characterized by shear cracking through the webs of CMUs around all four boundaries with little development of bending induced tensile

cracks; and for a flexible frame, the tensile cracks developed as indicated by the inclined cracks although the final failure is still characterized as shear cracking through the webs of CMUs. A comparison of Figure 5.19(b) and (c) shows that for a given bounding frame, as the slenderness of infill increases, the cracking pattern shifts from a predominantly shear cracking developed through the webs of CMUs in the vicinity of top and bottom boundaries to a yield line pattern initiated by tensile cracks along the diagonal lines as a result of more flexural behaviour. The damage on the frame is increasingly developed as the slenderness increases.

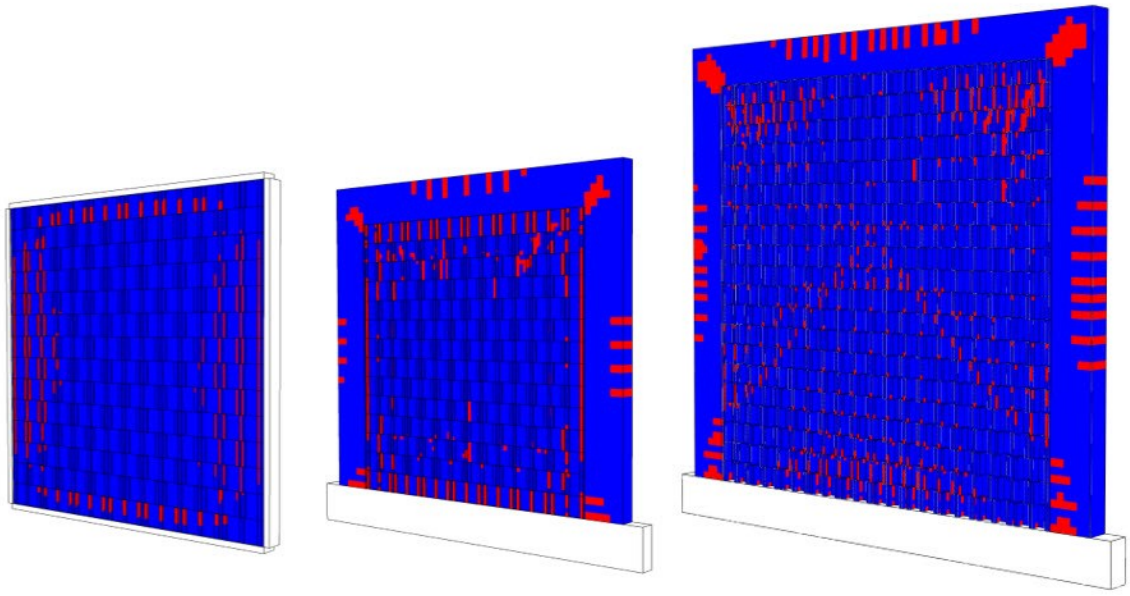

(a) h/t=14, rigid frame (b) h/t=14, model frame (c) h/t=20, model frame

Figure 5.19. Cracking patterns shown at mid-plane of infill at ultimate pressure for slenderness ratio study: h/l=1

5.6.4 Effect of Size and Aspect Ratio of Openings

Three opening sizes representing 13%, 23%, and 36% of the infill area while having the same opening aspect ratio (h_0/l_0=1) were considered on model AR3 as shown in Figure 5.20(a). Figure 5.20(b) plots the normalized strength of infills with openings with respect to the corresponding solid infill vs. opening area ratio. The figure indicates that the infills with openings attained higher strengths than the solid infills and the larger the opening, the higher the strength. The rate of strength increase as a function of opening area ratio appears to be linear for opening areas investigated. This finding, in line with observation made by Mays et al. (1998), is believed to apply to non-blast resisting openings where the out-of-plane pressure was only applied to the solid parts of the infill and no force was applied to the opening area. This results in a reduction in the total force applied to the infill as well as the area available for arching. In the case of a blast-resisting opening, the opening study was repeated for models OS1 to OS3 where the pressure acting on the opening area was simulated as a line load on the boundary of the opening. The results in terms of normalized strengths are also plotted in Figure 5.20(b). It shows that for blast resisting opening, the presence of opening results in a strength reduction around 20%, and this reduction seems to remain more or less the same for three opening sizes considered.

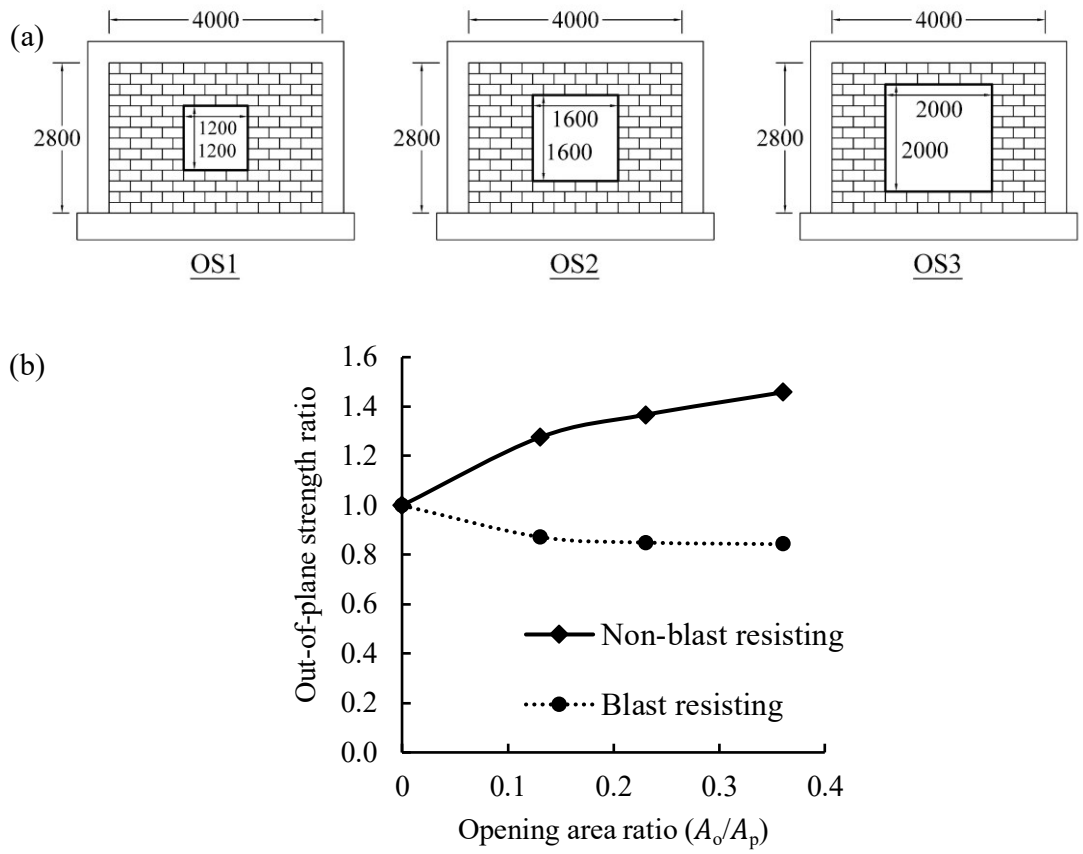

Figure 5.20. Infill opening size study: (a) geometry of models with different opening sizes; (b) normalized strength vs. opening area ratios

For opening aspect ratio study, three aspect ratios (h_0/l_0=1, 0.65, 1.54) were considered while maintaining an opening-to-infill area ratio of about 23%, as shown in Figure 5.21(a). The out-of-plane pressure vs. displacement curves plotted in Figure 5.21(b) show that the out-of-plane responses of models OAR1 and OAR2 through the loading history were almost identical with similar ultimate strengths (55.6 vs. 56.5 kPa), while the model OAR3 showed softening in the response at earlier loading and reached a strength at 46.3 kPa. The lower strength for model OAR3 is believed to be associated with the orientation of the opening in relation to the infill. In this case, the long side of the opening is perpendicular to the long side of the infill and thus the available bandwidth (masonry below and above

the opening) in the vertical direction is more significantly reduced when compared to model OAR2.

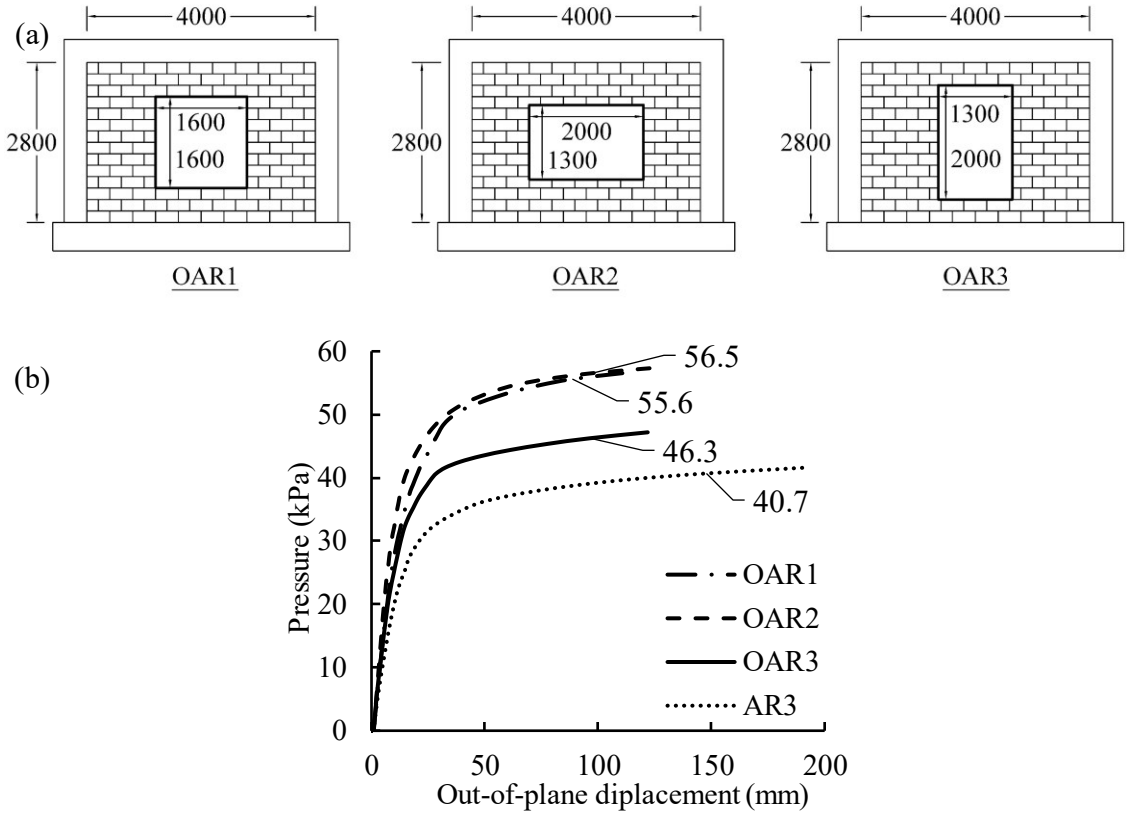

Figure 5.21. Infill opening aspect ratio study (FE results): (a) geometry of models; and, (b) out-of-plane pressure vs. displacement curves

Cracking pattern in these cases at the out-of-plane pressure of 42.0 kPa is shown in Figure 5.22. It can be seen that in the case of model OAR3, extensive cracking on the top beam indicates that the main load transfer direction is towards the top beam and vertical arching is the main load resisting mechanism. Infill cracks are more concentrated at two sides of the opening towards the column regions. The results suggest that the effect of infill opening area on ultimate strength also depends on the opening aspect ratio. For a given opening area, the opening with an aspect ratio closer to the infill aspect ratio is the least detrimental

to the out-of-plane strength of the infill. It is noted that the above observations and discussions are only intended for central window opening cases and are not directly applicable to the case of door openings and offset openings.

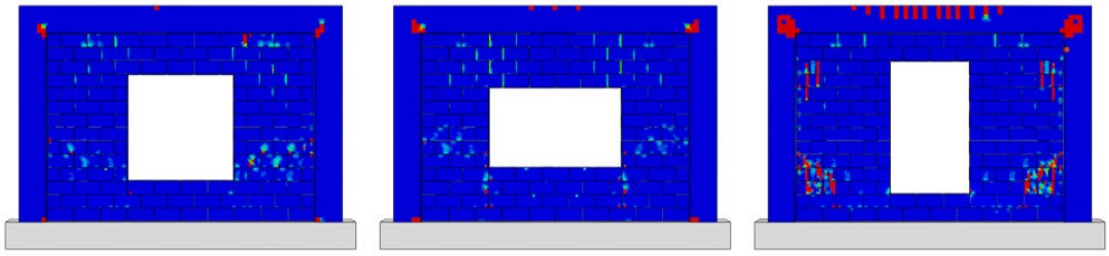

Figure 5.22. Cracking pattern for different opening aspect ratios at 42 kPa pressure

5.6.5 Effect of Interfacial Gaps

Gaps at the frame-to-infill interface are not uncommon due to shrinkage or settlement of masonry wall or defective workmanship in construction. As infills may rely on arching action for their out-of-plane resistance, the interfacial gaps could conceivably influence the arching action and thus change the out-of-plane response of infilled frames. In this study, three gap scenarios on model AR3 were considered, including: 1) a gap between the infill and the top beam of the frame (labeled as BG); 2) gaps between the infill and the frame columns (labelled as CG); and 3) a full separation gap at the frame and the infill interfaces (labelled as AG). Gaps were introduced into the model by creating actual separation between the infill and the frame. This was achieved by increasing the length of the columns or beam and knowing that the maximum gap size is 6 mm, the increase in the frame size would not have any significant influence on the behaviour of the frame. When these surfaces become in contact, a Coulomb friction criterion (described in 3.2) controls the shear behaviour of the contact. The presence of gap at either frame beam-to-infill (BG) or

frame column-to-infill interface (CG), regardless of the size, will reduce a potential two-way to one-way arching action in the direction (Dawe and Seah 1989b). Presence of gap (regardless of size) will reduce the frame member to zero stiffness at the gap location. Hence, when the out-of-plane pressure is applied, the infill will crack in the direction perpendicular to the gap and all the out-of-plane pressure will be transferred to the side with tight contact (high stiffness boundary) through arching action. However, in the case of a full separation gap (AG), depending on the gap size, one-way arching may still develop after some degree of overturning of the infill. To confirm this theory, three gap sizes of 2, 4, and 6 mm for each gap scenario were considered and, in each model, the gap size was assumed to be present at each interface involved.

The out-of-plane pressure vs. displacement curves for all three gap cases applied to model AR3 are shown in Figure 5.23(a). The figure confirms that for BG and CG cases, all considered gap sizes (identified as 1, 2, and 3 for 2, 4, and 6 mm in the figure) yielded identical load-displacement curves and the ultimate strength (only 2 and 4 mm are plotted for clarity) whereas for AG case, the ultimate strength and behaviour are dependent on the gap size. Further, for the given infill, the column gap is the least detrimental to the out-of-plane strength, and the full separation gap results in the most out-of-plane strength reduction. A sharp increase in stiffness observed in response curves of all AG gap cases indicates the engagement of infill with the frame after a certain amount of rotation of the infill. As the gap size increases, the rotation of infill required for making contact with the frame increases and the ultimate strength decreases. For BG and CG gap cases, a much greater initial stiffness indicates that engagement of the infill occurred at the onset of loading, albeit in only one direction. Figure 5.23(b) plots the normalized strength variation

vs. gap size for all three gap cases where the strength is normalized with respect to model AR3 without gaps. The reduction in strength for AG gap case is not linear and rather, the rate of reduction diminishes with an increase in the gap size. For BG and CG gap cases, reductions are 54% and 48%, respectively and they are independent of gap sizes.

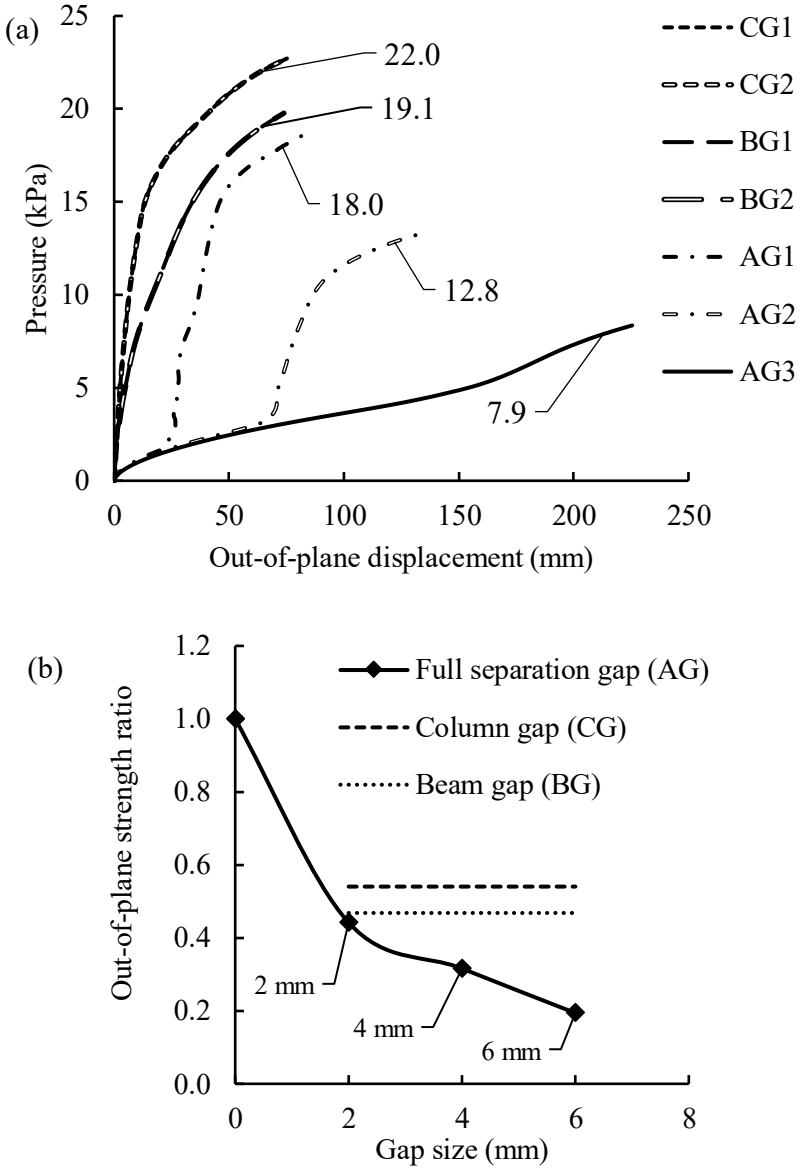

Figure 5.23. Interfacial gap study: (a) out-of-plane pressure vs. displacement curves; and (b) normalized strength for different gap sizes/locations

It is reasonable to deduce that the gap related strength reduction is dependent on the infill aspect ratio as the arching action is developed in one direction. To further demonstrate the gap effect, the gap size of 6 mm was also applied to models AR1 to AR4 for BG and CG cases. The results are plotted in Figure 5.24 where the strength is normalized with respect to model AR3 without gaps. It confirms that the gap effect is dependent on the infill aspect ratio and both gap cases, in general, result in increasingly greater strength reduction as the infill aspect ratio decreases. It is noted that below certain aspect ratio, approximatley 0.85 in this case, the CG case shows higher strength and the trend reverses as the aspect ratio exceeds 0.85. The manner by which two gap cases affect infill strength is believed to be associated with two factors, geometry of the CMUs in the vertical and horizontal directions and boundary conditions for BG and CG cases. The number of CMUs and the configuration of blocks in the vertical and horizontal directions are different. In the case of column gap, the shear stress transfer in the vertical direction is through the web length while in the case of beam gap, the transfer in the horizontal direction is through the web thickness, which makes the beam gap more detrimental to strength reduction from shear stress transfer standpoint. On the other hand, the compressive stresses for column gap case are developed at the two beam-to-infill interfaces while for beam gap case, compressive stresses were also developed at the bottom beam-to-infill interface as shown by the FE compressive stress contours in Figure 5.25. This additional boundary support provides potential strength increase for beam gap case than column gap case. It is reasoanble to deduce that at a certain aspect ratio, the two effects achieve a balance and beam gap and column gap result in the same strength reduction. Away from this aspect ratio, the strength reduction depends on which factor predominates. Also shown in Figure 5.24 is the comparison between the BG

and CG gap cases and no-gap case (plotted in a solid line) which suggests that two-way arching action results in greater out-of-plane strengths by an average of 180% than one-way arching.

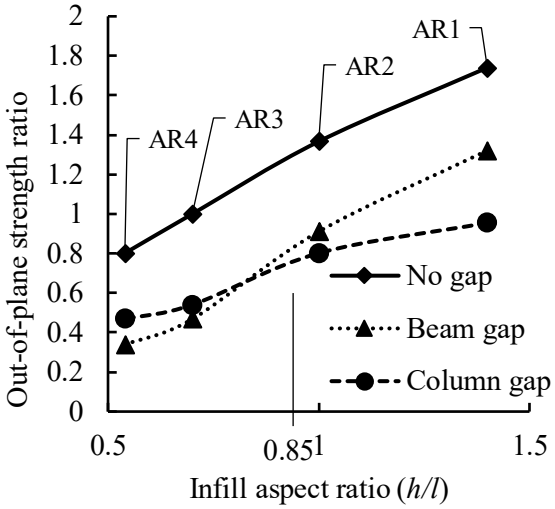

Figure 5.24. Effect of beam gap and column gap on the infills with different aspect ratios

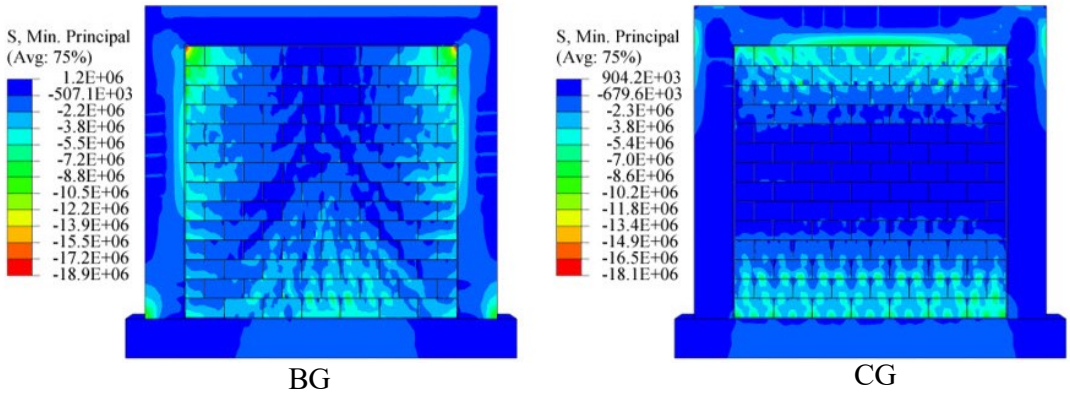

Figure 5.25. Maximum compressive stress contours (unit: N/m^2) for model AR2 with gaps at 32 kPa out-of-plane pressure

5.6.6 Effect of CMU Web Thickness

It was observed in the model validation stage that the failure of infill after development of arching was initiated by cracking in the webs of the CMUs. The infill slenderness section

also suggests that web failure in the CMUs predominates for infills with intermediate or short slenderness. In this section, two additional CMU web thicknesses of 20 and 40 mm implemented to model AR3 were studied. The normalized out-of-plane strength with respect to model AR3 (30 mm web) vs. web thickness is illustrated in Figure 5.26. The figure shows that for a given slenderness, an increase in the web thickness of CMUs results in an increase in the ultimate out-of-plane strength.

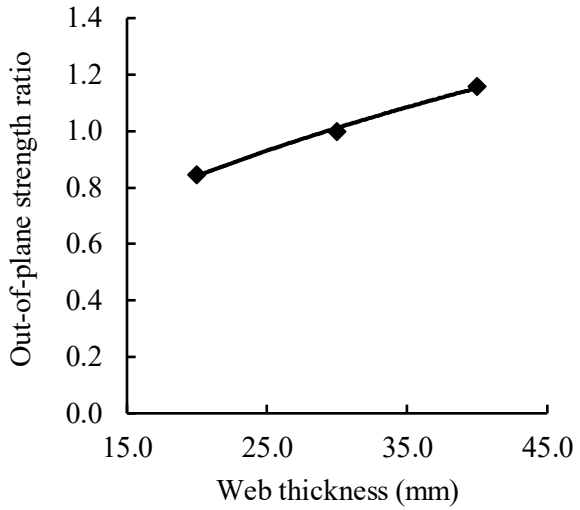

Figure 5.26. CMU web thickness study: normalized strength vs. web thickness

A close-up view on the cracking development of one CMU from the bottom course of infill is shown in Figure 5.27 for the three web thicknesses. It indicates that the extent of cracking (shown in red) is much greater in CMUs with thinner webs. It should be noted that at this pressure no cracking or crushing was observed in the face shells of CMUs, indicating that failure was initiated by cracking of the webs. Thus, when the infill failure is caused by shear failure of the webs of CMUs, using CMUs with thicker webs can significantly increase the out-of-plane strength of the infill wall. Note that either flange taper or web flare was not considered, and the constant flange and web thickness was assumed in the

above analysis. However, since the failure is governed by web shear failure rather than crushing of the flanges, the web flare is conceivable to lead to a higher infill capacity than a constant web thickness. The flange taper, on the other hand, is not considered to be as influential. The relationship presented above can then be considered on the conservative side.

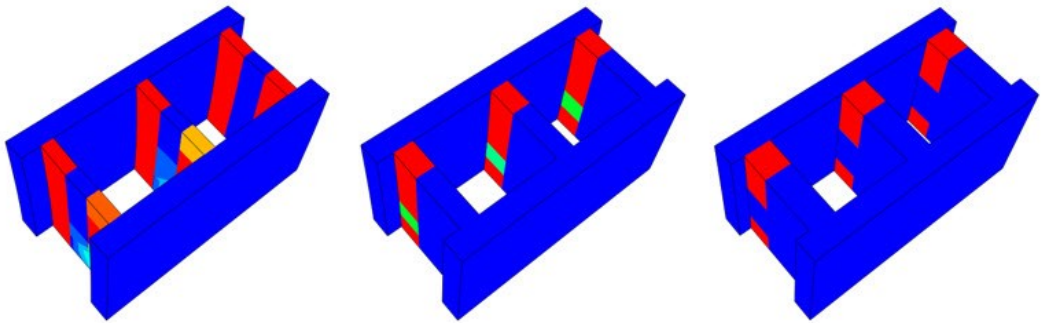

Figure 5.27. Cracking development in the webs of different thickness at 30 kPa out-of-plane pressure

5.7 Conclusion

A finite element study was performed to investigate the effect of several critical geometric parameters on the out-of-plane behaviour and strength of concrete masonry infills bounded by RC frames. A three-dimensional finite element model was developed for this purpose and its accuracy and effectiveness were verified using test results of a concurrent experimental program on four masonry infilled RC frame specimens. Conclusions from this study are as follows:

- The 3D model developed is capable of producing accurate ultimate strength results and simulating reasonably well the load vs. displacement behaviour. The model is

also capable of providing detailed stress distribution, crack pattern and failure modes that may not be fully predicted by a 2D model.

- For a given infill height, a reduction in the aspect ratio (*h/l*) results in a significant reduction in the out-of-plane strength. The degree of this reduction is associated with the bounding frame stiffness. The higher stiffness of the bounding frame, the lower rate of the reduction.
- For a given infill aspect ratio, the bounding frame flexural stiffness is influential in the infill strength by ensuring the arching action. A correlation between the frame flexural stiffness and the infill strength was suggested.
- For a given infill aspect ratio, an increase in the infill slenderness (*h/t*) results in an exponential decreasing trend for the infill strength. The failure mode was shown to shift from a yield line pattern for high slendernesses to a web-shear failure pattern for low slendernesses.
- When compared with the infills without openings, the infills with non-blast resisting openings are shown to have higher strengths while infills with blast-resisting opening are shown to have lower strengths. The strength increase for the former opening is a function of opening size while the strength decrease for the latter opening remains almost constant for varying opening sizes.
- For a given gap size, the full separation gap results in the most significant reduction in infill strength. The reduction as a result of the beam gap or column gap does not depend on the gap size, rather, it depends on the infill aspect ratio. The aspect ratio at which the beam or column gap results in the same reduction in infill strength was identified.

- Both experimental and FE results in this study showed that for certain range of infill slenderness, failure of the infills is initiated by cracking developed in the CMU webs, rather than compressive crushing of masonry. In this case, increasing the web thickness of CMUs results in a marked increase in infill strength. A relationship between the web thickness and infill strength was proposed.

5.8 Acknowledgement

The authors wish to recognize the contribution of financial assistance by the Canadian Concrete Masonry Producers Association and Natural Sciences and Engineering Research Council of Canada.

Chapter 6 Study of Arching Behaviour and Strength of Concrete Masonry Infills under Out-of-Plane Loading

Ehsan Nasiri, Yi Liu

Published in Canadian Journal of Civil Engineering

https://doi.org/10.1139/cjce-2018-0662

6.1 Abstract

A numerical study using a three-dimensional finite element model was conducted to investigate the arching behaviour and strength of concrete masonry infills bounded by RC frames subjected to out-of-plane loading. Physical specimens were concurrently tested to provide results for validation of the model as well as evidence of directional characteristics of arching behaviour of masonry infills. A subsequent parametric study using the model included a wide range of infilled frame geometric properties. The results showed in detail the difference in one-way and two-way arching in terms of both strength and failure mechanism, and the contributing factors to this difference. Evaluation of the two main design equations for out-of-plane strength of masonry infills led to proposal of modifications to provide a more rational consideration of directional behaviour of concrete masonry infills. A comparison study using the available test results showed a marked improvement of strength prediction based on the proposed modification.

Keywords: concrete masonry infills; RC frames; out-of-plane; strength; finite element; arching action; nonlinear analysis

6.2 Introduction

Masonry walls, when constructed within either a reinforced concrete (RC) or steel frame, are often referred to as masonry infills. It is well recognized that the behaviour and failure mode of masonry infills under loading are affected by confinement provided by the bounding frame and thus are different from those without confinement. In the context of out-of-plane behaviour, masonry infills were shown to be able to attain much higher capacity than their flexural wall counterparts (Abrams et al. 1996, Anderson 1984, Dawe and Seah 1989b, Flanagan 1994, Gabrielsen and Kaplan 1976). While the conventional flexural walls derive their ultimate capacity through masonry tensile strength, masonry infills were shown to develop a large portion of their capacity after tensile cracking which indicates a different failure mechanism. This mechanism, known as "arching", was first taken into account by McDowell et al. (1956a) for analysis of out-of-plane strength of infills. Their model proposed that subsequent to flexural cracking, the rotation of cracked segments of the infill panel is restrained by the bounding frame, creating in-plane compressive forces which delay further cracking and thus increase the ultimate capacity. In their model, the capacity was related to the compressive strength of masonry instead of tensile stresses as in the case of flexural walls, and slenderness ratio of the infill, as shown in Eq. (6.1).

$$q_u = \frac{\gamma f'_m}{2(\frac{h}{t})^2} \tag{6.1}$$

where γ is a function of *h/t* ratio and f'_m is the compressive strength of masonry.

Stemming from the basic arching concept, two main approaches have been developed and become widely referenced analytical methods for calculating the out-of-plane strength of masonry infills. Both were adopted in different design standards in North America, albeit with some modifications. One was initially proposed by Dawe and Seah (1989b) where they expanded McDowell et al.'s method to include two-way arching and also introduced the boundary frame stiffness as an influential parameter in the strength calculation. The model combined the arching action with the plate yield-line theory and assumed the compressive crushing of masonry as the failure mode for ultimate capacity calculation. They proposed the following equations to calculate the ultimate out-of-plane capacity q_{ult} for two situations of infills.

$$q_{ult} = 4.5(f'_m)^{0.75} t^2 \alpha / L^{2.5} \quad \text{(infill panel bounded on three sides and top side is free)} \tag{6.2}$$

$$q_{ult} = 4.5(f'_m)^{0.75} t^2 \{\alpha / L^{2.5} + \beta / H^{2.5}\} \quad \text{(infill panel bounded on four sides)} \tag{6.3}$$

and,

$$\alpha = {}^{1}/_{H} (E I_c H^2 + G J_c t H)^{0.25} \leq 50 \ (\leq 75 \text{ for panel bounded on three sides}) \tag{6.4}$$

$$\beta = {}^{1}/_{L} (E I_b L^2 + G J_b t L)^{0.25} \leq 50 \tag{6.5}$$

where *t, L*, and *H* are the thickness, length, and height of the infill panel. Parameters α and β are factors accounting for the stiffness effect of boundary frame where E and G are the Young's modulus and shear modulus of the frame members respectively, and *I* and *J* are the moment of inertia and torsional constant of the frame members with subscript *b* and *c* indicating beam and columns respectively. An upper limit is set for α and β, indicating

that the effect of boundary frame stiffness diminishes as the stiffness becomes greater and at the set limit, the frame can be considered as rigid. The method also provides simple treatment for gaps at frame-to-infill interface, by setting α or β equal to zero for frame-column or frame-beam gap, respectively.

Flanagan and Bennett (1999a) suggested that for most practical frames, the GJ_ctH and GJ_btL terms in Dawe and Seah's method are much smaller than the EI_cH^2 and EI_bL^2 terms. Thus, they eliminated the torsional terms (GJ_ctH and GJ_btL) in their method while maintaining the remaining of the strength formulation of Dawe and Seah's method with a small change of constant (4.5 to 4.1). Flanagan and Bennett's simplified formulation was adopted in the current American masonry design standard TMS 402/602-16 for design of masonry infills subjected to out-of-plane loading.

The second main approach for calculating out-of-plane strength based on arching was proposed by Angel et al. (1994). Their analytical model was developed considering both compressive crushing of masonry at the boundaries and snap-through of the panel due to buckling as potential failure modes for smaller and larger slenderness ratios. The contribution of the model was to include prior in-plane damage effect in the out-of-plane capacity calculation. The method is expressed as follows:

$$q = \frac{2f'_m}{(\frac{h}{t})} R_1 R_2 \lambda \tag{6.6}$$

$$R_2 = 0.357 + 2.49 \times 10^{-14} EI \leq 1.0 \tag{6.7}$$

$$\lambda = 0.154\exp\left(-0.0985\frac{h}{t}\right) \quad (6.8)$$

The term R_1 is a reduction factor for prior in-plane damage; R_2 is a reduction factor accounting for bounding frame stiffness where EI is the least flexural stiffness of the bounding frame members; and λ is a function of h/t. Note that this design equation was originally formulated based on a one-way arching mechanism but was calibrated using two-way arching tests on infills with 1.5 aspect ratio for the constant terms in the equations. This method was adopted with some modification by FEMA-356 (2000) and ASCE/SEI41-13. (2013) "guideline for the seismic rehabilitation of buildings".

A close examination of the two methods identified the following issues. In the case of Dawe and Seah's method, the two-way arching strength is simply a summation of vertical and horizontal arching strengths which are calculated in a same manner. Therefore, for infills with *h/l=2* and *h/l=0.5*, the out-of-plane capacity would be equal for a given infill material property and frame section. This raises a question since the masonry, in general, shows a pronounced directional behaviour under compression and shear. Further, the boundary conditions for infills in the vertical and horizontal directions are not likely to be the same, which will conceivably result in different strengths in the vertical and horizontal directions. In the case of Angel et al.'s method, the contribution from horizontal direction arching is totally ignored as the equation is solely dependent on *h/t*. Also, the stiffness factor is expressed only in terms of *EI* values of frame members and the length effect on stiffness is not explicitly considered.

The performance of the above presented two main approaches was evaluated in several studies (Flanagan and Bennett 1999a, Pasca et al. 2017, Ricci et al. 2018) using

experimental results available in the literature. It should be pointed out that the results on out-of-plane tests of masonry infills were, in general, limited and those reported in the literature were of a great variety in terms of masonry infill type and its mechanical property, bounding frame type and condition, and out-of-plane load application method. With that in mind, it is not surprising that the three studies yielded significantly different mean values of experimental-to-analytical strength ratios with high coefficient of variations for both methods. However, the general conclusions can be drawn as follows. Overall, Dawe and Seah's method provided closer estimates to the test results especially for steel framed masonry infills. Performance of both methods for RC framed infills was inconclusive as so few results were available. The level of COVs for both methods (as high as 70%) suggests a large scatter in estimated capacities vs. experimental results, indicating neither method can provide estimates for a variety of infill and frame properties with consistent accuracy. Pasca et al. (2017) recognized that it may not be possible to have one equation that can be universally applicable to all types of masonry infills and frames and more reliable results, both numerical and experimental, were needed to provide a more thorough assessment of analytical models.

In view of the above, the aim of this study was to assess validity of the two main analytical methods for calculating out-of-plane strength of masonry infills through an extensive finite element study. Concrete masonry unit (CMU) infills were used as they are a primary infill material used in Canada. The focus of the assessment was to understand one-way and two-way arching and the relationship between the two in influencing the out-of-plane strength of RC framed concrete masonry infills. A 3D finite element (FE) model was used for simulation of behaviour of masonry infilled RC frames of varying parameters. The model

was thoroughly validated using results of a concurrent experimental program. Three specimens' results were presented and discussed in detail to demonstrate the model's capability as well as to provide experimental evidence of relationship between the one-way and two-way arching. A subsequent parametric study focusing on several critical geometric parameters was conducted using the model and the results were used to propose modifications to an existing analytical model for out-of-plane strength calculation.

6.3 Finite Element Modelling Method

A three-dimensional FE model was developed to simulate the behaviour of the concrete masonry infills bounded by RC frames. The development of the model and its validation using test results of infilled frames under in-plane and out-of-plane loading are described in detailed in Nasiri and Liu (2017, 2019a) and thus are not repeated herein. The following however, provides a summary of some key modelling aspects of various components of masonry infilled RC frames. The masonry infill was modeled as ungrouted and mortar was assumed to be applied through both bed and head joints. The "simplified micro-modelling" technique (Lourenco 1996) was used where the mortar joints were not physically modeled and the CMU dimensions were thus increased by half thickness of the mortar joint in both horizontal and vertical directions and the discrete CMUs were connected and interact with each other through zero-thickness interface elements.

6.3.1 Nonlinear Behaviour of Concrete and CMUs

The three-dimensional geometry of CMUs was considered in this method and the corresponding nonlinear mechanical behaviour was defined through the tensile and compressive stress-strain curves implemented in concrete damaged plasticity (CDP)

constitutive model in ABAQUS (D.S.Simulia 2010). These curves can be obtained experimentally or by using existing behaviour models for concrete and masonry. In this study, the compressive behaviour of concrete and CMUs is defined using the stress-strain constitutive model proposed by Sima et al. (2008) as follows:

$$\begin{cases} \sigma_c = \varepsilon_c E_0 & \varepsilon_c \le \varepsilon_{c0} \\ \sigma_c = \left[\varepsilon_{c0}(1-A) + A\varepsilon_c e^{\left(\frac{\varepsilon_{c0}-\varepsilon_c}{\varepsilon_c'}\right)}\right] E_0 & \varepsilon_c > \varepsilon_{c0} \end{cases}$$

$$A = \frac{f_c' - \varepsilon_{c0} E_0}{E_0\left(\varepsilon_c' e^{\left(\frac{\varepsilon_{c0}}{\varepsilon_c'}-1\right)} - \varepsilon_{c0}\right)} \tag{6.9}$$

where σ_c and ε_c are the compressive stress and strain values, respectively; f_c' is the compressive strength of the material; ε_{c0} is the linear elastic strain limit; ε_c' is the strain at the peak stress and E_0 is the Young's modulus of the material.

The tensile behaviour model used in this study adopted an averaged tensile stress-strain curve between cracked and uncracked concrete suggested by Maekawa et al. (2003) to account for the tension stiffening effect. This model was shown to be independent of element size, crack spacing, and orientation of reinforcement. For concrete material, the tensile stress-strain curve used in this study can be expressed using Eq. (6.10).

$$\begin{cases} \sigma_t = \varepsilon_t E_0 & \varepsilon_t \le \varepsilon_{t0} \\ \sigma_t = \sigma_{t0}\left(\frac{\varepsilon_{t0}}{\varepsilon_t}\right)^{0.4} & \varepsilon_t > \varepsilon_{t0} \end{cases} \tag{6.10}$$

where σ_t and ε_t are the tensile stress and strain values, respectively; σ_{t0} and ε_{t0} are the linear elastic stress and strain limits, respectively.

For CMUs, the tension stiffening effect described above is non-existent due to the absence of steel reinforcement. The tensile behaviour is better described by a linear elastic behaviour in the pre-cracking phase and a stress-crack displacement curve in the post-cracking phase. The area under the curve represents the Mode I fracture energy of the material (G_f) which can be related to the compressive strength of CMUs using Eq. (6.11) as suggested by Fib: Model Code (2012).

$$G_f = 73\, f_c^{\,0.18} \tag{6.11}$$

6.3.2 Behaviour Model of Interface Elements

The surface-based cohesive behaviour model in ABAQUS was used for the interface between the CMUs and between the CMUs and the frame. This behaviour model uses the traction-separation constitutive relationship incorporating shear and tensile failure criteria to capture the possible failure modes of interface. The behaviour model is schematically illustrated in Figure 6.1. In the elastic state, the traction-separation law is controlled by an elastic response for both normal and transverse deformations as expressed in Eq. (6.12). Traction stress vector t consists of three components, t_n, t_s and t_t, which represent the tensile and two shear tractions. The corresponding separations are denoted by δ_n, δ_s and δ_t.

$$t = \begin{Bmatrix} t_n \\ t_s \\ t_t \end{Bmatrix} = \begin{bmatrix} K_{nn} & 0 & 0 \\ 0 & K_{ss} & 0 \\ 0 & 0 & K_{tt} \end{bmatrix} \begin{Bmatrix} \delta_n \\ \delta_s \\ \delta_t \end{Bmatrix} = K \tag{6.12}$$

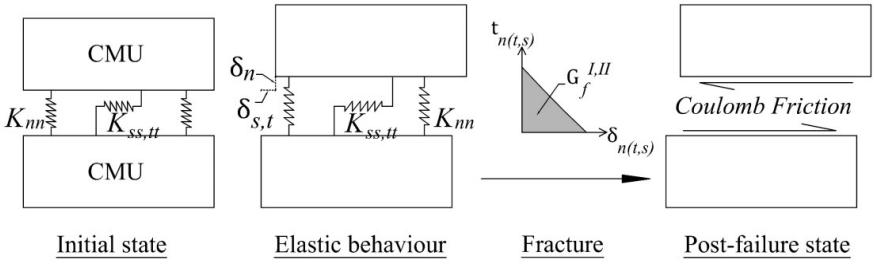

Figure 6.1. Behaviour of the interface interaction

Once failure is detected when tensile or shear stress reaches its limit, two damage models (normal and shear stress damage) control degradation and elimination of the interaction. Upon full degradation of the interface, the model adopts the Coulomb frictional contact between the CMUs or between the CMUs and the frame.

The explicit analysis method was adopted to solve the nonlinear problem. The explicit analysis is preferred for computation problems involving complicated nonlinear constitutive laws and large deformations and is especially effective for prediction of post-failure behaviour. The procedure uses a large number of small time increments to ensure the accuracy of analysis.

6.4 One-Way Arching with Rigid Supports

While previous experimental studies have shown that the infill is capable of developing two-way arching for resisting out-of-plane loading, it is not clear on the distribution of resistance in vertical or horizontal directions. As discussed above, the two main existing analytical models, i.e. Dawe and Seah's and Angel et al.'s methods, deviate in this regard significantly. Therefore, the one-way arching in infills was first studied to understand the directional behaviour of infills under out-of-plane loads. As shown in Figure 6.2, two

configurations of masonry panels were considered, namely, the vertical strip and horizontal strip with rigid boundary supports. In each case, the strips, consisting of standard 200 mm masonry blocks, were 800 mm wide with lengths varying from 2000 to 12000 mm to achieve slenderness ratios ranging from 10 to 60. The dimensions of the block were obtained from CSA Standard A165-14 "Concrete Block Masonry Units". It should be mentioned that although infills with slenderness ratios beyond 40 may not be practical, they were considered in order to cover all potential failure modes for the completeness of the study. A uniformly distributed out-of-plane pressure was applied to the surface of the infill and monotonically increased until the ultimate capacity of the panel was reached.

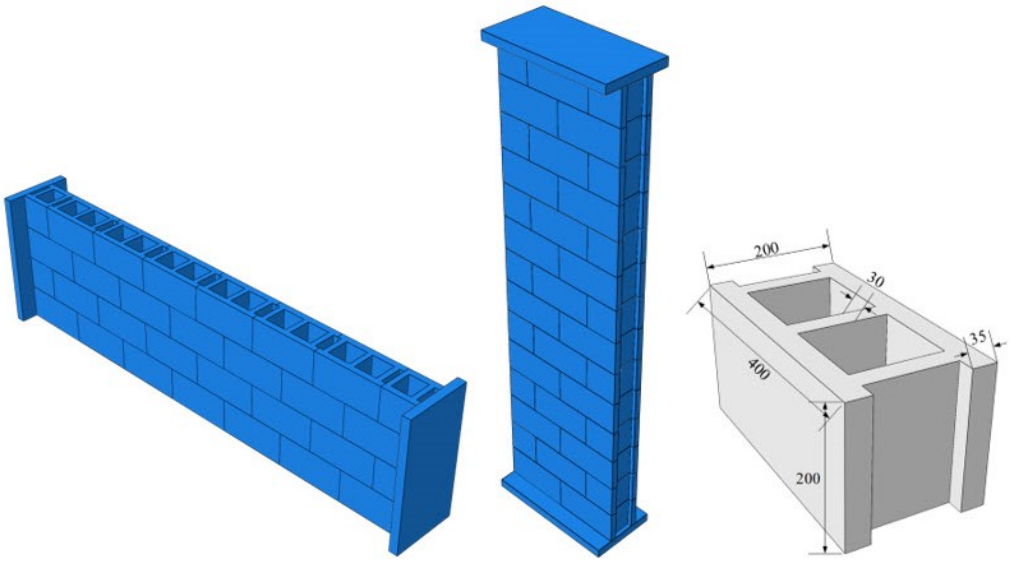

Figure 6.2. Geometric configuration of vertical and horizontal strips and masonry block dimensions

Figure 6.3 shows the out-of-plane strength vs. slenderness ratio for both vertical and horizontal strips. It can be seen that for both cases, the out-of-plane strength decreases and the rate of decrease diminishes as the slenderness ratio increases. The decrease trend is, more or less, in line with what those two analytical methods would suggest. However, for

the entire range of slenderness ratio, the horizontal arching strength is smaller than the vertical arching strength and the difference is most pronounced for slenderness less than 40 and diminishes for slenderness beyond that point. This observation differs from Dawe and Seah's method which suggests an equal strength for vertical and horizontal strips for a given slenderness.

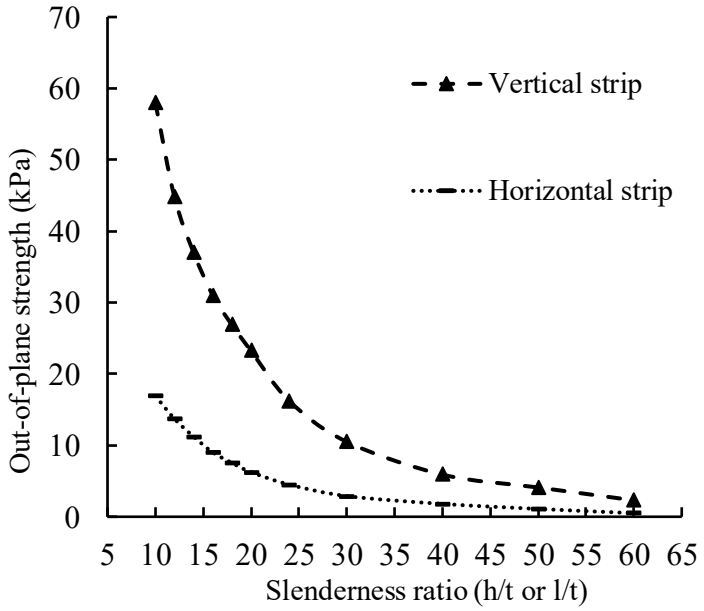

Figure 6.3. Out-of-plane strength in vertical and horizontal arching vs. slenderness ratio

The FE results also showed distinctively different failure mechanisms for the two strip cases which are believed to attribute to the difference in their capacity. In the case of vertical strips, three failure modes were identified (see Figure 6.4) and they are dependent on the slenderness ratio of the strip. Note that the red contours show the elements with tensile stresses beyond the cracking stress of the CMU (cracked elements) and white contours representing the elements with compressive stresses beyond the compressive capacity of the CMU (crushed elements). The FE results showed that for *h/t* smaller than 24, the failure was characterized by shear failure of the webs of the CMUs ultimately

causing the spalling of faceshells and sudden loss of the strength. The failure zone is focused in the top and bottom regions close to boundary supports. For slenderness ratios between 24 and 50, failure was characterized by compressive crushing of the faceshells at the boundary and mid-height regions. For slenderness ratios beyond 50, failure was by elastic buckling of the strip where no cracking or crushing in the arched segments was observed. In the case of horizontal strips, failure modes as affected by slenderness, are different.

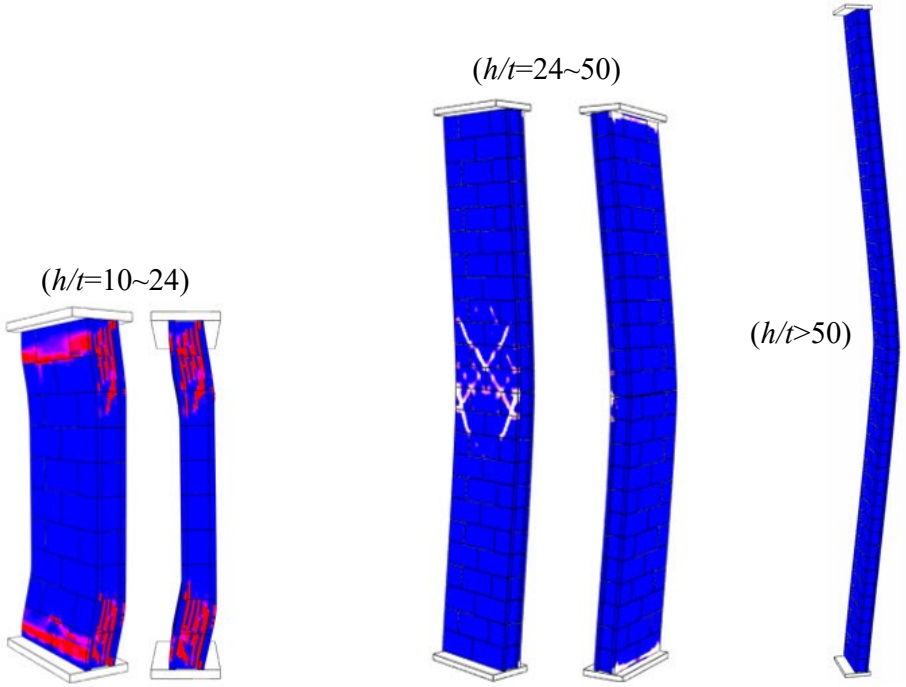

Figure 6.4. Failure modes in vertical strips with different h/t ratios (5× magnified deformations)

As shown in Figure 6.5, for *l/t* smaller than 40, the failure was characterized by shear cracking of the webs followed by tensile cracking through the faceshells. For *l/t* greater than 40, no shear cracking in the webs was observed and the failure was controlled by the tensile cracks through the faceshells of the blocks and mortar joints. It should be pointed

out that no compressive crushing on the faceshells was observed in any of the horizontal strips.

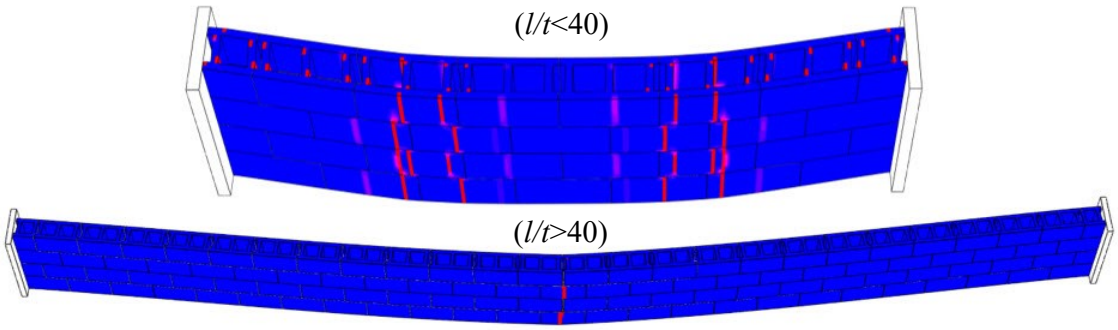

Figure 6.5. Failure modes in horizontal strips with different l/t ratios (5 × magnified deformations)

The above discussion identified that shear failure of webs of CMUs is the controlling failure mode for some slenderness in the vertical strips and for majority of slenderness in the horizontal strips. This failure mode was not recognized in the development of existing analytical methods which often assumed that the failure mechanism is by masonry compressive crushing. The web shear failure is believed to be the main factor attributing to a much smaller capacity for horizontal than vertical strips. For horizontal strips, the cracking in webs was caused by shear stresses acting through the thickness of the webs (perpendicular to the plane of the webs) whereas these stresses act through the length of the webs (in the plane of the webs) for vertical strips. For an ungrouted infill, shear stress transfer for the former (through the web thickness) is not continuous as there is no continuous mortar bedding connecting one web to another whereas for the latter (through the web length), it can be considered continuous as webs are aligned in the vertical direction. This further underscores that anisotropic characteristics of masonry requires its geometry and configuration to be taken into consideration in strength evaluation.

6.5 Two-Way Arching with Rigid Bounding Frames

The previous section demonstrates that horizontal arching yields much less capacity than vertical arching. This section expands the strips into four-side confined infill panels and investigates the contributions from horizontal and vertical arching to the two-way arching strength of an infill. In this case, a square infill bounded by fully rigid boundaries at four sides was used as an example. Figure 6.6 presents the out-of-plane capacity results for two-way arching models and the one-way arching capacity for either horizontal and vertical strips from the previous section is also included for comparison.

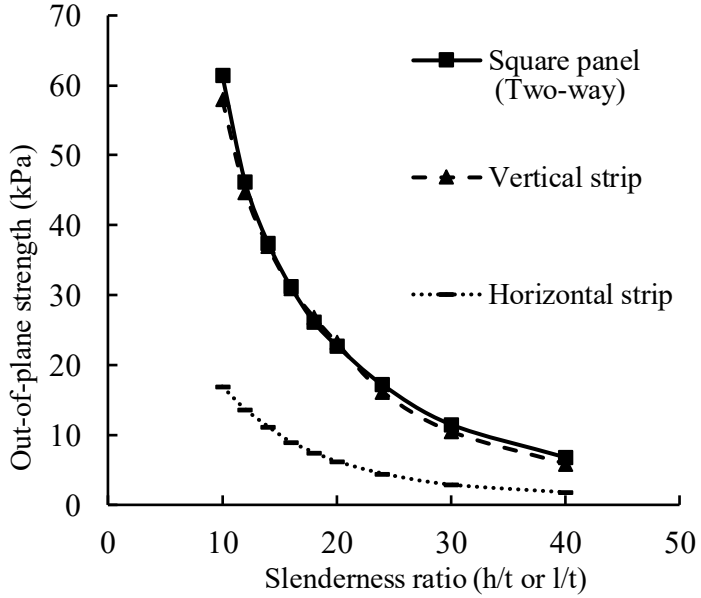

Figure 6.6. Two-way and one-way arching comparison for rigid frames

Figure 6.6 indicates that the out-of-plane capacity attained in a square panel is almost equal to that attained in its corresponding vertical strip, and much greater than that attained in its corresponding horizontal strip. The difference is more pronounced in the low to intermediate slenderness range (10~30) than in the high slenderness range (>30). Figure 6.7 compares the arching force applied to the horizontal and vertical boundary members

with the overall load vs. displacement response of the infill. Both arching force and applied load are normalized with respect to their maximum values. It shows that the web shear cracking around the left and right boundary caused a reduction in overall stiffness and the horizontal arching force reached maximum soon after while the infill strength continued to increase until the vertical arching force reached its maximum. At ultimate, the vertical arching force was about 4 times greater than the horizontal force. The above discussion seems to support that Angel et al.'s method to ignore the horizontal arching strength is valid for fully rigid frames.

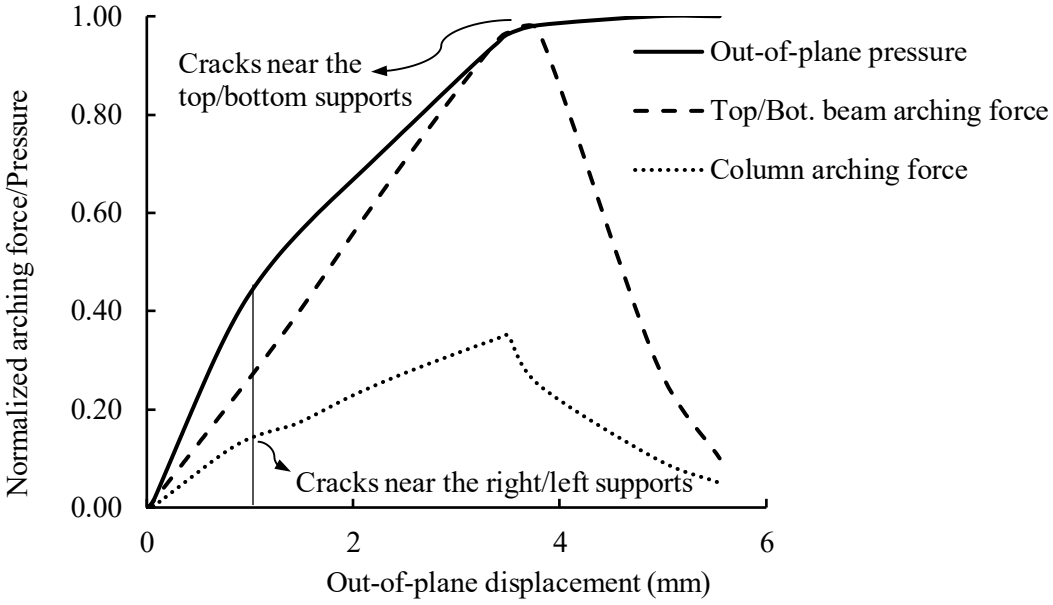

Figure 6.7. Normalized pressure and arching froces in vertical and horizontal directions

6.6 Experimental Investigation

Concurrent with the finite element modeling, an experimental study was conducted to obtain test results on out-of-plane behaviour and strength of concrete masonry infilled RC frames with varying parameters (Sepasdar 2017, Wang 2017). The specimens and results

discussed in the following were used to validate the capability of the model as well as to provide physical evidence of one-way and two-way arching correlations for "real" bounding frames. Three specimens were RC framed concrete masonry infills measuring 1350×980 mm ($l \times h$), constructed with standard half-scaled 200 mm CMUs laid in the running bond. The RC frame consisted of two 180 mm square columns and a 180 mm square top beam and a 250 mm square bottom beam. The dimension and reinforcement details for the specimens are shown in Figure 6.8 and specimen properties and parameters are summarized in Table 6.1.

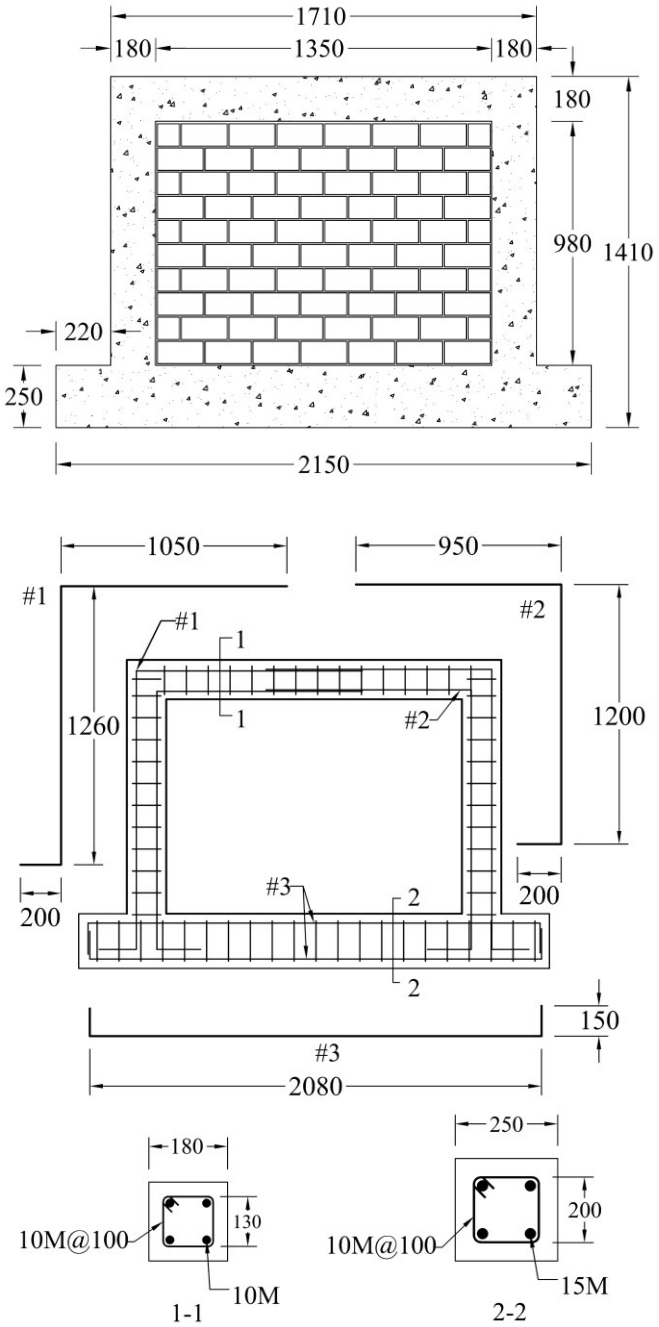

Figure 6.8. Geometric properties of specimens and reinforcement details in the RC frames

Table 6.1. Details of tested RC framed masonry infill specimens

Ref. (Original ID)	Specimen ID	Concrete		Masonry		Reinforcement		Parameter
		E (MPa)	f_c' (MPa)	E (MPa)	f_m' (MPa)	E (MPa)	f_y (MPa)	
Sepasdar 2017 (IF-ND)	IFNG	27800	43.8	2980	17.1	220000	440	Control specimen
Wang 2017 (IF-RC-TG)	IF-TG	20400	42.4	2980	17.1	220000	440	5mm top gap
Wang 2017 (IF-RC-SG)	IF-SG	16900	38.5	2980	17.1	220000	440	5mm side gap

The specimens included one control specimen (IFNG), one specimen with a 5 mm gap at the infill-to-column interface on each side (side gap, IF-SG) and one specimen with a 5 mm gap at the infill-to-the-top-beam interface (top gap, IF-TG). The out-of-plane loading was applied through a self-equilibrating system as shown in Figure 6.9. An airbag housed in a stiffened wood reaction box was used to apply the load and the load was applied at a rate of approximately 1.5 kPa per minute until failure of the specimen. During the testing, the specimen was clamped down to the strong floor to prevent potential lateral or transverse movement. The experimental and finite element out-of-plane load vs. displacement responses for the three specimens are compared in Figure 6.10(a)~(c) where the ultimate capacities are indicated in the diagram. It shows that the FE results compare well with experimental values with the experimental-to-FE capacity ratio, $\frac{q_{u,\mathrm{EXP}}}{q_{u,\mathrm{FE}}}$, of 1.06, 1.10 and 1.02 for IFNG, IF-SG and IF-TG, respectively.

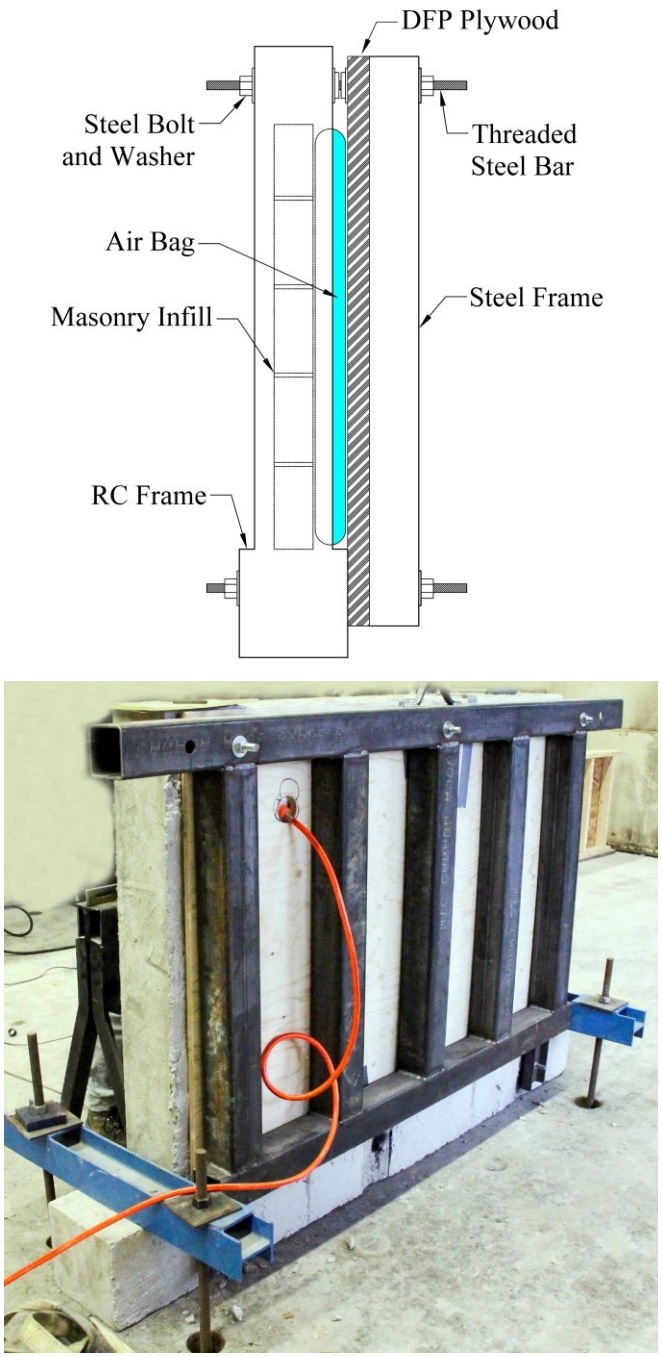

Figure 6.9. Test set-up for out-of-plane loading of the specimens

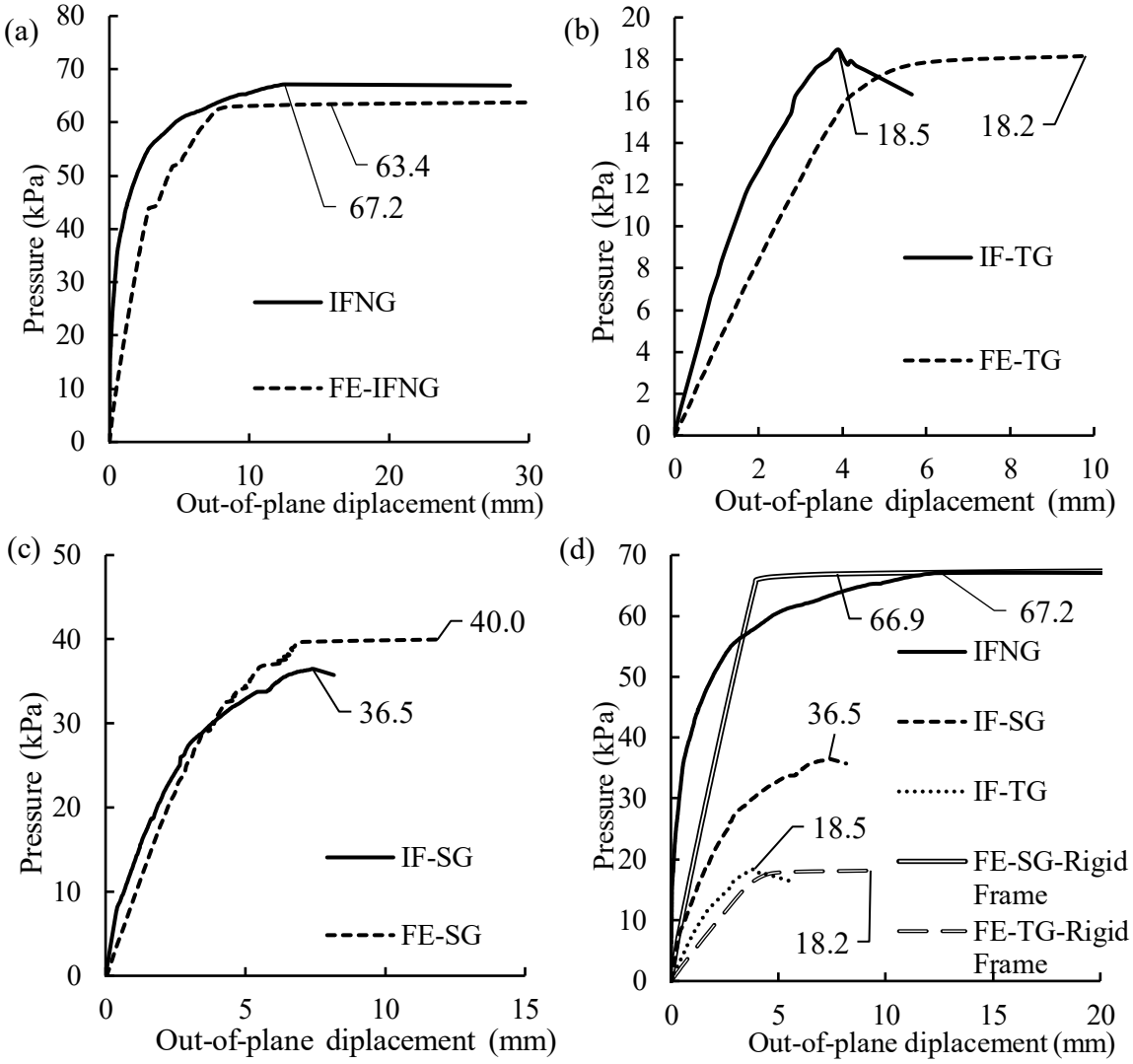

Figure 6.10. Comparison of out-of-plane pressure vs. displacement curves obtained from tests and FE analysis: (a) IFNG; (b) IF-TG; (c) IF-SG; and (d) Combined results

The failure mode comparison presented in Figure 6.11 demonstrates that the FE model can also predict the cracking pattern and failure mode with a good accuracy. The cracking pattern in IFNG shown in Figure 6.11(a) compares well with the observed cracking on the surface of the infill during the test. This includes the vertical cracks on the faceshells along the column regions, horizontal cracks through the mortar joints at the infill center and near the top and bottom boundaries and, cracks towards the corners of the infill. It is noted

though that both FE analysis and experimental observation suggest that the final failure was governed by cracking through the webs of CMUs. The failure of side gapped specimen (IF-SG) was initiated with a horizontal crack through the middle of the infill which was followed by inclined cracks through the CMUs and mortar joints towards the corners of the infill. This shows that the arching force was mainly transferred towards the corners of the infill as the top beam deflected. The cracks through concrete frame members were also accurately predicted in the FE model. On the other hand, the presence of top gap (IF-TG) resulted in an essentially three-side bounded panel. The largest out-of-plane deformation was observed at the top of the infill as shown in Figure 6.11(c) and the cracking pattern is in line with the yield-line pattern for a three-side supported slab but with vertical cracks developed along two column regions and inside the CMUs through the webs. Again, the final failure was governed by the web shear failure. Overall, the FE model is shown to produce capacity results and predict behaviour and failure both accurately.

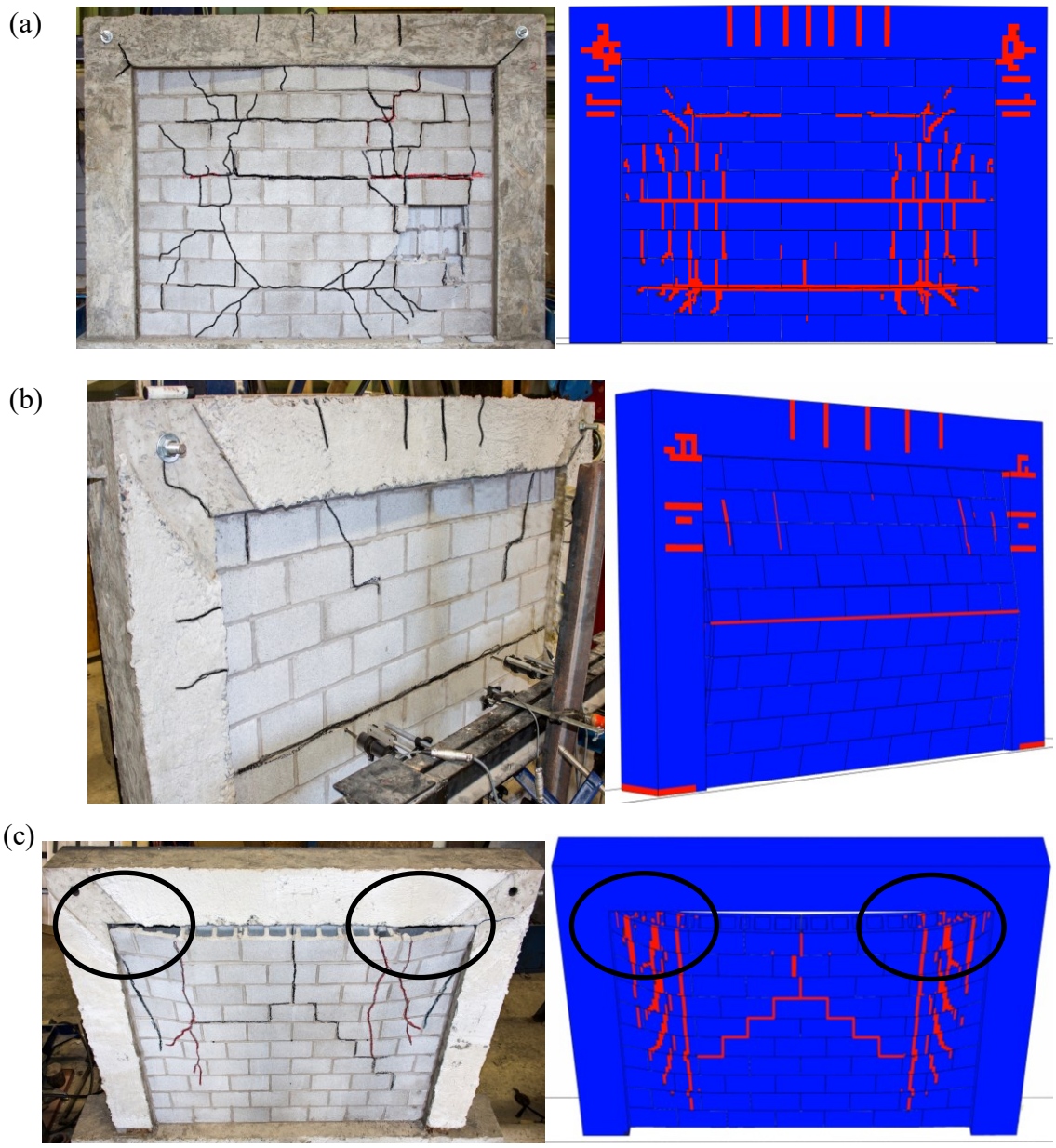

Figure 6.11. Comparison of FE and experimental results for cracking patterns: (a) IFNG; (b) IF-SG; and (c) IF-TG

Figure 6.10(d) combines the FE and experimental results to illustrate the relationship between two-way and one-way arching in both a fully rigid frame and a "real" frame allowing deformations. It can be assumed that specimen IF-SG reflects the vertical arching behaviour whereas specimen IF-TG reflects the horizontal arching behaviour, albeit with

an additional bottom boundary. In previous section, it was shown that for a fully rigid frame boundary, the vertical arching strength is more or less equal to the two-way arching strength. This observation is still supported herein by comparing curves of FE-SG-Rigid Frame and IFNG in the figure. However, when the test results on "real" frames are considered, the side gap (IF-SG) resulted in a strength reduction of 46% whereas the top gap (IF-TG) resulted in an even higher strength reduction, at 72%, by comparing curves of IF-SG, IF-TG and IFNG. Clearly, the hypothesis of vertical arching equal to two-way arching is not realized in a "real" frame situation. The reduction of strength in IF-SG is attributed to the deflection of the top beam at the centre enabled by the frame flexibility creating a less stiff support for the infill and thus less arching strength, indicating the stiffness of the frame plays an important part in the strength of the infill. For specimen IF-TG, the strength reduction is at much higher level indicating that horizontal arching is much weaker. The fact that the fully rigid boundary assumption does not change the predicted strength (comparing curves of FE-TG-Rigid Frame and FE-TG) suggests that horizontal arching strength is insensitive to frame stiffness.

6.7 Two-Way Arching in Flexible Bounding Frames

The previous sections discussed the relationship between one-way and two-way arching using both the FE and experimental results. It can be concluded that for a less than rigid bounding frame, the vertical arching strength is not equal to the two-way arching strength of an infill. Also, it was found that the horizontal arching yielded much less capacity than vertical arching of a panel with the same slenderness and the two-way arching capacity is not a simple addition of vertical and horizontal arching strengths. In this section, results of

a parametric study using full-scale FE models are presented to further demonstrate the correlation between the one-way and two-way arching and they are also used to evaluate the current two main analytical models. Note that since only minor cracking is expected in the frame, a linear elastic behaviour model was considered for the concrete frame members in this study. It also eliminated the effect of reinforcement details on the behaviour of frame members and thus focused the comparison of different available methods on the infill behaviour and strength. Details of each model are summarized in Table 6.2 and Figure 6.12. The masonry compressive strength was assumed to be 12 MPa for all models. The key parameters were aspect ratio (0.8, 1.0, 1.3 and 1.4) and bounding frame stiffness. Three different sections, including 200×200, 350×350 and 500×500 mm square sections were chosen for the bounding frame members to cover a range of low, intermediate to high stiffness expected in practice for RC frames. Also listed in the table are strength values obtained using FE analysis, q_{FE}, Dawe and Seah's method, $q_{D\&S}$, and Angel et al.'s method, q_{Angel}, and FE-to-analytical ratios.

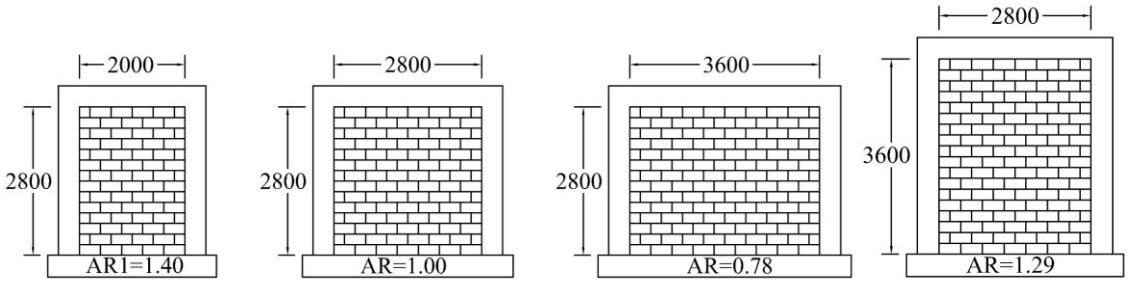

Figure 6.12. Geometric configuration of the models in parametric study

Table 6.2. Summary of FE model results

Model	Infill dimensions ($l \times h$) (mm)	h/l	h/t	Beam/Col section (mm)	EI/L $\times 10^{-10}$ (N/mm)	Dawe and Seah			Angel et al.		q_{FE} (kPa)	$\frac{q_{FE}}{q_{D\&S}}$	$\frac{q_{FE}}{q_{Angel}}$
						α	β	$q_{D\&S}$ (kPa)	R_2	q_{Angel} (kPa)			
1	2000×2800	1.4	14.0	500×500	7.8	68(50)	80(50)	82.6	4.2(1.0)	66.5	39.8	0.48	0.60
2	2000×2800	1.4	14.0	350×350	1.9	47	56(50)	79.5	1.3(1.0)	66.5	37.7	0.47	0.57
3	2000×2800	1.4	14.0	200×200	0.2	27	32	47.2	0.5	30.4	26.1	0.55	0.86
4	2800×2800	1.0	14.0	500×500	5.6	68(50)	68(50)	49.7	4.2(1.0)	66.5	36.2	0.73	0.54
5	2800×2800	1.0	14.0	350×350	1.3	47	47	47.1	1.3(1.0)	66.5	32.1	0.68	0.48
6	2800×2800	1.0	14.0	200×200	0.1	27	27	26.9	0.5	30.4	20.8	0.77	0.69
7	3600×2800	0.8	14.0	500×500	4.3	68(50)	59(50)	38.1	4.2(1.0)	66.5	33.9	0.89	0.51
8	3600×2800	0.8	14.0	350×350	1.0	47	42	33.3	1.3(1.0)	66.5	27.8	0.84	0.42
9	3600×2800	0.8	14.0	200×200	0.1	27	24	19.0	0.5	30.4	17.0	0.89	0.56
10	2800×3600	1.3	18.0	500×500	5.6	59(50)	68(50)	38.1	4.2(1.0)	34.9	28.0	0.73	0.80
11	2800×3600	1.3	18.0	350×350	1.3	42	47	33.3	1.3(1.0)	34.9	24.1	0.72	0.69
12	2800×3600	1.3	18.0	200×200	0.1	24	27	19.0	0.5	15.9	14.4	0.76	0.90

Figure 6.13 compares strength values from the three sources vs. infill aspect ratio for three frame stiffnesses and Figure 6.14 compares strength values vs. stiffness of the bounding frame for three infill aspect ratios. The slenderness of infills is kept the same (h/t=14) for both figures. The frame stiffness was defined using EI/L, rather than EI as in Angel et al.'s method, to include the effect of member length. The top beam stiffness was used in the plot as arching in the vertical direction is the primary contributor to the overall strength as discussed previously. Both figures show that overall, the two analytical methods predict much higher strengths than the FE results, and this overestimation is more pronounced for bounding frames of intermediate to high stiffness and infills of large aspect ratio. Further, as shown in Figure 6.13, q_{Angel} remains constant as aspect ratio varies due to the fact that Angel et al.'s method does not take the infill aspect ratio into strength consideration. On the other hand, both FE results and Dawe and Seah's method suggest an increasing trend for strength as aspect ratio increases but the difference is noted in the high aspect ratio region where the latter predicts much higher strengths than the FE analysis. This marked overestimation by Dawe and Seah's method in high aspect ratio regions can be explained as follows. Since Dawe and Seah's method considers the horizontal and vertical arching strengths in a same manner and the shorter the span, the higher the strength. An increase in aspect ratio in this case corresponds to an increasingly shorter horizontal span, and the method would then yield an increasing horizontal strength. As the FE analysis shows that the horizontal arching is much weaker than the vertical arching, the difference in treating the horizontal arching is believed to attribute to the significant disparity in strength predictions between the FE analysis and Dawe and Seah's method. This point is further demonstrated in Table 6.2 by comparing results for models of 3600 × 2800 mm and 2800

× 3600 mm**.** Dawe and Seah's method results in an equal strength for these two different aspect ratios but the FE results for the latter are lower than the former and both are lower than Dawe and Seah's predicted values.

Figure 6.14 shows that there exists a stiffness limit beyond which the strength increase levels off and this stiffness limit is dependent on the infill aspect ratio. However, three methods show different stiffness limits. For the aspect ratios considered, the FE results suggest that the stiffness EI/L (calculated using the top beam) greater than 2×10^{-10} N/mm has a diminishing effect on increasing the arching strength. Referring to Table 6.2, columns of α and β (Dawe and Seah's method) and R_2 (Angel et al.'s method) and noting that the number in brackets is the limit set by the corresponding method, the FE results seem to agree more with Dawe and Seah's method on the stiffness limit. Although calculated differently, both methods show a cut-off point in a general agreement. For Angel et al.'s method, it defines a smaller stiffness limit and also does not reflect the dependence of the stiffness limit on the aspect ratio as R_2 factor remains constant for different aspect ratios.

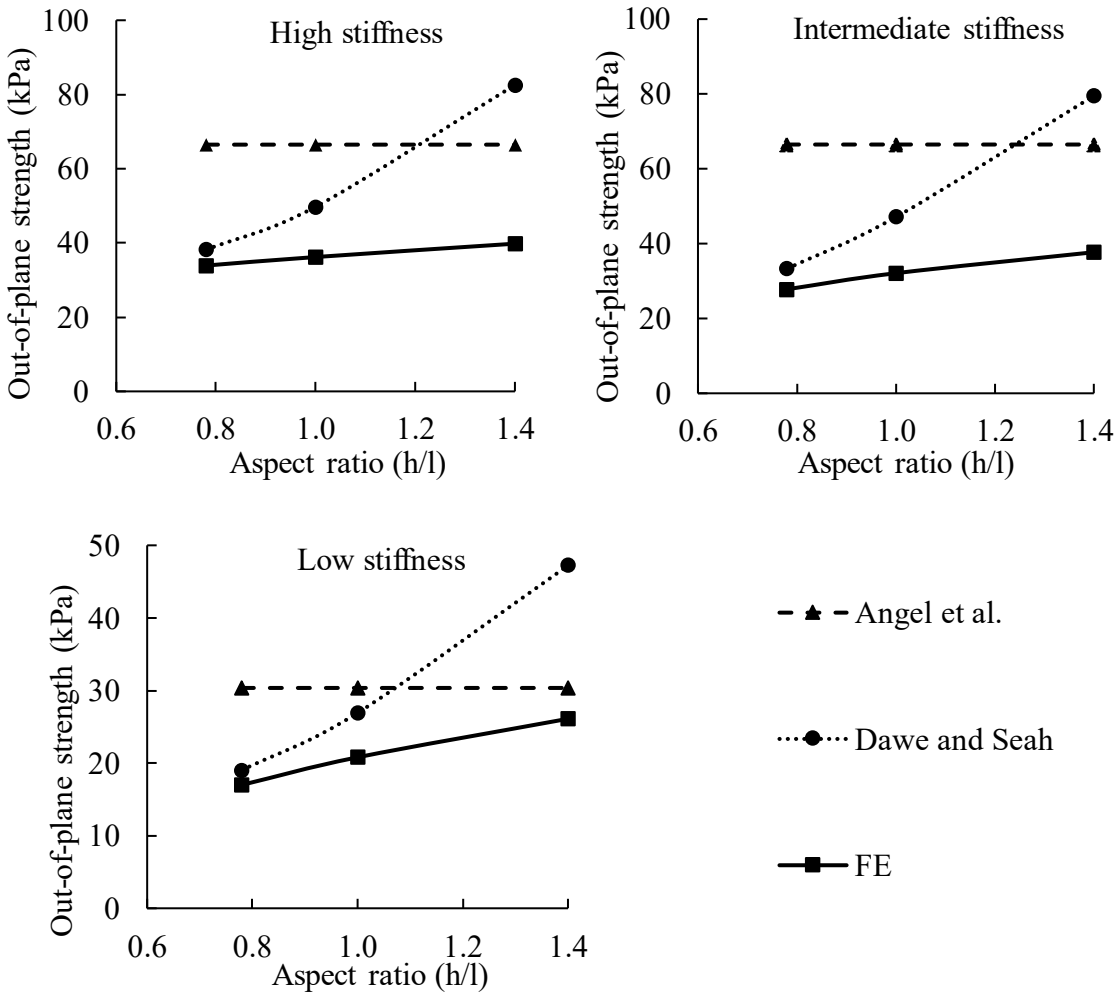

Figure 6.13. Comparison of strength value vs aspect ratio for different frame stiffness

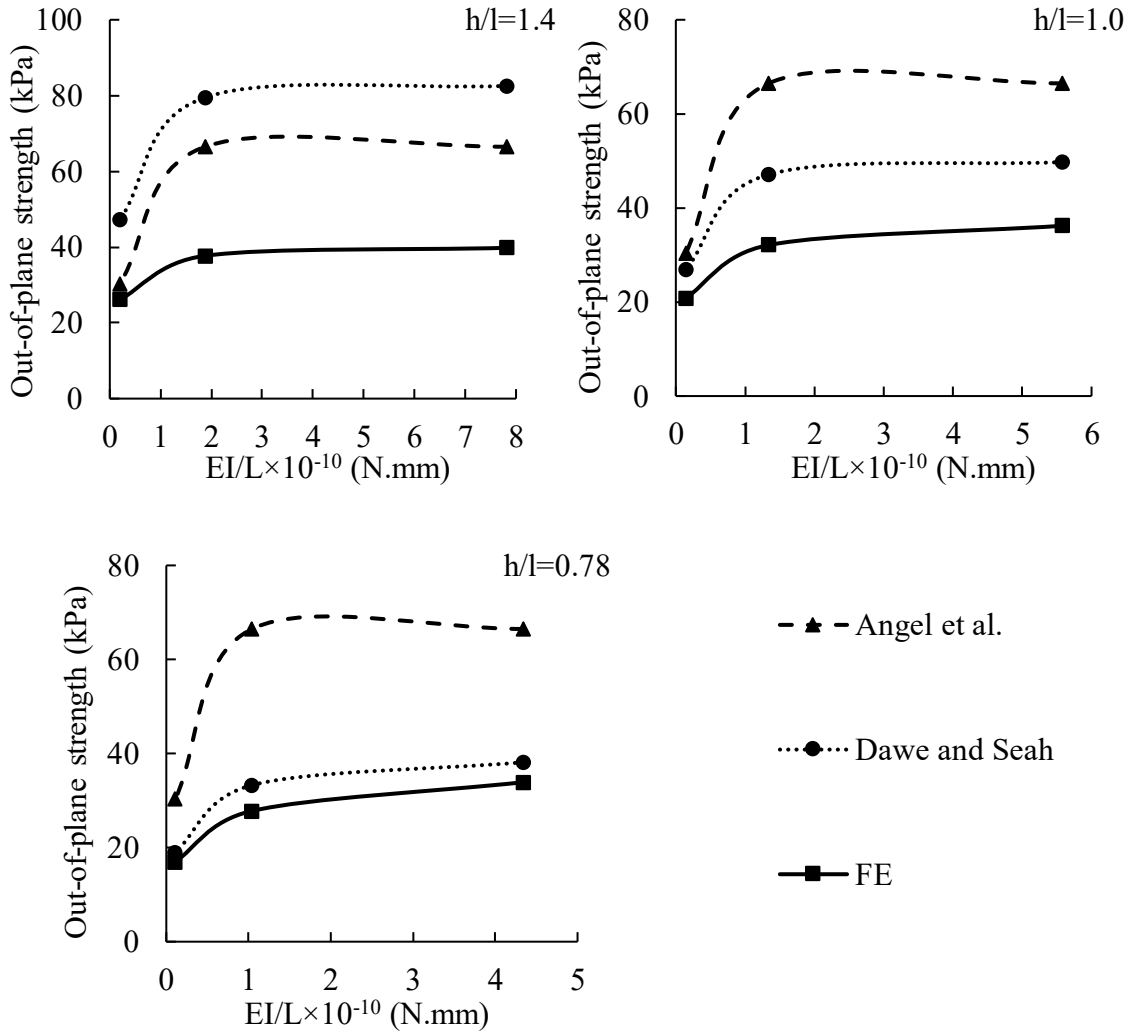

Figure 6.14. Comparison of strength value vs frame stiffness for different infill aspect ratio

6.7.1 Proposed Modification Based on Dawe and Seah's Method

The above discussion shows that the FE results share a more similar overall trend with Dawe and Seah's method than Angel et al.'s method with respect to infill aspect ratio and bounding frame stiffness. It was then decided to use Dawe and Seah's method as basis to propose modifications to improve the accuracy of the strength equation. Noting that the exponential strength decrease trend with respect to slenderness (h/t) of an infill has been

well established in the available literature (Abrams et al. 1996, Dawe and Seah 1989b, Flanagan and Bennett 1999b), the modification is then focused on the manner in which the horizontal and vertical arching strengths are calculated, i.e, α and β terms in the method. To understand the distribution of two-way strength in horizontal and vertical directions for non-rigid bounding frames, the models in

Table 6.2 were analyzed again for one-way arching in vertical (SG) and horizontal (TG) directions. This was achieved by providing an artificial gap at either the top beam-to-frame interface or column-to-frame interface to reduce a two-direction arching to one direction only. Results are plotted in Figure 6.15. First, the figure confirms that for a less than rigid bounding frame, the vertical arching strength contributes to a portion of the infill strength, which was also suggested by the experimental results. Second, the vertical arching strength is about 1.0 to 3.6 times the horizontal strength for the range of aspect ratio and bounding frame stiffness considered. Third, the stiffness of the bounding frame has a pronounced and similar effect on the vertical and two-way arching strengths while insignificant effect on the horizontal arching strength. Last, the comparison of the vertical arching with two-way arching strengths shows that as the aspect ratio increases, the vertical arching strength assumes an increasingly large portion of the two-way arching strength and become the predominant strength contributor. Based on these observations and through a regression analysis of FE results, the following modification based on Dawe and Seah's method was proposed. The contribution of horizontal arching strength to the two-way capacity was modified by introducing a factor of 3/4 for a two-arching infill. The constants of equation were changed as a result of regression analysis (4.5 to 4). The upper limits of α and β were changed to 30 and 70, respectively, to reflect the different stiffness effect on horizontal and

vertical arching. For gapped infills, either α (side gap) or β (top gap) can be set to zero according to gap locations.

$$q_{ult} = 4(f'_m)^{0.75} t^2 \left\{ \frac{3}{4}\alpha/L^{2.5} + \beta/H^{2.5} \right\} \tag{6.13}$$

where:

$$\alpha = {}^{1}/_{H} (EI_c H^2 + GJ_c tH)^{0.25} \leq 30 \tag{6.14}$$

$$\beta = {}^{1}/_{L} (EI_b L^2 + GJ_b tL)^{0.25} \leq 70 \tag{6.15}$$

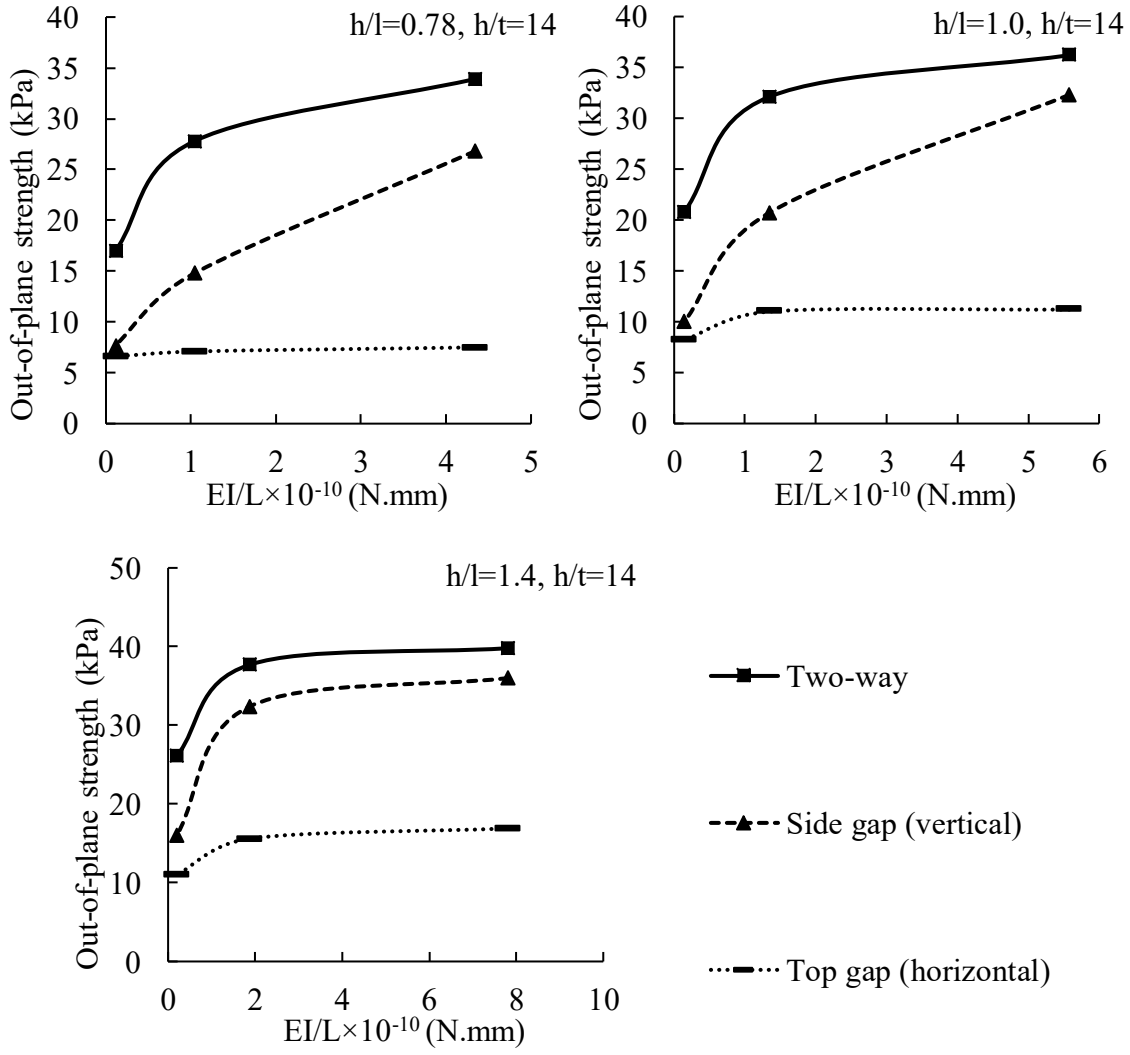

Figure 6.15. Two-way and one-way arching comparison for non-rigid frames

6.7.2 Performance of the Proposed Equation

The performance of the proposed equation was first evaluated against the FE results and a summary is shown in Table 6.3 together with the two analytical methods. It can be seen that the overall average of q_{FE}/q_{eqn} is close to unity with a COV of 23%. Both indicators are improved from Dawe and Seah's and Angel et al.'s methods, suggesting a better performance in predicting the strength. When the gapped cases were examined separately, the average q_{FE}/q_{eqn} are 0.92 for the top gap cases and 1.10 for the side gap cases with COVs of 28% and 22%, respectively. This, when compared with the average $q_{FE}/q_{D\&S}$ of 0.51 and 1.11 with COV of 35% and 30% for results by Dawe and Seah's method, shows that the proposed modifications also provide improved predictions for gapped boundary conditions.

Table 6.3. Comparison of results from FE analysis and proposed equation

Spec.	Infill dimension (l×h) (mm)	h/l	h/t	Beam/Column section (mm)	q_{ult} (kPa)		Ratio of FE results to predicted loads		
							D&S	A et al.	Modified equation
FE1	2000×2800	1.4	14	500×500	Two-way	39.8	0.48	0.60	0.69
					Top gap	16.9	0.29	-	0.63
					Side gap	36.0	1.45	0.54	1.16
FE2	2000×2800	1.4	14	350×350	Two-way	37.7	0.47	0.57	0.73
					Top gap	15.6	0.29	-	0.58
					Side gap	32.4	1.30	0.49	1.30
FE3	2000×2800	1.4	14	200×200	Two-way	26.1	0.55	0.86	0.75
					Top gap	11.0	0.35	-	0.53
					Side gap	16.0	1.00	0.53	1.12
FE4	2800×2800	1.0	14	500×500	Two-way	36.2	0.73	0.54	0.87
					Top gap	11.2	0.45	-	0.96
					Side gap	32.3	1.30	0.49	1.08
FE5	2800×2800	1.0	14	350×350	Two-way	32.1	0.68	0.48	0.99
					Top gap	11.0	0.47	-	0.95
					Side gap	20.7	0.88	0.31	0.99
FE6	2800×2800	1.0	14	200×200	Two-way	20.8	0.77	0.69	0.99
					Top gap	8.2	0.61	-	0.91
					Side gap	10.0	0.74	0.33	0.84
FE7	3600×2800	0.8	14	500×500	Two-way	33.9	0.89	0.51	1.04
					Top gap	7.5	0.57	-	1.21
					Side gap	26.8	1.08	0.40	1.02
FE8	3600×2800	0.8	14	350×350	Two-way	27.8	0.84	0.42	1.13
					Top gap	7.1	0.57	-	1.15
					Side gap	14.8	0.71	0.22	0.80
FE9	3600×2800	0.8	14	200×200	Two-way	17.0	0.89	0.56	1.11
					Top gap	6.6	0.92	-	1.38
					Side gap	7.7	0.65	0.25	0.73
FE10	2800×3600	1.3	18	500×500	Two-way	28.0	0.73	0.80	1.02
					Top gap	11.0	0.44	-	0.95
					Side gap	23.4	1.76	0.67	1.47
FE11	2800×3600	1.3	18	350×350	Two-way	24.1	0.72	0.69	1.06
					Top gap	9.5	0.46	-	0.82
					Side gap	16.6	1.32	0.48	1.49
FE12	2800×3600	1.3	18	200×200	Two-way	14.4	0.76	0.90	1.01
					Top gap	8.0	0.68	-	1.01
					Side gap	8.0	1.11	0.50	1.25
						Avg.	**0.78**	**0.53**	**0.99**
						COV (%)	**0.44**	**0.33**	**0.23**

Next, the proposed equation was evaluated using the available experimental results obtained in the literature. A summary of the comparison study is presented in Table 6.4. The experimental results were divided into two categories. Since the proposed equation was developed for concrete masonry block infills, the tests involving concrete masonry infills were considered first. Results of 11 specimens from three studies were collected and compared with the proposed equation as well as the two analytical methods. It is noted that this study and Angel et al.'s study used RC frames whereas Dawe and Seah's study used steel frames. Specimens IF-TG and WE6, had a gap at the top beam-to-infill interface and thus were excluded from Angel et al.'s method calculations. Also, the reported strengths for specimens 4b and 5b (Angel et al.'s study) were not exactly the "ultimate" strengths as the tests were terminated before the specimens reaching the ultimate load. They were however included to demonstrate the relative performance between different methods. Based on the results in Table 6.4, the modified equation provides the best estimate of out-of-plane strength in each set of tests considered. It should be pointed out that the modified equation performed better than Dawe and Seah's method for the tests conducted by Dawe and Seah. Angel et al.'s method is the least accurate one due to the mean experimental-to-analytical ratio being far from unity and with the highest COV of all three methods. Next, the performance of the proposed equation was assessed using experimental results on other types of masonry infills from three studies (Flanagan and Bennett 1999b, Frederiksen 1992, Fricke et al. 1992). These results were also used in the studies (Flanagan and Bennett 1999a, Pasca et al. 2017, Ricci et al. 2018) mentioned in the introduction section. All three studies used steel bounding frames. The results were in line with those of concrete masonry infills that Dawe and Seah's and proposed methods provide comparable predictions with

the latter showing an improved overall experimental-to-analytical mean value while Angel et al.'s method performed the worst of the three. Combining the entire data points, the proposed equation yielded a mean experimental-to-analytical ratio of 1.02 with a COV of 33% in comparison of 0.75% with a COV of 28% obtained using Dawe and Seah's method.

It should be pointed out that the proposed equation was developed and calibrated based on results of concrete masonry infills with consideration of their characteristic failure mode (web shear failure). The comparison above showed that it also provided reasonable predictions for other types of masonry infills. It is cautioned though, due to the limited data points, further validation is needed for applicability of the proposed method to a range of masonry infill and frame types.

Table 6.4. Comparison of results from the proposed equation and experimental studies

Ref.	Spec.	Infill dimensions (l×h) (mm)	t (mm)	h/l	h/t	Beam/Column section (mm)	f'_m (kPa)	q_{ult} (kPa)	Ratio of experimental-to-predicted load		
									D&S	A et al.	Modified equation
Concrete masonry infills											
This study	IFNG	1350×980	90	0.7	10.9	180×180	17100	67.2	0.71	0.97	0.90
	IF-TG	1350×980	90	0.7	10.9	180×180	17100	18.5	0.61	-	0.97
	IF-SG	1350×980	90	0.7	10.9	180×180	17100	36.5	0.66	0.56	0.75
								Avg.	**0.66**	**0.77**	**0.87**
								COV (%)	**8**	**38**	**13**
Dawe and Seah (1989)	WE1	3600×2800	190	0.8	14.7	B: W200×46 C: W250×58	30500	22.3	0.60	0.33	0.76
	WE2	3600×2800	190	0.8	14.7	B: W200×46 C: W250×58	28100	19.2	0.55	0.31	0.70
	WE4	3600×2800	140	0.8	20.0	B: W200×46 C: W250×58	22700	11.2	0.70	0.51	0.88
	WE8	3600×2800	140	0.8	20.0	B: W200×46 C: W250×58	27400	13.4	0.72	0.50	0.91
	WE5	3600×2800	90	0.8	31.1	B: W200×46 C: W250×58	20200	7.8	1.28	1.84	1.61
	WE6 (TG)	3600×2800	190	0.8	14.7	B: W200×46 C: W250×58	22300	10.6	0.84	-	1.26
								Avg.	**0.78**	**0.70**	**1.02**
								COV (%)	**34**	**93**	**34**
Angel et al. (1994)	4b	2400×1600	90	0.7	18.1	B:250×300 + Slab C: 300×300	22897	29.8	0.69	0.45	0.77
	5b	2400×1600	140	0.7	11.6	B:250×300 + Slab C: 300×300	21463	32.2	0.32	0.18	0.36
								Avg.	**0.50**	**0.31**	**0.56**
								COV (%)	**51**	**62**	**51**
Clay Tile Infill with Steel Frame											
Flanagan and Bennett (1999a)	22	2240×2240	330	1.0	6.8	B: W460×113 C: W410×60	2290	39.5	0.76	1.77	1.23
	18	2240×2240	195	1.0	11.5	B: W310×52 C: W250×45	5590	26.6	0.81	1.40	1.30
	25	2240×2240	93	1.0	24.1	B: W310×52 C: W250×45	5590	8.1	1.09	3.09	1.74
Fricke et al. (1992)	1	8470×3660	195	0.4	18.8	B: W360×216 C: W760×161	4300	6.1	1.00	0.55	1.19
								Avg.	**0.92**	**1.70**	**1.37**
								COV (%)	**17**	**62**	**18**
Clay Brick Infill with Steel Frame											
Frederiksen (1992)	86-3	680×970	29.5	1.4	23.3	Rigid	10600	18.0	0.75	4.62	1.08
	90-3	680×970	29.5	1.4	23.3	Rigid	15500	31.7	0.66	3.28	0.95
	91-3	680×970	29.5	1.4	23.3	Rigid	21200	40.2	0.73	3.22	1.06
								Avg.	**0.71**	**3.71**	**1.03**
								COV (%)	**7**	**21**	**7**
Overall performance								**Avg.**	**0.75**	**1.47**	**1.02**
								COV (%)	**28**	**93**	**33**

6.8 Conclusion

A finite element study was conducted to investigate the effect of arching action in both one-way and two-way on the out-of-plane strength of RC framed concrete masonry infills. The results were used to assess validity of the two main analytical methods for out-of-plane strength calculation and further propose a modification based on Dawe and Seah's method. Some conclusions drawn from this study are as follows:

- For infills constructed with concrete masonry units, web shear failure was identified as a predominant failure mode and also a main contributor to difference in strength in horizontal and vertical arching.
- For a fully rigid bounding frame, the two-way arching strength is practically equal to the vertical arching strength and horizontal arching is negligible. For a less than rigid bounding frame, both vertical and horizontal arching contribute to the overall two-way strength with the former being a more significant contributor. The distribution between the two depends on geometrical properties of the infill and stiffness of the frame. The two-way arching capacity is not a simple addition of vertical and horizontal arching strength.
- The stiffness of the bounding frame has more effect on vertical arching strength than the horizontal arching strength.
- A strength equation based on Dawe and Seah's method was proposed showing an improved performance when compared with the two existing analytical models.

- The equation was developed and validated using concrete masonry infills and more reliable experimental results are needed to evaluate its applicability for other infill materials.

6.9 Acknowledgement

The authors wish to recognize the contribution of financial assistance by the Canadian Concrete Masonry Producers Association and Natural Sciences and Engineering Research Council of Canada.

Chapter 7 Effect of Prior In-Plane Damage on the Out-of-Plane Performance of Concrete Masonry Infills

Ehsan Nasiri, Yi Liu

Submitted to Engineering Structures

7.1 Abstract

This paper presents results of a study on the out-of-plane behaviour and strength of concrete masonry infills bounded by reinforced concrete (RC) frames with prior in-plane damage. The experimental portion of the study consisted of testing four physical infilled frame specimens at varying levels of in-plane damage. A finite element (FE) model was concurrently developed and validated using the test results. A parametric study using the model was performed to further study the effect of several influential geometric and material parameters including infill aspect ratio, masonry strength, and slenderness ratio. The correlation between the prior in-plane damage sustained by the infill and its out-of-plane strength as affected by each parameter was discussed in detail. The impact of cyclic vs. monotonic loading was also studied. The efficacy of the existing analytical method for calculating the strength reduction was evaluated using both the experimental and FE results. A new reduction factor equation was proposed and the comparison with the existing analytical method against the available results showed an improvement in providing an estimate of residue out-of-plane strength for infills with prior in-plane damage.

Keywords: concrete masonry infills; RC frames; out-of-plane; in-plane damage; finite element; arching action; nonlinear analysis

7.2 Introduction

Masonry walls are often built within concrete and steel frames in modern building construction to either form the building envelope or act as partition walls. It is well recognized that accurate prediction of the behaviour and strength of these infilled frames under various loading conditions must consider the interaction between the frame and the infill wall. When subjected to in-plane lateral loading, the frame behaviour is shown to be significantly affected by the infill as the latter increases the stiffness and strength as well as alters the dynamic characteristics of the frame structure. On the other hand, when subjected to out-of-plane loading, behaviour of the infill wall is largely impacted by confinement provided by the bounding frame so that the failure mechanism of the infill is changed from a flexure-controlled failure to a compression-controlled failure. Both in-plane and out-of-plane behaviour of the infilled frame has been studied in the past six decades, albeit with less research contributed to the latter. Some design guidelines for simple infilled frame situations have been established (CSA S304-14, TMS 402/602-16) for both in-plane and out-of-plane loading conditions. In the case of in-plane loading, the formation and development of tensile cracking in the diagonal direction of the infill followed by masonry crushing at the loaded corners is identified as the most common failure mode (Asteris et al. 2013, El-Dakhakhni et al. 2003, Flanagan and Bennett 1999c, Mehrabi et al. 1996). Hence, the diagonal strut concept where the entire infill is simply replaced by a diagonal strut connecting loaded corners was thus developed to simulate the infill effect on the stiffness and strength of the frame system. The strut width is dependent on the contact area between the infill and the bounding frame (El-Dakhakhni et al. 2003, Flanagan and Bennett 1999c, Smith 1962). In the case of out-of-plane loading, presence of

the boundary frame was shown to provide confinement for masonry infills which attain much higher capacity than their flexural wall counterparts (Abrams et al. 1996, Anderson 1984, Dawe and Seah 1989b, Flanagan 1994, Gabrielsen and Kaplan 1976). This capacity increase was attributed to a failure mechanism, known as "arching". It was proposed that subsequent to flexural cracking, the rotation of cracked segments of the infill wall panel was restrained by the bounding frame, creating in-plane compressive forces which delayed further cracking and the failure was caused by masonry compressive stress reaching its limit. As masonry compressive strength is higher than its tensile strength, the masonry infills failing by "arching" action attained higher capacity than flexural walls failing by tension cracking. Previous studies (Angel et al. 1994, Dawe and Seah 1989b, Flanagan and Bennett 1999b, Varela-Rivera et al. 2012) focused on the effect of several important parameters on the out-of-plane strength including masonry compressive strength, infill slenderness and aspect ratio, and bounding frame stiffness. One important work conducted by Dawe and Seah (1989b) formed the basis of design provisions contained in the American masonry standard (TMS 402/602-16) for out-of-plane strength of masonry infills. Nasiri and Liu (2017, 2019a, 2019b) proposed some modifications to Dawe and Seah's equation by considering both one-way and two-way arching action as affected by infill geometry and frame stiffness.

This paper is motivated to investigate the interaction between in-plane and out-of-plane behaviour, in particular, the effect of prior in-plane damage on the out-of-plane strength of the masonry infills. As infills are considered to participate in load sharing with the bounding frame, they often experience both in-plane and out-of-plane loading such as in an earthquake event. Conceivably, the infill may sustain varying levels of damage caused

by in-plane loads and how these damages affect the infill out-of-plane load carrying capacity is an important design consideration for the stability of the infills. A review of available literature on the subject showed a general observation among existing studies that the prior in-plane damage results in reductions in out-of-plane strength of infills (Angel et al. 1994, Flanagan and Bennett 1999b, Komaraneni et al. 2011). However, due to the limited results and difference in the type of infills and out-of-plane loading methods used, the findings in terms of the correlation between the extent of reduction and levels of damage were not consistent. For example, Flanagan and Bennett (1999b) tested a 2.2×2.2 m square clay tile infill bounded by a steel frame. An in-plane cyclic displacement of 0.85% drift corresponding to 80% of the in-plane capacity of the specimen was first applied. At this point, diagonal cracks were developed but no corner crushing was observed. Then the lateral load was removed, and out-of-plane pressure was applied to the panel surface using an airbag to the failure of the specimen. This in-plane drift resulted in an 18% reduction in the infill out-of-plane strength. They concluded that damaged infills can still carry a significant out-of-plane pressure although with greater deformation. Furtado et al. (2016) tested one full-scale clay masonry infilled RC frames under cyclic in-plane and out-of-plane loading. The specimen was subjected to a 0.5% cyclic in-plane drift which was twice the drift at the ultimate load before being tested under out-of-plane loading. This in-plane damage resulted in a 75% reduction in out-of-plane strength when compared with the undamaged control specimen. Calvi and Bolognini (2001) investigated the out-of-plane performance of in-plane damaged weak clay block masonry infills in RC frames. They used 0.4 and 1.2% drift levels (serviceability and collapse limit states, respectively) and conducted the out-of-plane test using the four-point loading scheme. Results indicated 73 and 82% reductions in out-of-plane strength in specimens with 0.4 and 1.2% prior in-plane drift, respectively. Angel et al.

(1994) tested two clay brick masonry infilled RC frames with 0.34 and 0.22% cyclic in-plane drift ratios and the out-of-plane strength reductions were found to be 51 and 27% respectively. In the same study, they also proposed an out-of-plane strength reduction factor equation to account for the effect of prior in-plane damage. The factor is a function of the ratio of applied in-plane displacement to the in-plane displacement at which the first crack occurred. This equation is the only analytical method available in the literature to account for prior in-plane damage. However, it should be pointed out that the equation was calibrated using one specimen as the reference for all other pre-damaged specimens of varying slenderness ratios and masonry materials, which raised the question of its efficacy. Di Trapani et al. (2017) implemented a macroelement model in OpenSees to investigate the out-of-plane strength of infills with in-plane damage. When compared with the specimens tested by Angel et al. (1994), it was concluded that the loss of strength predicted by Angel et al.'s method was significantly higher than that predicted using their model.

This study, consisting of both experimental testing of physical specimens and a finite element study, was conducted to further investigate the effect of prior in-plane damage on the out-of-plane strength of masonry infills bounded by RC frames. Concrete masonry unit (CMU) infills were used as they are a primary infill material used in North America. A 3D finite element (FE) model was used for simulation of out-of-plane behaviour and strength of masonry infilled RC frames with in-plane damage. A concurrent experimental program was conducted on testing of four concrete masonry infilled RC frame specimens with varying levels of prior in-plane damage. The test results were used to validate the model as well as to provide experimental evidence of correlation of prior damage and out-of-plane strength reduction. A subsequent parametric study focusing on several critical parameters

was conducted using the model. A bi-linear equation for calculating the out-of-plane strength reduction factor considering prior in-plane damage was proposed based on both the FE and experimental results.

7.3 Finite Element Modelling Method

A three-dimensional FE model was developed in ABAQUS to simulate the behaviour of the concrete masonry infills bounded by RC frames. The detailed development of the model and its validity in both the in-plane and out-of-plane analysis of the infilled frames are described in Nasiri and Liu (2017) and thus are not repeated herein. The following however, provides a summary of some key modelling aspects of various components of concrete masonry infilled RC frames. The "simplified micro-modelling" technique (Lourenco 1996) was used where the mortar joints were not physically modeled and the CMU dimensions were thus increased by half thickness of the mortar joint in both horizontal and vertical directions. The three-dimensional geometry of CMUs were considered in this method and the corresponding nonlinear mechanical behaviour was defined through the tensile and compressive stress-strain curves implemented in concrete damaged plasticity (CDP) constitutive model in ABAQUS. These curves can be obtained experimentally or by using existing behaviour models for concrete and masonry.

The surface-based cohesive behaviour model in ABAQUS was used to model the interface between the CMUs and between the CMUs and the frame. This behaviour model uses the traction-separation constitutive relationship incorporating shear and tensile failure criteria to capture the possible failure modes of interface. The behaviour model is schematically illustrated in Figure 7.1. In the elastic state, the traction-separation law is controlled by an

elastic response for both normal and transverse deformations as expressed in Eq. (7.1). Traction stress vector t consists of three components, t_n, t_s and t_t, which represent the tensile and two shear tractions. The corresponding separations are denoted by δ_n, δ_s and δ_t.

$$t = \begin{Bmatrix} t_n \\ t_s \\ t_t \end{Bmatrix} = \begin{bmatrix} K_{nn} & 0 & 0 \\ 0 & K_{ss} & 0 \\ 0 & 0 & K_{tt} \end{bmatrix} \begin{Bmatrix} \delta_n \\ \delta_s \\ \delta_t \end{Bmatrix} = K \tag{7.1}$$

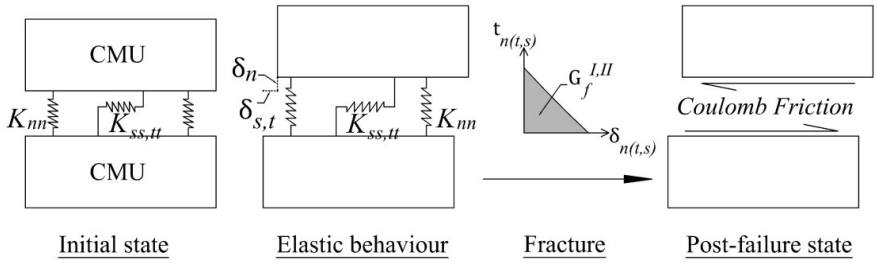

Figure 7.1. Behaviour of the interface interaction

Once failure is detected when tensile or shear stress reaches its limit, two damage models (normal and shear stress damage) control degradation and elimination of the interaction. Upon full degradation of the interface, the model adopts the Coulomb frictional contact between the CMUs or between the CMUs and the frame (see Figure 7.1). The concrete frame was modeled using solid elements with the nonlinear behaviour assigned through the CDP model. Nonlinear material model for steel reinforcement in concrete considering bond-slip effect was implemented (Nasiri and Liu 2017). The explicit analysis method was adopted to solve the nonlinear problem. The explicit analysis is preferred for computation problems involving complicated nonlinear constitutive laws and large deformations and is especially effective for prediction of post-failure behaviour.

7.4 Experimental Investigation

Four concrete masonry infilled RC frame specimens were tested to provide physical results on the effect of in-plane damage on the infill out-of-plane behaviour. As summarized in Table 7.1, the four specimens included one control specimen IF-ND, and three with different extents of prior in-plane damage, IF-D1, IF-D2 and IF-D3. The damage was defined using the drift ratio measured at the frame top beam level, and in this case, drift ratios of 0.66, 1.37 and 2.7% were used for IF-D1, IF-D2 and IF-D3, respectively.

Table 7.1. Details of RC framed masonry infill specimens

Specimen ID	In-plane drift (Δ/h)	Concrete		Masonry		$q_{u,EXP}$ (kPa)	$\frac{q_{u,\mathrm{EXP}}}{q_{u,\mathrm{FE}}}$
		E (MPa)	f_c' (MPa)	E (MPa)	f_m' (MPa)		
IF-ND	0	27800	43.8	2980	17.1	67.2	1.06
IF-D1	0.66%	16900	38.5	2980	17.1	44.4	1.01
IF-D2	1.37%	16900	38.5	2980	17.1	37.6	0.96
IF-D3	2.7%	16900	38.5	2980	17.1	26.4	0.83
						Avg.	0.97
						COV (%)	10

The loading procedure consisted of two steps. First, the in-plane loading was applied at the top beam level monotonically to the desired drift ratio and corresponding physical damage was noted. Next, the in-plane load was removed, and the damaged specimens were tested to failure under out-of-plane load. The in-plane load was applied using a hydraulic actuator whereas the out-of-plane load was applied as a pressure acting on the surface of the infill through an airbag. During the test, the specimens were prevented from lateral and

transverse movement at the base beam level. All specimens had the same dimensions yielding an aspect ratio (h/l) of 0.7 as seen in Figure 7.2.

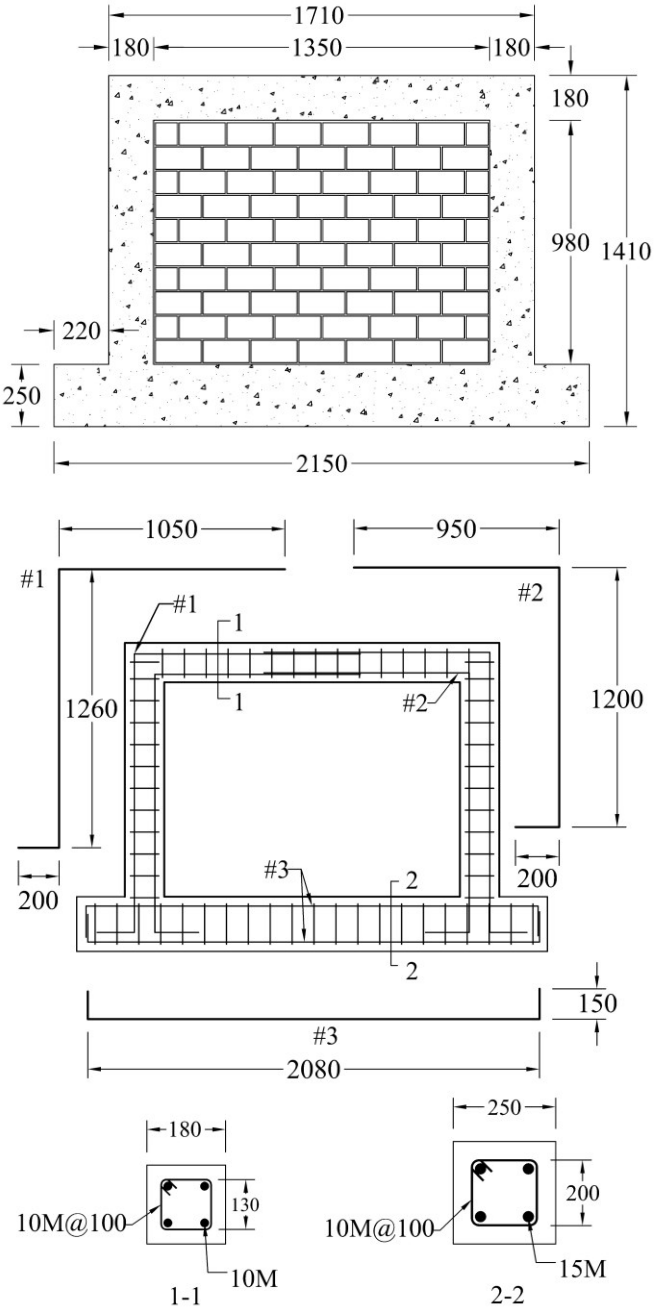

Figure 7.2. Geometric properties of specimens and reinforcement details in the RC frame

The infills were constructed using half-scale standard 200 mm concrete units (CMUs) laid in the running bond. The frame top beam and columns had a 180 mm square section reinforced with four 10M deformed rebars and 10M stirrups spaced at 100 mm centre-to-centre. The base beam had a 250 mm square cross-section reinforced with four 15M longitudinal rebars and 10M stirrups with a spacing of 100 mm centre-to-centre. In addition, four 300 mm by 300 mm L-shaped made from 10M rebars were used to further reinforce the top beam-column corners. Details of the reinforcement are shown in Figure 7.2.

The obtained in-plane load vs. lateral displacement curves for these specimens are shown in Figure 7.3. Damaged conditions of the specimens at the end of in-plane loading is shown in Figure 7.4. Based on the experimental observations, the response can be approximately divided into four stages during which a specific failure mode predominated. For instance, the diagonal cracking region began when the first macro crack appeared on the infill up to the point that crushing of the infill was identified. Referring to both figures, it shows that drift ratios of IF-D1, IF-D2, and IF-D3 corresponded to the failure of diagonal cracking, corner crushing, and post-ultimate.

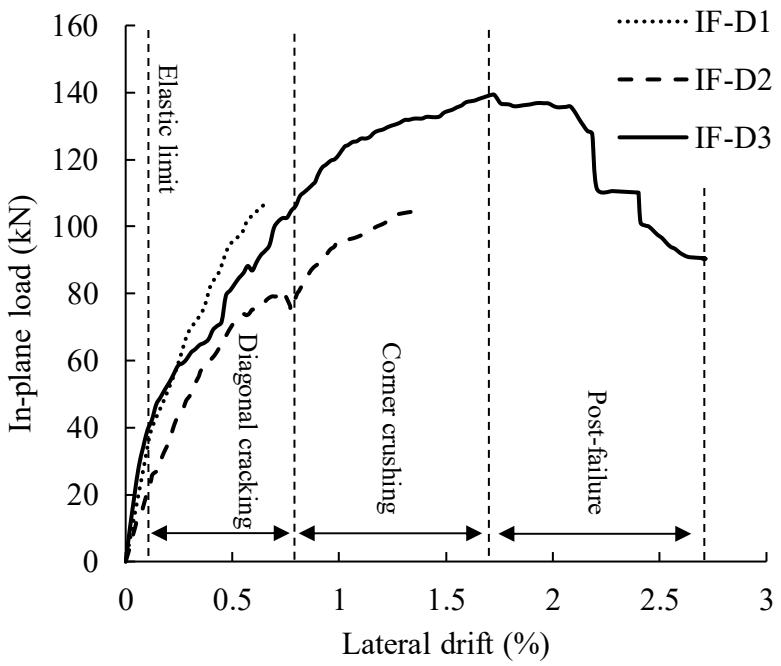

Figure 7.3. Lateral load vs. drift ratio obtained from in-plane tests

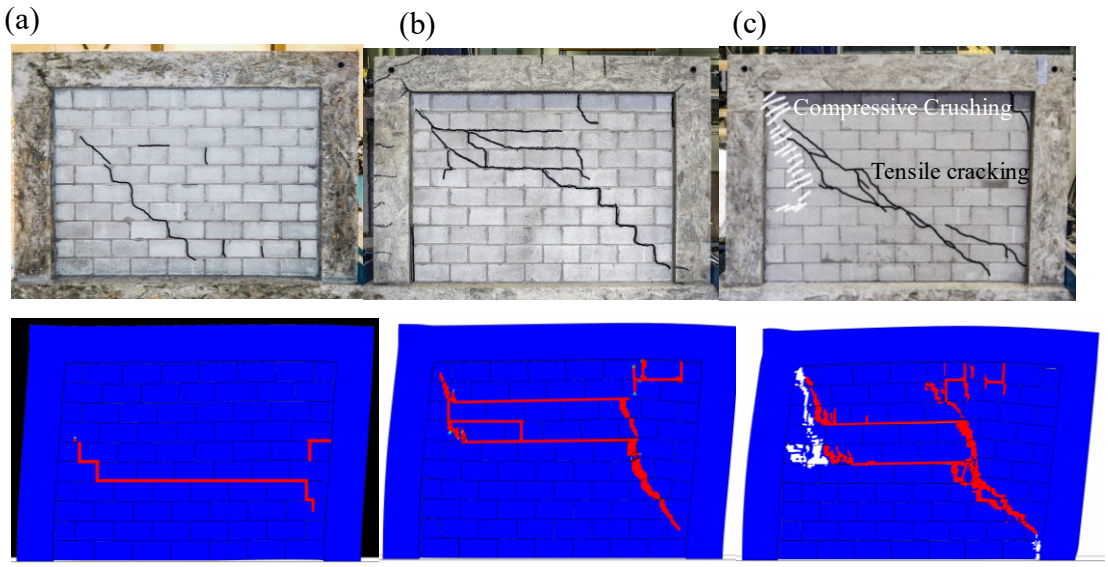

Figure 7.4. Comparison of FE and experimental results for cracking patterns: (a) IF-D1; (b) IF-D2; and (c) IF-D3 (magnified deformation)

The out-of-plane strength vs displacement curves of all four specimens are compared in Figure 7.5 (a) with the ultimate strength attained by each specimen indicated on the curve. For all specimens, LVDT reading at the center of the infill was used in the plots. It can be seen that the prior in-plane damage resulted in a reduction in the specimen out-of-plane strength and increased softness in its behaviour. The greater the damage (higher the drift ratio), the greater the reduction. The normalized strength with respect to the control specimen vs. applied in-plane drift is plotted in Figure 7.5 (b). A 34% reduction was observed in the specimen with 0.66% in-plane drift (IF-D1) which was followed by a 45% reduction in the specimen with 1.23% in-plane drift (IF-D2). The greatest reduction of strength was about 60% observed in IF-D3 with a 2.7% prior in-plane drift, in which case, the specimen has reached well into its post-ultimate stage. In other words, the specimen still had about 40% out-of-plane strength remaining after reaching its in-plane capacity.

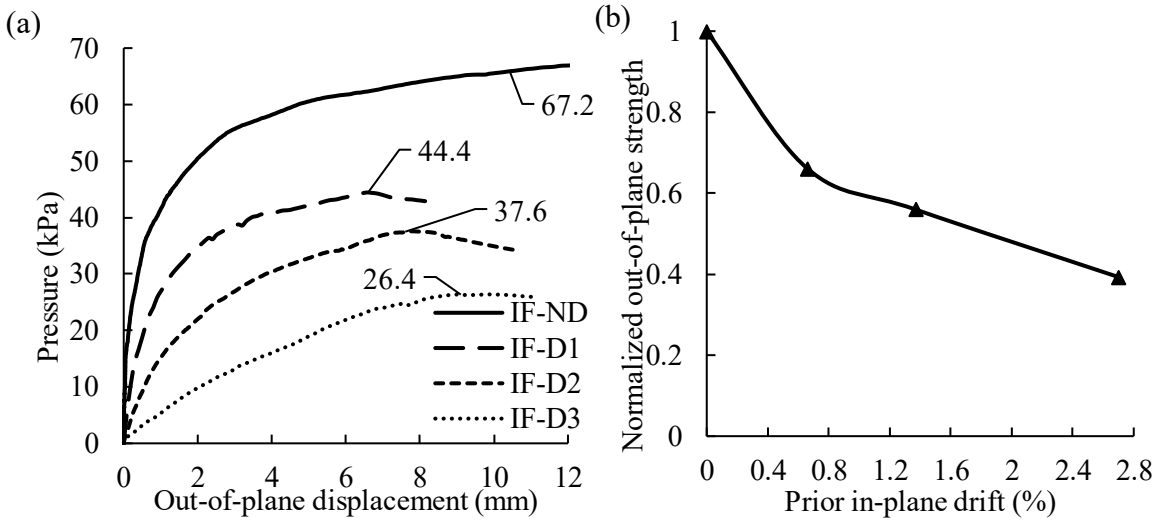

Figure 7.5. Out-of-plane test results: (a) Out-of-plane pressure vs displacement curves; and (b) normalized out-of-plane strength vs. prior in-plane drift

Experimental observations also showed that the cracks from the in-plane loading stage reduced the stiffness of the system during the out-of-plane testing in the initial loading phase. At the onset of the out-of-plane loading, the deformation increased through opening up of existing cracks, however, as the loading increased, new cracks with an X-shaped pattern similar to the control specimen appeared on the leeward face of the damaged infills. Similar to the control specimen, the failure of pre-damaged specimens was also sudden and abrupt, and the failure was initiated by shear cracking of the webs of CMUs near the bounding frame members. It can be observed that the in-plane damage undermined the out-of-plane strength through the following mechanisms: a) compromising the integrity of the infill and reducing the stiffness of the infill panel; b) weakening the infill/frame interface in the form of mortar joint cracking/crushing and gap formation, and c) reducing the stiffness of the bounding frame due to tensile cracking and yielding of reinforcement.

7.5 Validation of the Model

The FE model was verified through three aspects of experimental results. First, the FE predicted damage during the in-plane loading stage is compared with the experimental results as shown in Figure 7.4. It can be seen that the FE model accurately predicted the in-plane cracking pattern and its extent as well as ultimate failure mode (masonry crushing) as drift ratio varied. Secondly, the out-of-plane load vs displacement curves obtained using the FE model are compared with the experimental curves in Figure 7.6 and the ultimate capacity comparison is presented in Table 7.1. It can be seen that the FE model is capable of predicting the out-of-plane behaviour and capacity with reasonable accuracy. As shown in Table 7.1, the average experimental-to-FE capacity ratio, $\frac{q_{u,\mathrm{EXP}}}{q_{u,\mathrm{FE}}}$, was determined to be

0.97 with an COV of 10%. The noticeable discrepancy between the FE and experimental stiffness of the curves (Figure 7.6) is believed to be attributed to the excess deformation in the FE model due to out-of-plane slippage of the masonry infill against the RC frame as well as between CMUs during the out-of-plane loading. It was assumed in the model that after the mortar joints crack, coulomb friction defined through a friction coefficient (0.8 in all models) controls the interaction between the CMUs and the CMUs and RC frame. The accuracy of this interaction is affected by the mesh density which in turn affects the capture of penetration or slippage between the surfaces required for interaction to take place. The discrepancy can be reduced by using a finer mesh and assuming a much higher contact stiffness or a smaller penetration tolerance value but all at the expense of a significant increase in computing time. Note that the ultimate capacity compares well with the experimental results and it is deemed that the assumptions used in this study achieved a balance of reasonable accuracy and computing efficiency. Thirdly, the FE predicted cracking pattern at the end of the out-of-plane test is compared with the experimental results in Figure 7.7 using IF-D2 as an example. In this figure, cracks developed during the in-plane loading stage is marked using black/red lines and those generated during the out-of-plane test, are highlighted in yellow lines. The comparison shows that the FE model accurately simulated the cracking formed and developed in the infill and RC frame. The out-of-plane cracking pattern in IF-D1 and IF-D3 were similar to IF-D2 but those specimens collapsed after the ultimate load, so no photographs were available for comparison. Overall, the FE model is shown to produce capacity results and predict both behaviour and failure accurately.

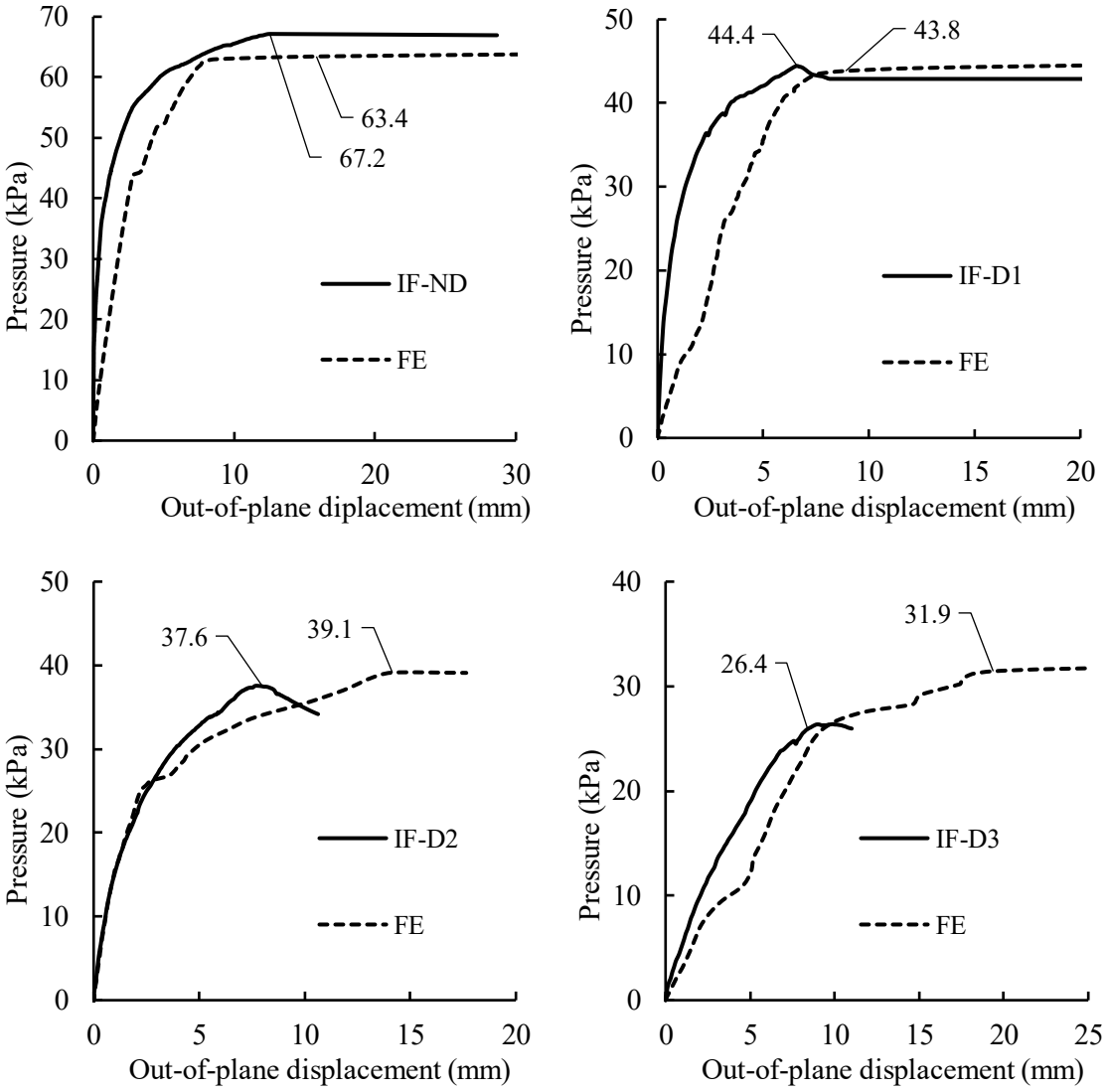

Figure 7.6. Comparison of out-of-plane pressure vs. displacement curves obtained from tests and FE analysis

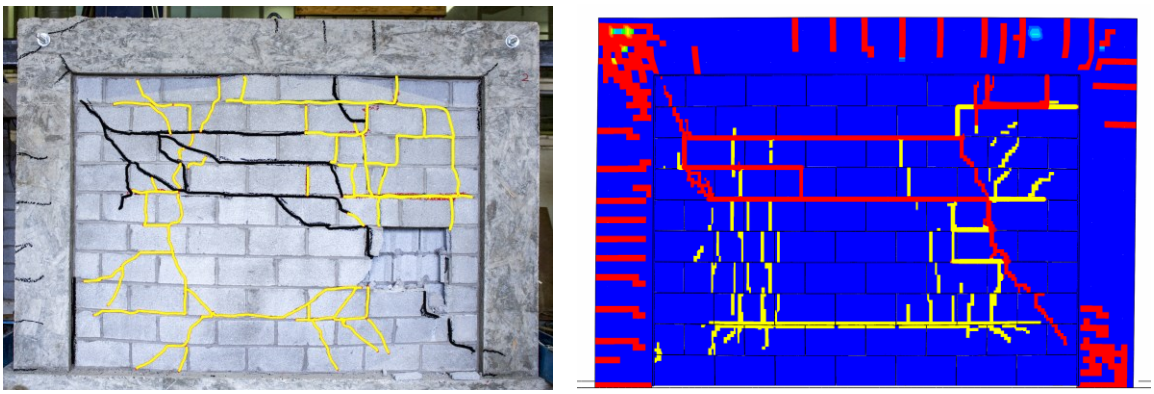

Figure 7.7. Comparison of FE and experimental cracking pattern in IF-D2 at out-of-plane loading stage

7.6 Parametric Study

This section presents results of the finite element study conducted to further the investigation on the effect of in-plane damage on the out-of-plane strength of the infill. In this study, drift ratios of 0.25, 0.5, 1 and 2% were considered to define varying extents of in-plane damage. Two main parameters, i.e. infill aspect ratio and infill masonry strength, were chosen to cover a range of geometrical and material properties of the infills. The infill aspect ratio and masonry strength are considered to be main factors influencing infill damage patterns and cracking extent under in-plane loads as well as infill out-of-plane strength (Nasiri and Liu 2017, 2019a). As shown in Figure 7.8, three aspect ratios, 0.78, 1.0, 1.29, were studied and they were selected to represent slender to squat infills in practice. For each aspect ratio, three compressive strengths of masonry f'_m, of 8, 12 and 16 MPa, were considered to cover a range of masonry strength from weak to strong. For all models, the mechanical properties and details of the RC frames were kept constant. The RC frame consisted of 350 mm square members with the bottom beam fully restrained to simulate the rigidity of a foundation beam. The design of the concrete frame was based on

CSA A23.3-14 in compliance with requirements for minimum flexural and shear reinforcement, reinforcement spacing, and concrete cover. It was done to ensure that adequate ductility is provided, and no shear or brittle failure occurs during analysis. The mechanical properties of the infill and RC frame used in the parameter study are summarized in Table 7.2.

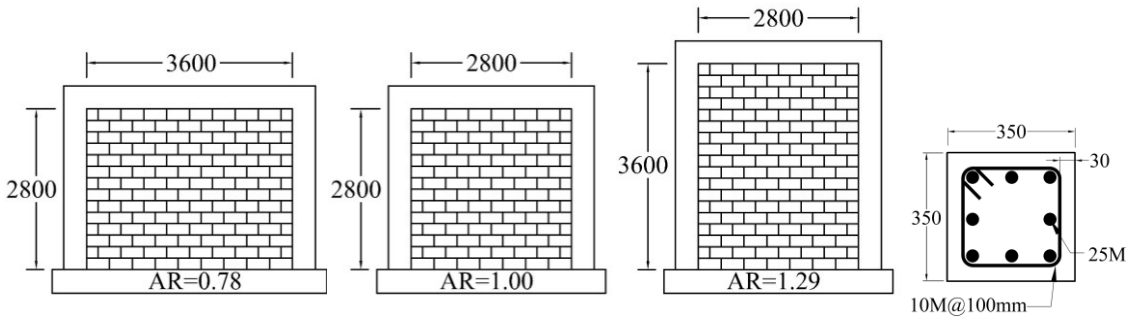

Figure 7.8. Geometric configuration of the models and reinforcement details in the RC frame in the parametric study

Table 7.2. Material properties used in the parametric study

		Compressive strength (MPa)	Elastic modulus (GPa)	Tensile strength (MPa)
Masonry	Weak	8	11.0	0.8
	Intermediate	12	14.0	1.2
	Strong	16	17.0	1.6
RC frame	Concrete	35	30.0	3.5
	Reinforcement	-	220.0	400 (600)*

* Yield and (ultimate) strength

7.6.1 In-Plane Behaviour

When bounded by a relatively strong and ductile RC frame, the in-plane behaviour and failure mode of the infill is controlled by either the tensile/shear cracking or compressive crushing of masonry. The former is characterized by the diagonal tensile cracking or stepped cracks through the mortar joints while the latter is associated with the compressive stress failure in loaded corners of the diagonal strut (corner crushing). Both failure modes are often observed in the in-plane testing of infilled frames (Mehrabi et al. 1996, Nasiri and Liu 2017) but the extent of each mode is different depending on the lateral drift level, infill aspect ratio, and mechanical properties of the infill. For example, Figure 7.9 plots the FE simulated damage for the model with f'_m = 16 MPa at 0.25 and 2% in-plane drifts. As the in-plane drift ratio increased, the damage pattern shifted from discrete diagonal cracking in the infill to extensive cracking throughout the infill, corner crushing and frame cracking. Figure 7.10 shows the damage patterns for a square panel with (a) weak, (b) intermediate, and (c) strong infill at a drift ratio of 2%. For the strong infill, there is more cracking and crushing through CMUs while for the weak infill, the same in-plane drift is accommodated mainly by shear sliding of mortar joints (indicated by the horizontal lines) and less damage to the CMUs. The failure pattern of the intermediate infill is somewhere in between. The in-plane load vs. displacement curves for a square panel with weak, intermediate and strong masonry infills as well as the bare frame response are shown in Figure 7.11. The strong infill reached the peak at lower drift ratios; the intermediate and weak infill curves showed increasingly ductile behaviour. For all models, the first major cracking occurred at drift ratios between 0.15 and 0.35%. This corresponded to the appearance of tensile cracking through the mortar joints and marks the end of elastic limit for the infilled frame. Beyond

this point, failure progressed through opening of new cracks and crushing of masonry. The ultimate strength was observed at 0.65% and 0.7% drifts for strong and intermediate infills, respectively and was considered at 2% for the weak infill as its response levels off and its residue strength is mainly controlled by the strength of the RC frame.

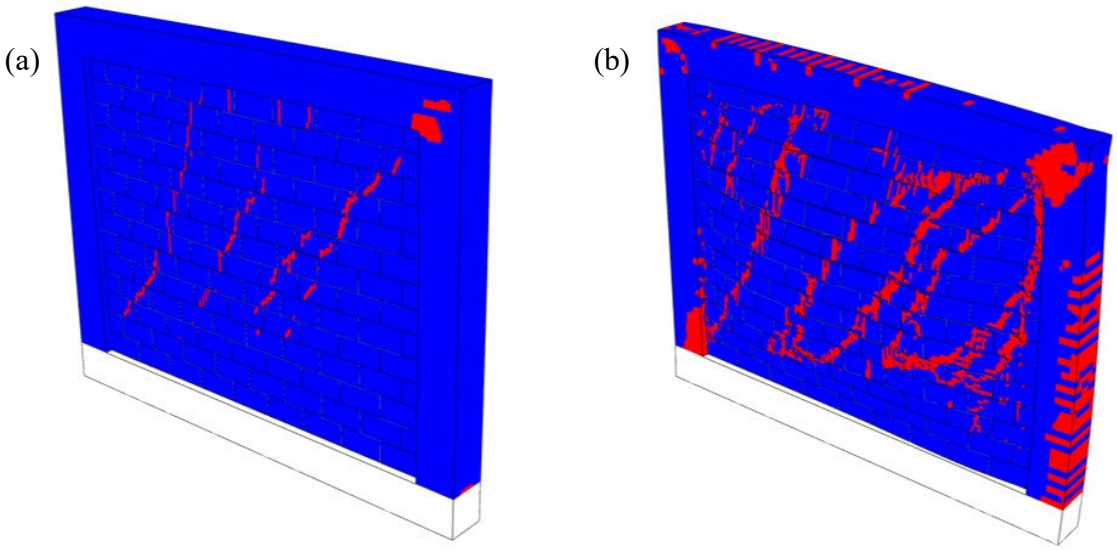

Figure 7.9. Prior damage pattern at: (a) 0.25%, and (b) 2% in-plane drift (AR=0.8, f'm = 16 MPa)

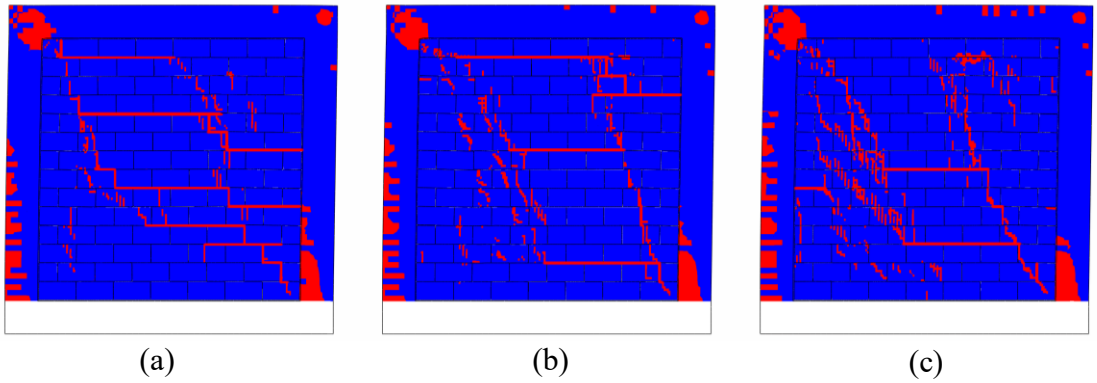

Figure 7.10. Damage patterns for a square panel with: (a) weak, (b) intermediate; and, (c) strong infill.

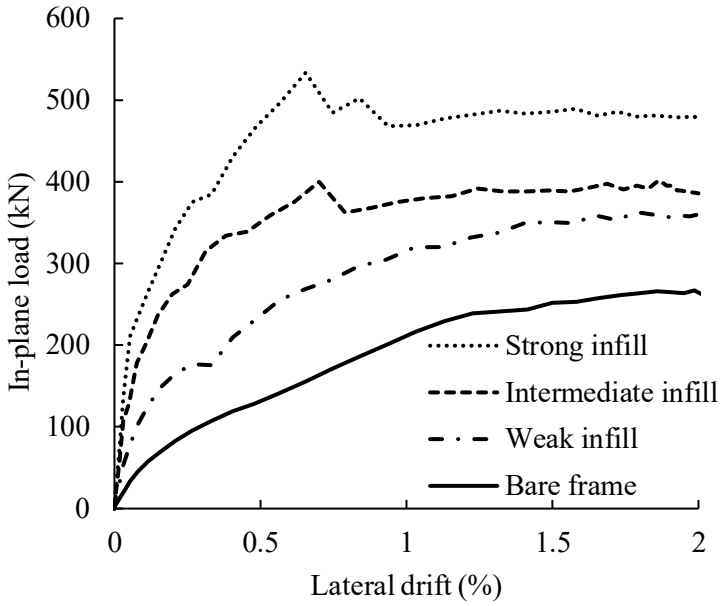

Figure 7.11. In-plane load vs. drift ratio for AR=1.0 model

7.6.2 Out-of-Plane Behaviour with In-Plane Damage

Similar to the experimental loading procedure, the FE analysis was also performed in two steps, i.e. first the in-plane loading step and then the out-of-plane loading step. During the in-plane step, the frame was applied with the desired level of drift and analyzed; and, during the out-of-plane step, the damaged model was analyzed under uniform out-of-plane pressure to failure. The in-plane drift levels were achieved by applying a monotonic displacement to the frame top beam and once the desired in-plane drift was achieved, the load was removed. During the out-of-plane step, the corners of the RC frame were restrained for out-of-plane displacement while the out-of-plane displacement and rotation were permitted along the lengths of the columns and the top beam. In both steps the bottom beam of the frame was fully restrained to simulate a rigid foundation beam.

The out-of-plane pressure vs displacement curves for all models are shown in Figure 7.12. For each case, the model with 0% drift (undamaged) is also included for comparison. It can be seen that the previous discussed experimental observation is also true for infills with different aspect ratio and masonry strength. The in-plane damage reduces the out-of-plane capacity and the amount of reduction is affected by the prior drift experienced by the infill. The higher the drift, the more the reduction. The out-of-plane stiffness of the infill is also highly reduced due to in-plane damage causing the infill to experience an increasingly larger deformation prior to failure as damage level increases.

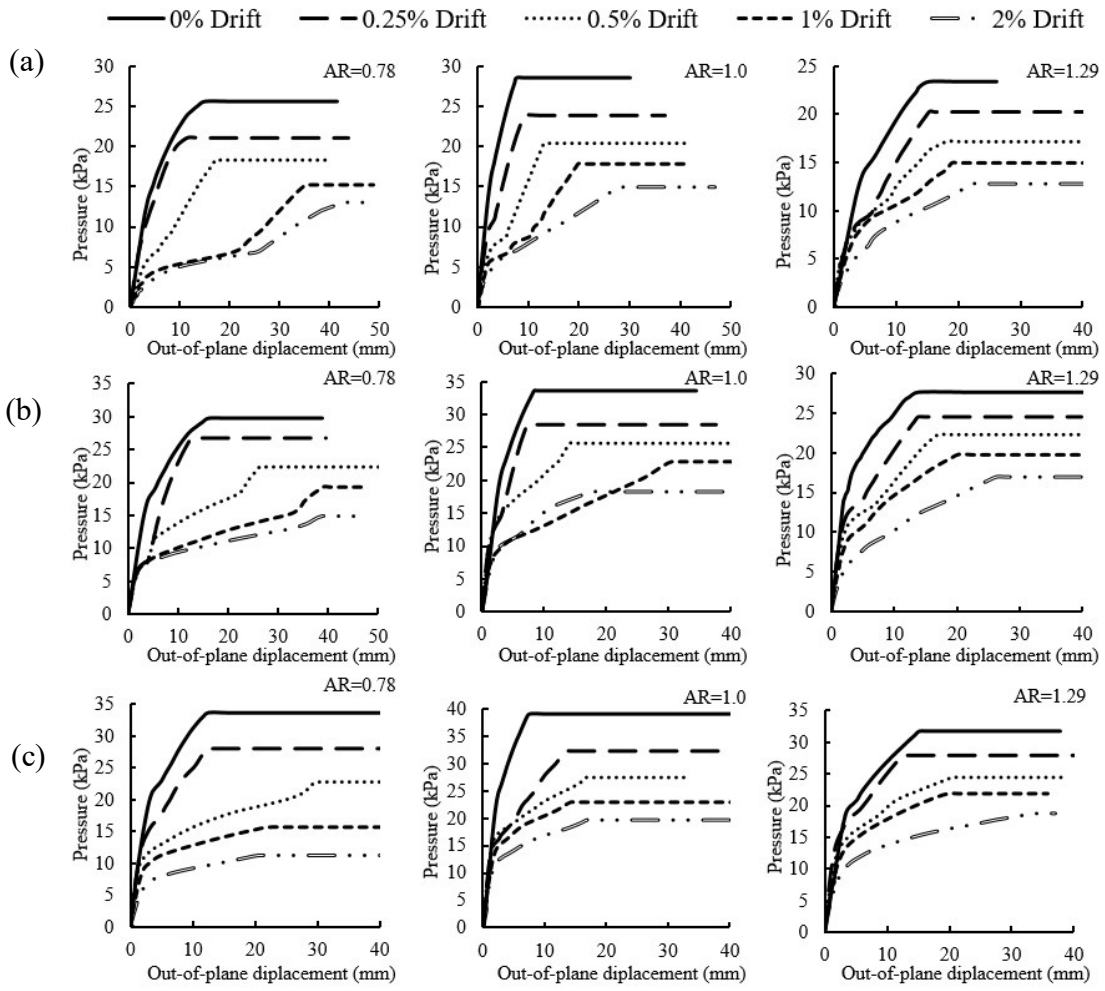

Figure 7.12. Pressure vs. displacement curves: (a) Weak; (b) Intermediate; and, (c) Strong infill

The out-of-plane strengths of damaged model normalized with respect to the undamaged model are plotted in Figure 7.13 (a~c) as a function of prior in-plane drift for weak, intermediate and strong infills. For all masonry strengths studied, the out-of-plane strength of infills shows a similar trend of degradation in which a significant reduction in strength is observed between 0.25 and 1.0% drift ratios and beyond that point, the rate of reduction is decreased. Further, the exact degree of reduction is influenced by both masonry strengths and infill aspect ratios. For the drift up to 0.25%, the effect of masonry strength and infill aspect ratio are insignificant, and all models show around 15% reduction in their out-of-plane strength. However, when the drift increases to 0.5% and beyond, the out-of-plane strength reduction shows marked difference depending on the masonry strength and infill aspect ratio. It appears that for all masonry strengths studied, as the infill becomes more squat, the reduction increases. This is believed to be due to the difference in the in-plane damage experienced by slender vs. squat infills. The squat infill develops a wider diagonal strut under the in-plane load that engages a greater area of the infill and hence causes greater compressive crushing whereas the slender infill has a narrower strut that sustains more cracking through the mortar joints and less crushing at loaded corners, under the same drift ratio. This effect is most pronounced for the strong infill. This is illustrated in Figure 7.14 where in-plane cracking pattern for AR=1.3 and AR=0.8 strong infills have been compared. In this figure more damage and cracking through the CMUs can be observed in AR=0.8 model while damage in AR=1.3 is mainly shear sliding through the mortar joints.

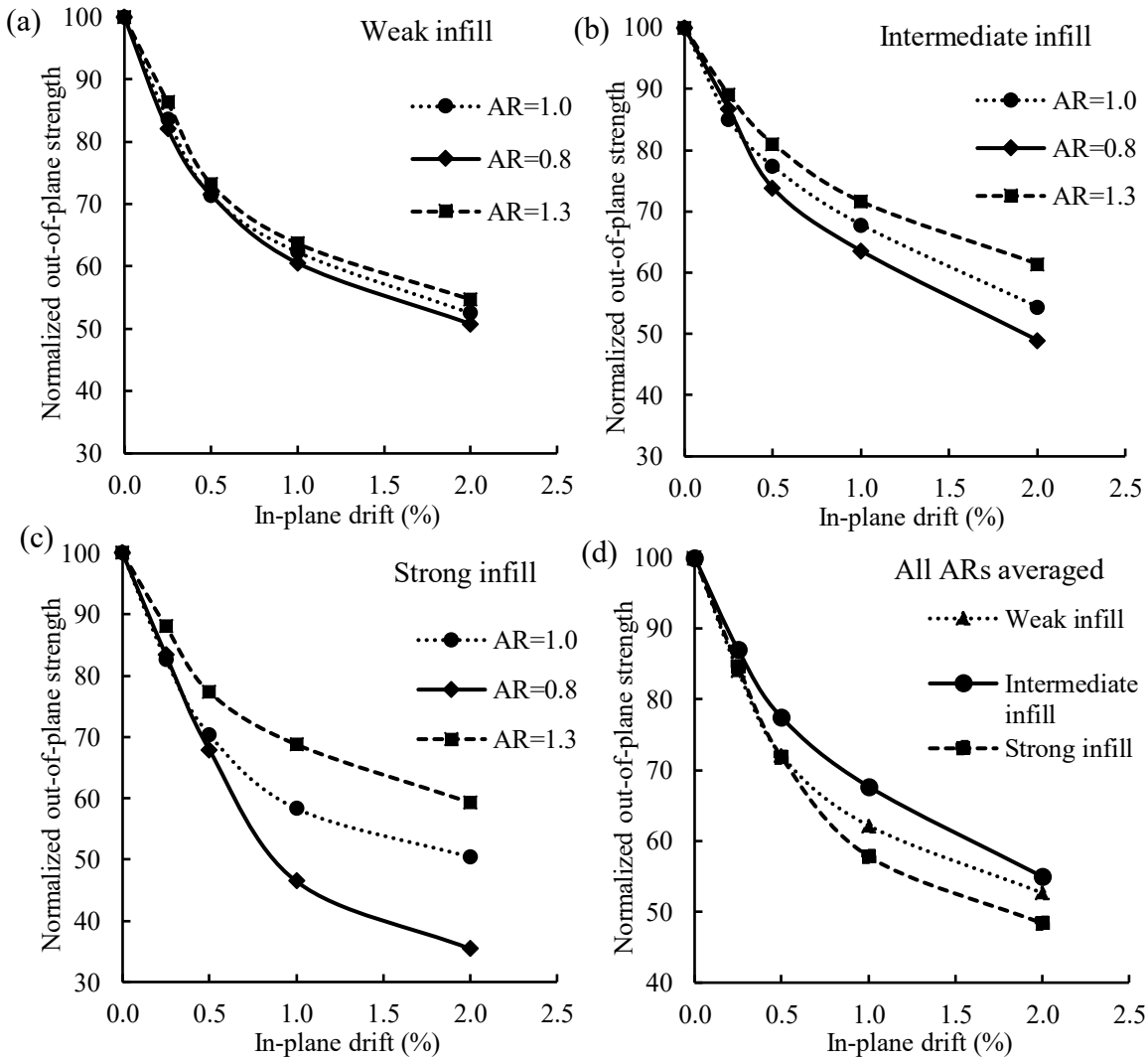

Figure 7.13. Normalized out-of-plane strength vs. in-plane drift ratios for different infill strength and aspect ratios: (a) Weak infill; (b) Intermediate infill; (c) Strong infill; and, (d) Average of all aspect ratios

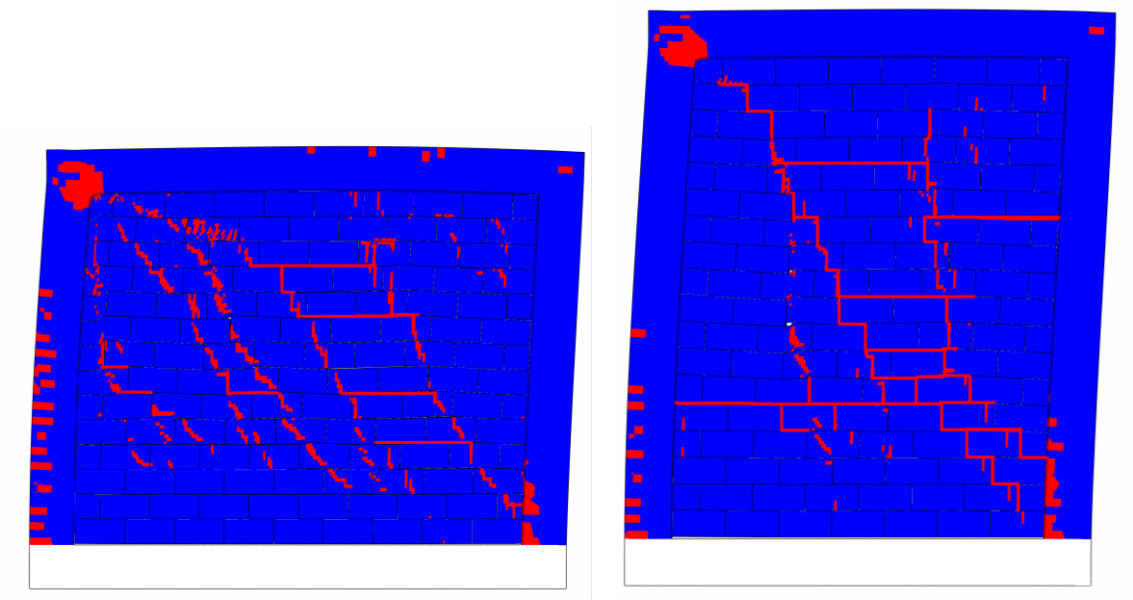

Figure 7.14. In-plane cracking pattern for AR=0.8 and AR=1.3 strong infill models at 1% drift

The effect of masonry strength is shown in Figure 7.13(d) where the normalized strengths averaged over three aspect ratios vs. drift ratios are plotted. For small in-plane drifts (up to 0.25%), the three infill strengths show a negligible difference on the strength reduction, but as the drift ratio increases (> 0.5%), the difference increases. Notedly, the intermediate strength shows an overall better performance when compared to the strong and weak infills. This is again attributed to the type and extent of damage as affected by different infill strengths. Referring to Figure 7.10, the strong infill experiences more damage through CMUs cracking and crushing and damage on the RC frame via the larger diagonal strut component acting on the RC frame. The weak infills suffer mainly from the cracking through the mortar joints and shear sliding. The intermediate infills lie somewhere in between and thus showed the least reduction at a given drift level.

7.6.3 Consideration of Infill Slenderness

The infill slenderness (h/t) is a relatively more researched parameter and its effect on the out-of-plane strength of the infill is relatively better understood (Angel et al. 1994, Dawe and Seah 1989b, Flanagan and Bennett 1999b). Angel et al.'s analytical equation for the out-of-plane strength reduction factor incorporates h/t as the only geometric parameter. In this study, the effect of infill slenderness was also investigated by repeating the analyses for AR=1.0 models with two other CMU thicknesses of 150 and 100 mm using the intermediate masonry strength infill (f'_m=12 MPa) as an example. These thicknesses, in addition to the original model thickness, provided slenderness ratios of 14.0, 18.6 and 28.0. The normalized out-of-plane strengths of the damaged models with respect to the undamaged model for the three slenderness ratios are plotted in Figure 7.15 as a function of prior in-plane drift. It shows that the variation in slenderness has a negligible effect on the strength reduction at a low drift level (<0.25%), which is in line with previous observations on aspect ratio and masonry strength. As the drift level increases beyond 0.5%, the figure shows that the increase in slenderness ratio results in an increase in strength reduction. However, the greatest reduction is approximately 10% when the slenderness ratio is increased from 14 to 28. This is illustrated in Figure 7.16 where the failure patterns obtained from the FE analysis for slenderness 14 and 28 did not show significant difference.

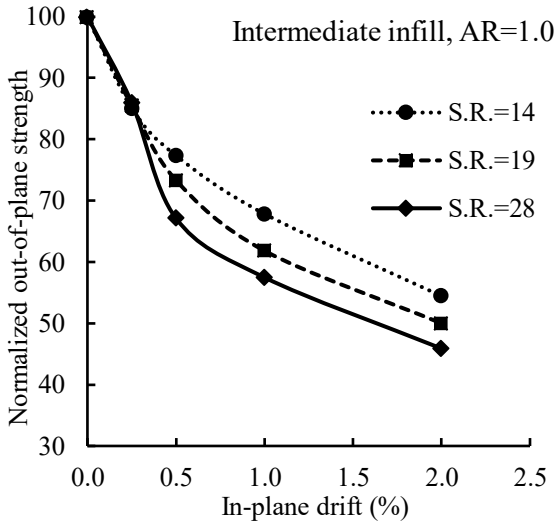

Figure 7.15. Normalized out-of-plane strength vs. prior in-plane drift curves for different slenderness ratios

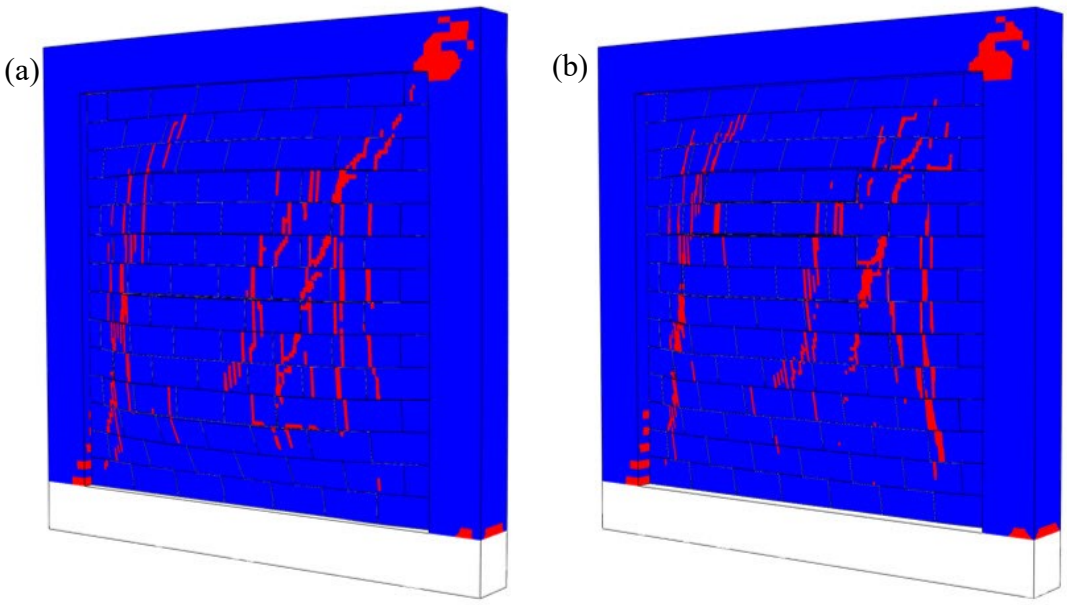

Figure 7.16. Cracking pattern for: (a) SR=14; and, (b) SR=28 with 0.5% in-plan drift at the ultimate out-of-plane pressure (magnified deformation)

7.6.4 Consideration of Cyclic Loading

The FE results showed that for most models, at a drift ratio of 2% which is considered at or beyond the ultimate in-plane capacity for typical infills in practice, there is still approximately 40-50% out-of-plane strength remaining. Noting that the in-plane loading was applied as monotonic in the models, the parametric study was extended to include analysis with cyclic in-plane loading in an effort to provide closer simulation of the in-plane damage in a practical lateral loading situation. The FE analyses were repeated by applying the cyclic in-plane displacement. Due to the lengthy computational time required to run for 3D models, only one cycle of in-plane drift was simulated and applied to the intermediate infills. The magnitudes of the cycles were chosen to be similar to the monotonic loading as shown in Figure 7.17(a).

The normalized out-of-plane strengths of cyclically loaded models are plotted and compared with the pre-monotonically loaded models in Figure 7.17(b to d). As expected, all pre-cyclically loaded models show a greater reduction in out-of-plane strength as a result of in-plane damage, and the largest difference between the cyclic loading and monotonic loading cases occurs in the range of drift ratios 0.25-1%. Beyond that range, the difference diminishes, which indicates that at a high drift ratio, the damage caused by monotonic loading is extensive enough to be comparable to the cyclic loading and thus their effect on out-of-plane strength is comparable. In terms of infill aspect ratio, the largest impact of the pre-cyclic loading vs the pre-monotonic loading occurs in AR=1.0 models with a maximum difference of 13% at a drift ratio of 0.5% (Figure 7.17 (c)). In other words, the damage caused by pre-cyclic in-plane loading results in a 13% more reduction in the

out-of-plane strength of the infill than that caused by pre-monotonic in-plane loading. Figure 7.18 shows a comparison between the in-plane and out-of-plane cracking patterns in AR=1.0 model for monotonic and cyclic loading at the drift ratio of 0.5%. The figure shows that cyclic loading generates a cracking pattern in a more or less symmetrical manner in the other side of the infill but the general cracking pattern (including the location and extent of cracking) between the two loading scenarios is similar. In the out-of-plane step, the pre-cyclically loaded model attains more damage but the arching and failure mechanism (Figure 7.17 (c and d)) appears similar in both loading scenarios, which explains that there is a noticeable difference in out-of-plane strength reductions by two loading scenarios but the difference is not overly significant.

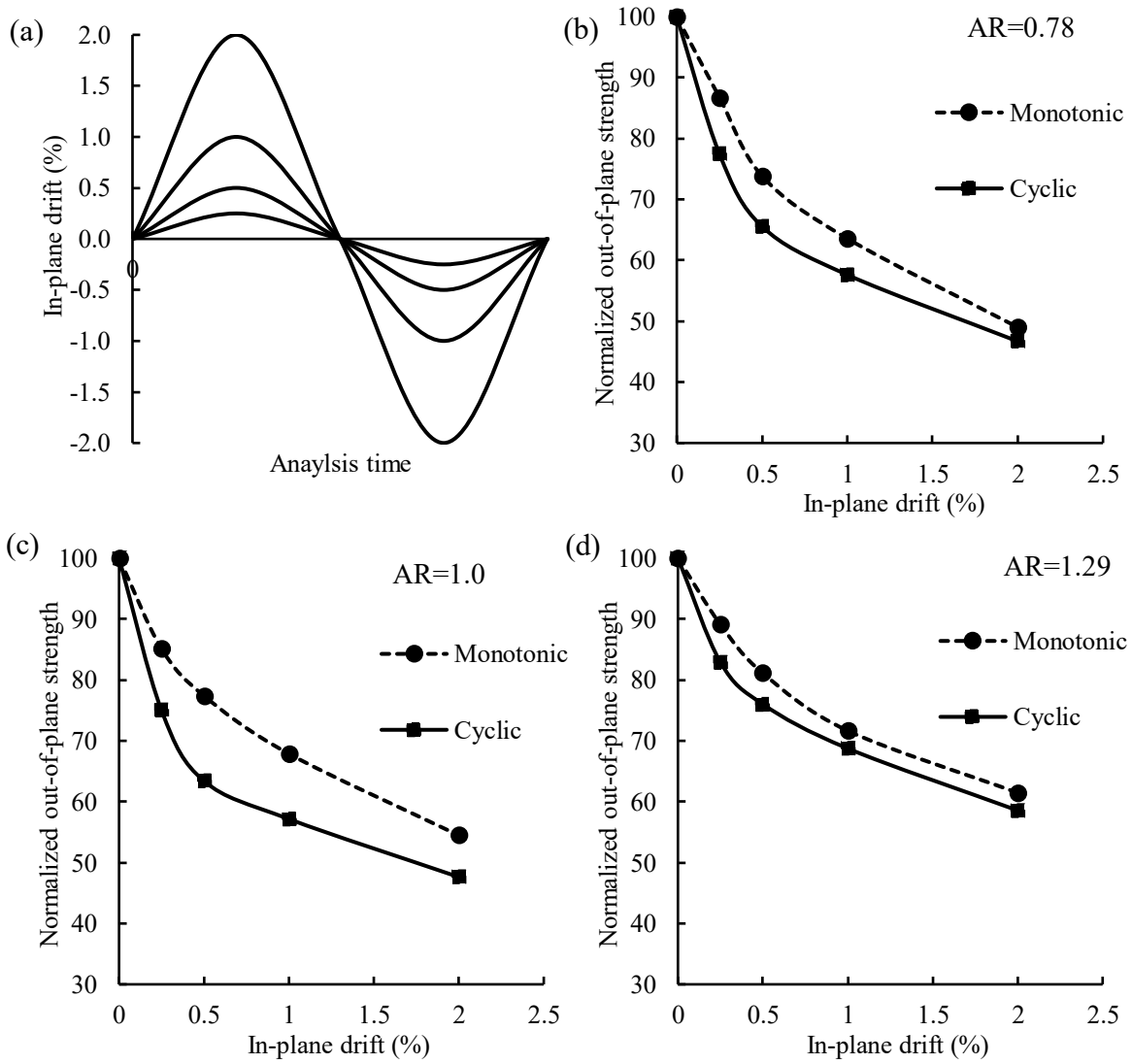

Figure 7.17. Cyclic in-plane loading analysis for out-of-plane strength reduction: (a) Cyclic loading history; (b) AR=0.8 infill; (c) AR=1.0 infill; and, (d) AR=1.3 infill

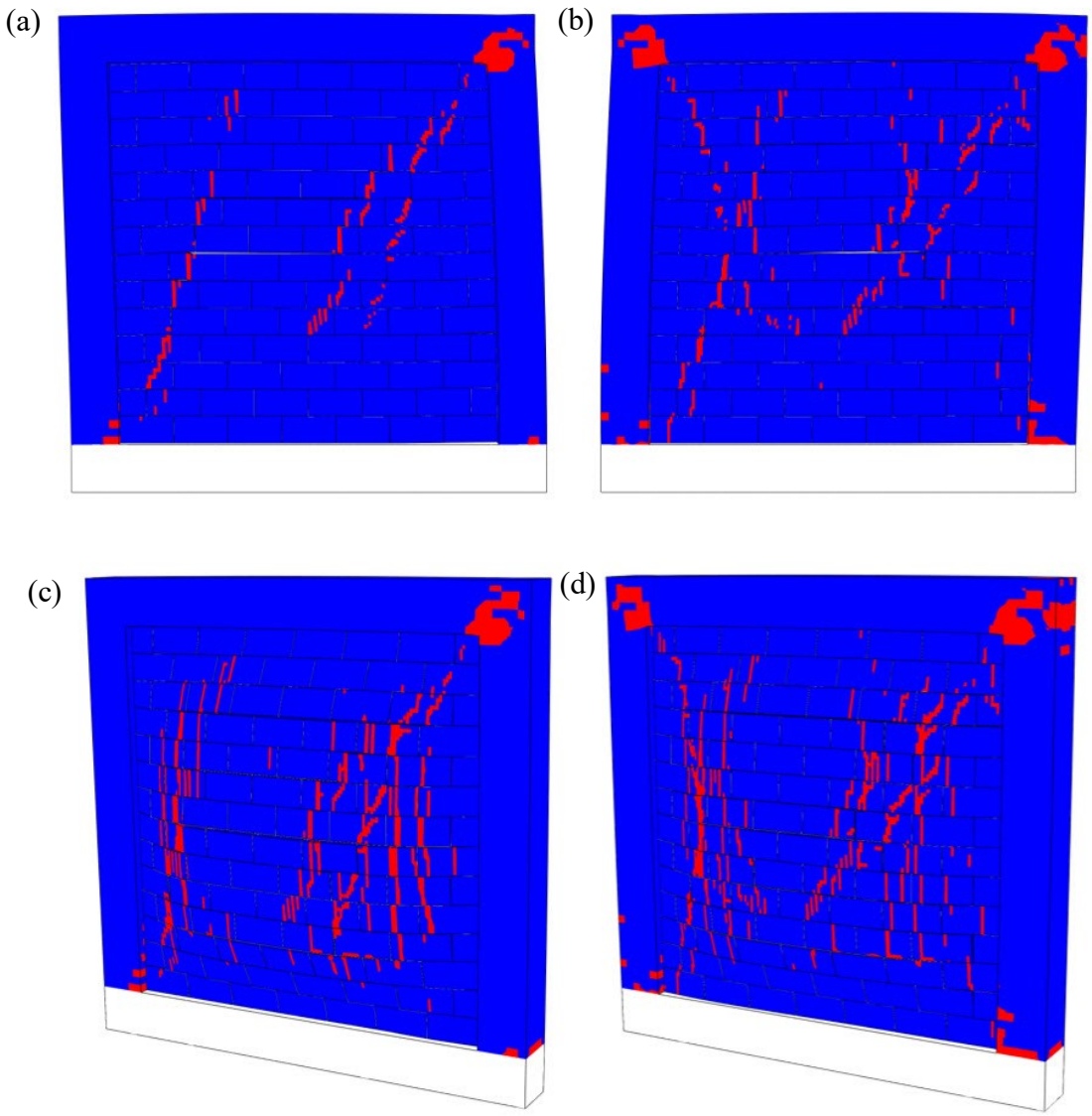

Figure 7.18. Cyclic and monotonic cracking comparison in different steps (6×magnified deformations): (a) Monotonic in-plane; (b) Cyclic in-plane; (c) Monotonic out-of-plane; and, (d) Cyclic out-of-plane

7.7 Evaluation of the Existing Analytical Method

This section examines the efficacy of the existing analytical model, i.e. Angel et al.'s method, using the results of this study. The method considers the effect of prior in-plane

damage on the infill out-of-plane strength through a strength reduction factor R_1 as expressed as follows:

$$R_1 = 1, \qquad \frac{\Delta}{\Delta_{cr}} < 1$$

$$R_1 = \left[1.08 + \left(\frac{h}{t}\right)\left(-0.015 + \left(\frac{h}{t}\right)\left(-0.00049 + 0.000013\left(\frac{h}{t}\right)\right)\right)\right]^{\frac{\Delta}{2\Delta_{cr}}}, \quad \frac{\Delta}{\Delta_{cr}} \geq 1 \tag{7.2}$$

where Δ is the maximum lateral deflection experienced by the infill and Δ_{cr} is the lateral deflection required for the cracking of the infill. This equation suggests that no reduction in out-of-plane strength is expected when no cracking occurs during the in-plane loading; and beyond the cracking displacement, there is a power relationship between the reduction of the strength and the in-plane displacement. The equation also suggests that the rate of reduction is highly dependent on the infill slenderness ratio. The higher the slenderness ratio, the higher the strength reduction. Figure 7.19 compares reduction factor vs. in-plane drift curves obtained using the method as well as the experimental and numerical results presented in the previous sections.

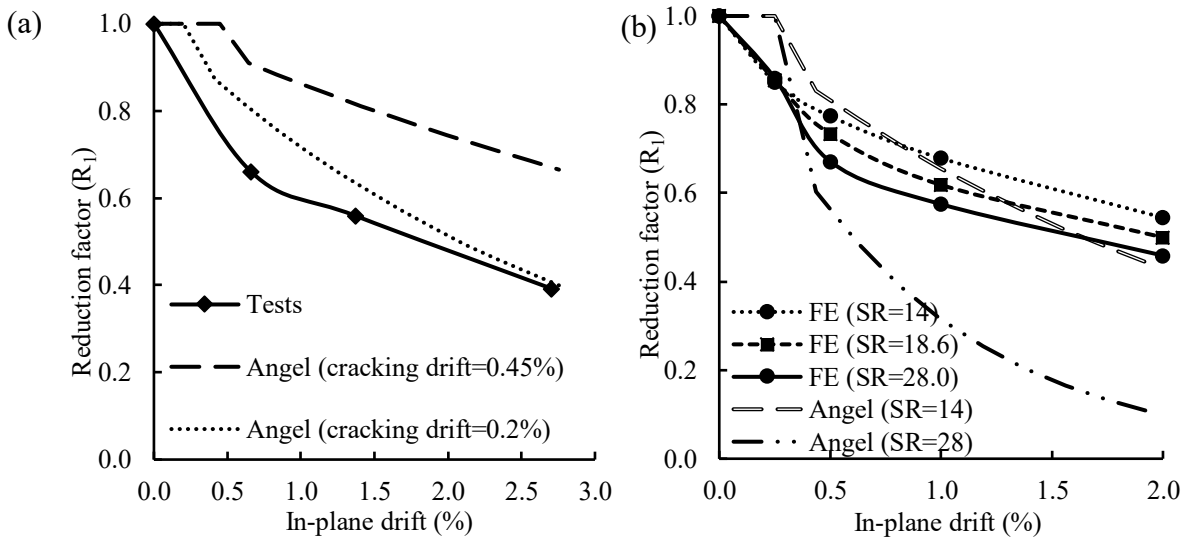

Figure 7.19. Out-of-plane strength reduction comparison between Angel et al.'s method and: (a) test results; and, (b) finite element results

Figure 7.19 (a) shows comparison of the test results (SR=11 for specimens) and the analytical values obtained assuming initial cracking drifts Δ_{cr}/h at 0.2 and 0.45% respectively. It indicates that the analytical value is sensitive to the initial cracking deflection and the variation in the predicted reductions increases significantly in higher drift ratios when different initial cracking deflections are used. The experimental results of the in-plane tests showed that the elastic limit was found to be at 0.15% drift and the initial cracking was observed in the range of 0.25~0.6% drift ratios for different specimens. This suggests a high level of inherent variance and uncertainty in the determination of point of initial cracking due to the randomness of masonry materials. Secondly, the definition of initial cracking was left to interpretation as it is not clear whether it refers to the first appearance of cracks or the formation of the first major crack as discrete cracks propagate in separate segments and form a continuous crack on the infill. The process of forming the latter major crack may place the infill in a different drift range. Figure 7.19 (b) compares

the FE results on slenderness ratio effect with the analytical values with the cracking deflection Δ_{cr}/h assumed at 0.25% drift ratio. It shows that Angel et al.'s method predicts a much more pronounced effect of slenderness ratio on the degree of reduction than the FE results. In addition, Angel et al.'s method produces an exponentially increasing reduction as drift ratio increases while the FE results shows a diminishing reduction rate. An assessment of Angel et al.'s method by Di Trapani et al. (2017) showed a similar overestimation of strength reduction by the method as infill slenderness increased.

7.8 Suggested Reduction Factor

A new reduction factor equation based on the afore-presented results is discussed in this section. In this effort, the upper and lower bound reduction curves as well as the mean reduction curve obtained from all FE models are plotted in Figure 7.20 together with the experimental results from this study. It is recognized that the effect of studied parameters is not independent and rather intertwined which makes the development of an equation incorporating all individual parameters difficult. Hence, the new reduction factor equation was based on the lower bound of the FE data as a conservative estimation. As shown, a bilinear curve was proposed to calculate the out-of-plane strength reduction due to prior in-plane damage. Expressed in Eq. (7.3), the proposed reduction factor is a function of in-plane drift Δ/h, instead of Δ/Δ_{cr}. Also note that Δ/h is expressed as a percentage in the equation.

$$\begin{aligned} R &= 1 - 0.83 \times {}^{\Delta}/_{h} && {}^{\Delta}/_{h} \leq 0.6 \\ R &= 0.5 - 0.1 \times ({}^{\Delta}/_{h} - 0.6) && {}^{\Delta}/_{h} > 0.6 \end{aligned} \tag{7.3}$$

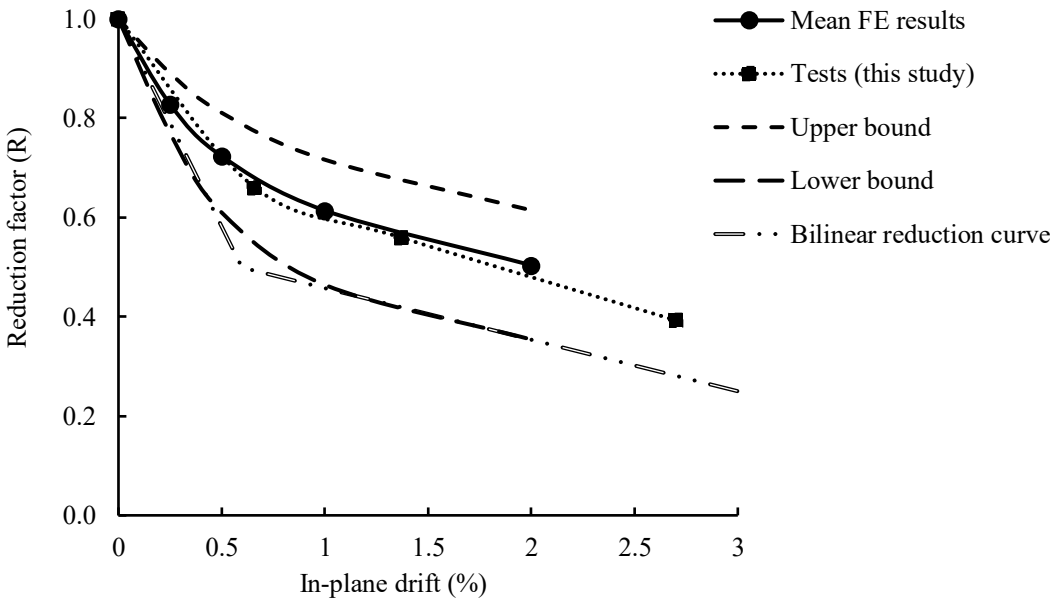

Figure 7.20. Proposed reduction factor equation with FE and test results

The performance of the proposed reduction factor equation is evaluated against the test results obtained from this study as well as those available in the literature. Table 7.3 shows a summary of this evaluation with infills in two categories of concrete masonry unit and solid maosnry brick respectively. It should be pointed out that the data sample size is small and also has an inherent large scatter, which makes any conclusive assessment of the equaiton difficult. However, some useful observations are made as follows. When compared with Angel et al.'s method, the proposed equation showed an overall improved and slightly conservative estimate while the former provides marked overestimate in residue out-of-plane strength. When two types of masonry infills are compared, the proposed reduction factor seems to perform better in the case of concrete masonry infills, providing consistently conservative estimate with a low COV. This is expected as the proposed equation was developed on concrete masonry infills and was intended to capture the lower bound of reduction. On the other hand, the proposed reduction factor seems to

overestimate the residue out-of-plane strength for solid brick infills. It suggests that the out-of-plane failure mechanism of solid brick infills might be different from concrete masonry infills which leads to much smaller residue strength. It is thus recommended that further assessment of the equation needs to be conducted with more data points to cover different infill types and infill/frame geometric and material properties.

Table 7.3.Comparison of experimental and analytical reduction factor

Ref.	Spec.	Infill dimensions (l×h) (mm)	t (mm)	h/l	h/t	Δ/h (%)	Δ_{cr} (mm)	R_{exp}	R_1 (Angel et al.)	R_{exp}/R_1	R (this study)	R_{exp}/R
Concrete Masonry Blocks												
This study	IF-D1	1350×980	90	0.7	10.9	0.66	6.3	0.66	0.93	0.71	0.45	1.47
	IF-D2	1350×980	90	0.7	10.9	1.37	5.5	0.56	0.85	0.66	0.42	1.33
	IF-D3	1350×980	90	0.7	10.9	2.7	5.9	0.39	0.74	0.53	0.28	1.40
Flanagan and Bennett (1999b)	19	2240×2240	195	1.0	11.5	0.85	4.5	0.82	0.74	1.10	0.48	1.54
							Avg.			**0.75**		**1.44**
							COV (%)			**33**		**6**
Solid Masonry Bricks												
Angel et al. (1994)	2b	2400×1600	50	0.7	34.0	0.34	2.8	0.49	0.52	0.94	0.71	0.69
	3b	2400×1600	50	0.8	34.0	0.22	1.8	0.73	0.50	1.46	0.82	0.89
Calvi and Bolognini (2001)	6	4200×2750	135	0.7	20.0	0.4	5.5	0.27	0.68	0.40	0.67	0.41
	2	4200×2750	135	0.7	20.0	1.2	6.5	0.18	0.40	0.45	0.44	0.41
							Avg.			**0.81**		**0.6**
							COV (%)			**61**		**39**
Overall performance							**Avg.**			**0.78**		**1.02**
							COV (%)			**47**		**47**

7.9 Limitations

The model developed in this study assumed that the frame is relatively strong and ductile with shear failure prevented. The in-plane damage is mostly concentrated in the infill and

the frame only experiences opening of tensile cracks and yielding of reinforcements. The results do not apply to the situation where the frame failure controls the system strength. Secondly, during either the monotonic or cyclic analysis, the damaged infill was assumed to remain in contact with the bounding frame to allow the arching action to develop. The results are not applicable to situations where the infill experiences significant separation from the frame and the infill may slip out of the frame.

7.10 Conclusion

This paper presents results of both an experimental and a numerical study on the effect of prior in-plane damage on the out-of-plane performance of masonry infills bounded by RC frames. The experimental results showed the correlation between the reduction in out-of-plane resistance and prior in-plane drift levels but also revealed that a significant residue out-of-plane strength can be expected from damaged infills which have reached their in-plane capacity. The numerical study using a 3D finite element model was performed to further the study on the correlation as affected by several influential geometric and material parameters. Some conclusions are summarized as follows:

1. For all models studied, the effect of geometric and material parameters was most pronounced for drift ratios between 0.25 and 1.5%. The rate of reduction began to diminish for greater drift ratios.
2. At a given in-plane drift ratio, the squat infills ($h/l<1$) showed more out-of-plane strength reduction when compared to slender infills ($h/l>1$). When comparing the effect of infill masonry strength, the intermediate masonry strength, on average, had more

residue out-of-plane strength than either the strong or weak infill. The slenderness ratio was shown to affect the out-of-plane strength reduction, but its effect is not significant.

3. The damage caused by cyclic in-plane loading resulted in more out-of-plane strength reduction than monotonic in-plane loading and the difference between the two loading situations was more pronounced in smaller drift ratios (<1%).
4. Evaluation of the existing analytical method suggested that the inherent randomness and uncertainty in defining the drift causing the first cracking could result in either under- or over-estimation of reduction factors for infills with different mechanical and geometric properties.
5. A bi-linear equation was proposed as a lower bound estimate for the out-of-plane strength reduction considering prior in-plane damage. The equation was shown to produce improved estimate when compared with the existing analytical method. It is cautioned that applicability of the proposed equation for solid brick masonry infills needs to be further investigated.

7.11 Acknowledgement

The authors wish to recognize the contribution of financial assistance by the Canadian Concrete Masonry Producers Association and Natural Sciences and Engineering Research Council of Canada.

Chapter 8 Summary and Conclusions

A finite element model was developed to simulate the in-plane and out-of-plane behaviour of masonry infills bounded by reinforced concrete frames. While it is understood that the frame is also a main contributor of the system behaviour, this research is focused on the behaviour of infills and thus the frame geometric and material properties were kept constant in both the experimental and numerical studies. The three-dimensional geometry of components as well as nonlinear behaviour of masonry block, concrete, steel, and mortar joint interface was considered in the modelling. Where relevant, information and reference for determination of each of the model input parameters were provided to make it easy to be adopted for other masonry infill geometry and configuration. Concurrent with the numerical modelling, a comprehensive experimental program was conducted to obtain physical data on the influence of a group of less-studied parameters on the behaviour of the infilled frames and provide detailed information for calibration of the FE model. Subsequent to validation of the model, parametric studies on several influential parameters on both in-plane and out-of-plane behaviour were carried out. Numerical and experimental findings were also used to evaluate the efficacy of the available methods for determination of out-of-plane strength and modifications were suggested to provide a more rational consideration of arching behaviour. Out-of-plane strength of masonry infills which sustained prior in-plane damage was also studied numerically and experimentally for a range of infill geometric and mechanical properties, and a simplified solution to count for the in-plane damage was proposed.

Conclusions drawn from the results of this research are summarized in the following.

8.1 In-Plane Behaviour

8.1.1 Experimental Observations

- When compared to the bare frame, presence of the infill resulted in 128% and 154% increases in the ultimate in-plane capacity and initial stiffness, respectively.
- Presence of gap between the infill and the RC frame reduced the ultimate in-plane capacity of the infilled frame. It suggests that the gap at the infill to the top beam of the frame resulted in more reduction than the gap at the infill-to-column interface whereas the latter gap resulted in a more reduction on the initial stiffness of the system.
- Presence of openings in the infill reduced the ultimate in-plane capacity of the infilled frame. The degree of the reduction is in proportion to the opening size. For a given opening size, the door opening resulted in a more significant reduction than the window opening.

8.1.2 FE Modelling

- The three-dimensional simplified micro-modelling approach was capable of capturing the behaviour of the system in terms of its initial stiffness, ultimate capacity, post-ultimate strength and load-displacement curves with good accuracy. Using 3D elements and modelled on the basic geometric and material level, this model was also capable of simulating the out-of-plane behaviour of masonry infills with a boundary frame.

- Failure modes, tensile cracking and compressive crushing patterns in masonry infills and RC frames were predicted accurately.
- Of all critical mortar interface parameters, the assumption of initial shear and tensile strength of the mortar joint, friction angle of the failure surface, and dilation angle were shown to have a significant effect on the simulation of failure mode, ultimate strength and load-displacement curves while the fracture energy release during failure was shown to have a negligible effect on the in-plane behaviour.

8.2 Out-of-Plane Behaviour

8.2.1 General behaviour

- In all the out-of-plane tests, the arching of masonry infills was observed to be the main load-resisting mechanism in specimens.
- All specimens tested under out-of-plane loading had a sudden failure characterized by out-of-plane collapse of the infill.
- Tensile cracks propagated on the infill surface throughout the out-of-plane loading, but the final failure mode was identified as web shear cracking in the CMUs initiated near the frame members.

8.2.2 Effect of Interfacial Gap

- Comparing with the control specimen, the presence of gaps at the infill-to-column (side gap) or infill-to-beam (top gap) interfaces, resulted in reduction of two-way arching to one-way arching under uniform out-of-plane loading.

- The cracking pattern of the specimen with top gap was similar to yield-line pattern of a wall supported on three sides, and the specimen with the side gap developed arching action in the vertical span direction.
- A 10 mm gap at the infill-to-beam interface (top gap) caused a more pronounced reduction in strength than the same sized gap but positioned at the infill-to-column interface (side gap). The top gap was found to be more detrimental than the side gap in the tests.
- Compared with both the top and side gap, a full separation gap (gaps all around the infill) resulted in a greater reduction in out-of-plane strength and reduced the two-way arching to one-way vertical arching.

8.2.3 Effect of Infill Opening

- The effect of window opening on the out-of-plane infill strength is dependent on the type of openings, i.e, blast resisting and non-blast resisting openings.
- Non-blast resisting openings increase the out-of-plane strength and this increase is a function of opening size.
- Blast-resisting openings reduce the out-of-plane strength; however, this reduction was almost equal in all infill opening sizes studied.

8.2.4 Effect of Infill Aspect Ratio

- For a given infill height, reduction in the aspect ratio results in a reduction of the out-of-plane strength of the infill. This reduction varies with the frame stiffness and

approaches a constant value for very small aspect ratios (extremely long infills) in infills with rigid boundary.

- For a given infill area and boundary frame stiffness, the infill with smaller aspect ratio has higher out-of-plane strength.

8.2.5 Effect of Infill Slenderness Ratio

- Slenderness ratio of the infill (*h/t*) has a significant effect on the out-of-plane strength. An increase in slenderness ratio results in an exponential reduction in strength.
- For small slenderness ratios the failure is characterized by pure shear failure near the supports while for larger slenderness ratios the failure shifts to flexural failure.

8.2.6 Effect of Frame Stiffness

- Development of arching action and thus out-of-plane resistance of the infills is highly affected by the flexural stiffness of the bounding frame; the higher the stiffness, the higher the expected out-of-plane strength.
- For CMU infills, the stiffness of the top beam is more influential on the out-of-plane strength than the columns due to higher arching forces generated in the vertical direction.

8.2.7 One-Way and Two-Way Arching

- Shear cracking through the webs of the CMUs was found to be the main failure mode in concrete masonry infills under arching. Due to the anisotropic characteristics of CMUs, a significant difference between the out-of-plane strength

in horizontal and vertical arching was observed in both the experimental and numerical studies.

- In a square panel made with standard CMUs laid in running bond and bounded by a rigid frame, the vertical and two-way arching strengths were found to be equal and both are significantly greater than the horizontal arching.
- When bounded by a flexible frame, the two-way arching strength is greater than the vertical and horizontal arching and it is not equal to the sum of the two.
- Modifications to Dawe and Seah (1989b) method was proposed based on the experimental and numerical findings for arching in concrete masonry infills that showed improved performance when compared with existing methods.

8.2.8 Effect of In-Plane Damage

- Prior in-plane damage was found to reduce the out-of-plane strength of infilled RC frames. The greater the damage, the greater the reduction.
- In all damaged specimens, two-way arching was still the main load resisting mechanism however, cracks from in-plane loading softened the out-of-plane behaviour and altered the pattern of cracks propagation during the out-of-plane loading.
- With an equal in-plane drift, the loss of out-of-plane strength in squat ($h/l<1$) and stronger infills is higher than the slender ($h/l>1$) and weak infills.
- Infills subjected to 0.25-1.5% in-plane drift was found to lose the out-of-plane strength at a higher rate when compared to infills with greater in-plane drifts.

- The cyclic in-plane loading resulted in more out-of-plane strength reduction than monotonic loading and this reduction was more pronounced in smaller drift ratios.
- A bi-linear equation was proposed for calculating reduction factor for the out-of-plane strength reduction considering prior in-plane damage and was shown to achieve a good agreement with FE and experimental results on concrete masonry infills.

8.3 Recommendations for Future Research

The following is recommended for future research:

1- All the tests conducted on the infilled frames were on specimens made with half-scaled CMUs. Experimental investigation on large-scaled specimens would provide valuable information on the behaviour in actual conditions.

2- Studies were focused on infills bounded by RC frames. Replacing the RC frame with steel frame could change the behaviour and lead to different failure mechanism due to factors such as local deformation in steel section, smaller torsional stiffness of steel sections, and weaker shear resistance available at the masonry-steel boundary. The steel bounding frame can be incorporated in the current proposed numerical model with relative ease.

3- A single frame configuration was used in this study. The validity of conclusions on multi-bay, multi-storey infilled frames needs further investigation. Moreover, monotonic loading was used in most analysis cases. Dynamic analysis can be incorporated in this model to evaluate the seismic behaviour of masonry infills;

however, the computational effort is the main barrier that may be overcome by using high performance computing.

4- More extensive parametric studies on the influential parameters such as gaps, openings, and CMU geometries should be conducted to draw comprehensive conclusions leading to design methods for each of these parameters. Furthermore, effect of axial load, grouting and reinforcing infills, concurrent in-plane and out-plane loading, and the effect of out-of-plane damage on in-plane behaviour and strength should be further investigated.

5- Some of the conclusions such as web shear failure are strictly applicable to concrete masonry units that meet the strength and geometric requirements of Canadian masonry standards (CSA-S304-14 and CSA-A165-14). The applicability of conclusions and proposed analytical equations on other masonry types and properties needs further investigation.

References

Abdeldjelil, B., and Thomas, T.C.H. Constitutive Laws of Concrete in Tension and Reinforcing Bars Stiffened By Concrete. Structural Journal 91(4).

Abrams, D.P., Angel, R., and Uzarski, J. 1996. Out-of-plane strength of unreinforced masonry infill panels. Earthquake Spectra 12(4): 825-844.

Akhoundi, F., Vasconcelos, G., Lourenço, P.B., and Silva, L. 2016. Out-of-plane response of masonry infilled RC frames: Effect of workmanship and opening, Taylor & Francis, pp. 1147-1154.

Al-Chaar, G., Mehrabi, A.B., and Manzouri, T. 2008. Finite element interface modeling and experimental verification of masonry-infilled R/C frames. The Masonry Society Journal 26(1): 47-65.

Alecci, V., Fagone, M., Rotunno, T., and De Stefano, M. 2013. Shear strength of brick masonry walls assembled with different types of mortar. Construction and Building Materials 40: 1038-1045.

Anderson, C. 1984. Arching action in transverse laterally loaded masonry wall panels. STRUCT. ENG. Struct. Eng. 62(1): 12.

Anderson, T.L., and Anderson, T. 2005. Fracture mechanics: fundamentals and applications. CRC press.

Angel, R., Abrams, D.P., Shapiro, D., Uzarski, J., and Webster, M. 1994. Behavior of reinforced concrete frames with masonry infills. University of Illinois Engineering Experiment Station. College of Engineering. University of Illinois at Urbana-Champaign.

ASCE/SEI41-13. 2013. Seismic Rehabilitation of Existing Buildings. American Society of Civil Engineers; Reston, VA.

Asteris, P.G., Cotsovos, D.M., Chrysostomou, C.Z., Mohebkhah, A., and Al-Chaar, G.K. 2013. Mathematical micromodeling of infilled frames: State of the art. Engineering Structures 56: 1905-1921.

ASTM. 2014. ASTM C270-14a Standard Specification for Mortar for Unit Masonry. ASTM International, West Conshohocken, PA.

ASTM. 2016a. ASTM C39/C39M Standard test method for compressive strength of cylindrical concrete specimens. *In* ASTM International, West Conshohocken, PA.

ASTM. 2016b. ASTM C140/C140M Standard Test Methods for Sampling and Testing Concrete Masonry Units and Related *In* ASTM International, West Conshohocken, PA.

ASTM. 2016c. ASTM C1314-16 Standard Test Method for Compressive Strength of Masonry Prisms. ASTM International, West Conshohocken, PA.

ASTM. 2016d. ASTM E8/E8M-16a Standard Test Methods for Tension Testing of Metallic Materials. ASTM International, West Conshohocken, PA.

Atkinson, R., Amadei, B., Saeb, S., and Sture, S. 1989. Response of masonry bed joints in direct shear. Journal of Structural Engineering 115(9): 2276-2296.

Bolhassani, M., Hamid, A.A., Lau, A.C.W., and Moon, F. 2015. Simplified micro modeling of partially grouted masonry assemblages. Construction and Building Materials 83: 159-173.

Buonopane, S., and White, R. 1999. Pseudodynamic testing of masonry infilled reinforced concrete frame. Journal of structural engineering 125(6): 578-589.

Calvi, G.M., and Bolognini, D. 2001. Seismic response of reinforced concrete frames infilled with weakly reinforced masonry panels. Journal of Earthquake Engineering 5(02): 153-185.

Chen, X. 2016. Numerical study of the in-plane behaviour of concrete masonry infills bounded by steel frames.

Chen, X., and Liu, Y. 2015. Numerical study of in-plane behaviour and strength of concrete masonry infills with openings. Engineering Structures 82: 226-235.

Chen, X., and Liu, Y. 2016. A finite element study of the effect of vertical loading on the in-plane behavior of concrete masonry infills bounded by steel frames. Engineering Structures 117: 118-129.

Chrysostomou, C.Z. 1991. Effects of degrading infill walls on the nonlinear seismic response of two-dimensional steel frames, Cornell University Ithaca, NY, USA.

Chrysostomou, C.Z., Gergely, P., and Abel, J.F. 2002. A six-strut model for nonlinear dynamic analysis of steel infilled frames. International Journal of Structural Stability and Dynamics 02(03): 335-353.

Crisafulli, F.J., and Carr, A.J. 2007. Proposed macro-model for the analysis of infilled frame structures. Bulletin of the New Zealand Society for Earthquake Engineering 40(2): 69-77.

Crisafulli, F.J., Carr, A.J., and Park, R. 2000. Analytical modelling of infilled frame structures-a general review. Bulletin-New Zealand Society for Earthquake Engineering 33(1): 30-47.

CSA. 2004. CAN/CSA-A23.3-04 - Design of Concrete Structures. Canadian Standard Association.

CSA. 2014a. CAN/CSA-A23.3-14 - Design of Concrete Structures. Canadian Standard Association.

CSA. 2014b. CAN/CSA-A165 SERIES-04 (R2014) - CSA standards on concrete masonry units Canadian Standard Association.

CSA. 2014c. CSA S304-14 - Design of masonry structures. Canadian Standard Association.

D.S.Simulia. 2010. ABAQUS Analysis User's Manual, Providence, RI, USA.

Dawe, J., and Seah, C. 1989a. Behaviour of masonry infilled steel frames. Canadian Journal of Civil Engineering 16(6): 865-876.

Dawe, J., and Seah, C. 1989b. Out-of-plane resistance of concrete masonry infilled panels. Canadian Journal of Civil Engineering 16(6): 854-864.

Dehestani, M., and Mousavi, S. 2015. Modified steel bar model incorporating bond-slip effects for embedded element method. Construction and Building Materials 81: 284-290.

Dhanasekar, M. 2010. Review of modelling of masonry shear. International Journal of Advances in Engineering Sciences and Applied Mathematics 2(3): 106-118.

Di Trapani, F., Shing, P., and Cavaleri, L. 2017. Macroelement model for in-plane and out-of-plane responses of masonry infills in frame structures. Journal of Structural Engineering 144(2): 04017198.

Dolatshahi, K.M., and Aref, A.J. 2011. Two-dimensional computational framework of meso-scale rigid and line interface elements for masonry structures. Engineering Structures 33(12): 3657-3667.

Drysdale, R.G., Hamid, A.A., and Baker, L.R. 1994. Masonry structures: behavior and design. Prentice Hall.

El-Dakhakhni, W.W., Elgaaly, M., and Hamid, A.A. 2003. Three-strut model for concrete masonry-infilled steel frames. Journal of Structural Engineering 129(2): 177-185.

Eurocode. 2004. E8: Design of structures for earthquake resistance. CEN, Comité Européen de Normalisation. pp. 1998-1991.

FEMA-356. 2000. Prestandard and commentary for the seismic rehabilitation of buildings. Federal Emergency Management Agency, Washington, DC.

FIB. 2012. Fib model code 2010. International Federation for Structural Concrete.

Flanagan, R.D. 1994. Behavior of structural clay tile infilled frames. Oak Ridge National Lab., TN (United States).

Flanagan, R.D., and Bennett, R.M. 1999a. Arching of masonry infilled frames: Comparison of analytical methods. Practice Periodical on Structural Design and Construction 4(3): 105-110.

Flanagan, R.D., and Bennett, R.M. 1999b. Bidirectional behavior of structural clay tile infilled frames. Journal of Structural Engineering 125(3): 236-244.

Flanagan, R.D., and Bennett, R.M. 1999c. In-plane behavior of structural clay tile infilled frames. Journal of Structural Engineering 125(6): 590-599.

Flanagan, R.D., and Bennett, R.M. 2001. In-plane analysis of masonry infill materials. Practice Periodical on Structural Design and Construction 6(4): 176-182.

Frederiksen, V. 1992. Membrane effect in laterally loaded masonry walls: a second order phenomenon, pp. 537-547.

Fricke, K., Jones, W., and Huff, T. 1992. In situ lateral load testing of an unreinforced masonry hollow clay tile wall, pp. 519-530.

Furtado, A., Rodrigues, H., Arêde, A., and Varum, H. 2016. Experimental evaluation of out-of-plane capacity of masonry infill walls. Engineering Structures 111: 48-63.

Gabrielsen, B., Wilton, C., and Kaplan, K. 1975. Response of arching walls and debris from interior walls caused by blast loading. DTIC Document.

Gabrielsen, B.L., and Kaplan, K. 1976. Arching in masonry walls subjected to out-of-plane forces.

Genikomsou, A.S., and Polak, M.A. 2015. Finite element analysis of punching shear of concrete slabs using damaged plasticity model in ABAQUS. Engineering Structures 98: 38-48.

Ghosh, A.K., and Amde, A.M. 2002. Finite Element Analysis of Infilled Frames. Journal of Structural Engineering 128(7): 881-889.

Griffith, M., and Vaculik, J. 2007. Out-of-plane flexural strength of unreinforced clay brick masonry walls. TMS Journal 25(1): 53-68.

Haach, V.G., Vasconcelos, G., and Lourenço, P.B. 2009. Experimental analysis of reinforced concrete block masonry walls subjected to in-plane cyclic loading. Journal of structural engineering 136(4): 452-462.

Hashemi, S.A. 2007. Seismic evaluation of reinforced concrete buildings including effects of masonry infill walls. University of California, Berkeley.

Hendry, A.W. 1981. Structural brickwork. Halsted Press.

Hillerborg, A., Modéer, M., and Petersson, P.-E. 1976. Analysis of crack formation and crack growth in concrete by means of fracture mechanics and finite elements. Cement and concrete research 6(6): 773-781.

Holmes, M. 1961. Steel frames with brickwork and concrete infilling. proceedings of the Institution of civil Engineers 19(4): 473-478.

Hu, C. 2015. Experimental study of the effect of interfacial gaps on the in-plane behaviour of masonry infilled RC frames, Civil and resource engineering, Dalhousie university, Halifax.

Jankowiak, T., and Lodygowski, T. 2005. Identification of parameters of concrete damage plasticity constitutive model. Foundations of civil and environmental engineering 6(1): 53-69.

Jiang, J.-F., and Wu, Y.-F. 2012. Identification of material parameters for Drucker–Prager plasticity model for FRP confined circular concrete columns. International Journal of Solids and Structures 49(3–4): 445-456.

Kakaletsis, D., and Karayannis, C. 2007. Experimental investigation of infilled R/C frames with eccentric openings. Structural Engineering and Mechanics 26(3): 231-250.

Klingner, R., Rubiano, N., Bashandy, T., and Sweeney, S. 1996. Evaluation and analytical verification of shaking table data from infilled frames. Part 2: Out-of-plane behavior, pp. 521-532.

Komaraneni, S., Rai, D.C., and Singhal, V. 2011. Seismic behavior of framed masonry panels with prior damage when subjected to out-of-plane loading. Earthquake spectra 27(4): 1077-1103.

Koutromanos, I., Stavridis, A., Shing, B., and Willam, K. 2011a. Numerical modeling of masonry-infilled RC frames subjected to seismic loads. Computers and Structures 89: 1026-1037.

Koutromanos, I., Stavridis, A., Shing, P.B., and Willam, K. 2011b. Numerical modeling of masonry-infilled RC frames subjected to seismic loads. Computers & Structures 89(11): 1026-1037.

Kupfer, H., Hilsdorf, H.K., and Rusch, H. 1969. Behavior of concrete under biaxial stresses, pp. 656-666.

Kwak, H.-G., and Kim, J.-K. 2006. Implementation of bond-slip effect in analyses of RC frames under cyclic loads using layered section method. Engineering Structures 28(12): 1715-1727.

Lee, J., and Fenves, G.L. 1998. Plastic-damage model for cyclic loading of concrete structures. Journal of engineering mechanics 124(8): 892-900.

Liauw, T., and Lo, C. 1988. Multibay infilled frames without shear connectors. Structural Journal 85(4): 423-428.

Liu, Y., and Manesh, P. 2013. Concrete masonry infilled steel frames subjected to combined in-plane lateral and axial loading – An experimental study. Engineering Structures 52: 331-339.

Liu, Y., and Soon, S. 2012. Experimental study of concrete masonry infills bounded by steel frames. Canadian Journal of Civil Engineering 39(2): 180-190.

Lotfi, H., and Shing, P. 1991. An appraisal of smeared crack models for masonry shear wall analysis. Computers & structures 41(3): 413-425.

Lotfi, H.R., and Shing, P.B. 1994. Interface model applied to fracture of masonry structures. Journal of structural engineering 120(1): 63-80.

Lourenco, P.B. 1996. Computational strategies for masonry structures, TU Delft, Delft University of Technology.

Lourenço, P.B. 2000. Anisotropic softening model for masonry plates and shells. Journal of Structural Engineering 126(9): 1008-1016.

Lourenço, P.B., and Rots, J.G. 1997. Multisurface interface model for analysis of masonry structures. Journal of engineering mechanics 123(7): 660-668.

Lourenço, P.B., Rots, J.G., and Blaauwendraad, J. 1998. Continuum model for masonry: parameter estimation and validation. Journal of Structural Engineering 124(6): 642-652.

Lubliner, J., Oliver, J., Oller, S., and Onate, E. 1989. A plastic-damage model for concrete. International Journal of solids and structures 25(3): 299-326.

Maekawa, K., Okamura, H., and Pimanmas, A. 2003. Non-linear mechanics of reinforced concrete. CRC Press.

Mainstone, R. 1971. On the stiffnesses and strengths ofinfilled frames. Proc. lnxtn cir. Engrs Suppl.

Maksoud, A., and Drysdale, R. 1993. Rational moment magnification factor for slender unreinforced masonry walls, pp. 6-9.

Mallick, D., and Garg, R. 1971. Effect of openings on the lateral stiffness of infilled frames. Proceedings of the Institution of Civil Engineers 49(2): 193-209.

Mallick, D., and Severn, R. 1967. The behaviour of infilled frames under static loading. Proceedings of the Institution of Civil Engineers 38(4): 639-656.

Manos, G., Soulis, V., and Thauampteh, J. 2012. The behavior of masonry assemblages and masonry-infilled R/C frames subjected to combined vertical and cyclic horizontal seismic-type loading. Advances in Engineering Software 45(1): 213-231.

Masia, M.J., Simundic, G., and Page, A.W. 2012. Assessment of the AS3700 relationship between shear bond strength and flexural tensile bond strength in unreinforced masonry.

Mays, G., Hetherington, J., and Rose, T. 1998. Resistance-deflection functions for concrete wall panels with openings. Journal of Structural Engineering 124(5): 579-587.

McDowell, E., McKee, K., and Sevin, E. 1956a. Arching action theory of masonry walls. Journal of the Structural Division 82(2): 1-8.

McDowell, E., McKee, K., and Sevin, E. 1956b. Arching action theory of masonry walls. J. Struct. Div 82(2): 915.

Mehrabi, A.B., Benson Shing, P., Schuller, M.P., and Noland, J.L. 1996. Experimental evaluation of masonry-infilled RC frames. Journal of Structural Engineering 122(3): 228-237.

Mehrabi, A.B., and Shing, P.B. 1997. Finite element modeling of masonry-infilled RC frames. Journal of structural engineering 123(5): 604-613.

Minaie, E., Moon, F.L., and Hamid, A.A. 2014. Nonlinear finite element modeling of reinforced masonry shear walls for bidirectional loading response. Finite Elements in Analysis and Design 84: 44-53.

Moghaddam, H., and Goudarzi, N. 2010. Transverse resistance of masonry infills. ACI Structural Journal 107(4): 461.

Mohebkhah, A., Tasnimi, A.A., and Moghadam, H.A. 2008. Nonlinear analysis of masonry-infilled steel frames with openings using discrete element method. Journal of Constructional Steel Research 64(12): 1463-1472.

Mohyeddin, A., Goldsworthy, H.M., and Gad, E.F. 2013. FE modelling of RC frames with masonry infill panels under in-plane and out-of-plane loading. Engineering Structures 51: 73-87.

Monk, C. 1958. Resistance of structural clay masonry to dynamic forces. Structural Clay Products Research Foundation.

Mosalam, K.M., White, R.N., and Gergely, P. 1997. Static response of infilled frames using quasi-static experimentation. Journal of Structural Engineering 123(11): 1462-4169.

Nasiri, E., and Liu, Y. 2017. Development of a detailed 3D FE model for analysis of the in-plane behaviour of masonry infilled concrete frames. Engineering Structures 143: 603-616.

Nasiri, E., and Liu, Y. 2019a. The out-of-plane behaviour of concrete masonry infills bounded by reinforced concrete frames. Engineering Structures 184: 406-420.

Nasiri, E., and Liu, Y. 2019b. Study of arching behaviour and strength of concrete masonry infills under out-of-plane loading. Canadian Journal of Civil Engineering.

Noor-E-Khuda, S., Dhanasekar, M., and Thambiratnam, D.P. 2016a. An explicit finite element modelling method for masonry walls under out-of-plane loading. Engineering Structures 113: 103-120.

Noor-E-Khuda, S., Dhanasekar, M., and Thambiratnam, D.P. 2016b. Out-of-plane deformation and failure of masonry walls with various forms of reinforcement. Composite Structures 140: 262-277.

Page, A. 1981. The biaxial compressive strength of brick masonry. Proceedings of the Institution of Civil Engineers 71(3): 893-906.

Pantò, B., Caliò, I., and Lourenço, P. 2018. A 3D discrete macro-element for modelling the out-of-plane behaviour of infilled frame structures. Engineering Structures 175: 371-385.

Pantò, B., Silva, L., Vasconcelos, G., and Lourenço, P. 2019. Macro-modelling approach for assessment of out-of-plane behavior of brick masonry infill walls. Engineering Structures 181: 529-549.

Pasca, M., Liberatore, L., and Masiani, R. 2017. Reliability of analytical models for the prediction of out-of-plane capacity of masonry infills. Structural Engineering and Mechanics 64(6): 765-781.

Polliakov, S.V.e. 1963. Masonry in framed buildings: An investigation into the strength and stiffness of masonry infilling. National Lending Library for Science and Technology, Boston Spa., Yorkshire.

Pujol, S., and Fick, D. 2010. The test of a full-scale three-story RC structure with masonry infill walls. Engineering Structures 32(10): 3112-3121.

Rahimi, R., and Liu, Y. 2017. Numerical Investigation on the in-plane behaviour of concrete masonry infilled RC frames under quasi-static cyclic loading., Halifax, Canada.

Ricci, P., Di Domenico, M., and Verderame, G.M. 2018. Empirical-based out-of-plane URM infill wall model accounting for the interaction with in-plane demand. Earthquake Engineering & Structural Dynamics 47(3): 802-827.

Roca, P., González, J., Oñate, E., and Lourenço, P. 1998. Experimental and numerical issues in the modelling of the mechanical behaviour of masonry. Structural Analysis of Historical Constructions II. CIMNE, Barcelona: 57-91.

Rots, J. 1991. Numerical simulation of cracking in structural masonry. Heron 36(2): 49-63.

Saneinejad, A., and Hobbs, B. 1995. Inelastic design of infilled frames. Journal of Structural Engineering 121(4): 634-650.

Sarhosis, V., Tsavdaridis, K., and Giannopoulos, I. 2014. Discrete element modelling (DEM) for masonry infilled steel frames with multiple window openings subjected to lateral load variations. Open Construction and Building Technology Journal 8: 93 - 103.

Schmidt, T. 1989. An approach of modelling masonry infilled frames by the FE method and a modified equivalent strut method. Annual Journal on Concrete and Concrete Structures." Darmstadt, Germany: Darmstadt University.

Sepasdar, R. 2017. Experimental investigation on the out-of-plane behaviour of the concrete masonry infilled RC frames, Civil and resource engineering, Dalhousie university, Halifax.

Shima, H., Chou, L.-L., and Okamura, H. 1987. Micro and macro models for bond in reinforced concrete. Journal of the Faculty of Engineering 39(2): 133-194.

Sima, J.F., Roca, P., and Molins, C. 2008. Cyclic constitutive model for concrete. Engineering structures 30(3): 695-706.

Smith, B.S. 1962. Lateral stiffness of infilled frames. Journal of the Structural Division 88(6): 183-226.

Smith, B.S. 1966. Behavior of square infilled frames. Journal of the Structural Division 92(1): 381-404.

Smith, B.S. 1967. The composite behaviour of infilled frames. *In* Tall Buildings. Elsevier. pp. 481-495.

Smith, B.S., and Carter, C. 1969. A method of analysis for infilled frames. Proceedings of the institution of civil engineers 44(1): 31-48.

Soon, S. 2011. In-plane behaviour and capacity of concrete masonry infills bounded by steel frames, Civil and resource engineering, Dalhousie university, Halifax.

Stavridis, A., and Shing, P. 2010. Finite Element Modeling of Nonlinear Behavior of Masonry-Infilled RC Frames. Journal of Structural Engineering 136(3): 285-296.

Syrmakezis, C., and Asteris, P. 2001. Masonry failure criterion under biaxial stress state. Journal of Materials in Civil Engineering 13(1): 58-64.

Syrmakezis, C., and Vratsanou, V. 1986. Influence of infill walls to RC frames response, p. 6.5.

Tasnimi, A., and Mohebkhah, A. 2011. Investigation on the behavior of brick-infilled steel frames with openings, experimental and analytical approaches. Engineering Structures 33(3): 968-980.

Thiruvengadam, V. 1985. On the natural frequencies of infilled frames. Earthquake engineering & structural dynamics 13(3): 401-419.

Thomas, F. 1953. The strength of brickwork. The Structural Engineer 31(2): 35-46.

TMS. 2016. TMS 402/602 Building Code Requirements and Specifications for Masonry Structures. The Masonry Society.

Turgay, T., Durmus, M.C., Binici, B., and Ozcebe, G. 2014. Evaluation of the predictive models for stiffness, strength, and deformation capacity of RC frames with masonry infill walls. Journal of Structural Engineering 140(10): 06014003.

Van der Pluijm, R. 1993. Shear behaviour of bed joints. *In* 6th North American Masonry Conference. Technomic Publ. Co, Philadelphia, Pennsylvania, USA.

Varela-Rivera, J., Moreno-Herrera, J., Lopez-Gutierrez, I., and Fernandez-Baqueiro, L. 2012. Out-of-plane strength of confined masonry walls. Journal of Structural Engineering 138(11): 1331-1341.

Wang, C. 2017. Experimental investigation on the out-of-plane behaviour of concrete masonry infilled frames, Department of Civil and Resource Engineering, Dalhousie University, Halifax, NS, Canada.

Yong, T.C. 1984. Shear strength of masonry panels in steel frames, Civil and resource engineering, University of New Brunswick, Fredericton.

Appendix A: Copyright Permissions

Copyright permission for Chapter 4

June 13th, 2019

Engineering Structures,

I am preparing my Ph.D. thesis for submission to the Faculty of Graduate Studies at Dalhousie University, Halifax, Nova Scotia, Canada. I am seeking your permission to include a manuscript version of the following paper as a chapter in the thesis:

[Ehsan Nasiri and Yi Liu, "Development of a detailed 3D FE model for analysis of the in-plane behaviour of masonry infilled concrete frames. Engineering Structures, Volume 143, 2017, pp. 603-616]

Canadian graduate theses are reproduced by the Library and Archives of Canada (formerly National Library of Canada) through a non-exclusive, world-wide license to reproduce, loan, distributor or sell these. I am also seeking your permission for the material described above to be reproduced and distributed by the LAX (NLC). Further details about the LAC (NLC) thesis program are available on the LAC (NLC) website (www.nlc-bnc.ca) Full publication details and a copy of this permission letter will be included in the thesis.

Yours Sincerely,

Ehsan Nasiri

Copyright permission for Chapter 5

June 13th, 2019

Engineering Structures,

I am preparing my Ph.D. thesis for submission to the Faculty of Graduate Studies at Dalhousie University, Halifax, Nova Scotia, Canada. I am seeking your permission to include a manuscript version of the following paper as a chapter in the thesis:

[Ehsan Nasiri and Yi Liu, "The Out-of-Plane Behaviour of Concrete Masonry Infills Bounded by Reinforced Concrete Frames", Engineering Structures, Volume 184, 2019, pp. 406-420]

Canadian graduate theses are reproduced by the Library and Archives of Canada (formerly National Library of Canada) through a non-exclusive, world-wide license to reproduce, loan, distributor or sell these. I am also seeking your permission for the material described above to be reproduced and distributed by the LAX (NLC). Further details about the LAC (NLC) thesis program are available on the LAC (NLC) website (www.nlc-bnc.ca) Full publication details and a copy of this permission letter will be included in the thesis.

Yours Sincerely,

Ehsan Nasiri

Copyright permission for Chapter 6

June 13th, 2019

Canadian Journal of Civil Engineering,

I am preparing my Ph.D. thesis for submission to the Faculty of Graduate Studies at Dalhousie University, Halifax, Nova Scotia, Canada. I am seeking your permission to include a manuscript version of the following paper as a chapter in the thesis:

[Ehsan Nasiri and Yi Liu, "Study of arching behaviour and strength of concrete masonry infills under out-of-plane loading", Canadian Journal of Civil Engineering]

Canadian graduate theses are reproduced by the Library and Archives of Canada (formerly National Library of Canada) through a non-exclusive, world-wide license to reproduce, loan, distributor or sell these. I am also seeking your permission for the material described above to be reproduced and distributed by the LAX (NLC). Further details about the LAC (NLC) thesis program are available on the LAC (NLC) website (www.nlc-bnc.ca) Full publication details and a copy of this permission letter will be included in the thesis.

Yours Sincerely,

Ehsan Nasiri

Copyright Clearance Center

Confirmation Number: 11820915
Order Date: 06/04/2019

Customer Information

Customer: Ehsan Nasiri
Account Number: 3001464477
Organization: Ehsan Nasiri
Email: ehsan.nasiri@dal.ca
Phone: +1 (902) 220-2725
Payment Method: Invoice

This is not an invoice

Order Details

Canadian journal of civil engineering : Revue canadienne de génie civil

Billing Status: **N/A**

Order detail ID:	71916256
ISSN:	0315-1468
Publication Type:	Journal
Volume:	
Issue:	
Start page:	
Publisher:	Canadian Science Publishing

Permission Status: **Granted**

Permission type:	Republish or display content
Type of use:	Republish in a thesis/dissertation
Order License Id:	4602201335253
Requestor type	Author of requested content
Format	Print, Electronic
Portion	chapter/article
The requesting person/organization	Ehsan Nasiri
Title or numeric reference of the portion(s)	Entire Paper
Title of the article or chapter the portion is from	Study of arching behaviour and strength of concrete masonry infills under out-of-plane loading
Editor of portion(s)	N/A
Author of portion(s)	Nasiri, Ehsan ; Liu, Yi
Volume of serial or monograph	N/A
Page range of portion	
Publication date of portion	Mar 14, 2019

Rights for	Main product
Duration of use	Life of current and all future editions
Creation of copies for the disabled	yes
With minor editing privileges	no
For distribution to	Worldwide
In the following language(s)	Original language of publication
With incidental promotional use	yes
Lifetime unit quantity of new product	Up to 499
Title	Study of arching behaviour and strength of concrete masonry infills under out-of-plane loading
Institution name	Dalhousie University
Expected presentation date	Jun 2019

Note: This item was invoiced separately through our **RightsLink service.** More info **$ 0.00**

Total order items: 1 **Order Total: $0.00**